TAMPEREEN TEKNILLINEN YLIOPISTO
TAMPERE UNIVERSITY OF TECHNOLOGY

Matti Javanainen

Diffusion of Lipids and Proteins in Complex Membranes

Julkaisu 1589 • Publication 1589

Tampere 2018

Tampereen teknillinen yliopisto. Julkaisu 1589
Tampere University of Technology. Publication 1589

Matti Javanainen

Diffusion of Lipids and Proteins in Complex Membranes

Thesis for the degree of Doctor of Science in Technology to be presented with due permission for public examination and criticism in Rakennustalo Building, Auditorium RN201, at Tampere University of Technology, on the 26th of October 2018, at 12 noon.

Tampereen teknillinen yliopisto - Tampere University of Technology
Tampere 2018

Doctoral candidate: Matti Javanainen
Biological Physics and Soft Matter Group
Laboratory of Physics
Faculty of Science and Engineering
Tampere University of Technology
Finland

Supervisor: Prof. Ilpo Vattulainen
Biological Physics and Soft Matter Group
Laboratory of Physics
Faculty of Science and Engineering
Tampere University of Technology
Finland

Pre-examiners: Prof. Petra Schwille
Cellular and Molecular Biophysics
Max Planck Institute of Biochemistry
Germany

Prof. Juha Vaara
NMR Research Unit
Faculty of Science
University of Oulu
Finland

Opponent: Assoc. Prof. Robert Vacha
Vacha Lab
CEITEC MU
Masaryk University
Czech Republic

ISBN 978-952-15-4230-5 (printed)
ISBN 978-952-15-4237-4 (PDF)
ISSN 1459-2045

ABSTRACT

Integral membrane proteins are tiny factories with big responsibilities in signaling and transport. These proteins are constantly looking for oligomerization partners and favorable lipid environments to perform their functions that are critical for our health. The search processes are driven by thermally-agitated lateral diffusion. Cellular membranes are crowded and highly heterogeneous entities. Their structure is assumed to couple to the dynamics of molecules within the membrane, rendering diffusion therein complex too. Clarifying this connection can help us to grasp how cells regulate dynamic processes by locally varying their membrane properties, and how this further affects protein function. Unfortunately, despite persistent experimental work, our understanding of this structure–dynamics–function coupling remains poor.

In this Thesis, we present our findings on how protein crowding and lipid packing affect the lateral dynamics of lipids and proteins in membranes and monolayers. We have employed molecular dynamics simulations using both atomistic and coarse-grained models to resolve how the rate and nature of diffusion are affected by these two factors. We also advanced the related methodology, which turned out to be beneficial for studying lipid membranes that are crowded with proteins.

We find that crowding and packing slow down lipid and protein diffusion and extend the anomalous diffusion regime. We demonstrate that models used to predict diffusion coefficients of lipids and proteins struggle in such conditions. Finally, we observe that protein crowding effects non-Gaussian diffusion that does not follow the diffusion mechanism observed for protein-free bilayers, nor any other known mechanism.

Our observations help us understand the dynamics in crowded membranes, and hence shed light on the kinetics of numerous membrane-mediated phenomena. The findings suggest that normal diffusion is likely absent in the membranes of living cells, where the motion of each lipid and protein is heavily affected by its heterogeneous surroundings. The results also pave the way towards understanding central processes in the utterly complex plasma membranes of living cells. Here, the possible future applications lie in pharmaceuticals that affect protein function by disturbing the formation of functional protein–protein or protein–lipid units by perturbing the dynamic properties of the membranes and monolayers.

TIIVISTELMÄ

Kalvoproteiinit kuljettavat viestejä ja molekyylejä solukalvon läpi. Nämä proteiinit toimivat usein monen proteiinin oligomeerinä, minkä lisäksi monet kalvojen lipidit säätelevät niiden toimintaa. Proteiinit ja lipidit ovatkin jatkuvassa diffuusioliikkeessä etsien suotuisia oligomerisaatiokumppaneita ja lipidiympäristöjä. Solujen kalvot ovat rakenteeltaan heterogeenisiä ja ne on pakattu täyteen kalvoproteiineja. Tästä monimutkaisesta rakenteesta johtuen myös kalvoissa tapahtuva diffuusioliike tunnetaan huonosti. Tämän tiedon avulla voitaisiin kuitenkin ymmärtää, kuinka solut säätelevät paikallisesti dynaamisia ominaisuuksiaan ja kuinka tämä puolestaan vaikuttaa proteiinien toimintaan. Vuosien pitkäjänteisestä työstä huolimatta emme toistaiseksi juurikaan tunne tätä yhteyttä rakenteen, dynamiikan ja toiminnallisuuden välillä.

Tässä väitöskirjassa selvitimme, miten solujen kalvoja vastaavat proteiinikonsentraatiot ja lipidien pakkaantuminen vaikuttavat lipidien ja kalvoproteiinien dynamiikkaan lipidikaksoiskalvoissa ja yksikerroskalvoissa. Karkeistettuihin ja atomitason malleihin pohjautuvien molekyylidynamiikkasimulaatioiden avulla selvitimme, kuinka nämä kalvojen epäideaalisuudet vaikuttavat diffuusioliikkeen nopeuteen ja luonteeseen. Kehitimme samalla menetelmiä, jotka mahdollistivat diffuusioilmiöiden laskennallisen tutkimuksen näissä täyteenpakatuissa lipidikalvoissa.

Havaitsimme, etteivät diffuusionopeutta ennustavat teoreettiset mallit ole sovellettavissa monimutkaisiin kalvoihin. Saimme selville, että kaksoiskalvojen täyteenpakkautuminen proteiineilla sekä yksikerroskalvojen puristaminen hidastavat lipidien ja proteiinien diffuusiota huomattavasti kasvattaen samalla anomaalin diffuusion aikaskaalaa. Osoitimme myös diffuusioliikkeen olevan ei-Gaussista täyteenpakatuissa kalvoissa, mitä ei voida selittää millään tunnetulla teoreettisella mallilla.

Tuloksemme auttavat ymmärtämään täyteenpakattujen kalvojen dynamiikkaa ja siten käsittämään useiden kalvoavusteisten ilmiöiden kinetiikkaa. Tutkimuksemme keskeisin löytö on, että normaalin diffuusioliikkeen rooli heterogeenisissa kalvoissa on olematon ja että kaikki näissä kalvoissa tapahtuva lipidien ja proteiinien liike riippuu hyvin paljon paikallisesta ympäristöstä ja jatkuvista vuorovaikutuksista muiden molekyylien kanssa. Havainnoillamme saattaa olla lääketieteellisiä sovelluksia, sillä vaikuttamalla proteiinioligomeerien ja proteiini–lipidi-kompleksien muodostumiseen lienee mahdollista vaikuttaa epäsuorasti myös itse näiden proteiinien toimintaan.

PREFACE

Putting this Thesis together took somewhat longer than I originally expected, but I would not trade away any of those six years. It is really a privilege to work on something so exciting that it feels like a hobby — and still get paid for it.

So what made it all so nice? First of all, I got to work on numerous projects that were interesting or important — and sometimes even both. I'm greatly thankful to Ilpo for always being supportive and feeding me with plenty of research questions to tackle, as well as for giving me the freedom to work on other topics I came across.

I am also grateful to other current and former members of our group, both in Tampere and in Helsinki. Special thanks go to Hector for our long and inspiring discussions (*i.e.* fights) that often resulted in successful research ideas. Science-wise I'm also very grateful to Fabio, Giray, and Waldek, yet everyone is to thank for the group spirit. And when I struggled at work, Sami and Maria were there to listen to me complain. I also owe a lot to all my roommates with whom I shared many interesting discussions, as well as to all the brilliant students I was honored to supervise.

I also had the pleasure to get to know Ralf and Pavel who joined the group as Finland Distinguished Professors. While the work conducted in collaboration with Ralf forms the backbone of this Thesis, I also got to visit Pavel's group in Prague repeatedly during my studies, eventually ending up as a member of his group.

Aside from the group members, I would like to thank my classmates in Tampere — with whom we have traveled the world in search of the perfect pint — as well as my good friends Samuli and Juha whose company has made any beer taste just fine.

Finally, I am the most grateful to my best friend Linda for all the love and understanding, to my son Lukas for all the joy and meaning he has brought to my life, and to my family for all the possible support they have provided throughout the years.

Prague, September 23rd, 2018

Matti Javanainen

CONTENTS

LIST OF SYMBOLS AND ABBREVIATIONS

AA	All-atom
AFM	Atomic force microscopy
APL	Area per lipid
ATP	Adenosine triphosphate
CG	Coarse-grained
CTRW	Continuous time random walk
DLPC	Dilinoleoylphosphatidylcholine
DPPC	Dipalmitoylphosphatidylcholine
EA-MSD	Ensemble-averaged mean squared displacement
EA-TA-MSD	Ensemble- and time-averaged mean squared displacement
EB	Ergodicity breaking parameter
EM	Electron microscopy
EXSY	Exchange spectroscopy
FA	Free area
FBM	Fractional Brownian motion
FCS	Fluorescence correlation spectroscopy
FLCS	Fluorescence lifetime correlation spectroscopy
FLE	Fractional Langevin equation
FRAP	Fluorescence recovery after photobleaching
FREE	Obstacle-free conditions
FRET	Förster resonance energy transfer
GPU	Graphics processing unit
INF	Lipid-to-protein ratio in a single protein system
iSCAT	Interferometric scattering
L_c	Liquid-condensed
L_d	Liquid-disordered
L_e	Liquid-expanded
L_o	Liquid-ordered
LJ	Lennard-Jones
LP	Lipid-to-protein ratio
MD	Molecular dynamics
MSD	Mean squared displacement
NMR	Nuclear magnetic resonance

OPLS	Optimized potential for liquid simulations
PBC	Periodic boundary conditions
PDB	Protein data bank
PDF	Probability distribution function
PFG	Pulsed field gradient
PM	Plasma membrane
PN	Plasmonic nanoantenna
POPC	Palmitoyloleoylphosphatidylcholine
POPG	Palmitoyloleoylphosphatidylglycerol
QENS	Quasi-elastic neutron scattering
SA	Strongly-aggregating proteins
SC	Strongly-confining obstacles
SD	Saffman–Delbrück
SPT	Single particle tracking
STED	Stimulated emission depletion
TA-MSD	Time-averaged mean squared displacement
TIP3P	Three-site transferable intermolecular potential
TIRFM	Total internal reflection fluorescence microscopy
TM	Trans-membrane
UA	United-atom
VMD	Visual molecular dynamics
WA	Weakly-aggregating proteins
WC	Weakly-confining obstacles

Φ	Particle concentration
t	Time
D	Diffusion coefficient
$P(r,t)$	Probability distribution function
r	Displacement
$\langle r^2(t)\rangle$	Ensemble-averaged MSD
l_D	Diffusion length
ξ	White Gaussian noise
δ	Delta function,
$\mathbf{r}$	Position
μ	Mobility
T	Temperature

k_{B}	Boltzmann constant
T	Temperature
N_{A}	Avogadro's constant
R	Universal gas constant
$\overline{\delta^2(\Delta)}$	Time-averaged MSD
$\langle\overline{\delta^2(\Delta)}\rangle$	Ensemble- and time-averaged MSD
Δ	Lag time
Θ	Measurement time
Γ	Overlap parameter in the free area model
v^*	Critical volume
v_f	Free volume
E_v^*	Activation energy at constant volume
$a(T)$	Average area of lipid at temperature T
M	Molar mass
a_0	Close-packed area
E_a	Activation energy
η	Viscosity
R	Radius
h	Membrane thickness
μ_{m}	Membrane viscosity
μ_{f}	Solvent viscosity
L_{SD}	Saffman–Delbrück length
γ	Euler–Mascheroni constant
α	Diffusion exponent
ξ_f	Fractional Gaussian noise
D^*	Effective diffusion coefficient
δt	Time interval
$C_{\delta t}(t)$	Displacement autocorrelation function
ϕ	Distribution function
τ	Waiting time
$\mathbf{a}$	Acceleration
$\mathbf{F}$	Force
m	Mass
ϵ	Energy parameter in the Lennard-Jones potential
D_0	Prefactor in the Arrhenius model
E_{Arrh}	Arrhenius activation energy
R_{eff}	Effective radius
ζ	Non-Gaussian exponent

LIST OF PUBLICATIONS

Publications III–VI consider research on lateral dynamics in membranes and monolayers, whereas publications I & II support this work by providing the necessary methodological developments.

I **M. Javanainen**, "Universal Method for Embedding Proteins into Complex Lipid Bilayers for Molecular Dynamics Simulations," *Journal of Chemical Theory and Computation*, vol 10, no. 6, pp. 2577–2582, 2014.

II **M. Javanainen**, H. Martinez-Seara, I. Vattulainen, "Excessive Aggregation of Membrane Proteins in the Martini Model", *PLoS One*, vol 12, no. 11, e0187936, 2017.

III **M. Javanainen**, L. Monticelli, J.B. de la Serna, I. Vattulainen, "Free Volume Theory Applied to Lateral Diffusion in Langmuir Monolayers: Atomistic Simulations for a Protein-Free Model of Lung Surfactant," *Langmuir*, vol 26, no. 19, pp. 15436–15444, 2010.

IV **M. Javanainen**, H. Martinez-Seara, R. Metzler, I. Vattulainen. "Diffusion of Integral Membrane Proteins in Protein-Rich Membranes," *The Journal of Physical Chemistry Letters*, vol 8, no. 17, pp. 4308–4313, 2017.

V **M. Javanainen**, H. Hammaren, L. Monticelli, J.-H. Jeon, M.S. Miettinen, H. Martinez-Seara, R. Metzler, I. Vattulainen. "Anomalous and Normal Diffusion of Proteins and Lipids in Crowded Lipid Membranes," *Faraday Discussions*, vol 161, pp. 397–417, 2013.

VI J.-H. Jeon*, **M. Javanainen***, H. Martinez-Seara, R. Metzler, I. Vattulainen. "Protein Crowding in Lipid Bilayers Gives Rise to Non-Gaussian Anomalous Lateral Diffusion of Phospholipids and Proteins," *Physical Review X*, vol 6, no. 2, 021006, 2016. *Jeon and Javanainen had an equal contribution to this publication, thus they shared the first-author status.

AUTHOR'S CONTRIBUTION

For Publication I, the author, as the only author in the article, was responsible for all steps of the research. The author conceptualized the research. He designed, set up, performed, and analyzed all simulations. The author wrote the paper with comments provided by colleagues. The author was also responsible for the publishing process.

For Publication II, the author co-conceptualized the research together with both coauthors. The author designed, set up, and performed all simulations. The author analyzed the simulations with the help of Hector Martinez-Seara. The author wrote the paper with the help of both coauthors.

For Publication III, Ilpo Vattulainen was mainly responsible for the conceptualization of the research. The author collected all data by setting up, performing, and analyzing the simulations. Luca Monticelli provided technical assistance with performing the simulations, whereas Ilpo Vattulainen supervised later steps of the research. The author participated in the writing process, mostly by contributing to sections considering methodology and results. The paper was mainly written by Ilpo Vattulainen with the help of all coauthors.

For Publication IV, the author co-conceptualized the research with Ilpo Vattulainen. The author designed, set up, performed, and analyzed all simulations with assistance provided by Hector Martinez-Seara. All authors participated actively in the interpretation of the results, and helped the author write the paper.

For Publication V, the author co-designed the simulations with Ilpo Vattulainen. The author set the simulations up, performed them, and analyzed most of the data. Minor parts of the analyses were performed by Jae-Hyung Jeon. The author wrote the methods and the results sections. Ilpo Vattulainen wrote the other sections of the paper with the help of all coauthors.

For Publication VI, the author co-conceptualized the research together with all coauthors. The author co-designed the simulations, set them up, performed them, and co-analyzed them. The author wrote parts of the paper, including the introduction. The rest was mainly written by Jae-Hyung Jeon and Ilpo Vattulainen with the help of all coauthors. A major fraction of the analyses and theoretical derivations were performed by Jae-Hyung Jeon, with whom the author shares the first-author status.

1. INTRODUCTION

Cellular membranes are utterly complex quasi-two-dimensional soft sheets of lipids that host a plethora of macromolecules such as membrane proteins and carbohydrates. These membranes encapsulate numerous organelles — including the nucleus — in the cytoplasm. Perhaps the most central of all cellular membranes is the plasma membrane, which separates this intracellular environment of a cell from its surroundings, hence regulating the transport of matter and messages to and from the cell [1]. The lipid bilayer — the main building block of cellular membranes — is made up of thousands of different types of lipids that are distributed unevenly both along the bilayer plane as well as across the two bilayer leaflets [2, 3]. Furthermore, the plasma membrane is also tremendously crowded by thousands of different kinds of membrane proteins — the small factories that are responsible for numerous cellular functions, such as signaling and transport [4, 5, 6]. The correct functioning of these proteins is of utmost importance for health, which is highlighted by the fact that a significant fraction of modern pharmaceuticals targets them [5].

In addition to being structurally complex, the plasma membrane is highly dynamic as its components are under constant motion driven by both thermal fluctuations and active transport processes [1]. Lipids and proteins diffuse along the membrane to form functional protein oligomers [7], lipid nanodomains [8], and to engage in specific lipid–protein interactions [9] that provide proteins with suitable environments to carry out their functions. These dynamic processes are certainly affected or perhaps even regulated by the complexity characteristic of biomembranes, yet the details of this structure–dynamics–function interplay have remained poorly understood to date.

Experimental efforts aiming to understand membrane dynamics have several limitations. Measurements of the dynamics in living cells suffer from rather poor spatiotemporal resolution as well as from the lack of proper control experiments. Model membranes allow for a more controlled and systematic approach and therefore provide a slight improvement in the obtained temporal and spatial resolutions.

Unfortunately, such model systems lack the proper non-equilibrium conditions that define living organisms.

Fortunately, experiments are not facing the aforementioned challenges alone. Theoreticians have studied dynamic processes for decades, and the field is currently as active as ever. Most importantly, molecular dynamics simulations of biomembranes have reached their golden era in the recent years. Notably, the simulation field has seen substantial improvements in both the accuracy of the used models as well as the time and length scales reachable by the ever improving multiscale simulation approaches and the increasing computing capacity. These scales are currently already overlapping with those achieved by the most precise experimental methods. Simulations can hence act as the "ultimate microscope" and complement experiments by providing one with a nanoscale picture of the studied phenomena. Such a multidisciplinary approach will certainly help us understand the dynamic processes taking place in complex membranes and therefore open new avenues to improve our health. In these efforts, computer simulations — such as those employed in this Thesis — will undoubtedly be an indispensable tool.

Research Objectives and the Scope of This Thesis

The motion of lipids and proteins in biomembranes is traditionally described by empirical parameters, such as the diffusion coefficient and the diffusion exponent. The diffusion coefficient describes the rate of diffusion, whereas the diffusion exponent distinguishes normal diffusion from its anomalous counterparts. Surprisingly little is actually known on how these two parameters depend on the structural complexities present in the plasma membrane. Moreover, the biological role of anomalous diffusion in membrane-associated processes has remained a mystery.

This Thesis has three central objectives related to improving our understanding of membrane dynamics. The first set of goals considers models that are commonly employed to predict lipid and protein diffusion coefficients. The free area model for lipid bilayers [10] assumes that lipids diffuse *via* jumps between vacant sites in a membrane. It provides the diffusion coefficient of a lipid as a function of two parameters — one describing the energy required for the lipid to break free from its old environment and the other related to the free area required for a jump. This model has successfully been adapted to lipid bilayers [10], even though the underlying mechanism has been questioned [11]. We put the free area model to the

test in lipid monolayers, where the area parameter can be readily varied. Here, the simulation approach provided a straightforward and self-consistent evaluation, since the parameters obtained by fitting the free area model to lipid diffusion coefficients can be readily compared to the corresponding parameters extracted directly from the simulations. The central question here was whether the parameters provided by the free area model to describe lipid motion are physically reasonable. If not so, the model is likely unable to capture the correct physical mechanism of lipid diffusion in monolayers, and hence its predictive power needs to be seriously questioned therein.

The Saffman–Delbrück model [12, 13] links protein diffusion coefficient to parameters describing the protein, the membrane, and the surrounding solvent. Notably, it suggests a weak logarithmic dependence between the protein diffusion coefficient and its radius. The Saffman–Delbrück model was derived for a single protein diffusing in an indefinitely large membrane sheet. However, the plasma membrane is exceptionally crowded with proteins [4], and it is, therefore, possible that the predictions of the model fail in such a crowded setting. We evaluated the ability of the Saffman–Delbrück model to describe the size dependence of protein diffusion in crowded membranes. The main question here was whether the model is valid under crowding and, if not, what replaces it in such a setting.

Our second set of objectives considers lipid and protein dynamics in crowded membranes, as well as lipid dynamics in packed monolayers. It is known that crowding slows down diffusion [14] and induces anomalous diffusion [15]. However, the details of anomalous diffusion, especially the underlying physical mechanisms, have remained unsolved. We studied lipid and protein motion in membranes with different levels of crowding. Here, we presented multiple research questions. What is the time regime in which anomalous diffusion manifests itself? How does the diffusion exponent vary as a function of lag time? Furthermore, how are these two related to the level of protein crowding? Similar questions were also tackled with the monolayer simulations, yet instead of protein crowding, here we systematically varied lipid packing. Moreover, we asked which mathematical model can describe anomalous subdiffusion in protein-crowded membranes: does the fractional Brownian motion — validated as the corresponding mechanism in protein-free membranes by us [16] — also hold in crowded conditions and, if not, what is the correct formulation.

Our third set of objectives considers methodology. Here, we aimed to provide an improved approach for embedding proteins in lipid membranes to foster studies on membrane protein systems. Moreover, we set an aim to improve the ability of

a commonly used simulation model to describe protein–protein interactions and hence provide reliable results for the dynamics of membranes crowded by proteins. We consider that both of these improvements were crucial for reaching the other objectives described above.

Finally, the grand aim of this Thesis is to combine my work and the work of others into a comprehensive state-of-the-art picture of the current understanding of lipid and protein diffusion in complex biomembranes.

Contents of This Thesis

After this Introduction, being Chapter 1, the remainder of the Thesis is structured as follows. An overview of the relevant biological concepts is provided in Chapter 2. Here, the current understanding of the structure of the plasma membrane, membrane proteins, and lipid monolayers are described. Most importantly, the complexity of biomembranes is highlighted in Chapter 2, and this complexity is connected to the peculiar observations on lipid and protein diffusion in Chapter 6.

The key theoretical concepts regarding lateral diffusion are described in Chapter 3. Here, the theoretical models that are used to describe the diffusion of lipids and proteins are briefly introduced. Moreover, the concept of anomalous diffusion that is prevalent in biomembranes is discussed. A few theoretical descriptions that lead to anomalous dynamics are also presented. The relevance of lateral diffusion — including anomalous one — for cellular functions is justified. The main experimental methods that are commonly employed to tackle the questions related to lateral dynamics of membranes are also reviewed in Chapter 3. Their primary operating principles and limitations are discussed and their spatial and temporal resolutions are reviewed. Chapter 3 is closed by a justification for the need for computer simulations in the studies of membrane dynamics.

A brief look into the theoretical background of the molecular dynamics method employed throughout this Thesis is provided in Chapter 4. The fundamental concepts related to this methodology are introduced, and some of its central limitations are discussed. A thorough description of all the simulation models used in this Thesis is also provided at the end of Chapter 4.

Findings of this Thesis are described in Chapter 5 that is divided into three parts. In the first one, the methodological contributions of this Thesis are described. This

work is covered by Publications I and II attached to this Thesis. In the second part of Chapter 5, the central results of this Thesis considering models describing normal diffusion of proteins and lipids are discussed. These findings have been reported in Publications III and IV attached to this Thesis. In the third section, the results of this Thesis on anomalous diffusion in membranes and monolayers are described. This work includes both qualitative and quantitative analysis of the effects of protein crowding and lipid packing on lipid and protein dynamics. This work is described in Publications V and VI attached to this Thesis.

A state-of-the-art picture of dynamics in biomembranes is provided in Chapter 6. The way the recent experimental and simulation efforts have improved our understanding of the interplay between plasma membrane complexity and dynamics is systematically reviewed. To close this Thesis, some central open questions and possible future directions in the field are discussed.

2. BIOLOGICAL FRAMEWORK

In this Chapter, the biological framework and its key players relevant for this Thesis are described. An overview of the structure of the plasma membrane is provided, highlighting its complexity. The biological roles of membrane proteins and lipid monolayers are also briefly discussed.

2.1 The Plasma Membrane

The plasma membrane (PM) surrounds every cell and acts as a barrier between intracellular and extracellular environments, regulating the transport of ions and molecules to and from the cell [1]. This regulation is required to prevent harmful substances from entering cells, to provide the cell with nutrients, and to maintain concentration gradients of ions that drive numerous processes [1]. The PM, depicted in Fig. 2.1, is a complex mixture of hundreds of thousands of different lipid species [17], thousands of distinct membrane proteins [6], and a group of other structurally diverse macromolecules. Fortunately, decades of joint efforts by scientists working on simplified model membranes, cellular extracts, living cells, theoretical models, and computer simulations have brought our understanding of the PM structure to the point where we can begin understand the link between this structure and cellular functions.

2.1.1 The Fluid Mosaic Model and Beyond

Our current understanding of the structure of lipid membranes, including the PM, is based on the fluid mosaic model, also known as the Singer–Nicholson model [19]. This model states that the PM consists of two leaflets of amphiphilic lipid molecules arranged so that their hydrophilic head groups (red in Fig. 2.1) face outward from the membrane core formed by their hydrophobic acyl chains (orange in Fig. 2.1). This "main fabric" constitutes most of the membrane area and provides the membrane with

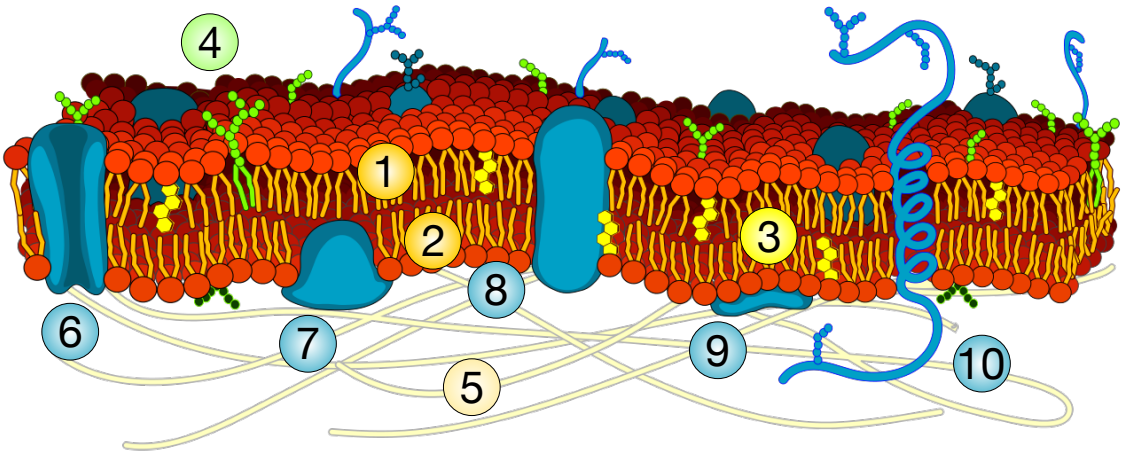

Figure 2.1 *Schematic picture of the PM with some key features highlighted by numbers. The lipids forming the bilayer are shown in red (head groups) and orange (acyl chains). The extracellular and the intracellular leaflets are indicated by 1 and 2, respectively. Cholesterol (3), drawn in yellow, resides in both leaflets. Carbohydrates on the extracellular side are shown in green. Here, they are attached to glycolipids (4). The actin cytoskeleton (5) covers the bilayer on the cytosolic side. Proteins of different types are shown in blue. Channel proteins (6) span the whole membrane and transport ions or molecules across the membrane. Many receptors possess a single alpha-helical trans-membrane domain (10) attached to large extra-membrane segments. In addition to trans-membrane proteins (6,8, and 10), integral membrane proteins can also span only one leaflet (7). Such proteins are referred to as integral monotopic proteins. Peripheral proteins (9) attach to the surface of the membrane with various mechanisms. The lipid complexity, lateral heterogeneity, trans-bilayer asymmetry, and membrane curvature, discussed in the text, are omitted in this simplified schematic [18].*

its fluidity and mechanical properties. It is also occupied by cholesterol molecules and proteins (yellow and blue in Fig. 2.1, respectively). Membrane proteins lie in the lipid fabric, whereas peripheral proteins are attached to the bilayer surface on either side. Carbohydrates (green in Fig. 2.1) are anchored to proteins and lipids on the extracellular leaflet. While this model has stood the test of time for more than four decades [20], it has been accompanied by numerous extensions sparked by later experimental observations [21]. Next, some of these central updates are reviewed.

Lateral Heterogeneity and Lipid Rafts

The membrane components are not uniformly distributed along the membrane plane. Instead, the PM is considered to be laterally heterogeneous, a fact that is

unfortunately omitted in Fig. 2.1. This *heterogeneity*, captured in the raft concept [22], provides membrane proteins with various distinct environments where they can facilitate their functions involved in, *e.g.*, signaling and trafficking [23]. It is considered that these environments are characterized by differences in membrane ordering; more ordered domains — coined rafts — are enriched in cholesterol and lipids with saturated chains such as sphingomyelin, whereas the less ordered regions are composed primarily of lipids with unsaturated chains [8]. The definition of a raft has evolved over the years, and the current view highlights their role as functional nanoscale domains [8]. The direct visualization of rafts is limited by their small size, which puzzles researchers even today [2, 18], and has also sparked alternative explanations for the indirect observations of rafts [24]. However, super-resolution fluorescence correlation spectroscopy measurements by independent teams have reported the cholesterol-dependent trapping of sphingomyelin in nanoscopic domains in the plasma membrane of living cells [25, 26, 27], providing strong support for the raft concept.

The picture of rafts is directly connected to *in vitro* experiments on ternary model membranes. Certain ternary lipid mixtures, including those containing cholesterol and sphingomyelin, spontaneously phase separate into microscopic liquid-ordered (L_o) and liquid-disordered (L_d) phases [28, 29]. This separation takes place typically at temperatures somewhat below the body temperature. Interestingly, giant plasma membrane-derived vesicles display phase separation at similar temperatures [30, 31], while their structure seems homogeneous at the body temperature. However, close to an immiscibility transition, critical fluctuations lead to the formation of transient domains [32] with the properties matching those postulated for lipid rafts. Indeed, such fluctuations are present in both model membranes and plasma membrane-derived vesicles [33, 34]. The critical fluctuation concept and its relation to lipid rafts is further supported by recent *in vivo* experiments demonstrating the reversible phase separation of a yeast vacuole membrane into two liquid phases upon temperature decrease [35].

Asymmetry, Leaflet Coupling, and Flip–Flops

In addition to being laterally heterogeneous, the compositions of the two membrane leaflets are also different as they face two distinct solvent environments [36]. This *asymmetry*, unfortunately omitted in Fig. 2.1, is crucial for maintaining the proper

membrane potential as an energy source for active transport [1]. Moreover, it also promotes specific interactions with proteins and other molecules that adsorb onto the membrane surface. Here, especially glycolipids and charged lipids have essential roles as receptors [37], while certain lipids are also involved in signaling [38]. The extracellular leaflet consists of neutral zwitterionic lipids such as phosphatidylcholine and sphingomyelin, as well as some glycolipids [3]. The intracellular leaflet, however, contains charged lipid moieties including phosphatidylserine, phosphatidylinositol, and phosphoinositides together with zwitterionic phosphatidylethanolamine [3]. Cholesterol occupies both leaflets of the bilayer to some extent, yet its precise distribution remains unknown [39, 40].

Curiously, model membranes mimicking the composition of the extracellular leaflet undergo spontaneous phase separation [29] and are therefore associated with rafts [22], whereas membranes consisting of the lipids present in the intracellular leaflet show no such tendency [41]. However, it is still somewhat unknown how heterogeneities in one leaflet couple to the other leaflet — and in case they do — are the structurally similar regions aligned across leaflets. These phenomena, coined interleaflet coupling and membrane registry, have been studied in experiments [42], in simulations [43], and theoretically [44]. While all these efforts point towards a coupling effect favoring membrane registry, its details remain poorly understood [45].

The formation of lateral heterogeneities is driven by passive diffusion, and lipids travel on average dozens of nanometers every millisecond. The diffusion of lipids across the bilayer with a thickness of about five nanometers, on the other hand, is significantly slower. This trans-bilayer diffusion is limited by the unfavorable partitioning of hydrophilic head groups into the membrane core, which helps cells maintain membrane asymmetry. Cholesterol spontaneously flip–flops in the millisecond time scale [46], whereas for phospholipids such events are very scarce and might take days [47]. This low rate is obviously inadequate to maintain bilayer structure as newly synthesized lipids frequently adsorb to its intracellular leaflet. Therefore, cell membranes are equipped with various lipid transport proteins. Energy-independent scramblases aid lipids to cross the bilayer without preferential direction [48]. Flippases use energy to keep phosphatidylserine from the extracellular leaflet, whereas floppases move lipids non-selectively in the opposite direction with the help of ATP [48, 49]. The well-controlled membrane asymmetry is the result of the interplay of these three protein classes as well as passive flip–flops.

Cytoskeleton and Glycocalyx

In addition to the structural complexity of the PM itself, it is also coupled on both sides to two very distinct structures — the *cytoskeleton* and the *glycocalyx*. The cytoskeleton (pale in Fig. 2.1) is a dynamic protein structure consisting of filaments and tubules in the cytoplasm. [1]. It functions as a highway for directed transport, maintains the shape of cells, and helps them deform and hence move [50]. The actin microfilaments of the cytoskeleton couple to the PM by anchoring to specific trans-membrane proteins — or "pickets" — thus immobilizing them [51]. Moreover, the actin skeleton meshwork lies on the cytoplasmic leaflet where the filaments — or "fences" — partition the membrane into distinct confined regions [51].

The extracellular side of the PM is covered by glycocalyx, a layer with a varying thickness of carbohydrates consisting of glycoproteins and glycolipids (green in Fig. 2.1) [52]. This network is anchored to the PM by trans-membrane domains of glycoproteins and the membrane-spanning parts of the glycolipids. Glycocalyx functions as an extra barrier against foreign molecules, acts as a cushion and adhesive between cells, and is involved in signaling [1].

Membrane Curvature

Even the smallest cells have a diameter of a few micrometers. Therefore, the PM curvature stemming from the size and shape of cells alone is relatively small. However, the PM *curvature* varies locally to a significant degree. Caveolae are membrane invaginations with a radius of a few dozen nanometers that cover up to a third of the cellular surface [53]. They are involved in membrane trafficking and host many proteins involved in signaling [54]. Certain peripheral proteins can also attach to the membrane and bend the membrane to follow their convex or concave shapes, act as wedges, or induce curvature by crowding effects [55, 56, 57]. Moreover, the various types of lipid molecules differ in their spontaneous curvatures, *i.e.* in their intrinsic ability to induce membrane curvature and to sort into regions of distinct curvatures [58]. The membrane shown in the schematic in Fig. 2.1 does not demonstrate any substantial local curvature.

Caveolae can bud out from the PM into the cytosol as vesicles [53]. This and other forms of endocytosis allow the transport of large molecules through the membrane [1]. In the reverse reaction, exocytosis, cargo from the cytosol is released into the

extracellular space by the fusion of a vesicle bilayer into the PM [1]. These trafficking processes keep the membrane under non-equilibrium conditions and maintain the rapid recycling of its constituents.

Protein Crowding

The fluid mosaic model pictured the PM to have a relatively dilute concentration of proteins [19]. However, it has recently become clear that approximately one-third of the cellular surface is covered by them [4, 21]. This level of *crowding* signals that proteins continuously collide and interact with each other, promoting their oligomerization. Moreover, there are only a few dozen lipids for each membrane protein. Considering that proteins bind lipids onto their surfaces [9] and perturb the structure and dynamics [59] of their lipid environment, it seems that no membrane lipids exhibit free bulk-like behavior. The concentration of proteins in the PM is somewhat underestimated by Fig. 2.1.

Crowding has substantial effects on lateral diffusion in the PM, as discussed later in this Thesis. Notwithstanding this, surprisingly little is known of its biological importance. Membrane protein clusters regulate membrane curvature [55, 60] and membrane phase behavior [60]. Moreover, oligomerization can regulate the signaling of the individual proteins [61]. The properties affected by crowding in the cytosol are better understood, and they cover, *e.g.*, reaction rates [62], diffusive motion [63], and protein stability [64]. Hence, it is safe to assume that crowding also plays essential roles in the processes taking place in the PM, such as the functions performed by membrane proteins.

2.1.2 Membrane Proteins

Membrane proteins are key molecules in the PM, occupying about a third of its surface area [4], corresponding to ∼30 % of the human proteome [6], and serving as targets for half of the current pharmaceuticals [5].

Structure and Function of Membrane Proteins

Membrane proteins (blue in Fig. 2.1) are the powerhouses of the cell and act as transporters, receptors, and enzymes [65]. As concrete examples, G protein-coupled

receptors bind a ligand — such as a neurotransmitter — at the extracellular side of the PM and undergo a conformational change, which induces a signaling cascade inside the cell. Voltage-gated ion channels respond to membrane potential and allow the passage of ions through the PM. Flippases and floppases use energy to transport lipids between the membrane leaflets.

Despite their medical importance and abundance, membrane proteins have been studied much less than their water-soluble counterparts. It was only in 1985 that the 3D structure of the first membrane protein was resolved [66] — 25 years after the high-quality structure of myoglobin appeared in the literature [67]. The numbers of known membrane protein and water-soluble protein structures have both seen exponential growth [68]. However, due to their head start, there are currently more than 100,000 known structures of water-soluble proteins, whereas the corresponding number for membrane proteins has yet to reach one thousand [69, 70]. The rate at which structures become available will likely grow in the near future, as cryo-EM is adapted more widely to complement X-ray and NMR techniques in structure determination [71].

Trans-membrane proteins (6, 8, and 10 in Fig. 2.1) are typically bundles of alpha-helices that span the entire membrane [72]. In the PM, they consist of a varying number of trans-membrane helices [65]. Typical examples are single-pass domains of receptor tyrosine kinases with large extra-membrane segments [73] and G protein-coupled receptors with seven trans-membrane helices [74]. Very few proteins contain more than 14 helices [65]. Bacteria and mitochondria also contain trans-membrane proteins with a beta-barrel as their secondary structure. The other classes of membrane proteins are integral monotopic proteins that span only one leaflet and peripheral proteins that attach to the membrane surface by inserting partially into the membrane, or by anchoring themselves via lipid anchors or electrostatic interactions (7 & 9 in Fig. 2.1) [1].

Membrane Protein Interactions

Recent experimental evidence suggests that instead of working as individual units, many trans-membrane proteins function in unison as clusters [7]. These oligomers can be homomers or heteromers, and the functions of the protein constituents can be coupled [61], highlighting the role of protein crowding.

Moreover, trans-membrane proteins also require a suitable lipid environment to function, as highlighted by the raft concept [22]. Indeed, lipids can modulate protein function by either binding to specific binding sites or by membrane-mediated effects, *i.e.* by altering membrane properties [9, 75, 76]. The tightly-bound lipids are often resolved together with the protein structure and can reside either within the protein structure as non-annular lipids or at the protein surface as annular lipids [77]. Along with the raft concept, cholesterol is suggested to be one of the primary lipids involved in direct interactions with proteins such as G protein-coupled receptors [78].

While the importance of membrane proteins is unquestioned, it is also worth highlighting that their functions are regulated by oligomerization and lipid–protein interactions, and the lipid–protein interactions in turn are controlled by their partitioning behavior between distinct membrane environments. All these phenomena rely on two-dimensional search processes that are driven by lateral diffusion, discussed in Chapter 3.

2.2 Lipid Monolayers

In addition to taking the shape of a bilayer when immersed in solution, lipid molecules can also be deposited at an interface between a polar solvent — such as water — and air. In this case, the lipids form a single layer at the interface, called a monolayer. While a monolayer seems to be merely one half of a bilayer, their physical behavior and hence biological roles are very different.

One liquid–air interface in the human body is found at the surface of an eye, where a layer of polar lipids is covered by non-polar waxes [79]. In the lungs, the tiny alveoli are lined by a pulmonary surfactant monolayer consisting of lipids and surfactant proteins [80]. This monolayer, together with other lipid structures connected to it, allows for the rapid transfer of gases between inhaled air and the bloodstream and prevents the alveoli from collapsing during exhaling [80]. The surfactant lipids display complex phase behavior that couples to lipid–protein interactions [81]. Notably, in both of these examples, the rapid spreading of the layer to the air–liquid interface is crucial due to the non-equilibrium conditions resulting from blinking and breathing.

From a physical perspective, bilayers and monolayers are very different. Bilayers minimize their free energy by relaxing to a tensionless equilibrium packing density. Above the main transition temperature this state is liquid, and its lateral compression

or expansion takes a lot of energy. Monolayers, on the other hand, have no such equilibrium packing density. Instead, they spread indefinitely unless they are physically confined to a particular density. This packing is characterized by area per molecule (APL), and restricting a monolayer to high packing densities increases its surface pressure. The surface pressure is equal to the ability of the monolayer to reduce the surface tension of the air–liquid interface to which it is deposited. Monolayers are often characterized by APL–surface pressure isotherms. Upon compression, a monolayer shifts from a two-dimensional gas into a liquid-expanded (L_e) phase and further into a liquid-condensed (L_c) phase. The two liquid phases bear a resemblance to L_d and gel phases observed in lipid bilayers, respectively. Upon further compression to a high enough pressure, the monolayer collapses, *i.e* part of its constituents escape the interface and form other lipid structures — such as vesicles — on the liquid side of the monolayer. In equilibrium, this takes place at surface pressures of ∼45 mN/m [82], yet by rapid compression metastable states with much higher pressures can be obtained. Notably, in equilibrium between a monolayer at 45 mN/m and the vesicles in the liquid phase, the structures of the lipids in monolayers and bilayers are similar [83]. Despite the apparent limitations of a monolayer to describe the physics of lipid membranes, monolayers have been extensively used as model systems for the PM. This primarily stems from the fact that they are much easier to treat in experiments. Moreover, monolayers allow systematic studies of the effects of compression on the structure and dynamics of lipid membranes.

3. LATERAL DIFFUSION

In this Chapter, the central properties of both normal and anomalous diffusion are described. The models that are used to describe the normal diffusion of lipids and proteins along membranes, as well as the mechanisms that characterize anomalous diffusion are introduced. This Chapter is primarily based on the reviews by Ralf Metzler and co-workers [84, 85].

3.1 Normal Diffusion

The movement of particles down a concentration gradient is coined diffusion, and it is traditionally described by the laws of Fick derived more than 150 years ago [86]. His second equation,

$$\frac{\partial \Phi}{\partial t} = D\nabla^2\Phi, \tag{3.1}$$

shows that the change in particle concentration Φ in time t is directly proportional to the second spatial derivative of the concentration, and the coefficient of proportionality, D, is called the (collective) diffusion coefficient. Here, it is assumed that D is independent of concentration, which does not always hold true. In a more general case, the right-hand side of Eq. (3.1) gets replaced by $\nabla \cdot (D\nabla\Phi)$.

Interestingly, diffusion does not only describe motion down a concentration gradient. In 1827 botanist Robert Brown observed the constant jittery motion of particles ejected by pollen granules under a microscope [87]. By witnessing similar behavior of inorganic particles, he could discard the possibility that this movement stems from pollen's origin as a part of a living organism. However, it took decades until the efforts of Albert Einstein [88] and Marian Smoluchowski [89] revealed the true nature of this "Brownian" motion. They explained the seemingly random movements of the particles by their repeated collisions with small water molecules driven by thermal motion. Einstein arrived in an equation similar to Eq. (3.1) with concentrations

replaced by probabilities $P(r,t)$ of finding a particle at position r at time t. For a released particle in two-dimensional space relevant for membranes, this equation has a solution

$$P(r,t) = \frac{1}{4\pi Dt} \times \exp\left(-\frac{r^2}{4Dt}\right), \tag{3.2}$$

i.e. the probability distribution function (PDF) of particle distances from their origin r is Gaussian and spreads in time. The rate of this spreading is defined by D. The maximum of the PDF remains at $r = 0$ whereas its variance, the mean squared displacement (MSD), grows linearly in time as

$$\text{MSD} = \langle r^2(t)\rangle = \int_0^\infty r^2 P(r,t) 2\pi r \mathrm{d}r = 4Dt. \tag{3.3}$$

Notably, the constant in front of D scales as $2d$, where d is the dimension of motion. Considering the average diffusion length $l_D^2 = \langle r^2(t)\rangle$, a very intuitive picture of diffusion is provided by noting that a particle undergoing normal diffusion travels on average a lateral distance of $l_D = \sqrt{2dDt}$ over a time t.

It is worth noting that to obtain Eq. (3.2), no concentration gradient is required in terms of Fick's second law ((Eq. (3.1)). Instead, it describes the self-diffusion or tracer diffusion of a single particle. The MSD in Eq. (3.3) is called the ensemble-averaged MSD (EA-MSD), as the PDF generally describes the motion of a set of identical self-diffusing particles. Fig. 3.1C demonstrates the spreading of the Gaussian distributions over time and the corresponding linear growth of the EA-MSD.

In 1908, Paul Langevin considered that when undergoing Brownian motion, a diffusing pollen grain feels a stochastic force by collisions to the solvent particles. He applied this white Gaussian noise ξ with the autocorrelation

$$\langle \xi_\mathrm{f}(t)\xi_\mathrm{f}(t')\rangle = 2D\delta(t-t') \tag{3.4}$$

(with Dirac delta function δ) to the equation of motion and considered the overdamped case where inertial effects are insignificant. This resulted in the Langevin equation

$$\frac{\mathrm{d}\mathbf{r}}{\mathrm{d}t} = \xi, \tag{3.5}$$

from which he was able to extract Eq. (3.3). At this overdamped limit, Eq. (3.5) no longer necessarily describes the motion of a physical object, yet converges to the

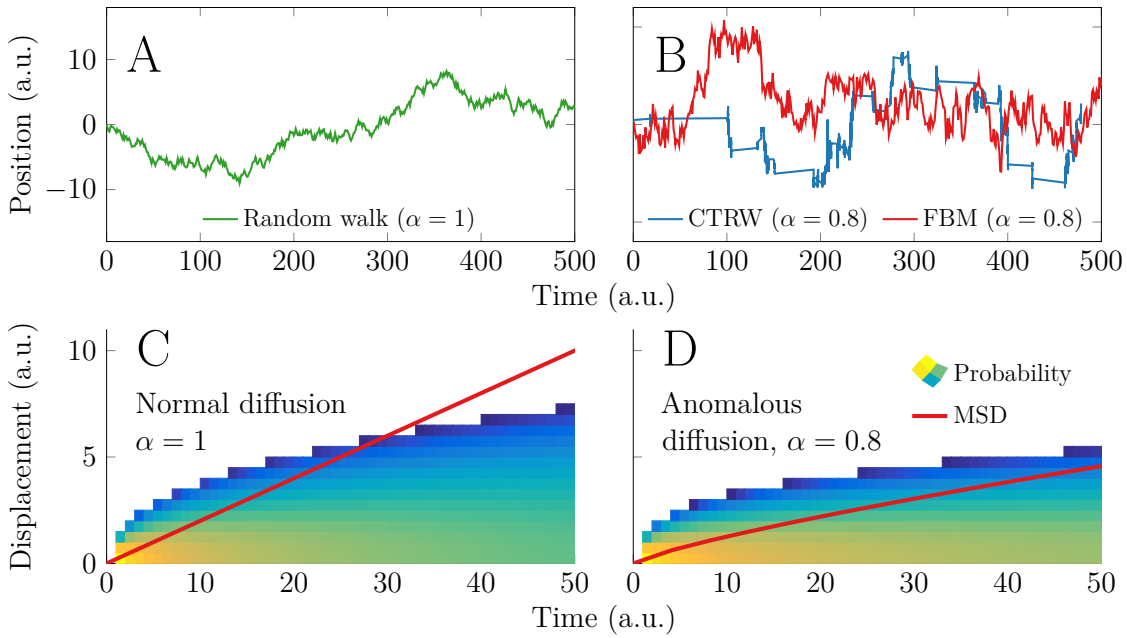

Figure 3.1 *Visualization of some key concepts related to diffusion. A) Sample trajectory of a 1-dimensional (1D) random walker modeling normal Brownian motion. B) Sample trajectories of 1D subdiffusive motion following the continuous time random walk (CTRW) and fractional Brownian motion (FBM) mechanisms. In both cases α is equal to 0.8. With such an exponent, FBM is essentially indistinguishable from regular Brownian motion in panel A. CTRW is recognized from its long waiting times. C) The probability distribution $P(r,t)$ is shown as a function of displacement r (only positive half plane is shown) and time t. For normal diffusion, this follows Eq.* (3.2)*. The red line shows the EA-MSD, Eq* (3.3)*. D) Same as panel C but for anomalous diffusion with $\alpha = 0.8$. Here, the distribution $P(r,t)$ follows Eq.* (3.17)*. This shape of $P(r,t)$ is characteristic for FBM, but not CTRW. The red line shows the EA-MSD that follows Eq.* (3.14)*, and applies to both FBM and CTRW.*

mathematical concept of a random walk.

In his seminal work, Einstein also derived an expression for the diffusion coefficient

$$D = \mu k_{\mathrm{B}} T, \tag{3.6}$$

where T is temperature, k_{B} the Boltzmann constant, and μ the mobility of the particle, *i.e.* the constant of proportionality between the particle's terminal velocity and a force applied to it. Experimental verification followed in 1909, when Jean Baptiste Perrin tracked the motion of colloidal particles, calculated their MSD, and extracted Avogadro's constant ($N_{\mathrm{A}} = R/k_{\mathrm{B}}$ with R the back-then known universal gas constant) from Eq. (3.6) [90].

3.1.1 Some Key Measurables

Next, a few fundamental concepts related to diffusion that are regularly encountered in the literature, including the remainder of this Thesis, are introduced.

Some experimental techniques track the motion of a single particle. Therefore, to obtain reasonable statistics, a single long measurement is performed over a time Θ, and the MSD is averaged over time and given as a function of lag time Δ. An MSD value at lag time Δ corresponds to the average MSD over all time intervals that have a length Δ present in the trajectory. This time-averaged (TA) MSD reads

$$\overline{\delta^2(\Delta)} = \frac{1}{\Theta - \Delta} \int_0^{\Theta-\Delta} \left[\mathbf{r}(t+\Delta) - \mathbf{r}(t)\right]^2 \mathrm{d}t, \tag{3.7}$$

and the integral is often discretized. In cases where many trajectories are measured, the TA-MSD can also be averaged over N different trajectories as

$$\langle\overline{\delta^2(\Delta)}\rangle = \frac{1}{N}\sum_{i=1}^{N} \overline{\delta_i^2(\Delta)} \tag{3.8}$$

to further improve the quality of the TA-MSD as an ensemble- and time-averaged MSD (EA-TA-MSD). Curiously, sometimes such a time average is not well-defined but depends on the duration of the measurement. This aging phenomenon is crucial for processes where waiting times are not bound, such as continuous time random walks discussed in Section 3.2.2.

Processes such as Brownian motion that fulfill $\langle r^2(\Delta)\rangle = \lim_{\Theta\to\infty} \overline{\delta^2(\Delta)}$ are called ergodic. However, it is relatively often observed in biological systems that the time and ensemble averages are not equal, and the system shows ergodicity breaking. This behavior can be characterized by the spread of TA-MSD curves, yet it is best captured in the ergodicity breaking parameter [91]

$$\mathrm{EB}(\Delta) = \langle\chi^2(\Delta)\rangle - \langle\chi(\Delta)\rangle^2 = \langle\chi^2(\Delta)\rangle - 1, \tag{3.9}$$

where

$$\chi(\Delta) = \frac{\overline{\delta^2(\Delta)}}{\langle\overline{\delta^2(\Delta)}\rangle}. \tag{3.10}$$

For ergodic processes, EB eventually converges to zero.

3.1.2 Free Area Model for Lipid Diffusion

Plenty of effort has been invested in developing models that predict diffusion coefficients based on other measurable quantities, as this would remove the need for carrying out often tedious and expensive measurements. The free volume and free area models describe diffusion as a process, where a particle diffuses by repeatedly jumping to an opening volume or area in its vicinity. The origin of such models lies in the free volume concept developed by Cohen and Turnbull to describe the three-dimensional diffusion in hard-sphere solutions [92]. Their purely geometrical reasoning was combined with the ideas of Eyring [93] by Macedo and Litovitz, who extended the model to include an energetic term [94]. Their equation reads

$$D \sim \exp\left[-\left(\frac{\Gamma v^*}{v_\mathrm{f}} + \frac{E_v^*}{RT}\right)\right], \tag{3.11}$$

where v^* is called critical volume, v_f is the available free volume, and Γ accounts for the overlap in this free volume. The activation energy in constant volume, *i.e.* the energy required for a diffusing particle to break free from its surroundings prior to jumping to another vacant site, is given by E_v^*, whereas R and T are the universal gas constant and temperature, respectively.

The free volume model evolved into a free area model as it was applied to planar lipid bilayers by several teams [95, 96, 97, 98]. However, the complete description was provided by Almeida *et al.* [10]. Their result replaces the critical area parameter Γa^* by the cross-sectional close-packed area of a diffusing lipid a_0 [95], and reads

$$D = 3.224 \times 10^{-5}\sqrt{\frac{Ta(T)}{M}}\exp\left[-\left(\frac{a_0}{a(T)-a_0} + \frac{E_\mathrm{a}}{RT}\right)\right]. \tag{3.12}$$

Here, $a(T)$ is the average area of a lipid at temperature T in units of Å^2, E_a is the activation energy, and M is the molar mass.

This model has been successfully employed to describe the temperature-dependence of lipid diffusion in protein-free model membranes [10]. Moreover, it links the decrease in diffusion coefficients due to the addition of cholesterol to the reduction in the free volume in the membrane [10] and fits the data measured for lipid monolayers [99].

The fundamental assumptions of the free area model are that 1) lipids are solid cylinders with a well-defined cross-sectional area, 2) the lipids move with discrete

and rapid jumps to a nearby pocket of approximately their own size, 3) these pockets open at a rate faster than the jumps occur, and 4) a jump only takes place if a lipid can break free from the interactions with its neighbors, *i.e.* overcome the activation energy barrier.

Some of these assumptions are clearly oversimplifications. The lipids are obviously not cylinders. Instead, their area varies drastically across the lipid leaflet [100]. Moreover, the link between the activation energy E_a and the similar Arrhenius activation energy concept remains unclear [101]. Computer simulations do not support the picture of discrete jumps, but instead suggest that lipids move as concerted flows of loosely-defined clusters along the membrane [11, 102]. Such flows have also been detected by experiments [103, 104].

3.1.3 The Saffman–Delbrück Model for Protein Diffusion

The well-known Stokes–Einstein relation is the application of Eq. (3.6) to spherical objects diffusing in three dimensions with a mobility of $\mu = (6\pi\eta R)^{-1}$. Here, η is the dynamic viscosity of the solvent and R the radius of the diffusing object. It would be tempting to derive a similar formulation for a two-dimensional system in which a disk, presenting a membrane protein, diffuses along a liquid sheet, presenting the membrane. Unfortunately, the infamous Stokes' paradox states that this problem does not have a steady-state solution.

Fortunately, this limitation can be overcome by applying some additional boundary conditions to the problem. In their seminal work, Philip Saffman and Max Delbrück studied three such cases, one of which considered a membrane being surrounded by a solvent with a non-zero viscosity [12, 13]. Also, they considered the cylindrical membrane proteins and the membrane to share a non-zero thickness. These assumptions led to the Saffman–Delbrück (SD) model [12, 13]

$$D_\mathrm{SD} = \frac{k_\mathrm{B}T}{4\pi\mu_\mathrm{m}h} \times \left[\ln\left(\frac{h\mu_\mathrm{m}}{\mu_\mathrm{f}R}\right) - \gamma\right], \tag{3.13}$$

where h is the thickness of the membrane, μ_m and μ_f are the viscosities of the membrane and the surrounding solvent, respectively, and γ is the Euler–Mascheroni constant equal to $\sim$0.577. The central difference to the Stokes–Einstein relation is the weak logarithmic size-dependence of the diffusion coefficients.

The applicability of the SD model is limited to objects smaller than the SD length $L_{\mathrm{SD}} = h\mu_{\mathrm{m}}/(2\mu_{\mathrm{f}})$. With a solvent such as water, the typical values of the SD length are ∼100 nm, which renders the model applicable to all membrane proteins. However, larger inclusions such as membrane domains require the use of an extension to the SD model by Hughes *et al.* [105] or its approximation [106], which find an asymptotic $D \sim 1/R$ dependence. Notably, the diffusion of lipids spanning only one leaflet is also poorly described by the SD model [107], even though some improvement is obtained by considering the contributions from interleaflet friction [108].

The SD model and its extensions have successfully described the diffusion of proteins in experiments [14, 109, 110, 111, 112] and simulations [113, 114, 115]. However, since lipids are known to diffuse together with the proteins [59], it remains unclear what the definition of the radius in the SD description is. Moreover, the parameters provided by SD model fits to experimental data might provide unphysical values [111]. Interestingly, some experiments report stronger dependence ($D \sim R^{-1}$ instead of $D \sim \ln R^{-1}$) of diffusion coefficients on protein size [116]. These observations have been associated with protein-induced deformations of the host membrane [117, 118], or explained by the limitations in the experimental setups [109].

3.2 Anomalous Diffusion

The normal Brownian diffusion only arises in case the motion is truly random, *i.e.* the particles move independently of each other and symmetrically along the studied dimension. Moreover, the displacements of the particle itself need to become independent at some time scale. Unfortunately, biological systems are rarely ideal, especially at all time scales.

Normal diffusion is characterized by a linear dependence between the EA-MSD and time (see Eq. (3.3)). Processes with directionality, coupling between diffusing particles, or memory effects often lead to anomalous diffusion, which instead displays

$$\langle r^2 \rangle \sim t^{\alpha}. \tag{3.14}$$

Here α is the diffusion exponent and characterizes the type of the motion. Anomalous superdiffusion ($1 < \alpha < 2$) and subdiffusion ($\alpha < 1$) are both present in biological systems [63, 84, 85, 119]. Superdiffusion does not contribute to membrane dynamics to a substantial degree, whereas subdiffusion is prevalent therein. Here α is often

time-dependent, and at the time regime with the strongest subdiffusion, it reaches values of ∼0.6–0.8 in fluid membranes [16, 120]. In the absence of confinement effects or binding events with divergent time scales (see Section 3.2.2 below), normal diffusion is usually eventually reached. In addition to long-time normal diffusion and anomalous diffusion present at intermediate times, the motion of membrane constituents over very short time intervals is ballistic, *i.e.* the molecules move at constant velocity ($\alpha = 2$) until they collide with their nearest neighbors.

Molecules undergoing subdiffusion cover a smaller area of the membrane in a fixed time as compared to normal diffusion, assuming equal values of the (effective) diffusion coefficient. This is highlighted in Fig. 3.1D, which demonstrates both the evolution of $P(r,t)$ over time and the connected sub-linear scaling of the EA-MSD. Moreover, in the anomalous regime, the diffusion coefficient gets replaced by an effective one, D^*, which has dimensions of length^2/time$^\alpha$. Importantly, the two parameters, D^* and α, describe two very different things. The former defines the rate of motion, whereas the latter represents the localization of this motion. Hence, it is possible for a molecule to rapidly sample a small region (large D^* and small α), or to explore larger regions with a slower pace (small D^* and large α). The heterogeneous structure and active processes present in the plasma membrane likely result in spatiotemporally varying values for these two parameters, thereby optimizing specific processes in certain environments and under certain conditions.

3.2.1 Fractional Brownian Motion

Anomalous subdiffusion can result from a multitude of mechanisms [84, 85]. Despite similar scaling of the EA-MSD with time, the mechanisms lead to distinct dynamics that uniquely manifest themselves in various physical observables.

Fractional Brownian motion (FBM), described by Mandelbrot and van Ness half a century ago [121], is a generalized case of Brownian motion whose subsequent steps are mutually correlated. Like regular Brownian motion, it is a continuous-time Gaussian process with a zero expectation value. Likely the most intuitive way to describe FBM is via the overdamped Langevin equation (compare to Eq. (3.5))

$$\frac{\mathrm{d}\mathbf{r}}{\mathrm{d}t} = \xi_\mathrm{f}(t), \tag{3.15}$$

where ξ_f is fractional Gaussian noise. Similar to Gaussian noise, it is normally distributed. However, it displays a power-law correlation with (compare to Eq. (3.4))

[84, 85]

$$\langle \xi_{\mathrm{f}}(t)\xi_{\mathrm{f}}(t')\rangle = \alpha(\alpha-1)D^* \left|t-t'\right|^{\alpha-2}. \tag{3.16}$$

This same noise also drives the related fractional Langevin equation (FLE) [122]. Since FLE and FBM are seldom carefully distinguished in the literature, it is worth pointing out their difference [123] here. FLE is a generalization of the Langevin equation and hence describes the motion of a physical particle and fulfills the fluctuation–dissipation theorem [122], whereas FBM is a generalization of the mathematical concept of Brownian motion. At short times, FLE leads to ballistic motion, whereas in the overdamped lipid it converges to FBM, just as at this limit the regular Langevin equation leads to Brownian motion. Hence, for subdiffusion in viscous membranes, FBM and FLE behave similarly and the terms are usually interchangeable.

For FBM, α describes the raggedness of the motion, and larger α values lead to smoother trajectories. We focus here on anomalous subdiffusion and note that with $\alpha < 1$, the motion is negatively correlated [84]. An example trajectory for FBM with $\alpha = 0.8$ is shown in Fig. 3.1B. Notably, depending on the value of α, FBM also describes normal diffusion and superdiffusion [84]. In anomalous diffusion, FBM leads to a sharper PDF (compare to Eq. (3.2) and see Fig. 3.1) [84]

$$P(r,t) = \frac{1}{4\pi D^* t^\alpha} \times \exp\left(-\frac{r^2}{4D^* t^\alpha}\right). \tag{3.17}$$

From the position autocorrelation function, it is evident that FBM is ergodic with the EA-MSD and EA-TA-MSD scaling as $\langle r^2(t)\rangle \sim t^\alpha$ and $\langle\overline{\delta^2(\Delta)}\rangle \sim \Delta^\alpha$, respectively [84]. Moreover, even the TA-MSD that is not averaged over many trajectories scales similarly ($\overline{\delta^2(\Delta)} \sim \Delta^\alpha$) with a sufficiently long trajectory.

The displacement (or discretized velocity) autocorrelation function,

$$C_{\delta t}(t) = \frac{1}{(\delta t)^2}\langle[\mathbf{r}(t+\delta t)-\mathbf{r}(t)]\cdot[\mathbf{r}(\delta t)-\mathbf{r}(0)]\rangle, \tag{3.18}$$

has a very characteristic and identical form for both FBM and overdamped FLE that — when normalized — reads [16, 124]

$$\frac{C_{\delta t}(t)}{C_{\delta t}(0)} = \frac{\left|t+\delta t\right|^\alpha - 2t^\alpha + \left|t-\delta t\right|^\alpha}{2\delta t^\alpha}. \tag{3.19}$$

The anti-persistent nature of the fractional Gaussian noise manifests itself in the displacement autocorrelation, which displays a negative correlation and hence a backflow of diffusing particles at intermediate times. This feature is characteristic of viscoelastic materials, such as lipid membranes [125]. FBM and FLE have been associated with many dynamic processes both in the cytosol as well as in membranes [16, 84].

3.2.2 Continuous Time Random Walks

Continuous time random walks (CTRWs) [126, 127] were also introduced half a century ago by Montroll, Scher, and Weiss. They are an extension of regular random walks, where steps are taken at fixed time intervals. In CTRW, in addition to the step sizes, the waiting time between consecutive steps is a random variable and independent of earlier steps. The distribution of steps is symmetric. When the mean waiting time and the mean squared step length are finite, normal ergodic Brownian motion is recovered. However, in case the waiting time distribution ϕ has a heavy tail in the form of

$$\phi(\tau) \sim \tau^{-1-\alpha}, \tag{3.20}$$

and the motion is subdiffusive with $\alpha < 1$, the expectation value of the waiting time τ,

$$\langle \tau \rangle = \int_{\tau_0}^{\infty} \tau' \phi(\tau') \mathrm{d}\tau', \tag{3.21}$$

diverges. Here τ_0 is some small value. The waiting times can be as long as the measurement meaning that subdiffusive CTRW motion displays aging. Indeed, the EA-TA-MSD scales as

$$\langle \overline{\delta^2(\Delta)} \rangle \sim D^* \frac{\Delta}{\Theta^{1-\alpha}}, \tag{3.22}$$

i.e. it has an explicit dependence on measurement time Θ [84]. Curiously, the properties of a system displaying aging also depend on the duration between the setting up of the system and the beginning of the measurement [128]. It is also noteworthy that the time-averaged MSD, Eq. (3.22), differs from the EA-MSD in Eq. (3.14). Hence, subdiffusive CTRW presents a non-ergodic process.

For subdiffusive CTRW, the displacement autocorrelation function, Eq. (3.18), reads

$$\frac{C_{\delta t}(t)}{C_{\delta t}(0)} = \begin{cases} 1 - (t/\delta t)^{\alpha}, & \text{if } t \leq \delta t \\ 0, & \text{if } t > \delta t, \end{cases} \tag{3.23}$$

i.e. the correlation is always non-negative for subdiffusion [124].

Natural causes for CTRW-like dynamics in biomembranes are persistent lipid–protein interactions, such as allosteric binding, protein–protein association, and trapping or confinement effects, which can lead to extended immobilization events. Indeed, CTRW-like diffusion has been observed in complex membranes [129, 130, 131].

3.2.3 Other Subdiffusion Models

A few other mechanisms leading to anomalous diffusion are also worth mentioning [85]. One such model is diffusion in a fractal [132], where a diffusing particle performs a random walk in labyrinth formed by, *e.g.*, confinement due to crowding or the interactions with the actin cytoskeleton. This labyrinth has dead ends at all length scales, and these can only be overcome by returning along the same route. Diffusion in a fractal has been reported for membrane proteins *in vivo* [129].

Non-ergodic subdiffusion can also arise from continuous Brownian motion if the diffusion coefficient varies spatially [133]. Such behavior has been observed in the membranes of living cells [134, 135].

Finally, processes that show non-Gaussian probability distributions of particle displacements (see Eq. (3.2)), yet linear scaling of MSD with time, have recently been under intensive research. Several models leading to such behavior have been suggested [136, 137], and they also likely play a role in the dynamics of crowded membranes [138].

Examples of all the discussed subdiffusion mechanisms are presented in Chapter 6.

3.3 Experimental Methods to Study Diffusion

In this Section, the main experimental techniques that are employed to extract diffusion coefficients of membrane lipids and proteins are reviewed. The resolutions

of all the considered methods — divided into three categories — are visualized in Fig. 3.2. To close the Section, the general limitations of experiments are discussed, and the justification for the use of computer simulations in studies of diffusion is provided.

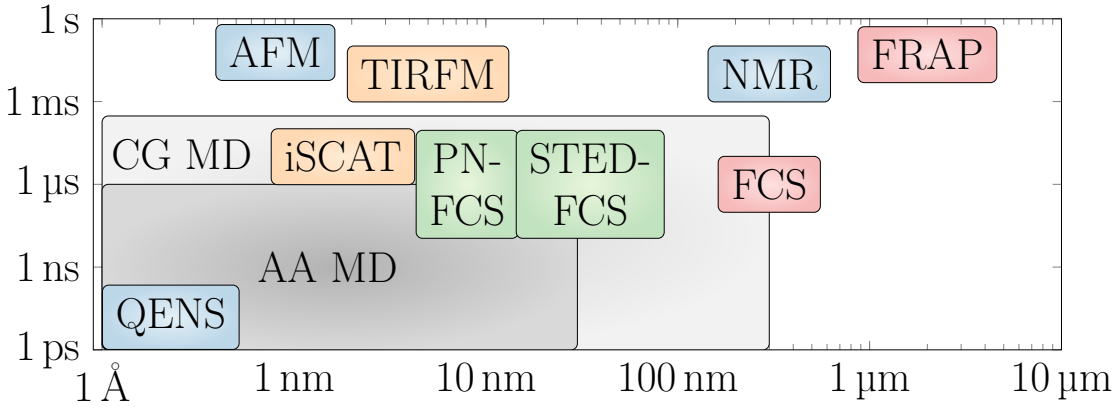

Figure 3.2 *Time and size scales at which the experimental techniques measure membrane dynamics. The fluorescence techniques probing ensemble dynamics — fluorescence recovery after photobleaching (FRAP) and fluorescence correlation spectroscopy (FCS) are shown in red. The super-resolution versions of FCS — based on plasmonic nanoantennas (PN) or stimulated emission depletion (STED) — are drawn in green. Super-resolution single-particle tracking methods — total internal reflection fluorescence microscopy (TIRFM) and interferometric scattering microscopy (iSCAT) — are shown in orange. All the methods mentioned above are applicable to both proteins and lipids, and — except for iSCAT — to both model membranes as well as the membranes of living cells, yet they require the use of labels. The other methods — atomic force microscopy (AFM), nuclear magnetic resonance (NMR), and quasi-elastic neutron scattering (QENS) — are shown in blue and free of such labels, but they are only applicable to certain molecule types in model membranes. The approximate scales covered by all-atom (AA) and coarse-grained (CG) molecular dynamics (MD) are shown in gray to highlight the overlap of their temporal and spatial resolution with some experimental techniques.*

3.3.1 Ensemble-Based Fluorescence Techniques Using Labels

Traditional fluorescence techniques are based on probing the collective motion of a set of fluorescent molecules to resolve the ensemble-averaged diffusion coefficients. Recent improvements in super-resolution microscopy have brought these old techniques back into the limelight.

Fluorescence Recovery After Photobleaching

In fluorescence recovery after photobleaching (FRAP) [139], a substantial fraction of the studied lipids or proteins is labeled with fluorophores resulting in laterally uniform fluorescence. The diffusion coefficients are extracted from a fit to the recovery of the fluorescence intensity after a micrometer-sized region is photobleached. This recovery, which usually takes tens of seconds, is due to the collective diffusion of fluorescent molecules back to the bleached area. The incomplete recovery also provides an estimate of the so-called immobile fraction of the labeled molecules.

The intensities are usually recorded every few dozen milliseconds, yet FRAP still essentially probes diffusion in a much longer timescale. Similarly, the spatial resolution of FRAP might seem poor at first. However, FRAP readily provides a collective diffusion coefficient in a single measurement that can be performed on lipids and proteins, and in model membranes as well as *in vivo* conditions [140]. Unfortunately, little effort has been invested in understanding anomalous transport with the aid of FRAP [141, 142], despite the existing theoretical framework [143].

Fluorescence Correlation Spectroscopy

In fluorescence correlation spectroscopy (FCS) [144], the number of fluorophores in the membrane is meager with preferably only one of them emitting under the illuminated spot at each moment. The diffusion coefficients are extracted from fits to the autocorrelation of the intensity data measured under this spot. The intensity fluctuations describe the motion of molecules across the spot of known area. With confocal microscopes, the illuminated and measured spot has a size of hundreds of nanometers. Interestingly, by repeating the measurement with varying spot sizes, FCS can resolve details of the underlying nanoscale membrane structure [145].

In an FCS measurement, the intensities can be recorded every microsecond, and the autocorrelation data are therefore typically fitted over multiple orders of magnitude in time, from microseconds to seconds [140], providing a long-time diffusion coefficient. FCS can be employed to study the motion of both proteins and lipids in model membranes and membranes *in vivo* [140]. The shape of the autocorrelation function distinguishes between different transport mechanisms, yet for anomalous diffusion a single anomalous exponent is assumed over the whole fitting interval [142].

Super-Resolution Techniques

The resolution of FCS can be improved by limiting the size of the illuminated spot. This is readily achieved with the stimulated emission depletion (STED) approach [146]. Here, one beam is used to illuminate a region of the sample, whereas another torus-shaped beam is used to deplete fluorescence at an area around the focal spot. Effectively, this reduces the diameter of the fluorescent spot down to a few dozen nanometers, an order of magnitude below the size achieved using confocal microscopy.

The STED-FCS method [147] can be applied to model membranes and live cells, and to study both lipids and proteins. With its small illuminated spot size, the intensity values are typically recorded every few microseconds [25]. By introducing pulsed excitation and time-gated detection into the STED methodology, its resolution can be further enhanced in FCS applications [148]. This can also be achieved by adapting fluorescence lifetime correlation spectroscopy (STED-FLCS) [27]. Moreover, scanning STED-FCS can provide spatiotemporal information of membrane dynamics with a similar resolution [149].

Another way to improve the resolution of FCS is to use planar plasmonic nanoantennas (PNs) that focus light to a region ∼10 nanometers wide [150]. In the PN-STED method, the intensities used to construct the autocorrelation curves can be sampled every few microseconds. This technique can be employed to study the dynamics of lipids and proteins in planar membranes — either model systems or deposited live cells [26, 151].

3.3.2 Single-Particle Tracking Techniques Using Labels

Single particle tracking (SPT) techniques are based on tracking a label — a fluorophore, a nanoparticle, or a quantum dot — attached to a diffusing entity such as a protein or a lipid [152]. Hence, SPT provides a trajectory of the label, which is assumed to resemble that of the labeled particle itself. The trajectories can be analyzed for information of the underlying diffusion mechanism. Traditional SPT techniques based on confocal microscopes do not usually provide adequate resolution for this. This caveat can, fortunately, be avoided by exploiting newly developed super-resolution techniques. Moreover, multiple-target tracking methods [153] can follow many labels simultaneously at an excellent resolution. SPT techniques are

generally applicable to both lipids and proteins and to live cells and model membranes [140].

Interferometric Scattering Optical Microscopy

In interferometric scattering (iSCAT) optical microscopy [154], the sample is illuminated, and the destructive interference of the light scattered from the tracked particle and the light reflected from the membrane-supporting interface provides information of the particle positions. The tracked particles can be even label-free proteins [155], but for measurements of diffusion in a membrane, the lipids or proteins need to be labeled by gold nanoparticles *via* linker molecules [156]. The iSCAT technique can obtain a spatial resolution down to a few nanometers and a temporal resolution of a couple dozen microseconds [157]. Furthermore, since no fluorescence is involved, a single measurement can last essentially forever, which provides detailed information on lipid dynamics and also covers the anomalous subdiffusive regime in protein-free model membranes [157]. However, the constant illumination increases the temperature of the sample locally near the nanoparticle, especially in case good temporal resolution is required. Currently, iSCAT has been applied to model membranes, yet live cell applications are under development [156].

Total Internal Reflection Fluorescence Microscopy

Alternatively, total internal reflection fluorescence microscopy (TIRFM) [158] can be exploited to improve the resolution of SPT. With TIRFM, the excitation of fluorophores is limited to a small region at the glass–water interface upon total internal reflection of the incident light. TIRFM-SPT is applicable to both lipids and proteins in live cells and in model membranes [129, 159]. When applied to protein diffusion in the membranes of living cells, TIRFM–SPT obtains a spatial resolution down to a few nanometers, and trajectories can be recorded every few dozen milliseconds [129].

3.3.3 Label-Free Methods

The methods described above are based on tracking labels attached to the studied particles. Such labels perturb the system, and often limit the measurements to short

time scales due to bleaching of the fluorescent labels. Therefore, label-free methods are desirable. The techniques described below all fall into this category, yet the downside is that they are only applicable to certain molecule types in a limited set of model systems.

Quasi-Elastic Neutron Scattering

In ensemble-based quasi-elastic neutron scattering (QENS) [160], lipid diffusion coefficients are extracted from the broadening of an elastic scattering peak of the neutrons upon their collision with the sample. This broadening corresponds to the relaxation times of structural fluctuations and hence to diffusion. Incoherent and coherent scattering techniques provide information of the movement of individual lipids and the collective motions in the membrane, respectively [161]. QENS can be used to study lipid motion in model membranes, where it attains a temporal resolution of dozens of picoseconds and a spatial resolution from Ångströms to a few nanometers [103, 104]. While it has not been applied to study anomalous diffusion, it can resolve between flow-like and jump-like motion of lipids [103, 104].

Nuclear Magnetic Resonance

Diffusion coefficient measurements using nuclear magnetic resonance (NMR) techniques are based either on the pulsed field gradient (PFG) or exchange spectroscopy (EXSY) techniques and can exploit many different NMR-detectable nuclei [162]. Both methods provide an ensemble-averaged diffusion coefficient. In stimulated echo PFG [163], the magnetization is dephased and rephased by a specific pulse sequence. For mobile particles, the refocus is not perfect, and its attenuation describes the movement, *i.e.* diffusion, of the studied molecules between the pulses. The PFG technique requires a well-defined orientation of a sample. The EXSY methods, on the other hand, are based on the anisotropy in certain measurable parameters [162]. This anisotropy can be exploited in spherical geometries such as vesicles [164], yet its validity depends on the accuracy of the estimate of the size of the used vesicles. Both NMR methods have only been applied to study lipid diffusion in model membranes. In general, diffusion studies by NMR are limited by the geometrical orientations of the studied molecules in the sample, the residual anisotropic interactions, and time frame at which measurements can be performed [162]. The resolution of a PFG

measurement depends on the time window between the pulses, and this "diffusion time" is usually of the order of a few dozen milliseconds [165]. Since the diffusion coefficient is extracted directly from the NMR spectra, there is no clear definition of a spatial resolution. In general, lipids move around 0.1–1 micrometers during the diffusion time.

Atomic Force Microscopy

In atomic force microscopy (AFM) [166], a nanoscopic tip at the end of a cantilever is dragged along the studied interface, and its motion due to the interactions with the surface is measured to create a topographic image. AFM is traditionally used to image biomembranes and other soft matter for structural purposes. However, by performing subsequent measurements, data on dynamics can also be extracted [167]. AFM images have a resolution of about one nanometer, and with high-speed AFM the images can be captured every few hundred milliseconds for up to minutes [168, 169]. With image processing, the trajectories of independent proteins can be resolved from these data, turning AFM essentially into an SPT technique with a multi-target tracking capability. Unfortunately, AFM is only applicable to molecules visible in the measured images, *i.e.* currently to membrane proteins in model membranes.

3.3.4 The Need for Computer Simulations

While the experimental techniques listed above provide a vast toolkit to probe the diffusion of membrane proteins and lipids in both model membranes and live cells, they all have their own limitations. First of all, the methods probe distinct temporal and spatial resolutions, and as shown in Fig. 3.2, they rarely excel on both fronts. The techniques with the best spatial resolution — AFM, QENS, and iSCAT — are currently only applicable to model membranes. Moreover, the methods that are able to resolve single particle trajectories do not usually provide very good temporal resolutions. Furthermore, many of the techniques require labels or tags that might perturb the dynamics of the labeled molecule or even the entire membrane. It is also unclear whether the motion of the labeled molecule is captured by the motion of the label, and even the lasers used to excite the probes can locally heat up the studied samples. However, label-free methods are much less flexible in terms of the studied sample. Finally, the experiments that do not track a single molecule are

based on some sort of a fit to the measured experimental data. The fitting functions are derived with some assumptions of the underlying diffusion process, which might not always hold — especially in the complex membranes of live cells [142].

Due to these limitations, there is growing demand for computational research on membrane dynamics. Molecular dynamics simulations readily provide a movie of the nanoscale events, including the trajectories of all molecules of the system allowing, *e.g.*, intuitive visualizations of lipid motion by flow patterns [170]. As highlighted in Fig. 3.2, coarse-grained molecular dynamics (CG MD) simulations can probe the dynamics of membranes with an edge length of a hundred nanometers for hundreds of microseconds, which already overlaps with the resolution of some experimental techniques. More detailed information can be extracted from all-atom molecular dynamics (AA MD) simulations that capture intricate interactions between the molecules. Both MD approaches can probe length scales down to the sub-nanometer level. Unfortunately, simulations are also error-prone, as discussed in detail in the Methods Section of this Thesis. Hopefully, with the spatial and temporal resolutions of experimental techniques rapidly improving and the probed time and size scales of computer simulations expanding, these two complementary approaches can soon be seamlessly combined to study the dynamics in biomembranes.

4. COMPUTATIONAL METHODS

In this Chapter, a brief overview of the molecular dynamics (MD) simulation method and the models used in biomembrane simulations is provided. All simulation models used in this Thesis are also introduced.

4.1 Simulation Models With Varying Levels of Detail

Computational research lays its foundation on some sort of a model, which is a mathematical description of the studied real-world object or phenomenon. Matter can be modeled at many levels of detail depending on the size and time scales relevant to the studied problem, as well as the required accuracy. Chemical reactions require the quantum-mechanical description of electrons, whereas macroscopic objects are very well modeled with empirical continuum models. Soft matter, such as biomembranes and monolayers modeled in this Thesis, is an extraordinary intermediate case: while structural rearrangements of molecules at the nanoscale define biological functions, these events do often not involve changes in chemical structure of matter, *i.e.* the electronic degrees of freedom remain unchanged. Moreover, at the temperature regime of interest, quantum effects are insignificant despite the atom-level description. Due to these particular features, biomembranes pose an ideal target for classical particle-based MD simulations.

4.1.1 Atomistic Models

In classical MD simulations employed in this Thesis, the models describe the properties of the involved particles and their mutual interactions. In atomistic models, each simulated particle describes an individual atom. Therefore, the parameters such as mass and charge reflect reality, and the parameters measured by, *e.g.*, spectroscopic methods are employed to describe interactions between atoms. Atomistic models used in biomolecular simulations are either all-atom (AA) models in which

explicit hydrogens are included, or united-atom (UA) models in which the non-polar hydrogens are merged into their host atoms [171].

Simulations of water-soluble proteins have traditionally been performed on AA models, while the biophysics of protein-free bilayers were studied using UA lipid models. However, with the growing interest towards membrane proteins, all major protein force fields can now be combined with their native all-atom lipid models. As examples of the models employed in the research presented in this Thesis, the OPLS-AA proteins [172] go together with an AA lipid model by Maciejewski *et al.* [173], and these proteins can also be combined [174] with the UA Berger lipid model [175].

Atomistic models are a natural choice to tackle many problems since they provide an accurate picture of physical interactions including hydrogen bonding and conformational entropy. A typical phospholipid contains 100–150 atoms, which is reduced to 50–100 in a UA scheme. The accuracy naturally comes with a high computational cost: the simulated membrane patches are usually relatively small, approximately 10×10 nm^2 in area, and contain 100–1000 lipids. Together with the explicit solvent and possible membrane proteins, this accumulates to a total of 50,000–1,000,000 particles. A typical AA simulation is performed for around a microsecond of simulation time [176].

Despite many atomistic force fields successfully reproducing the central properties of lipid bilayers [177] and lipid–protein interactions [178], they still struggle with some tasks. These include predicting the conformations of intrinsically disordered proteins [179], modeling the interactions at water–air interfaces and the monolayers adsorbed therein [180], and describing lipid head group conformations and their interactions with ions [181, 182]. Fortunately, these limitations are not expected to compromise the research presented in this Thesis.

4.1.2 Coarse-grained Models

Computing power has seen a steady increase during the last decade along with improvements in software optimization [183, 184]. Still, the size and length scales reached by atomistic simulations are inadequate to study large-scale structural reorganization in membranes, let alone reliably capture the dynamics of such processes. Fortunately, the specific interactions are often meaningless in such applications,

dealing with, *e.g.*, membrane elasticity, large-scale diffusion, and phase behavior. Coarse-grained (CG) models provide an efficient way to sample extended time and size scales without completely compromising chemical specificity. These models are based on quasi-particles — or "beads" — each of which describes the interactions of multiple heavy (non-hydrogen) atoms [185, 186]. Such averaging reduces the number of simulated particles by around ten-fold and hence decreases the number of degrees of freedom substantially [185, 186]. Moreover, coarse-graining also results in a smoother energy landscape, which speeds up the dynamics of the system [187]. These features of coarse-graining allow for the increase in the simulation timescale to hundreds of microseconds [188, 189], and the simulated membranes commonly have areas of up $\sim$100$\times$100 nm^2 [188].

The Martini CG model [190] and its derivatives [191, 192] have become a method of choice for CG biomolecular simulations thanks to its extensive selection of molecule types, including various kinds of lipids [186, 187] and proteins [193, 194]. Furthermore, the model is accompanied by a wide selection of tools [195] that make its adaptation straightforward. Martini is mainly based on a four-to-one mapping, in which on average four heavy atoms are described by one bead. The number of bead types is relatively limited, yet large enough to capture adequate chemical specificity. Martini is mainly parametrized based on partitioning free energies between oil and water [190], and it can be simulated with and without an explicit solvent [196].

CG models undoubtedly suffer from their own issues too. The reduction in the degrees of freedom means that part of the entropy is captured in energetic interactions, which can lead to these two being incorrectly balanced [185]. Moreover, the applicability of coarse-grained models to different temperatures, and the transferability of the models can also be compromised due to this simplification [185]. The speed-up in the dynamics due to the smoothened energy landscape also leads to issues. The factor of this increase differs from system to system, and hence the relation between simulation time and real time becomes ill-defined. Furthermore, the Martini model suffers from two particular issues — the overbinding of both water-soluble and membrane proteins [197, 198], and the poor representation of the surface tension of water [187].

In this Thesis, we apply the Martini model and its derivatives to study membrane dynamics. Importantly, in all this work, Martini is considered at a temperature that is close to the one where it was parameterized. Moreover, we focus on dynamics where the energy–entropy balance is likely not crucial, and we study trends that are not affected by the ill-defined description of simulation time. We use models that are

parameterized to work together [187, 193, 194]. Our systems do not involve interfaces, yet they are likely affected by excessive protein–protein interactions. However, we partially corrected this issue for Publication IV, as discussed in Section 5.1.2 and in Publication II.

4.1.3 Multi-scale Modelling

Many biological processes cannot be comprehensively described solely by AA or CG models. As an example, the large-scale arrangement of a protein complex can be efficiently sampled using a CG model, while the details of the protein–lipid interactions around this complex can only be accessed using an AA approach. Fortunately, recent tools allow for straightforward transformations between different resolutions. As examples, the `martinize` tool readily converts AA protein models to CG ones in the Martini scheme to be readily embedded into a membrane with the `insane` tool [195], whereas the `backward` tool [199] fine-grains CG models back to an AA resolution.

4.2 The Molecular Dynamics Method

In an MD simulation, the particles move along the trajectories defined by their mutual interactions [200, 201]. Notably, unlike some alternative methods, MD provides both structural and dynamic information on the studied system. Below, some central aspects of the MD method are discussed.

4.2.1 Simulation Workflow

Running an MD simulation requires three things. First, the simulation begins with an initial configuration of molecules, where no forces are excessive, and that is reasonably close to its equilibrium configuration. The forces for the initial conformation can be minimized using general optimization algorithms. Still, the relaxation to equilibrium from a poorly chosen initial state can be sluggish. Second, the descriptions of the properties of all involved particles and their mutual interactions — captured in the force field described below — needs to be provided. The third crucial piece is the set of simulation parameters that define the conditions under which the simulation is performed.

In classical MD simulations, the dynamics of the system is modeled by integrating Newton's second equation of motion, $\mathbf{a} = \mathbf{F}/m$, numerically for each simulated particle. The integration is repeatedly performed at discrete time steps. Here, due to the additive nature of classical non-polarizable force fields, the total force $\mathbf{F}$ is the sum of all forces acting on the particle with a mass m. The acceleration $\mathbf{a}$ provides the change of velocity over time, and the velocity further describes the evolution of particle position over time. There are many algorithms with different features that execute this integration [202]. For stability, the integration is performed with a tiny time step. Still, as the number of simulation steps is large, the small displacements lead to large-scale movements of the simulated particles. It is noteworthy that in some contexts MD is considered to cover a plethora of methods based on numerical integration of the equation of motion, such as dissipative particle dynamics and Langevin dynamics. However, in this Thesis, MD refers to the classical method where all forces are described by the force field, and no additional random or dissipative forces are considered. Still, depending on the choice of resolution and simulation parameters, very different conditions can be described.

4.2.2 Force Field

A fundamental concept in MD simulations is the force field, which maps particle coordinates to forces between them. In classical non-polarizable MD, the Born–Oppenheimer approximation allows the simulation to track only the positions of the atomic nuclei, to which the spherically symmetric interactions are assigned. Notably, in the non-polarizable force fields used in this Thesis, all forces are additive, and no many-body non-bonded interactions are considered.

The force field consists of two parts: the formulas that describe relevant physical interactions and a set of particle-specific interaction parameters. These parameters are derived from experiments, quantum-chemical calculations, or empirically. While the various force fields employed to study soft matter differ to some degree — especially in the way the empirical parameters are obtained — the same five interaction terms are commonly considered [171].

The three bonded terms describe bond-stretching between two particles, angle-bending among three particles, and dihedral-twisting among four particles. The first two interactions are commonly presented by harmonic potentials with their reference values and force constants derived from experiments. Proper dihedrals

describe rotation around a bond and are often described by a sum of cosines of the twisting angle. The parameters for proper dihedrals are derived from fits to quantum-chemical calculations. Improper dihedrals, on the other hand, are used to maintain the planarity of four-atom groups, the chirality of stereospecific centers, or in some cases the desired *cis–trans* isomerism around a double bond. Improper dihedrals are usually described using a harmonic potential.

The two non-bonded terms contain Lennard-Jones (LJ) interactions — capturing both steric repulsion and van der Waals dispersion at short and intermediate inter-particle distances, respectively — and long-range electrostatic interactions described by Coulomb's law. Parameters for the former are often fit to reproduce some experimental observables such as density and heat of vaporization [173]. The partial charges, describing the distribution of charge within a molecule, are usually derived by reproducing an electrostatic potential surface obtained from quantum-chemical calculations by an optimized set of partial point charges [173].

4.2.3 Simulation Engine

The numerical integration is performed by a simulation engine. Many such pieces of software are available either *via* a license, free of charge, or some even as open source software. However, the various engines differ drastically in the functionality they provide, as well as their compatibility with force fields, file types, and analysis software. Still, perhaps the most crucial factor is the speed at which the software performs the integration and other related computations.

In this Thesis, the GROMACS package [184] is exclusively employed for a variety of reasons. First of all, it is very fast with good parallelization and GPU support [183]. Second, it supports various atomistic and coarse-grained force fields, such as Martini [187, 193], Berger [175], and OPLS-AA [172, 173], all employed in this Thesis. Third, it provides a great deal of built-in analysis tools that can be extended by, *e.g.*, Visual Molecular Dynamics (VMD) software [203] or the MDAnalysis Python library [204], both of which are compatible with GROMACS output formats. Fourth, GROMACS provides plenty of methods for free energy calculations and enhanced sampling techniques that can be complemented by the PLUMED package [205]. Fifth and finally, it is a public domain software with the source code readily available for modifications, and all possible issues such as bugs are openly discussed to ensure their rapid elimination.

4.2.4 Standard Simulation Settings

In this Section, a few common features of MD simulations that are regularly employed to enhance the quality or speed of the computation are presented.

Simulation Ensembles

Without any additional modifications, and assuming that the integrator and the time step are well chosen to preserve energy, the system reproduces the microcanonical ensemble, where the number of particles, the volume of the system, and the total energy remain constant over time. Unfortunately, this does not correspond to the setups used in experiments. Therefore, thermostat and barostat algorithms are employed to keep the temperature and the pressure of the system constant, thus reproducing the canonical (constant temperature and volume) or the isothermal–isobaric (constant temperature and pressure) ensembles. These are natural choices for systems with interfaces — such as lipid monolayers deposited at the air–water interface — and for continuous fluid systems — such as lipid bilayers — respectively.

Handling of Non-Bonded Interactions

An MD engine uses plenty of optimizations, each with its imperfections. Long-range non-bonded interactions are costly to calculate between all particles. Therefore, LJ interactions are usually cut off at around 1 nm distance, meaning that all interactions between particles beyond this distance are omitted. Such cut-offs lead to the loss of some potential energy [206], yet as this scheme is used throughout the force field parametrization, the missing interactions are likely accounted for by the empirical LJ interaction parameters, and partially by approximate dispersion corrections [206].

Electrostatic interactions are usually somewhat stronger than LJ ones. The Coulomb's law is directly employed to find forces between particles within approximately 1 nm distance. Additionally, long-range electrostatic interactions are often included by interpolating the charges in a grid and calculating the forces in the Fourier space. The commonly employed Particle Mesh Ewald [207] and its smooth variant [208] perform this calculation at a rapid rate, yet might lead to the loss of momentum conservation. For efficiency, such long-range electrostatics are generally not considered with CG models [186].

The use of cut-offs speeds up the calculation drastically, yet finding the particles within the cut-off radius is also a demanding task. This neighbor search is speeded up by the use of neighbor lists that are not updated at every time step. Traditional group-based lists lead to lousy energy conservation due to the exchange of particles within the cut-off length between the updates. Modern buffered neighbor lists solve this issue without significant hits on simulation performance [209].

Combination Rules

In the optimal situation, the parameters describing LJ interactions between all pairs of particle types are derived exclusively. However, this is rarely feasible, and instead, each particle type is assigned with its own pair of LJ parameters. Then, for each combination of these particle types, the respective interaction parameters are calculated using combination rules, which essentially corresponds to taking a geometric or an arithmetic average of the parameters of the two interacting particles. This drastically simplifies force field development, yet often leads to poor accuracy [210]. The Martini model employs an interaction matrix with fixed interaction levels instead of combination rules [187].

Periodic Boundary Conditions

MD simulations can only treat fairly small systems, yet by using periodic boundary conditions (PBCs) the simulation box or the "unit cell" can be replicated to effectively describe an infinite system consisting of copies or "images" of the unit cell. In this setup, a particle exiting the simulation box from one side reappears on the other side, removing the need to use walls at the edge of the simulation box. This is a natural choice for lipid bilayers that are essentially planar at the size of the current simulations, and hence with PBCs they form a continuous bilayer across the box edges. With the minimum image convention, a particle only interacts with the closest images of other particles. PBCs introduce translational symmetry and hence ensure the conservation of total momentum. Although the system is effectively infinite, the length scales of processes, such as correlations of lipid motion or undulations of the bilayer, are still limited by the size of the simulation box.

4.2.5 Possible Pitfalls

The workflow of an MD simulation seems somewhat intuitive and straightforward compared to many other simulation methods. However, the MD approach is internally flawed. On the one hand, long simulations are pursued to sample the whole phase space in order to extract reliable averages of the physical observables. On the other hand, numerical errors accumulate throughout the simulation indicating that its quality actually decreases over time. Hence, being aware of and in control of these errors is of utmost importance.

Recently, the rapid development of user-friendly tools and increase in computing power have brought MD simulation within the reach of almost everyone. MD engines are freely available and easy to install. Databases now provide simulation-ready protein structures [211, 212], or such systems can be readily constructed for atomistic or coarse-grained schemes and different simulation engines using web portals [213, 214, 215] or standalone tools [195]. Moreover, analysis software is improving rapidly, which removes the requirement of programming skills [216].

This development is desirable to attract more people into the MD community, yet it also poses the risk that MD becomes a black box in the hands of inexperienced users. The force fields are built on years of intense development, yet they are susceptible to even small changes in simulation parameters. Available algorithms, their mutual compatibility, or even details of their implementation vary between MD engines. Therefore, the models, tools, and results should always be double checked against earlier results and verified by experiments and proper control simulations.

Unfortunately, even if everything is done correctly by the book, the software still contains bugs, and the force fields might fail in certain setups. Fortunately, the MD community drives active development and self-evaluation in both of these fields [171, 178, 181, 182, 186]. More of the issues and suggestions related to MD are highlighted in the recent reviews by us [216] and others [217].

4.3 Overview of the Simulation Models Used in This Thesis

In this Section, the models used in this Thesis are described. The simulation parameters are omitted, since they are described in detail in the original publications.

Publication I

In Publication I, we introduced a method for embedding proteins into lipid membranes by applying lateral pressure to a system, where the protein was placed next to a pre-existing lipid bilayer. The validity of this method was demonstrated by inserting an adenosine A_{2A} receptor into a palmitoyloleoylphosphatidylcholine (POPC) lipid bilayer using both OPLS-AA [172, 173] and CG Martini schemes [187, 193, 194]. Snapshots of the initial AA and CG setups before applying the pressure are shown in Figs. 4.1A and 4.1B, respectively. These figures, as well as all snapshots presented in this Section, are rendered with `tachyon` ray tracer using VMD [203].

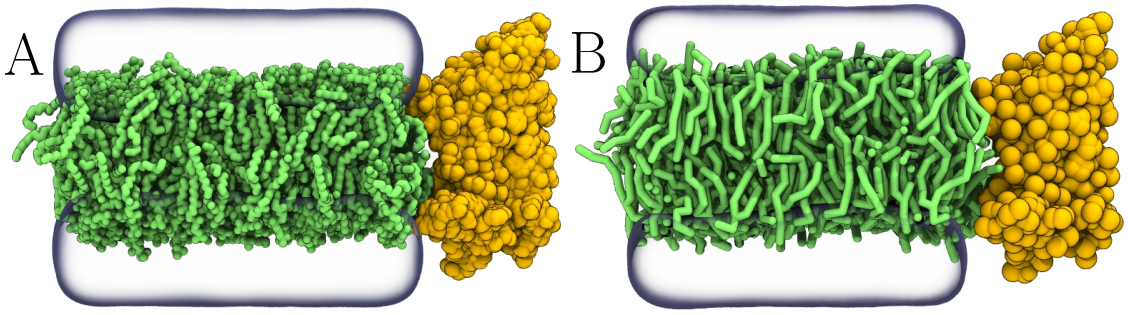

Figure 4.1 *Simulation models employed in Publication I. The initial configurations before the insertion of the protein. Here, the adenosine A_{2A} receptor (yellow) is to be embedded to a POPC (green) membrane. A) AA system with hydrogens in the lipid structures omitted for clarity. B) The corresponding CG system. In both panels, water is shown as a transparent surface and ions are not shown.*

Publication II

In Publication II, we evaluated the ability of the Martini model [187, 193, 194] to capture the experimental dimerization free energies of selected trans-membrane peptides. These values were used to assess the level of protein–protein interactions in the model. To this end, we performed umbrella sampling simulations on two trans-membrane domain dimers, EphA1 and ErbB1, exploiting the dimer structures that had been resolved by NMR [218, 219]. In the umbrella sampling technique, we can restrain the inter-peptide distance — our reaction coordinate — using a bias potential to remain around a certain value despite possible high energy barriers. Combining multiple such simulations along the reaction coordinate provides a biased probability distribution, which can be unbiased to obtain the potential mean force

that approximates the free energy profile of the dimerization process. Moreover, the corresponding experimental dimerization free energies for the studied domains had been obtained using Förster resonance energy transfer (FRET) experiments [220, 221]. We mimicked the experimental conditions and embedded the dimer structures into dilinoleoylphosphatidylcholine (DLPC) bilayers. The ion concentrations were also adjusted to follow the experimental setups used in FRET studies. A snapshot of the membrane with an embedded EphA1 dimer is shown in Fig. 4.2A.

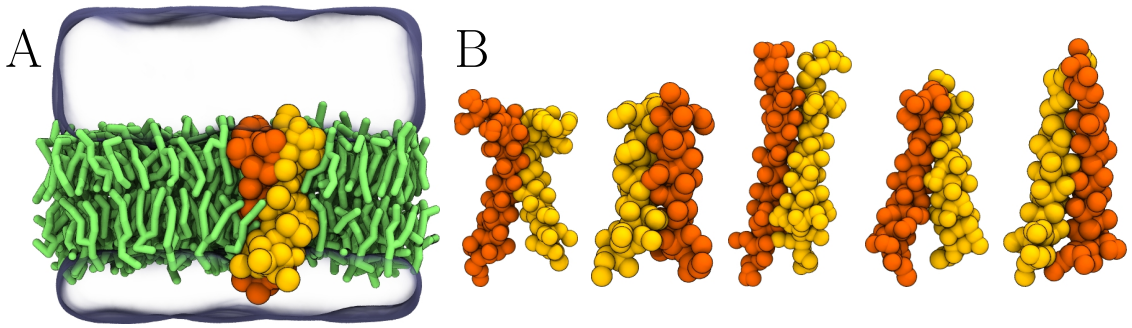

Figure 4.2 *Simulation models employed in Publication II. A) A snapshot of a DLPC membrane (green) with an embedded EphA1 dimer (peptide monomers shown in yellow and orange) in CG scheme. Water is shown as a transparent surface and ions are omitted. This setup is employed in umbrella sampling simulations used to evaluate the dimerization free energy of the peptides. A similar configuration was also used for the ErbB1 dimer. B) CG structures of the five dimers employed in the spontaneous dimerization simulations. These peptides were embedded in a membrane similar to that shown in panel A. The structures from left to right correspond to PDB identifiers: 1AFO, 2HAC, 2K9J, 2KA1, and 2L34.*

Additionally, we analyzed the structures of spontaneously forming dimers of transmembrane peptides and compared them to the corresponding structures resolved by NMR. The CG NMR structures of these peptides are shown in Fig. 4.2B. More information is available in the original publication [198].

Publication III

In Publication III, we evaluated the validity of the free area model to describe diffusion in lipid monolayers. To this end, we simulated protein-free pulmonary surfactant monolayers composed of 60 mol% dipalmitoylphosphatidylcholine (DPPC), 20 mol% palmitoyloleoylphosphatidylcholine (POPC), 10 mol% palmitoyloleoylphosphatidylglycerol (POPG), and 10 mol% cholesterol, mimicking the lipid composition of the native surfactant [80]. Two monolayers, each containing a total of 100 lipids, were

separated by a slab of water. Additionally, 150 mM of NaCl, together with counter ions for POPG, was included. Different monolayer compression states, with mean areas per lipid (APL) in the range 44–68 Å^2 were simulated at 310 K. Snapshots of the most compressed and the most expanded monolayers are shown in Figs. 4.3A and 4.3B, respectively.

The lipids were modeled in the UA scheme with phospholipid parameters adapted from the Berger description [175]. For cholesterol, the parameters of Höltje *et al.* were used [222]. Water was described with the TIP3P potential [223], and ions with the GROMOS-derived "ffgmx" parameters. Full details of the simulation models and simulation protocol can be found in the original publication [224].

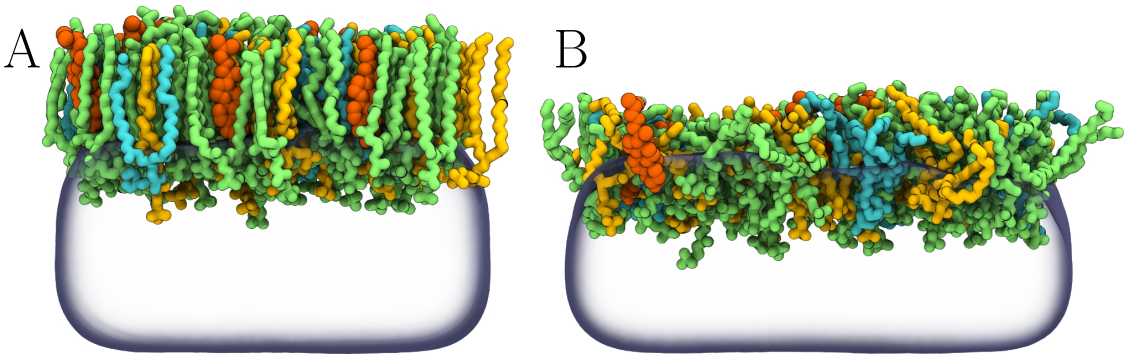

Figure 4.3 *Examples of simulation systems used in Publications III and V. Lipid monolayer models with APL equal to A) 44 Å^2 (L_c phase) and B) 68 Å^2 (L_e phase). DPPC is shown in green, POPC in yellow, POPG in blue, and cholesterol in orange. Water is shown as a transparent surface, and the ions are omitted for clarity. Due to the use of PBCs, each simulated system contains two monolayers.*

Publication IV

In Publication IV, we put the Saffman–Delbrück model to the test in membranes with different levels of trans-membrane protein crowding. To this end, we simulated lipid bilayers with an increasing number of proteins in the CG scheme. Equal amounts of the seven membrane proteins with different radii and minimal extramembrane domains, shown in Fig. 4.4A, were included in the systems. Complete proteins were either taken from the RCSB Protein Data Bank [225] or the OPM database [211], whereas structures of the proteins with missing atoms were completed by MODELLER [226].

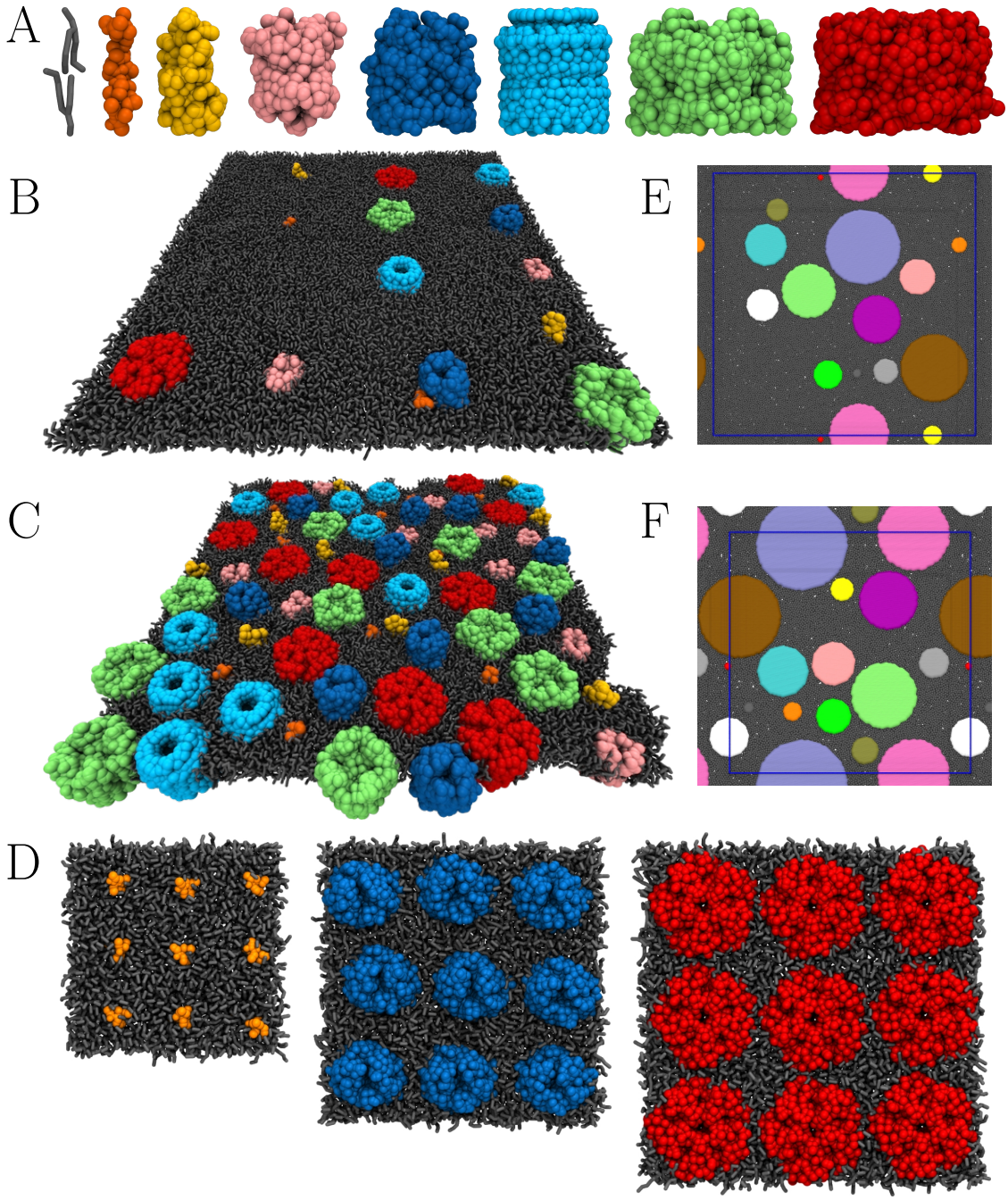

Figure 4.4 *Simulated systems in Publication IV. A) CG structures of a DPPC lipid and the seven proteins with increasing radii. B) A CG membrane with dilute ($LP = 400$) concentration of a polydisperse set of proteins. There are two copies of each of the seven proteins, respectively, and they — as well as the lipids — are colored as in A. Water beads and ions are omitted for clarity. E) A dilute (1000 free particles per disk) 2DLJ system. The 15 inclusions of different size are shown in different colors, while the individual particles are shown in gray. Systems E and F are not drawn to scale. C & F) Crowded ($LP = 50$) membrane with ten copies of each of the proteins (C), and the corresponding 2D system (Panel F, 400 free particles per disk). D) Examples of the systems with crowded ($LP = 50$) concentration of a monodisperse set of proteins. A similar system was considered for each studied protein. Coloring again follows that of Panel A. Snapshots adapted with permission from Ref. 188, Copyright 2017 American Chemical Society.*

Having all protein types in the membrane in these polydisperse systems ensures that they experience on average the same membrane environment. The leaflet-wise lipid-to-protein (LP) ratios of 50 (highly crowded), 75, 100, 200, and 400 (dilute) were considered, and the systems with two LP ratios are shown in Figs. 4.4B and 4.4C. In addition to the proteins, the membranes contained ∼10000 DPPC lipids, and had a size of ∼60×60 nm^2. The solvent composed of water and antifreeze beads, as well as 150 mM of NaCl together with counterions. All in all, the simulated systems contained a total of ∼300,000 Martini beads each.

In addition to the systems where all protein types were present, each protein was also simulated independently in a DPPC bilayer to evaluate its effective radius. Finally, we also simulated monodisperse systems, one for each protein type. These systems contained nine copies of the protein embedded in a crowded (LP = 50) DPPC bilayer. The purpose of these simulations was to provide additional support for the findings of the polydisperse systems under crowded conditions. Snapshots of three such systems are shown in Fig. 4.4D. For these two extra sets of simulations, we also considered two other proteins — not present in the polydisperse systems — to increase the reliability of our results.

The Martini model was used to describe the lipids [187] and the proteins [193, 194]. The elastic network [227] was applied to the proteins, and the protein–protein interactions were slightly reduced to prevent irreversible and excessive protein aggregation [198] (see also Publication II). The undulations of the membrane were suppressed by applying a soft restraint to the phosphate beads in the direction normal to the membrane plane. This substantially reduced the number of required solvent particles, and hence speeded up the calculation.

Additionally, we complemented these simulations by two-dimensional (2D) simulations of atoms, whose interactions were described by the LJ potential. To model protein crowding in a bilayer in the most minimalistic model, we included 15 mobile disks of different radii into the system together with 4500 to 15000 free atoms. Hence, there were 300–1000 free atoms per disk, providing a very similar area coverage as the Martini systems described above. Examples of dilute and crowded 2DLJ systems are shown in Figs. 4.4E and 4.4F, respectively. For more details on all the models and simulation parameters, see the original publication [188].

Publication V

In Publication V, we studied the effect of protein crowding on the nature of normal and anomalous diffusion. To this end, we simulated lipid membranes with various concentrations of the Na^+ complex of the NaK channel (PDB id: 2AHY) in the CG scheme. The systems had LPs equal to 50, 75, 100, 150, or 200, corresponding to an area coverage between 11 % and 34 %. The number of protein copies was varied between 4 and 16 so that in every case the bilayer edge was 23–32 nm long. Additionally, very dilute conditions were simulated by embedding a single protein in a membrane formed by ∼2000 lipids (LP = INF). Importantly, the membrane consisted of either DPPC or DLPC. These two lipids form bilayers with different thicknesses, and DPPC drives the aggregation of the NaK channel proteins due to hydrophobic mismatch. We refer to weakly-aggregating and strongly-aggregating systems as "WA" and "SA", respectively. The membranes were solvated by water. Snapshots of the weakly-aggregating and strongly-aggregating systems with LP = 50 are shown in Figs. 4.5A and 4.5B, respectively. Additionally, a snapshot of the SA LP = INF system is shown in Fig. 4.5C. The lipids were described using the Martini model [187], while the Martini-based Bondini model [192] was used for proteins.

We also studied lipid diffusion in lipid monolayers at different APLs. To this end, we employed the simulations of protein-free pulmonary surfactant monolayer models used already in Publication III (see details above). Further information on all models and the simulations is found in the original publication [120].

Publication VI

In Publication VI, we looked in more detail into the nature of subdiffusion of lipids and proteins in protein-crowded membranes. To this end, we employed the LP = 50 and LP = INF membranes from Publication V, shown in Figs. 4.5A–4.5C. Moreover, we considered both weakly-aggregating and strongly-aggregating membranes to resolve the role of aggregation-induced confinement. While the model systems were equal to those in Publication V, the simulations were significantly extended to provide better statistics on protein dynamics.

Additionally, we set up 2DLJ systems where free particles diffused among immobile obstacles. We modeled conditions where the obstacles were arranged to result in

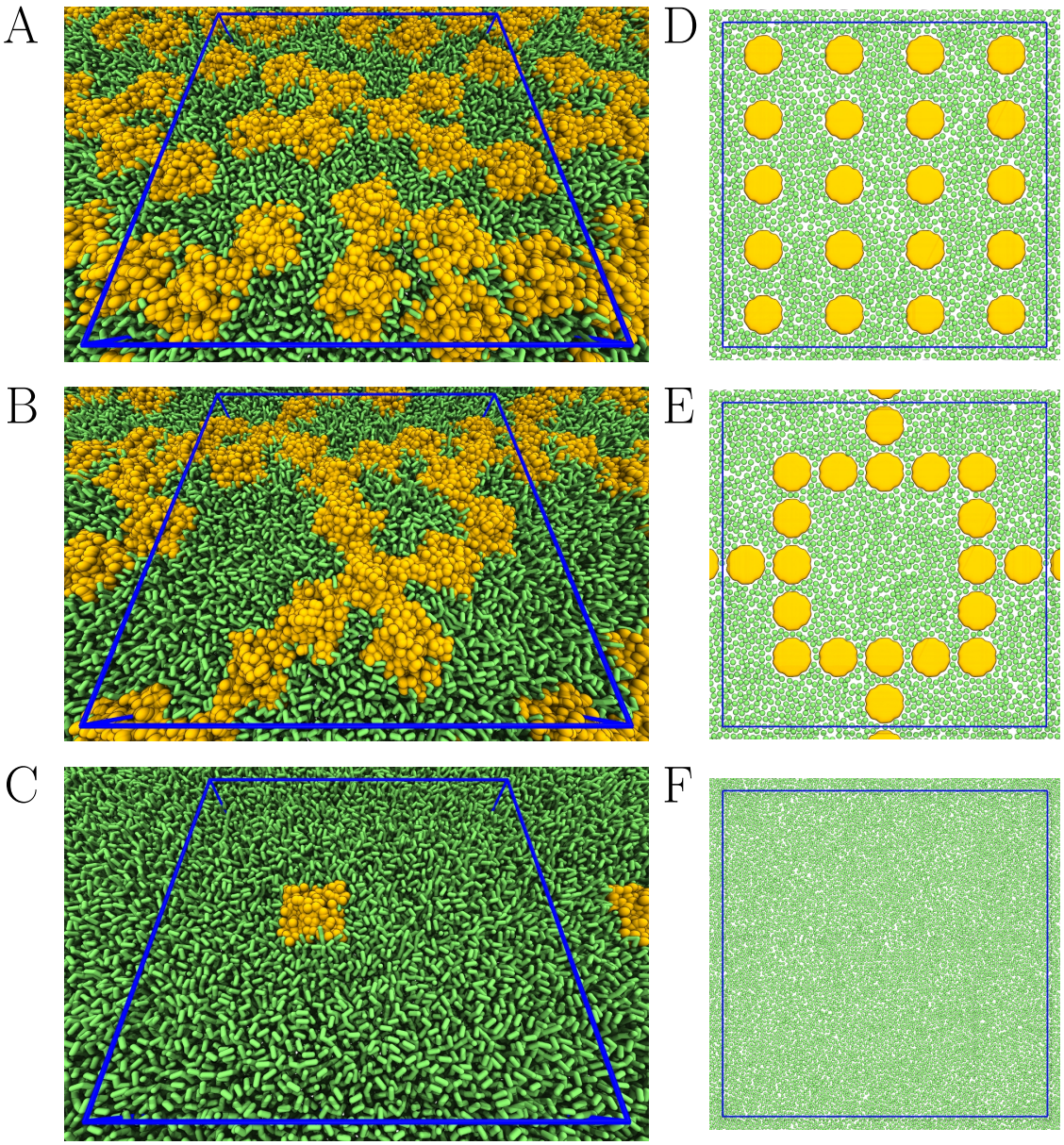

Figure 4.5 *Examples of simulation systems used in Publications V and VI. A) A crowded weakly-aggregating membrane with LP = 50 in the CG scheme. The proteins are shown in yellow and DLPC in green. Water beads and ions are omitted for clarity. The blue lines indicate the simulation box. D) 2DLJ-WC system with free particles shown in green and immobile obstacles in yellow. B & E) Same as A & D but with the strongly-aggregating membrane consisting of DPPC lipids, corresponding to the 2DLJ-SC system. C & F) DPPC membrane with LP = INF, and the corresponding 2DLJ-FREE system.*

either weak ("WC") or strong confinement ("SC") effects, corresponding to the weakly-aggregating and strongly-aggregating CG systems. Snapshots of these systems are

shown in Figs. 4.5D and 4.5E, respectively. Additionally, we considered a system without any obstacles ("FREE") as a simple model for a membrane with no proteins, a snapshot of which shown in Fig. 4.5F.

5. NEW INSIGHTS AND ADVANCEMENTS PROVIDED BY THIS THESIS

5.1 Methodological Improvements

In this Section, our work on method development is described. This work enabled the studies on protein and lipid diffusion in membranes crowded by proteins. Publications I and II consider this work.

5.1.1 Membrane Protein Insertion

As described in Chapter 4, prior to an MD simulation, an initial configuration of the simulated components needs to be set up. Unfortunately, generating such configurations for membrane protein simulations has traditionally been tedious, as lipid chains show a plethora of conformations that need to be fitted to complex protein surfaces. Luckily, many tools have been developed for this purpose [228, 229, 230, 231, 232, 233]. These tools either embed a protein into an existing bilayer or generate the whole system from scratch. Unfortunately, all of them suffer from a few limitations. The tools that insert proteins into existing bilayers require the removal of lipids. With new lipidomics data fostering simulations of multi-component membranes, this might result in unwanted changes in their lipid compositions. Most tools are also compatible only with specific models and simulation software or require the installation of third-party software. Moreover, they are merely suitable for creating a single-protein configuration.

To tackle these issues, we developed a protocol for embedding proteins into pre-existing lipid bilayers. This approach is based on pushing a protein into a membrane from its side by applied pressure. Briefly, the simulation box around the bilayer is increased in the plane of the bilayer so that the protein can be placed next to the bilayer without any overlap of atoms. This configuration is visualized in

Figs. 4.1A and 4.1B for AA and CG models, respectively. Next, a set of restraints are applied to maintain the integrity of the bilayer and the structure of the protein. Finally, significant pressure is applied in the plane of the membrane, which causes the fluid membrane to encapsulate the protein. Simultaneously, the lateral size of the box shrinks as the initial vacuum around the membrane disappears. After a brief simulation of approximately one nanosecond, the membrane is again continuous, yet now hosts the protein. This process is visualized in Fig. 5.1.

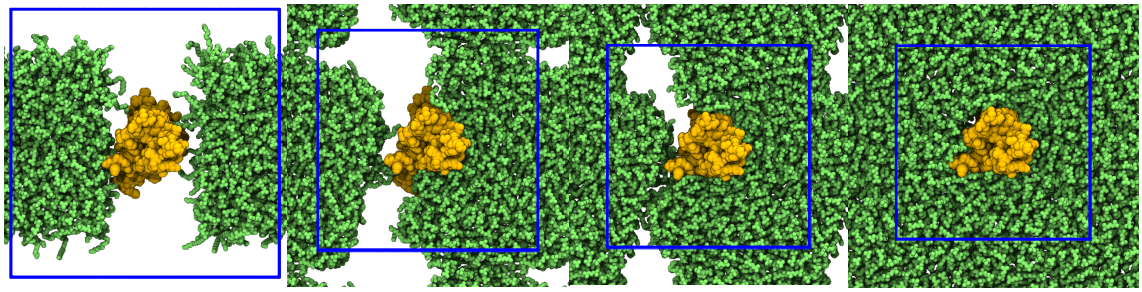

Figure 5.1 *Snapshots (top view) of the embedding process with an AA system. The protein is shown in yellow and the POPC lipids in green. Water and ions are omitted for clarity. Periodic images of the system are displayed to visualize the process better. The simulation box (unit cell) is highlighted in blue.*

This new protocol avoids most of the pitfalls of the earlier methods. It is universal to all models and independent of simulation software. Instead, any molecular dynamics engine can be employed as long as it implements the standard functions required – a barostat and position restraints. Most importantly, our approach does not require the removal of any lipids. Unfortunately, it does not come without limitations. The approach is not compatible with doughnut-shaped proteins that enclose lipids within their structure, and it is limited to work only with planar geometries. Finally, it is worth emphasizing that since making our protocol accessible for the community, two other tools, CHARMM-GUI [213, 214, 215] and `insane` [195], have emerged and rendered our approach obsolete in some cases.

5.1.2 Adjustment of Protein–Protein Interactions

During the research presented in this Thesis, it became apparent that the Martini model is not well parametrized for protein–protein interactions. This issue manifests itself in the excessive aggregation of membrane proteins under crowded conditions [189, 234, 235] (see Publication II for more examples). Without exception, simulations

performed using the Martini model result in a superaggregate that contains all the simulated proteins clustered together in a nonspecific manner. What is more, the estimated dimerization free energies of both trans-membrane (TM) peptides and proteins show incredibly high values of up to ∼160 kJ/mol [235]. Such energies refer to an entirely irreversible association, which is in disagreement with experimental observations and our intuitive picture of biological processes.

To systematically evaluate the level of protein–protein interactions in Martini, we performed umbrella sampling simulations on two TM domain dimers of known structures and dimerization free energies (see Section 4.3). An example conformation is shown in Fig. 4.2A. Additionally, the dimerization free energies of both dimers had been estimated in earlier Martini simulations [236, 237], yet using different simulation parameters and membrane compositions. We mimicked the experimental setups as closely as possible in our simulations. Additionally, we simulated the spontaneous formation of five dimers of TM domains, for which NMR structures are available. These dimers are shown in the CG scheme in Fig. 4.2B.

As expected and as shown in Table. 5.1, we find that the dimerization free energies of the TM domains extracted from umbrella sampling simulations using Martini are of the order of ∼35–40 kJ/mol. In contrast, the Förster resonance energy transfer (FRET) experiments provide values of around ∼10–15 kJ/mol (see Table 5.1). Furthermore, as demonstrated in Table 5.1, using the polarizable Martini model [238] does not improve this agreement. Our analysis also highlights that the peptides form higher-order oligomers or even a superaggregate in a simulation containing multiple membrane-embedded peptides. This result is in disagreement with the FRET studies that report the lack of such higher-order oligomers [220, 221].

Table 5.1 *EphA1 and ErbB1 TM domain dimerization free energies (in kJ/mol).*

	EphA1	ErbB1
FRET experiments [220, 221]	-15.4 ± 0.5	-10.5 ± 0.4
Standard Martini	-29.9 ± 1.0	-39.5 ± 1.0
Polarizable Martini	-33.5 ± 1.0	–
Scaled (Publication II)	-15.2 ± 1.0	-15.3 ± 0.3
Previous studies [236, 237]	-60 ± 2	-38 ± 3

Considering next the structures of the spontaneously formed dimers, the comparison with NMR data (not shown here) unfortunately reveals that Martini is unable to

correctly predict any of the dimer structures. Moreover, the 10 replicas simulated for each dimer provide a very diverse set of structures, indicating that any protein–protein contact can lead to irreversible protein aggregation.

Following the approach of Stark *et al.* applied to water-soluble proteins [197], we scaled down the Lennard-Jones (LJ) interactions between the protein beads by various amounts and repeated the simulations. We applied this scaling to either all protein beads or only to those that resided mostly in water. The former approach turns out to be more successful, and a subtle 10 % decrease in the LJ energy parameter (ϵ) brings the dimerization free energies to the same ballpark with experiments (see Table 5.1). Also, the oligomer sizes in multi-peptide simulations decrease, and the peptides no longer form a single superaggregate, in more reasonable agreement with experiments.

Unfortunately, the quality of the structures of the spontaneously formed dimers of TM domain peptides does not improve in this process. Instead, we still observe dimerization interfaces and dimer conformations that drastically differ from those resolved by NMR.

Despite the issues that prevent the general adaptation of the scaled Martini protein model, certain types of studies can significantly benefit from it. These include research on membrane dynamics in crowded environments, where excessive protein–protein interactions lead to abnormal protein aggregation and subsequently to strong confinement effects by these aggregates. In such cases, the scaling down of the protein–protein interactions can provide more realistic transient aggregation behavior. This is the case in Publication IV, where the proposed scaling approach is applied to crowded membranes.

5.2 Models for Normal Diffusion

In this Section, our work considering models describing normal diffusion is described. The validity of these models, introduced in Sections 3.1.2 and 3.1.3, is evaluated in biologically relevant conditions. Publications III and IV consider this work.

5.2.1 The Free Area Model Provides Nonphysical Parameters

The free area (FA) model [10] (see Section 3.1.2) has been successfully adapted to lipid bilayers, where it captures the temperature dependence of diffusion coefficients. Furthermore, it has explained the decrease in lipid diffusivities upon the addition of cholesterol by the reduction in the available free area [10]. However, there is still debate on the validity of the model and especially on the underlying diffusion mechanism [11, 100, 101]. We put the FA model to the test in a different setting. Lipid monolayers and their dynamics are crucial for lung function [81]. Moreover, monolayers allow for a systematic probing of diffusion as a function of both lipid area and temperature in both simulations and experiments. Also, with the use of simulations, the parameters provided by the FA model fits can be directly compared to the corresponding physical properties of the monolayer. We chose this approach and simulated protein-free pulmonary surfactant monolayers at different APLs, as described in Section 4.3.

Visualization of the lipid motion (see Fig. 5.2A already reveals flow-like patterns and suggests that hopping between vacant sites is not the correct physical description of diffusion. However, as Fig. 5.2B demonstrates, the lipid diffusion coefficients as a function of APL are reasonably well fitted with the FA model (Eq. (3.12), solid line), in line with experiments [99]. Here, data for DPPC — the most abundant lipid in the mixture — are shown. The fit provides activation energies E_a of $\sim$14 kJ/mol for all lipid species, whereas for the close-packed areas of the lipids, a_0, we obtain values of $\sim$40 Å^2, again similar across all lipid moieties.

The activation energy can also be extracted *via* an Arrhenius analysis, assuming that diffusion is an activated process. Following the Arrhenius equation,

$$D = D_0 \times \exp\left(-\frac{E_\mathrm{Arrh}}{RT}\right), \tag{5.1}$$

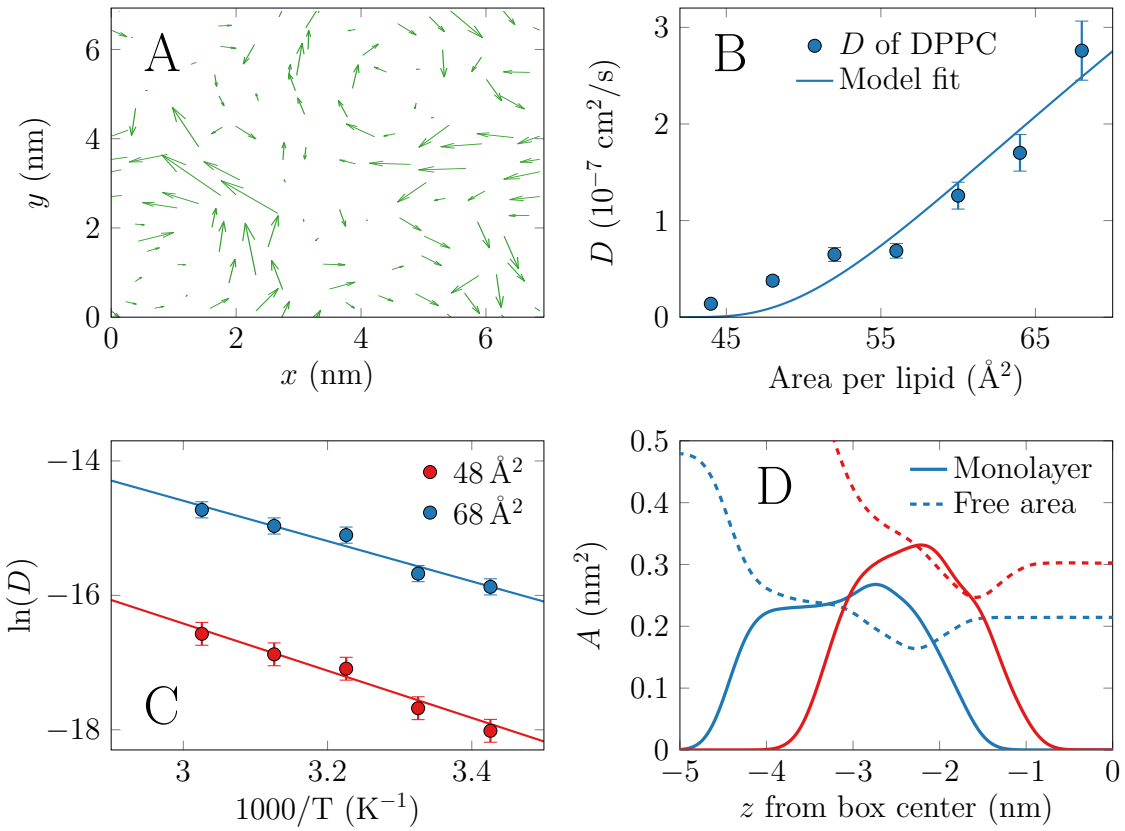

Figure 5.2 *Key results from Publication III: A) Typical flow patterns of lipids in the monolayer with an APL of 48 Å^2 over a 10 ns interval. B) Diffusion coefficients of DPPC as a function of APL (markers) together with a FA model fit (solid line). C) Diffusion coefficients (markers) in systems with APLs of 48 Å^2 and 68 Å^2 plotted in the Arrhenius manner (see Eq. (5.1)). Solid lines show the linear fits. D) Profiles of close-packed cross-sectional areas of DPPC (solid lines). The dashed curves show the free volume profiles. Data are displayed for systems with APLs of 48 Å^2 (red) and 68 Å^2 (blue).*

a plot of $\ln D$ against T^{-1} provides a slope of E_{Arrh}/R, *i.e.* the Arrhenius activation energy divided by the universal gas constant. Hence, to extract E_{Arrh}, we simulated monolayers with APLs equal to 48 and 68 Å^2 at different temperatures. These data, shown in Fig. 5.2C for DPPC in monolayers with APLs of 48 Å^2 (red) and 68 Å^2 (blue), provide activation energies of 31 and 25 kJ/mol, respectively. While these values are in line with the values measured for liquid-disordered bilayers [239], they are approximately twice as large as the values predicted by the FA model fits. This discrepancy between E_{Arrh} and E_{a} has also been demonstrated for lipid bilayers [101].

The close-packed cross-sectional area profiles for DPPC are shown by solid curves in Fig. 5.2D for systems with APLs equal to 48 Å^2 (red) and 68 Å^2 (blue). For lipids

(solid lines), the curves reach maximum values of ∼25 and ∼35 Å^2, respectively, only somewhat smaller than the value of ∼40 Å^2 obtained from the FA model fits. It must be kept in mind, though, that a lipid is not a rigid rod and its cross-sectional area varies drastically along its length [100]. Therefore — considering the inaccuracies of our calculation — the values of a_0 seem to be in the right ballpark. However, if the values of a_0 given by the FA model are considered quantitatively, the situation is more complicated. The area parameter a_0 should describe the cross-sectional close-packed area of a lipid (see Eq. (3.12)), but the deviation from the true cross-sectional close-packed area we determined from the data is of the order of 50 %. The obvious question is whether a_0 describes any physical parameter realistically, or whether it serves just as a fitting parameter.

5.2.2 Crowding Breaks Down The Saffman–Delbrück Model

The Saffman–Delbrück (SD) model [12, 13] (see Section 3.1.3) has been successfully applied to describe the diffusion of membrane proteins in the protein-poor limit [14, 109, 110, 111, 112]. The central feature of the SD model is that it predicts a weak logarithmic size-dependence for the diffusion coefficients of proteins ($D \sim \ln R^{-1}$ with protein radii R). Notably, the SD model is a fundamental concept for explaining protein motion and hence diffusion-controlled reactions in biomembranes. However, even though cellular membranes are incredibly crowded with proteins, the SD model has not been put to the test under such conditions, neither experimentally nor in simulations. To fill this gap, we simulated CG membranes with different concentrations of a polydisperse set of proteins as well as 2DLJ fluids with embedded disks of different radii. Moreover, we also considered crowded membranes with monodisperse sets of proteins. All these models are described in Section 4.3.

The protein diffusion coefficients, shown in Fig. 5.3A, display a nonlinear decrease upon protein crowding, and this decrease is the most drastic for the smallest proteins. For the estimation of protein radii, we performed single-protein simulations and analyzed the dynamics of lipids in the vicinity of the proteins. It is established that membrane proteins diffuse together with a tightly-bound lipid shell [59], which needs to be taken into account when considering the protein's hydrodynamic radius. Such "effective" radii (R_{eff}) are shown in Fig. 5.3B together with the radii of the 2DLJ disks. Notably, the CG proteins span the typical size range of known membrane proteins.

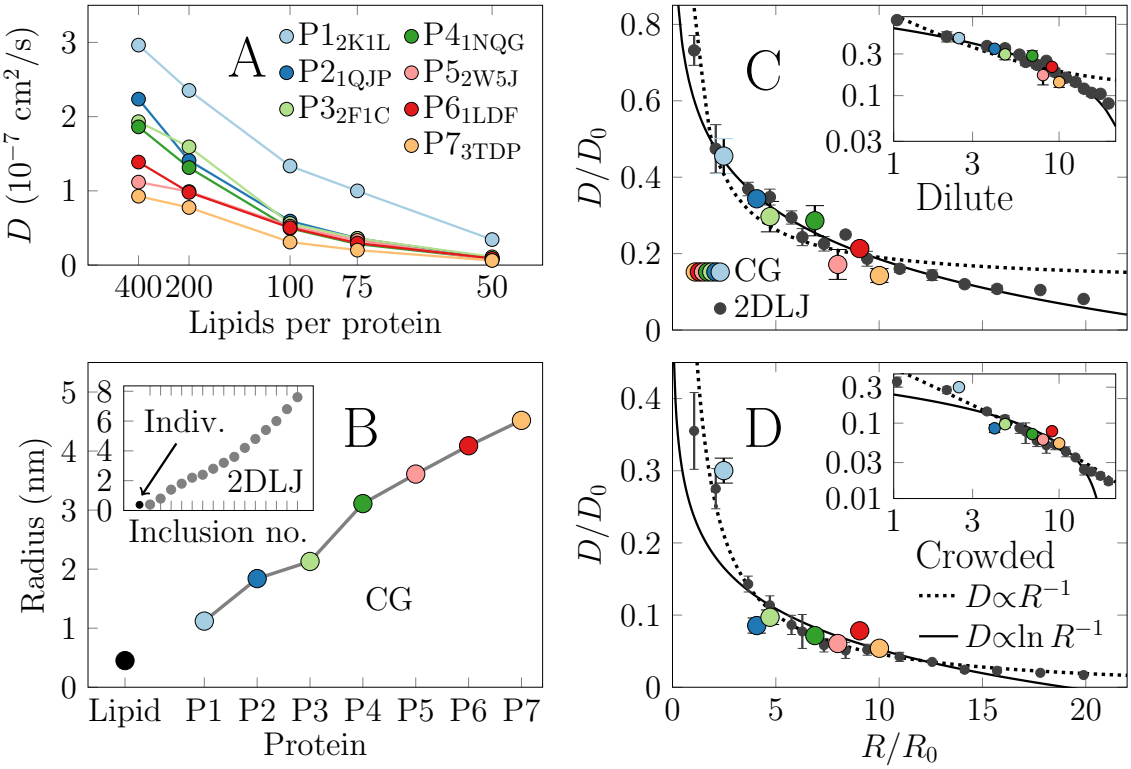

Figure 5.3 *Key results from Publication IV. A) The diffusion coefficients of the proteins at different LP ratios. B) The R_{eff} of the proteins in the CG simulations (main plot) and the radii of the 2DLJ disks (inset). "Indiv." stands for an individual (free) 2DLJ particle. C) Diffusion coefficients as a function of protein size in dilute systems. Data are shown in reduced units for a direct comparison between the CG and 2DLJ systems. The insets show data in logarithmic scale. The solid and dashed lines indicate fits of the SD model and Stokes-like scaling, respectively. D) Diffusion coefficients as a function of protein size in crowded systems.*

The protein diffusion coefficients are shown as a function of R_{eff} in Figs. 5.3C and 5.3D for dilute and crowded conditions, respectively. In the CG systems, these correspond to LP = 400 and LP = 50, respectively, whereas in the 2DLJ systems there are 1000 and 300 free particles per disk. The use of reduced units reveals a striking similarity between the behaviors of the CG (colored markers) and 2DLJ (black markers) systems. Here, the diffusion coefficients and radii of the proteins and the disks are scaled by the diffusion coefficients (D_0) and radii (R_0) of the lipids and the free LJ particles, respectively. Importantly, while the SD-like weak dependence $D \sim \ln R^{-1}$ (solid line) fits the data under dilute conditions well, a stronger Stokes-like law $D \sim R^{-1}$ (dashed line) arises under crowding. This crossover is most convincingly demonstrated in the logarithmic scale, as shown in the insets in

the panels of Figs. 5.3C and 5.3D. The Stokes-like law is also observed for crowded membranes with a monodisperse set of proteins, shown in Fig. 4.4 (see Publication IV for details).

5.3 Anomalous Diffusion in Membranes

In this Section, our research that examined the nature of lipid and protein diffusion in crowded membranes is described. Publications V and VI consider this work.

5.3.1 Lipid Packing Promotes Anomalous Diffusion

As explained in Section 2.2, lipid monolayers do not have an equilibrium area. Instead, their area and hence the level of lipid packing can be varied continuously by the applied pressure. Indeed, pulmonary surfactant monolayers undergo repeated compression–expansion cycles due to breathing. The surfactant forms a dynamic system that arranges itself into domains that promote lipid–protein interactions and folds away from the interface into lipid reservoirs during exhaling [81]. Therefore, lipid dynamics might prove to be a fundamental aspect of lung function. To study the coupling between monolayer packing and dynamics, we exploited the same monolayer models as in the research considering the validity of the free area model.

As demonstrated in Fig. 5.4A, the MSD curves reveal the different diffusion modes when plotted on the logarithmic scale. Here, data are shown in blue and red for monolayers with APLs equal to 44 Å^2 and 68 Å^2, corresponding to the L_c and L_e phases, respectively. Fig. 5.4B shows the diffusion exponent α as a function of lag time. Here, the short-time ballistic behavior is likely not entirely captured due to the limited sampling rate of the simulation. At intermediate lag times between 1 ps and 1 µs, lipid motion is subdiffusive with α values as small as 0.3 for the L_c phase monolayer. Finally, normal diffusion is reached at a 100 ns to 1 µs timescale, depending on the level of packing.

5.3.2 Crowding Extends the Anomalous Diffusion Regime

FCS experiments have revealed that protein crowding induces anomalous subdiffusion in model membranes [15]. These experiments consider α to be constant over the whole

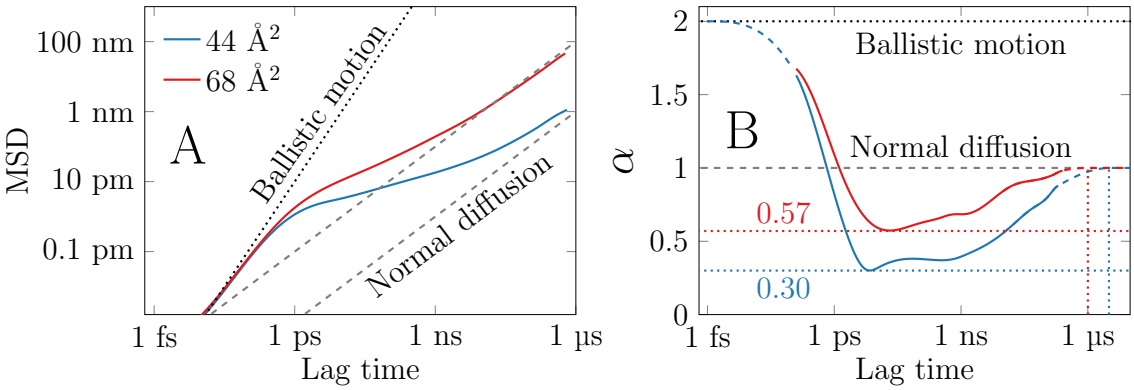

Figure 5.4 *Key results for lipid monolayers from Publication V: A) The MSD versus lag time shown on the logarithmic scale. Data for systems with APL equal to 44 Å² and 68 Å² are shown in blue and red, respectively. The dashed lines highlight a slope of 1, corresponding to normal diffusion, whereas the dotted line shows a slope of 2, corresponding to ballistic motion. B) Evolution of α versus lag time. Coloring as in panel A. The minimum values for both curves are shown, and the colored dashed lines extrapolate the curves to both ballistic (α = 2) and normal (α = 1) regimes. Note that lag time on the abscissa is given in the logarithmic scale.*

extended fitting interval, which seems like a bold assumption based on the monolayer data above. Due to this experimental limitation, the (lag) time dependence of α on protein crowding has remained unknown. To gain this knowledge, we simulated a set of membranes with different degrees of crowding. Moreover, the proteins in these membranes displayed strong (SA) or weak (WA) aggregation tendencies (see Section 4.3).

The diffusion coefficients of lipids and proteins in the SA (red) and WA (blue) systems are shown as a function of LP in Figs. 5.5A and 5.5B, respectively. In line with experiments [14], the diffusion coefficients show a decrease upon protein crowding. This decrease is linear for lipids, yet steeper for proteins. In general, the values measured for the WA systems are somewhat larger, as expected. The dependence of α on lag time is shown for lipids in WA and SA systems in Fig. 5.5C. Along with the behavior observed for monolayers (see Fig. 5.4), diffusion is anomalous at short lag times. However, in LP = INF membranes normal diffusion is reached at the ∼100 ns timescale, in line with the behavior of the L_e phase monolayer (see Fig. 5.4B). However, at around this timescale, a new subdiffusive regime emerges in the crowded membranes. This regime ranges from ∼100 ns up to macroscopic time scales in systems with a realistic level of crowding [4]. In the crowded SA membranes, the values of α decrease to ∼0.6 before they begin their recovery towards

one and hence normal diffusion. The values of α observed in the WA membranes are somewhat larger. The extent of this second subdiffusive regime apparently depends on the level of crowding, as well as the aggregation tendency of the proteins.

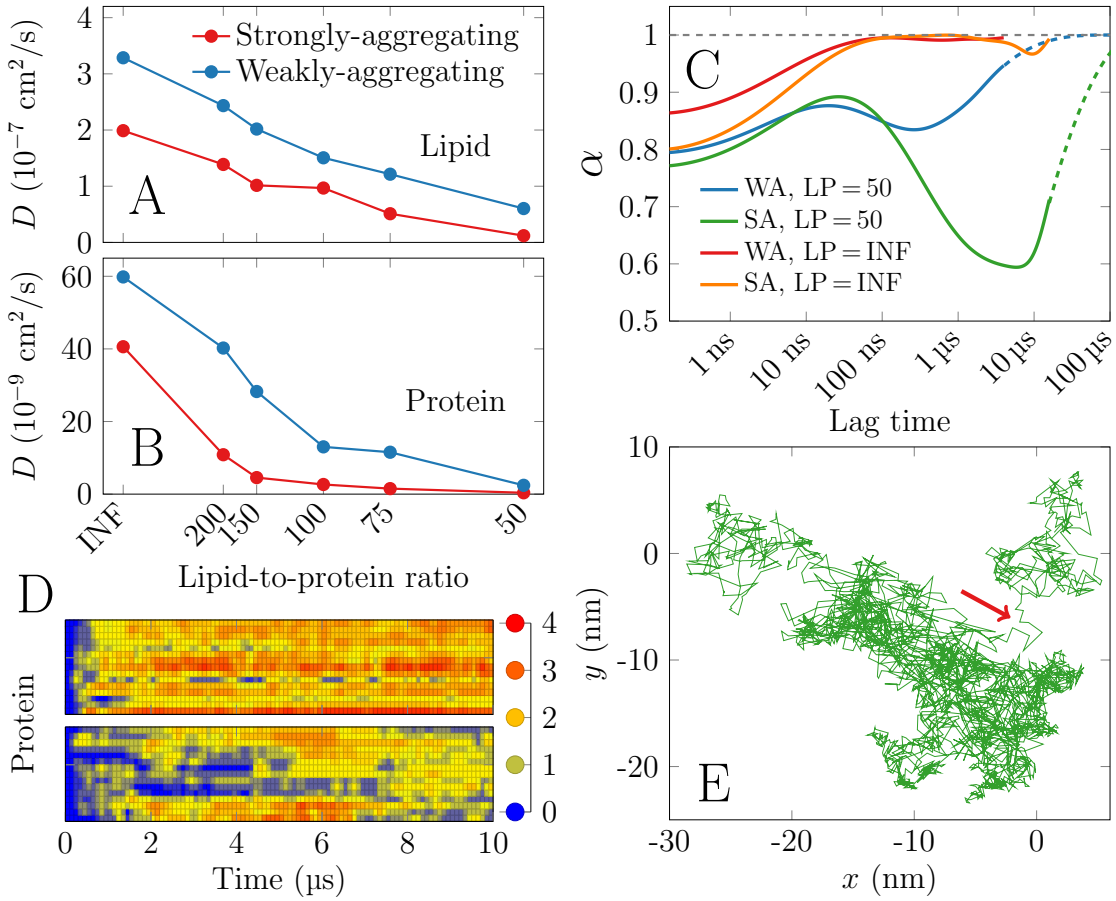

Figure 5.5 *Key results for crowded membranes from Publication V: A & B) Diffusion coefficients of A) lipids and B) proteins as a function of LP. Data are shown for red) SA and blue) WA systems. C) α as a function of lag time in WA and SA systems with LP = 50 and LP = INF. The dashed gray line highlights normal diffusion ($\alpha = 1$). The dotted lines estimate where this is reached by the calculated curves or their extrapolations (dashed line). D) The formation of protein clusters in top) SA or bottom) WA LP = 50 system. Each row corresponds to a protein, and the coloring of each cell shows the number of other proteins in contact with it at a given time. E) Sample trajectory of a lipid in the SA LP = 50 system. The red arrow points to an escape event from confinement.*

This membrane-dependent tendency of the proteins to aggregate is demonstrated in Fig. 5.5D. The data are shown for top) SA and bottom) WA systems with LP = 50. Each line provides data for a single protein, and the coloring reveals the number of other proteins bound to it. In the SA system, each protein rapidly associates with

2–4 others, whereas in the WA system the clusters are somewhat smaller and their formation takes substantially longer. This observation suggests that the substantial dip in α in the SA systems could originate from protein aggregates that restrict lipids into pools. These lipids need to escape this confinement before the regime of normal diffusion is reached. This behavior is indeed observed in sample lipid trajectories, such as that shown for the SA system with LP = 50 in Fig. 5.5E. Here, the red arrow highlights an event where the tracked lipid escapes confinement.

5.3.3 Protein Crowding Changes the Subdiffusion Mechanism

In our earlier study [16], we discovered that anomalous subdiffusion in protein-free bilayers follows the FBM/FLE mechanism (see Section 3.2.1). Notably, this feature holds throughout L_d, L_o, and even gel phases, and manifests itself in numerous ways: the subdiffusion is ergodic and Gaussian and it does not display aging [16]. Moreover, the calculated displacement autocorrelation function matches precisely that predicted for FBM (see Eq. (3.18)). These findings conclusively showed that subdiffusion in protein-free lipid membranes follows the FBM/FLE description. However, with the drastic effects of protein crowding on membrane dynamics, it is not evident that this mechanism also applies to subdiffusion in crowded membranes. To clarify this issue, we further analyzed the dynamics in the crowded (LP = 50) and dilute (LP = INF) WA and SA membranes shown in Figs. 4.5A–4.5C and discussed above. The simulations were extended to collect reliable statistics of protein diffusion, and the CG simulations were complemented by 2-dimensional Lennard-Jones (2DLJ) systems with obstacles, depicted in Figs. 4.5D–4.5F.

The radial PDFs, $P(r, \Delta)$, of lipids are shown Figs. 5.6A and 5.6B for the SA systems with LP = INF and LP = 50, respectively. Lipids in the dilute system follow a Gaussian distribution ($P(r, \Delta) \sim \exp(-r^2)$), highlighted by the gray dashed line. However, in the case of the crowded membrane, the Gaussian fit fails and gets replaced by a sum of two terms of a more general form ($P(r, \Delta) \sim \sum \exp(-r^{\zeta_i})$) with the values of ζ_i highlighted in Fig. 5.6B. This fit is shown by a solid line. The data for lipids in the crowded WA membrane as well as proteins in WA and SA membranes follow the same behavior (data not shown here). The non-Gaussianity already suggests that diffusion in crowded membranes does not follow the FBM/FLE mechanism, so we pursued indicators of alternative descriptions (see Sections 3.2.2 and 3.2.3). Characteristic examples of the TA-MSD curves of lipids with a fixed lag time (Δ =100 ns) are shown for the dilute LP = INF and crowded LP = 50 SA

membranes in Figs. 5.6C and 5.6D, respectively. In the dilute system, all trajectories rapidly converge to the mean value $\langle\overline{\delta(\Delta)}\rangle$, shown by a black dashed line. Hence, the dilute system does not display aging. Moreover, the corresponding ergodicity breaking parameter (see Eq. (3.9)), plotted in Fig. 5.7A, shows the typical $\sim \Theta^{-1}$ convergence of FBM/FLE [84] with both $\Delta = 100$ ns (blue) and $\Delta = 5$ µs (red), respectively. The TA-MSD data of lipids for the crowded membrane displays drastically different behavior (see Fig. 5.6D). While most trajectories converge to their mean value (examples given by reddish curves), some show a constant decline (bluish curves), a rapid increase (greenish curves), or even a combination of both (orangish curves). The decline events likely initiate when a lipid gets confined, whereas their release from such confinement leads to a rapid increase in the MSD. Despite this heterogeneity, $\langle\overline{\delta(\Delta)}\rangle$ is constant over measurement time, indicating that no aging takes place. Hence, CTRW is ruled out as a possible subdiffusion mechanism.

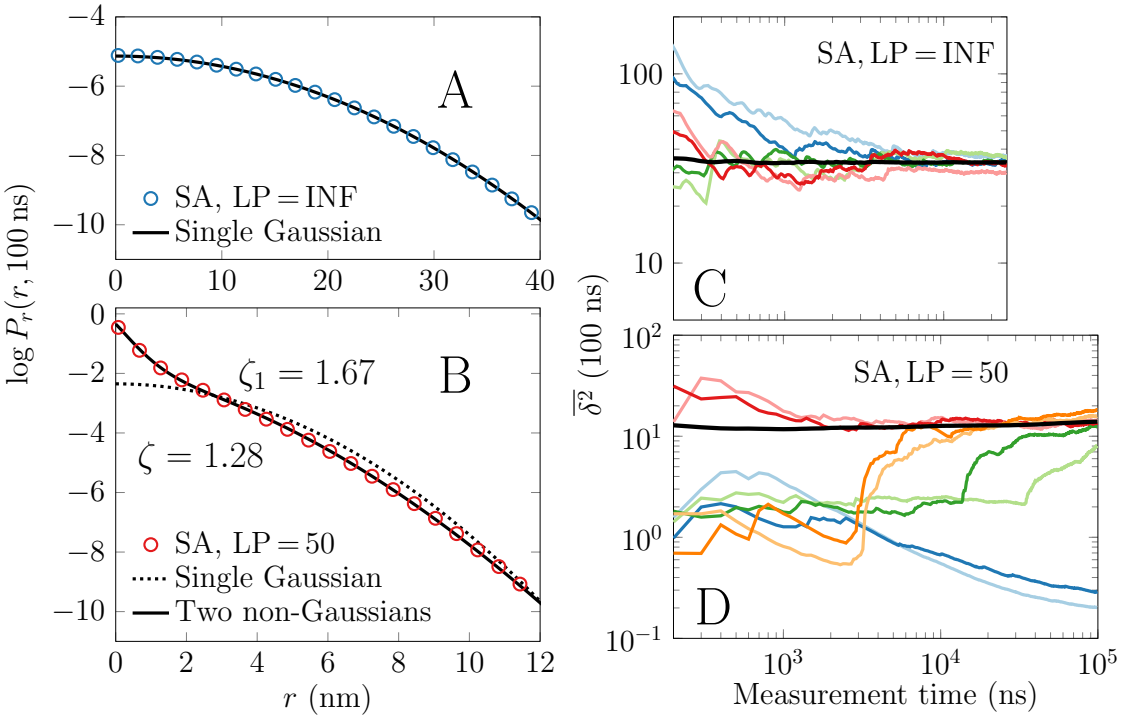

Figure 5.6 *First set of results for coarse-grained simulations in Publication VI. A & B) Radial PDFs for lipids in the A) dilute (LP = INF) and B) crowded (LP = 50) SA systems over a lag time of 100 ns. Dashed lines show Gaussian fits, while the solid lines are fits to the non-Gaussian exponents (see text for details). C & D) Examples of TA-MSD curves for C) dilute LP = INF and D) crowded LP = 50 SA systems.*

The ergodicity breaking parameters of lipids for the crowded LP = 50 case, shown

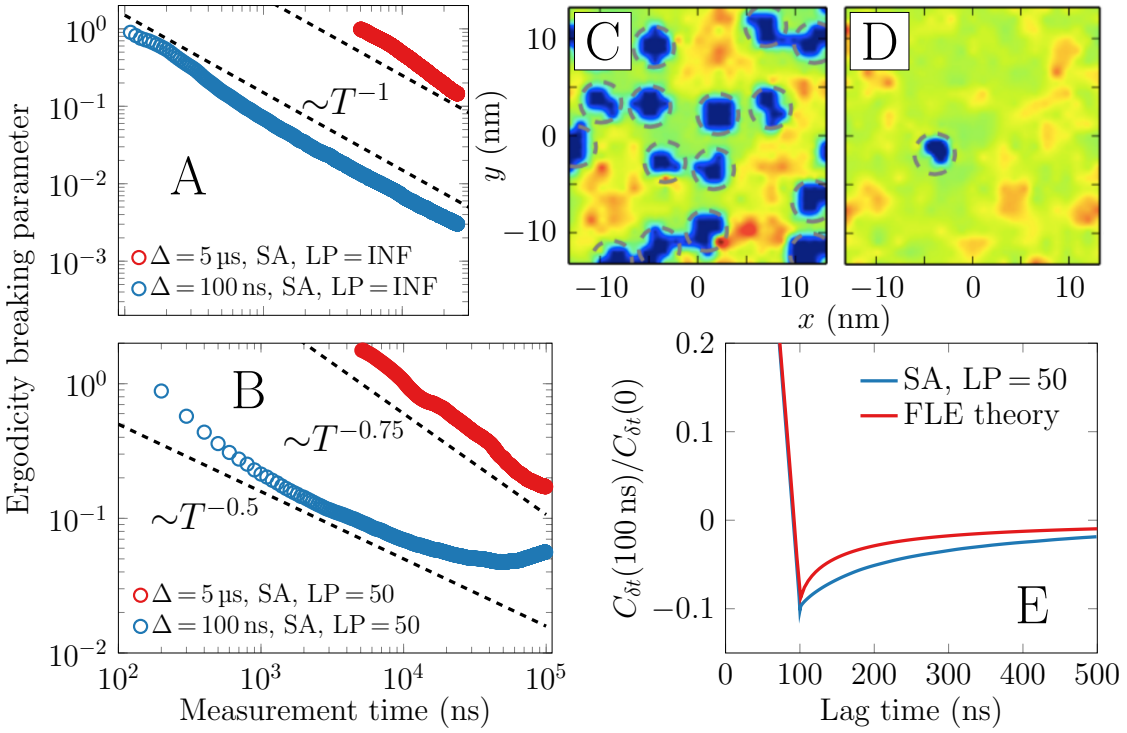

Figure 5.7 *Second set of results for coarse-grained simulations in Publication VI. A & B) Ergodicity breaking parameter for lipids with $\Delta = 100$ ns (blue) and $\Delta = 5$ µs (red) in A) dilute LP = INF and B) crowded LP = 50 SA systems. C & D) Example maps of MSD over a 10 ns time interval in the C) LP = 50 SA and the D) LP = INF SA (I) systems. E) Normalized displacement autocorrelation of lipids in the crowded (LP = 50) SA system.*

in Fig. 5.7B for both $\Delta = 100$ ns (blue) and $\Delta = 5$ µs (red), converge towards zero, although slower than what is predicted for FBM/FLE. The displacement autocorrelation of lipids (Eq. (3.18)), shown in Fig. 5.7E for the crowded LP = 50 SA membrane, displays the negative dip characteristic for FMB/FLE, yet does not entirely follow the theoretical prediction. Nevertheless, the CTRW model (Eq. (3.23)) does not explain the data either. Figs. 5.7C and 5.7D, show examples of the spatial variation of the MSD of lipids over a time interval of 1 ns in the C) SA LP = 50 and D) LP = INF systems. For the crowded case, protein arrangement effects a heterogeneous diffusivity landscape that also varies with time, whereas in the dilute membrane the variations are milder. Further modeling work (see Publication VI) suggests that this spatiotemporal heterogeneity is the reason behind the observed non-Gaussian yet ergodic subdiffusion.

Central results for the 2DLJ systems (see Fig. 4.5D–F) are shown in Fig. 5.8. The EA-TA-MSD curves are shown in Fig. 5.8A. The differences in the curves are best

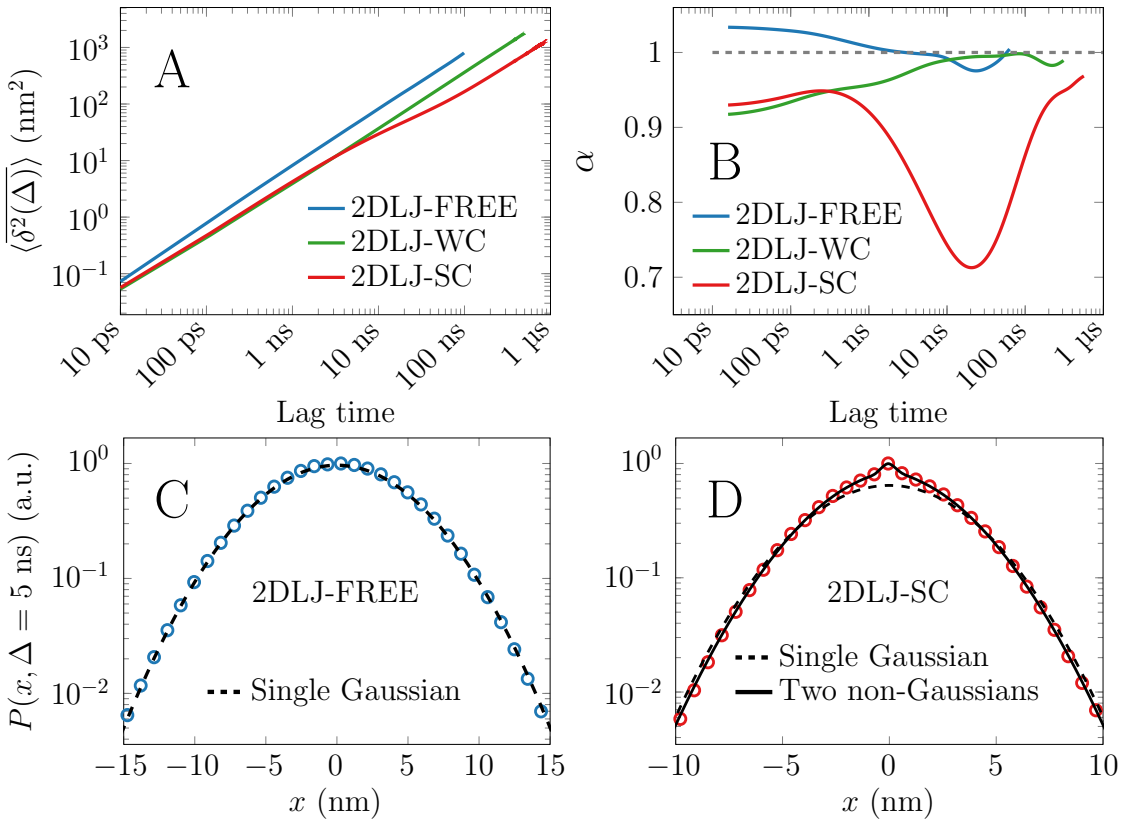

Figure 5.8 *Key results for 2DLJ simulations in Publication VI. A) TA-EA-MSD shown in double logarithmic scale. B) Diffusion exponent α as a function of lag time. C & D) 1D displacement distributions over a 5 ns time interval for the C) 2DLJ-FREE and D) 2DLJ-SC systems.*

highlighted by plotting the time evolution of α in lag time, shown in Fig. 5.8B. Notably, Fig. 5.8B shows that the convergence of α to one is observed in all systems. However, the SC system shows a dip in α, similar to what is observed in the LP = 50 SA system above (compare Figs. 5.8B and 5.5C). In the WC system, the obstacles somewhat extend the anomalous diffusion regime, yet do not lead to a similar dip in α. As shown in Fig. 5.8C the particles in the 2DLJ-FREE system show Gaussian diffusion. However, in the 2DLJ-WC (not shown here) and 2DLJ-SC system (see Fig. 5.8D), the obstacles effect a non-Gaussian displacement distribution described by two generalized Gaussians, in line with the behavior of the crowded CG systems.

5.4 Discussion and Conclusions

Beginning by considering the methodological advancements presented in this Thesis, we first introduced a technique for generating initial setups for membrane protein simulations. The proposed approach excels in its universality compared to other methods and has promoted the rest of the research presented in this Thesis. Next, the results demonstrating the shortcomings of the Martini model in describing protein–protein interactions were described. We proposed a simple correction that allows studies of lipid diffusion in the absence of excessive protein aggregation. Indeed, this approach was exploited in our further research on crowded membranes.

Moving on to discuss our work on lipid monolayers, we first assessed the validity of the free area model using lipid monolayers that allow for a systematic variation of area per lipid. We showed that while the model fits diffusion coefficient data reasonably well across different monolayer compression states, the fitting parameters have somewhat nonphysical values. It is not surprising that the free area model based on thermally-activated and discrete jumps fails, considering that we observed flow-like motion of the lipids. Such flow-like motion has also been demonstrated by simulations [11, 100, 102] and QENS experiments for lipid bilayers [103, 104]. We also examined the nature of anomalous diffusion in lipid monolayers. We found that lipid packing *via* monolayer compression results in the decrease of both diffusion coefficients and diffusion exponents and extends the subdiffusive regime to the microsecond time scale. These findings shape our understanding of lateral search processes in the pulmonary surfactant, where lipid–protein interactions regulate the transfer of lipids between the interface and the aqueous subphase — a key mechanism for breathing [81].

Proceeding to discuss our work on membranes crowded with proteins, we first considered the applicability of the Saffman–Delbrück model to protein-crowded membranes. We found that crowding decreases the diffusion coefficients of proteins of all sizes, yet this decrease is less radical for smaller proteins. Due to this size-dependent behavior, the Saffman–Delbrück model gets replaced by a stronger Stokes-like size-dependence between diffusion coefficients and protein radii in the crowded environment. The stronger scaling relation changes the picture of lateral search processes in cellular membranes drastically: in dilute conditions where the Saffman–Delbrück model holds true, proteins of different sizes diffuse at almost equal rates, whereas in crowded conditions the smaller proteins move around significantly faster

compared to larger ones that are virtually immobile. Hence, the Saffman–Delbrück model has to applied with extreme care to estimate diffusion-limited reactions in the heterogeneous and crowded plasma membrane. Unfortunately, a theoretical picture of the crossover from the Saffman–Delbrück model to the Stokes-like model is currently lacking. Furthermore, a systematic experimental study of the size-dependence of protein diffusion at different levels of crowding has not been performed. Such a study is likely further complicated by other non-idealities present in cellular membranes, described in Chapter 2.

Next, our findings on anomalous diffusion in crowded membranes were described. We observed that protein crowding has surprisingly similar effects as lipid packing: it lowers the rate of diffusion, decreases the values of α, and extends the subdiffusive regime. Notably, we found that substantial protein aggregation leads to confinement effects that maintain anomalous diffusion up to macroscopic time scales. Regarding the anomalous diffusion mechanism, our results convincingly suggest that protein crowding leads to deviations from the FBM/FLE concept, which has been found to be valid in dilute conditions [16]. Instead, the diffusion of both lipids and proteins becomes non-Gaussian and highly heterogeneous, while maintaining its ergodic nature. Unfortunately, the exact mechanism behind this peculiar behavior remains partially unknown. Curiously, our simulation work suggests that the findings might be explained by a combination of a fluctuating diffusion model — accounting for the spatiotemporal variations in local diffusivity induced by protein–lipid and protein–protein interactions — and non-Gaussian PDFs due to proteins acting as geometric obstacles. This finding was supported by our simulations on 2D models that reproduced the non-Gaussian behavior. However, as discussed in Section 5.1.2, our findings might be somewhat affected by excessive protein aggregation, even though we did not use the Martini model but its derivative.

All in all, our results help understand how lipid packing and protein crowding affect the dynamics of lipids and proteins in conditions matching those present in the lung surfactant and at the surface of cells. Our observations provide further evidence that diffusion in lipid layers takes place via flow-like motion with viscoelastic effects, yet the presence of proteins complicates this picture substantially to a degree where no single known mechanism captures the nature of the motion. At long times — which in crowded and packed systems likely means milliseconds — the size dependence of protein diffusion heavily relies on crowding, which alters our picture of diffusion-controlled processes in the crowded plasma membrane. These findings

will undoubtedly pave the way towards understanding processes that depend on the formation of functional protein oligomers [189] and the regulation of protein function by specific lipids [176]. Still, plenty of more research is required before a comprehensive model for diffusion-controlled processes in complex conditions can be formulated. Moreover, the role of anomalous dynamics and especially the importance of the underlying subdiffusion mechanism for biological functions remains an intriguing puzzle for theoretical research to solve in the future.

6. THE BIG PICTURE AND FUTURE OUTLOOK

In the previous Chapters, the fundamental concepts related to lateral diffusion were introduced, along with the many faces of the complexity of the plasma membrane. The central experimental methods used to probe the dynamics within these membranes were also reviewed. Moreover, the primary results of our simulation-based research were presented. In this Chapter, to conclude this Thesis, the essential findings of both experiments and simulations regarding lateral diffusion are highlighted. All in all, the aim is to provide a state-of-the-art view on how molecules move in the plasma membrane, and how their diffusion is affected by membrane complexity. Model lipid membranes are discussed first, followed by model membranes with embedded proteins, and finally diffusion in the membranes of live cells is reviewed. The Chapter and the Thesis are closed by a discussion on the possible future directions in the field.

6.1 Diffusion in Protein-Free Model Membranes

MD simulations have revealed that lipid diffusion can be characterized by a flow-like motion of loosely defined lipid clusters [11, 102, 224]. As described in Section 3.1.2, the alternative free area concept sees lipid diffusion as a series of jumps between vacant sites [10]. However, QENS methods applied to protein-free model membranes are in agreement with flow-like motion lipids at very short times [103, 104]. Still, the concept of activation energy, also present in the free area model, seems to capture the exponential temperature dependence of lipid diffusion observed in NMR measurements [239]. However, the link between Arrhenius-like activation energies and those associated with the free area model remains unclear [224].

At intermediate time scales, lipid motion can be described by anomalous subdiffusion [16, 240, 241], which usually extends up to the 100 ns timescale. Moreover, simulation

data have suggested that this anomalous diffusion follows the fractional Brownian motion mechanism [16]. Notably, the same mechanism describes the motion in all phases, namely L_d, L_o, and gel phases [16, 242]. Cholesterol extends the time regime at which anomalous diffusion is observed [16], and the onset of normal diffusion has been found to result from the circumrotation of membrane lipids [243]. In the gel phase, simulations have reported swing motion [244] and dynamic subpopulations with very small diffusion exponents [245].

Considering phase-separated systems modeling lateral heterogeneity in the plasma membrane, NMR has revealed that diffusion within a domain is on average uniform for all its constituents [246]. As the presence of cholesterol slows down lateral diffusion, it is not surprising that the particles in the L_o phase have been found to be less mobile than in the L_d phase [239]. Curiously, even the dynamics within the individual phases are not uniform across lipid molecules. Instead, iSCAT has revealed that the L_o phase contains ordered subdomains [157], and similar observations have been reported for both L_o and L_d phases by nanoantenna-based FCS measurements [151].

The effects of inter-leaflet coupling — in the form of lipid chain interdigitation — on lipid diffusion are relatively poorly understood. Nevertheless, recent iSCAT-based super-resolution SPT techniques have revealed that in the case of ganglioside GM1, inter-leaflet coupling to a GM1 cluster can lead to lipid trapping in the opposite leaflet [247].

6.2 Effects of Proteins on Membrane Dynamics

In membranes with sufficiently dilute concentrations of proteins, the celebrated Saffman–Delbrück model has successfully explained protein diffusion coefficients measured by FRAP and FCS [109, 110, 112]. Such dilute protein concentrations already have implications on lipid dynamics: computer simulations have demonstrated that membrane proteins slow down the diffusion of lipids in their vicinity, and the strength of this effect seems to heavily depend on protein size, as well as specific protein–lipid interactions [59, 115, 188].

As the protein concentration increases, the membrane dynamics gets significantly more complex [60, 63, 85]. FRAP and FCS measurements have demonstrated the decrease of protein diffusion coefficients upon increasing protein concentration in

model membranes [14, 109]. Moreover, FCS experiments on avidin proteins in model membranes have observed that protein crowding also effects anomalous subdiffusion [15].

The slowing-down of lipid and protein diffusion upon protein crowding has also been demonstrated by numerous simulation studies [115, 120, 188, 234, 248, 249]. Moreover, this effect has been found to be dependent on protein size, which leads to the breakdown of the Saffman–Delbrück model upon protein crowding [188]. The effect of crowding in extending the regime of anomalous diffusion of lipids and proteins has also been reported by numerous simulation studies [115, 120, 188, 248, 249]. Simulations have also demonstrated that the FBM mechanism no longer dictates anomalous dynamics in crowded membranes [249]. Instead, a more complex model accounting for both the spatiotemporal variations in diffusivity and the geometric effects has been suggested to arise in such conditions [249].

As protein crowding reaches the levels present in the plasma membrane [4], there are approximately 50 lipids per protein. Considering specific lipid–protein interactions and the nonspecific dynamic lipid shells [59, 115, 188], it is apparent that no free lipids exist in the membrane. Fortunately, high-speed AFM [168, 169] is able to provide information on diffusion in such extremely crowded membranes. It has demonstrated how protein aggregation leads to heterogeneous dynamics where the outer membrane protein F displays characteristics of both free diffusion and trapping [168]. Furthermore, AFM has revealed the heterogeneity in the motion of lysenin protein in crowded model membranes, where the proteins can become confined in solid-like environments, display more or less fluid-like glassy dynamics, or get trapped at different time scales [169].

6.3 Dynamics in the Membranes of Living Cells

Moving on to membranes of living cells, SPT has found that in the cytoplasmic leaflet of *E. coli*, membrane protein diffusion follows the Saffman–Delbrück model [111] at long times. However, at shorter times, the diffusion in the *in vivo* membranes becomes anomalous, as has been demonstrated by FCS [250].

This anomaly can result from a multitude of factors. STED-FCS and STED-FLCS have readily detected the transient trapping of sphingomyelins in small raft-like membrane domains [25, 149], whereas scanning STED-FCS has suggested that this

trapping arises from protein–lipid interactions instead [27]. The trapping of sphingomyelins has further been demonstrated by confocal microscopy exploiting multiple illumination spots [251] and FCS measurements based on planar nanoantennas [26]. Moreover, in addition to lipids, certain membrane proteins have also been found to get trapped in such raft-like domains [252].

Cytoskeleton-associated pickets and fences substantially affect the dynamics of both membrane leaflets, where they are assumed to lead to confinement effects [51]. Indeed, single-particle tracking has shown that both lipids [253] and proteins [254] undergo rapid diffusion within confined regions and perform hopping motion between these compartments in live cells. This behavior has also been observed for both lipids and proteins in MD simulations modeling the presence of pickets [255]. In line with these observations, STED-FLCS has demonstrated that actin depolymerization reduces the trapping of sphingomyelin, and generally reduces the spatiotemporal heterogeneity in the plasma membrane dynamics [27]. Conclusive evidence for the role of the actin meshwork in obstructing free diffusion has been provided by a combination of experimental techniques [256]: the confinement effects in channel diffusion observed with SPT were explained by the interactions with the actin meshwork, which was readily visualized by super-resolution microscopy [256].

The interactions with the cytoskeleton can also result in anomalous dynamics [111], which has been explained by numerous mechanisms. The dynamics of Kv1.4 and Kv2.1 ion channels affected by the meshwork have been described by an obstructed diffusion model [256], whereas certain proteins have been found to get trapped by membrane corrals formed by the cytoskeleton, which leads to dynamics best described by the CTRW formalism [130, 131]. Curiously, the trapped proteins showed aging, yet they were replaced by freely diffusing ones *via* constant vesicular trafficking [130, 131]. In line with this observation, the motion of Kv2.1 potassium channels has been found to display non-ergodic diffusion reminiscent of CTRW due to transient binding to the actin cytoskeleton [129]. However, this motion was accompanied with ergodic diffusion influenced by macromolecular crowding.

The relative roles of the cytoskeleton and crowding seem somewhat puzzling. Some reports have suggested that the perturbations caused by the anchored trans-membrane pickets and actin filament fences dominate over those induced by protein crowding, membrane heterogeneity, and the extracellular matrix [257]. However, these two effects often seem to be coupled. STED microscopy and STED-FCS measurements have concluded that protein diffusivity decreases as they cluster at the mesoscale,

and this clustering is dependent on their interactions with the cytoskeleton [258].

The combined effects of different aspects of membrane complexity also manifest themselves in spatiotemporal variations in diffusivity. SPT measurements have demonstrated that 3-grabbing nonintegrin proteins display ergodicity breaking and heterogeneous diffusion in the plasma membrane due to such spatiotemporally varying diffusion coefficients [134]. Similarly, TIRFM-SPT has revealed ergodicity breaking in the motion of three different membrane proteins in the membranes of neuronal cells [135]. This behavior has been explained in terms of the proteins switching between free and confined diffusion [135].

6.4 Future Directions

Concluding, the dynamics in the plasma membrane are dominated by lateral and transbilayer heterogeneity, protein crowding, and the interactions between the membrane and the actin cytoskeleton. These features effect the emergence of anomalous diffusion and other peculiar phenomena, such as aging and non-ergodicity, which have been explained by a plethora of mechanisms. Unfortunately, the numerous and diverse reports of these effects seem somewhat perplexing, highlighting the need for further research. A fundamental and common discovery is that normal Brownian diffusion is virtually nonexistent in biological membranes, which questions the picture of diffusion-limited reactions provided by dilute model systems.

One of the main challenges in the field is to connect the plethora of reports on anomalous diffusion and the related mechanisms with biological functions. While it is commonly assumed that membrane dynamics are locally shaped by the structural complexities to optimize the performance of biological processes, a consistent theoretical framework is currently missing. Moreover, so far, our understanding on membrane dynamics has led to very few applications. However, it is tempting to speculate that by perturbing membrane dynamics, we could regulate the formation of protein oligomers and lipid–protein complexes and therefore inhibit or promote the function of membrane proteins [259, 260]. Unfortunately, such medical applications likely lie still very far ahead.

Encouragingly, recent advances in experimental methodologies have enabled studies of dynamics in the plasma membranes of living cells at an unforeseen resolution. The full capabilities of such experiments are best exploited if they are coupled to theoretical

efforts and the descriptive power of ever more advanced computer simulations. With such a toolkit, we are poised to eventually reach a breakthrough in understanding the interplay of membrane dynamics and biological functions. Hopefully, the small steps taken in this Thesis will turn out to be useful in guiding the work of such interdisciplinary attempts.

REFERENCES

[1] B. Alberts, D. Bray, K. Hopkin, A. Johnson, J. Lewis, M. Raff, K. Roberts, and P. Walter, *Essential Cell Biology*. Garland Science, 2009, ISBN: 0815341296.

[2] E. Sezgin, I. Levental, S. Mayor, and C. Eggeling, "The Mystery of Membrane Organization: Composition, Regulation and Roles of Lipid Rafts", *Nature Reviews Molecular Cell Biology*, vol. 18, no. 6, p. 361, 2017.

[3] A. Zachowski, "Phospholipids in Animal Eukaryotic Membranes: Transverse Asymmetry and Movement.", *Biochemical Journal*, vol. 294, no. Pt 1, pp. 1–14, 1993.

[4] A. D. Dupuy and D. M. Engelman, "Protein Area Occupancy at the Center of the Red Blood Cell Membrane", *Proceedings of the National Academy of Sciences of the United States of America*, vol. 105, no. 8, pp. 2848–2852, 2008.

[5] J. P. Overington, B. Al-Lazikani, and A. L. Hopkins, "How Many Drug Targets Are There?", *Nature Reviews Drug Discovery*, vol. 5, no. 12, pp. 993–996, 2006.

[6] A. Krogh, B. Larsson, G. Von Heijne, and E. L. Sonnhammer, "Predicting Transmembrane Protein Topology with a Hidden Markov Model: Application to Complete Genomes", *Journal of Molecular Biology*, vol. 305, no. 3, pp. 567–580, 2001.

[7] M. Bouvier, "Oligomerization of G-Protein-Coupled Transmitter Receptors", *Nature Reviews Neuroscience*, vol. 2, no. 4, pp. 274–286, 2001.

[8] D. Lingwood and K. Simons, "Lipid Rafts as a Membrane-Organizing Principle", *Science*, vol. 327, no. 5961, pp. 46–50, 2010.

[9] A. Laganowsky, E. Reading, T. M. Allison, M. B. Ulmschneider, M. T. Degiacomi, A. J. Baldwin, and C. V. Robinson, "Membrane Proteins Bind Lipids Selectively to Modulate Their Structure and Function", *Nature*, vol. 510, no. 7503, pp. 172–175, 2014.

[10] P. F. Almeida, W. Vaz, and T. Thompson, "Lateral Diffusion in the Liquid Phases of Dimyristoylphosphatidylcholine/Cholesterol Lipid Bilayers: A Free Volume Analysis.", *Biochemistry*, vol. 31, no. 29, pp. 6739–6747, 1992.

[11] E. Falck, T. Róg, M. Karttunen, and I. Vattulainen, "Lateral Diffusion in Lipid Membranes through Collective Flows", *Journal of the American Chemical Society*, vol. 130, no. 1, pp. 44–45, 2008.

[12] P. Saffman and M. Delbrück, "Brownian Motion in Biological Membranes", *Proceedings of the National Academy of Sciences of the United States of America*, vol. 72, no. 8, pp. 3111–3113, 1975.

[13] P. Saffman, "Brownian Motion in Thin Sheets of Viscous Fluid", *Journal of Fluid Mechanics*, vol. 73, no. 4, pp. 593–602, 1976.

[14] R. Peters and R. J. Cherry, "Lateral and Rotational Diffusion of Bacteriorhodopsin in Lipid Bilayers: Experimental Test of the Saffman-Delbrück Equations", *Proceedings of the National Academy of Sciences of the United States of America*, vol. 79, no. 14, pp. 4317–4321, 1982.

[15] M. R. Horton, F. Höfling, J. O. Rädler, and T. Franosch, "Development of Anomalous Diffusion among Crowding Proteins", *Soft Matter*, vol. 6, no. 12, pp. 2648–2656, 2010.

[16] J.-H. Jeon, H. M.-S. Monne, M. Javanainen, and R. Metzler, "Anomalous Diffusion of Phospholipids and Cholesterols in a Lipid Bilayer and Its Origins", *Physical Review Letters*, vol. 109, no. 18, p. 188 103, 2012.

[17] L. Yetukuri, K. Ekroos, A. Vidal-Puig, and M. Orešič, "Informatics and Computational Strategies for the Study of Lipids", *Molecular Biosystems*, vol. 4, no. 2, pp. 121–127, 2008.

[18] J. B. de la Serna, G. J. Schütz, C. Eggeling, and M. Cebecauer, "There is No Simple Model of the Plasma Membrane Organization", *Frontiers in Cell and Developmental Biology*, vol. 4, p. 106, 2016.

[19] S. Singer and G. L. Nicolson, "The Fluid Mosaic Model of the Structure of Cell Membranes", *Science*, vol. 175, no. 4023, pp. 720–731, 1972.

[20] G. L. Nicolson, "The Fluid–Mosaic Model of Membrane Structure: Still Relevant to Understanding the Structure, Function and Dynamics of Biological Membranes After More Than 40 Years", *Biochimica et Biophysica Acta (BBA) - Biomembranes*, vol. 1838, no. 6, pp. 1451–1466, 2014.

[21] D. M. Engelman, "Membranes Are More Mosaic Than Fluid", *Nature*, vol. 438, no. 7068, pp. 578–580, 2005.

[22] K. Simons and E. Ikonen, "Functional Rafts in Cell Membranes", *Nature*, vol. 387, no. 6633, pp. 569–572, 1997.

[23] K. Simons and D. Toomre, "Lipid Rafts and Signal Transduction", *Nature Reviews Molecular Cell Biology*, vol. 1, no. 1, pp. 31–39, 2000.

[24] E. Sevcsik and G. J. Schütz, "With or without Rafts? Alternative Views on Cell Membranes", *Bioessays*, vol. 38, no. 2, pp. 129–139, 2016.

[25] C. Eggeling, C. Ringemann, R. Medda, G. Schwarzmann, K. Sandhoff, S. Polyakova, V. N. Belov, B. Hein, C. von Middendorff, A. Schönle, and S. W. Hell, "Direct Observation of the Nanoscale Dynamics of Membrane Lipids in a Living Cell", *Nature*, vol. 457, no. 7233, pp. 1159–1162, 2009.

[26] R. Regmi, P. M. Winkler, V. Flauraud, K. J. Borgman, C. Manzo, J. Brugger, H. Rigneault, J. Wenger, and M. F. García-Parajo, "Planar Optical Nanoantennas Resolve Cholesterol-Dependent Nanoscale Heterogeneities in the Plasma Membrane of Living Cells", *Nano Letters*, vol. 17, no. 10, pp. 6295–6302, 2017.

[27] G. Vicidomini, H. Ta, A. Honigmann, V. Mueller, M. P. Clausen, D. Waithe, S. Galiani, E. Sezgin, A. Diaspro, S. W. Hell, and C. Eggeling, "STED-FLCS: An Advanced Tool to Reveal Spatiotemporal Heterogeneity of Molecular Membrane Dynamics", *Nano Letters*, vol. 15, no. 9, pp. 5912–5918, 2015.

[28] S. L. Veatch and S. L. Keller, "Separation of Liquid Phases in Giant Vesicles of Ternary Mixtures of Phospholipids and Cholesterol", *Biophysical Journal*, vol. 85, no. 5, pp. 3074–3083, 2003.

[29] S. L. Veatch and S. L. Keller, "Miscibility Phase Diagrams of Giant Vesicles Containing Sphingomyelin", *Physical Review Letters*, vol. 94, no. 14, p. 148 101, 2005.

[30] T. Baumgart, A. T. Hammond, P. Sengupta, S. T. Hess, D. A. Holowka, B. A. Baird, and W. W. Webb, "Large-Scale Fluid/Fluid Phase Separation of Proteins and Lipids in Giant Plasma Membrane Vesicles", *Proceedings of the National Academy of Sciences of the United States of America*, vol. 104, no. 9, pp. 3165–3170, 2007.

[31] I. Levental, F. J. Byfield, P. Chowdhury, F. Gai, T. Baumgart, and P. A. Janmey, "Cholesterol-Dependent Phase Separation in Cell-Derived Giant Plasma-Membrane Vesicles", *Biochemical Journal*, vol. 424, no. 2, pp. 163–167, 2009.

[32] A. R. Honerkamp-Smith, S. L. Veatch, and S. L. Keller, "An Introduction to Critical Points for Biophysicists; Observations of Compositional Heterogeneity in Lipid Membranes", *Biochimica et Biophysica Acta (BBA) - Biomembranes*, vol. 1788, no. 1, pp. 53–63, 2009.

[33] S. L. Veatch, O. Soubias, S. L. Keller, and K. Gawrisch, "Critical Fluctuations in Domain-Forming Lipid Mixtures", *Proceedings of the National Academy of Sciences of the United States of America*, vol. 104, no. 45, pp. 17 650–17 655, 2007.

[34] S. L. Veatch, P. Cicuta, P. Sengupta, A. Honerkamp-Smith, D. Holowka, and B. Baird, "Critical Fluctuations in Plasma Membrane Vesicles", *ACS Chemical Biology*, vol. 3, no. 5, pp. 287–293, 2008.

[35] S. P. Rayermann, G. E. Rayermann, C. E. Cornell, A. J. Merz, and S. L. Keller, "Hallmarks of Reversible Separation of Living, Unperturbed Cell Membranes into Two Liquid Phases", *Biophysical Journal*, vol. 113, no. 11, pp. 2425–2432, 2017.

[36] J. A. Op den Kamp, "Lipid Asymmetry in Membranes", *Annual Review of Biochemistry*, vol. 48, no. 1, pp. 47–71, 1979.

[37] M. A. Lemmon, "Membrane Recognition by Phospholipid-Binding Domains", *Nature Reviews Molecular Cell Biology*, vol. 9, no. 2, pp. 99–111, 2008.

[38] S. McLaughlin, J. Wang, A. Gambhir, and D. Murray, "PIP_2 and Proteins: Interactions, Organization, and Information Flow", *Annual Review of Biophysics and Biomolecular Structure*, vol. 31, no. 1, pp. 151–175, 2002.

[39] M. Mondal, B. Mesmin, S. Mukherjee, and F. R. Maxfield, "Sterols Are Mainly in the Cytoplasmic Leaflet of the Plasma Membrane and the Endocytic Recycling Compartment in CHO Cells", *Molecular Biology of the Cell*, vol. 20, no. 2, pp. 581–588, 2009.

[40] S.-L. Liu, R. Sheng, J. H. Jung, L. Wang, E. Stec, M. J. O'Connor, S. Song, R. K. Bikkavilli, R. A. Winn, D. Lee, K. Baek, K. Ueda, I. Levitan, K.-P. Kim, and W. Cho, "Orthogonal Lipid Sensors Identify Transbilayer Asymmetry of Plasma Membrane Cholesterol", *Nature Chemical Biology*, vol. 13, no. 3, pp. 268–274, 2017.

[41] T.-Y. Wang and J. R. Silvius, "Cholesterol Does Not Induce Segregation of Liquid-Ordered Domains in Bilayers Modeling the Inner Leaflet of the Plasma Membrane", *Biophysical Journal*, vol. 81, no. 5, pp. 2762–2773, 2001.

[42] M. D. Collins and S. L. Keller, "Tuning Lipid Mixtures to Induce or Suppress Domain Formation across Leaflets of Unsupported Asymmetric Bilayers", *Proceedings of the National Academy of Sciences of the United States of America*, vol. 105, no. 1, pp. 124–128, 2008.

[43] J. D. Perlmutter and J. N. Sachs, "Interleaflet Interaction and Asymmetry in Phase Separated Lipid Bilayers: Molecular Dynamics Simulations", *Journal of the American Chemical Society*, vol. 133, no. 17, pp. 6563–6577, 2011.

[44] M. Schick, "Strongly Correlated Rafts in Both Leaves of an Asymmetric Bilayer", *The Journal of Physical Chemistry B*, vol. 122, pp. 3251–3258, 2017.

[45] S. May, "Trans-Monolayer Coupling of Fluid Domains in Lipid Bilayers", *Soft Matter*, vol. 5, no. 17, pp. 3148–3156, 2009.

[46] J. A. Hamilton, "Fast Flip-Flop of Cholesterol and Fatty Acids in Membranes: Implications for Membrane Transport Proteins", *Current Opinion in Lipidology*, vol. 14, no. 3, pp. 263–271, 2003.

[47] D. Marquardt, F. A. Heberle, T. Miti, B. Eicher, E. London, J. Katsaras, and G. Pabst, "^{1}H NMR Shows Slow Phospholipid Flip-Flop in Gel and Fluid Bilayers", *Langmuir*, vol. 33, no. 15, pp. 3731–3741, 2017.

[48] D. L. Daleke, "Regulation of Transbilayer Plasma Membrane Phospholipid Asymmetry", *Journal of Lipid Research*, vol. 44, no. 2, pp. 233–242, 2003.

[49] F. Contreras, L. Sánchez-Magraner, A. Alonso, and F. M. Goñi, "Transbilayer (Flip-Flop) Lipid Motion and Lipid Scrambling in Membranes", *FEBS Letters*, vol. 584, no. 9, pp. 1779–1786, 2010.

[50] D. A. Fletcher and R. D. Mullins, "Cell Mechanics and the Cytoskeleton", *Nature*, vol. 463, no. 7280, pp. 485–492, 2010.

[51] A. Kusumi, C. Nakada, K. Ritchie, K. Murase, K. Suzuki, H. Murakoshi, R. S. Kasai, J. Kondo, and T. Fujiwara, "Paradigm Shift of the Plasma Membrane Concept from the Two-Dimensional Continuum Fluid to the Partitioned Fluid: High-Speed Single-Molecule Tracking of Membrane Molecules", *Annual Review of Biophysics and Biomolecular Structure*, vol. 34, no. 1, pp. 351–378, 2005.

[52] J. M. Tarbell and L. Cancel, "The Glycocalyx and Its Significance in Human Medicine", *Journal of Internal Medicine*, vol. 280, no. 1, pp. 97–113, 2016.

[53] R. G. Parton and K. Simons, "The Multiple Faces of Caveolae", *Nature Reviews Molecular Cell Biology*, vol. 8, no. 3, pp. 185–194, 2007.

[54] R. G. Anderson, "The Caveolae Membrane System", *Annual Review of Biochemistry*, vol. 67, no. 1, pp. 199–225, 1998.

[55] J. C. Stachowiak, E. M. Schmid, C. J. Ryan, H. S. Ann, D. Y. Sasaki, M. B. Sherman, P. L. Geissler, D. A. Fletcher, and C. C. Hayden, "Membrane Bending by Protein–Protein Crowding", *Nature Cell Biology*, vol. 14, no. 9, pp. 944–949, 2012.

[56] J. Zimmerberg and M. M. Kozlov, "How Proteins Produce Cellular Membrane Curvature", *Nature Reviews Molecular Cell Biology*, vol. 7, no. 1, pp. 9–19, 2006.

[57] H. T. McMahon and J. L. Gallop, "Membrane Curvature and Mechanisms of Dynamic Cell Membrane Remodelling", *Nature*, vol. 438, no. 7068, pp. 590–596, 2005.

[58] M. M. Kamal, D. Mills, M. Grzybek, and J. Howard, "Measurement of the Membrane Curvature Preference of Phospholipids Reveals only Weak Coupling between Lipid Shape and Leaflet Curvature", *Proceedings of the National Academy of Sciences of the United States of America*, vol. 106, no. 52, pp. 22 245–22 250, 2009.

[59] P. S. Niemelä, M. S. Miettinen, L. Monticelli, H. Hammaren, P. Bjelkmar, T. Murtola, E. Lindahl, and I. Vattulainen, "Membrane Proteins Diffuse as Dynamic Complexes with Lipids", *Journal of the American Chemical Society*, vol. 132, no. 22, pp. 7574–7575, 2010.

[60] G. Guigas and M. Weiss, "Effects of Protein Crowding on Membrane Systems", *Biochimica et Biophysica Acta (BBA) - Biomembranes*, vol. 1858, no. 10, pp. 2441–2450, 2016.

[61] S. Ferré, "The GPCR Heterotetramer: Challenging Classical Pharmacology", *Trends in Pharmacological Sciences*, vol. 36, no. 3, pp. 145–152, 2015.

[62] A. P. Minton, "How Can Biochemical Reactions within Cells Differ from Those in Test Tubes?", *Journal of Cell Science*, vol. 119, no. 14, pp. 2863–2869, 2006.

[63] J. A. Dix and A. Verkman, "Crowding Effects on Diffusion in Solutions and Cells", *Annual Reviews in Biophysics*, vol. 37, pp. 247–263, 2008.

[64] Y. Wang, M. Sarkar, A. E. Smith, A. S. Krois, and G. J. Pielak, "Macromolecular Crowding and Protein Stability", *Journal of the American Chemical Society*, vol. 134, no. 40, pp. 16 614–16 618, 2012.

[65] M. S. Almén, K. J. Nordström, R. Fredriksson, and H. B. Schiöth, "Mapping the Human Membrane Proteome: A Majority of the Human Membrane Proteins Can be Classified according to Function and Evolutionary Origin", *BMC Biology*, vol. 7, no. 1, p. 50, 2009.

[66] J. Deisenhofer, O. Epp, K. Miki, R. Huber, and H. Michel, "Structure of the Protein Subunits in the Photosynthetic Reaction Centre of *Rhodopseudomonas Viridis* at 3 Å Resolution", *Nature*, vol. 318, no. 6047, pp. 618–624, 1985.

[67] J. Kendrew, R. Dickerson, B. Strandberg, R. Hart, D. Davies, D. Phillips, and V. Shore, "Structure of Myoglobin", *Nature*, vol. 185, no. 422, pp. 427–1960, 1960.

[68] S. H. White, "The Progress of Membrane Protein Structure Determination", *Protein Science*, vol. 13, no. 7, pp. 1948–1949, 2004.

[69] S. Jayasinghe, K. Hristova, and S. H. White, "MPtopo: A Database of Membrane Protein Topology", *Protein Science*, vol. 10, no. 2, pp. 455–458, 2001.

[70] H. Berman, K. Henrick, and H. Nakamura, "Announcing the Worldwide Protein Data Bank", *Nature Structural and Molecular Biology*, vol. 10, no. 12, p. 980, 2003.

[71] K. Shimizu, W. Cao, G. Saad, M. Shoji, and T. Terada, "Comparative Analysis of Membrane Protein Structure Databases", *Biochimica et Biophysica Acta (BBA) - Biomembranes*, vol. 1860, pp. 1077–1091, 2018.

[72] G. von Heijne, "Membrane-Protein Topology", *Nature Reviews Molecular Cell Biology*, vol. 7, no. 12, pp. 909–918, 2006.

[73] A. Ullrich and J. Schlessinger, "Signal Transduction by Receptors with Tyrosine Kinase Activity", *Cell*, vol. 61, no. 2, pp. 203–212, 1990.

[74] B. K. Kobilka, "G Protein Coupled Receptor Structure and Activation", *Biochimica et Biophysica Acta (BBA) - Biomembranes*, vol. 1768, no. 4, pp. 794–807, 2007.

[75] R. Phillips, T. Ursell, P. Wiggins, and P. Sens, "Emerging Roles for Lipids in Shaping Membrane-Protein Function", *Nature*, vol. 459, no. 7245, pp. 379–385, 2009.

[76] A. G. Lee, "How Lipids Affect the Activities of Integral Membrane Proteins", *Biochimica et Biophysica Acta (BBA) - Biomembranes*, vol. 1666, no. 1, pp. 62–87, 2004.

[77] H. Palsdottir and C. Hunte, "Lipids in Membrane Protein Structures", *Biochimica et Biophysica Acta (BBA) - Biomembranes*, vol. 1666, no. 1, pp. 2–18, 2004.

[78] G. Gimpl, "Interaction of G Protein Coupled Receptors and Cholesterol", *Chemistry and Physics of Lipids*, vol. 199, pp. 61–73, 2016.

[79] A. Bron, J. Tiffany, S. Gouveia, N. Yokoi, and L. Voon, "Functional Aspects of the Tear Film Lipid Layer", *Experimental Eye Research*, vol. 78, no. 3, pp. 347–360, 2004.

[80] J. Goerke, "Pulmonary Surfactant: Functions and Molecular Composition", *Biochimica et Biophysica Acta (BBA) - Molecular Basis of Disease*, vol. 1408, no. 2–3, pp. 79–89, 1998.

[81] J. Pérez-Gil, "Structure of Pulmonary Surfactant Membranes and Films: The Role of Proteins and Lipid–Protein Interactions", *Biochimica et Biophysica Acta (BBA) - Biomembranes*, vol. 1778, no. 7, pp. 1676–1695, 2008.

[82] H. M. Mansour and G. Zografi, "Relationships between Equilibrium Spreading Pressure and Phase Equilibria of Phospholipid Bilayers and Monolayers at the Air–Water Interface", *Langmuir*, vol. 23, no. 7, pp. 3809–3819, 2007.

[83] R. MacDonald and S. Simon, "Lipid Monolayer States and Their Relationships to Bilayers", *Proceedings of the National Academy of Sciences of the United States of America*, vol. 84, no. 12, pp. 4089–4093, 1987.

[84] R. Metzler, J.-H. Jeon, A. G. Cherstvy, and E. Barkai, "Anomalous Diffusion Models and Their Properties: Non-Stationarity, Non-Ergodicity, and Ageing at the Centenary of Single Particle Tracking", *Physical Chemistry Chemical Physics*, vol. 16, no. 44, pp. 24 128–24 164, 2014.

[85] R. Metzler, J.-H. Jeon, and A. Cherstvy, "Non-Brownian Diffusion in Lipid Membranes: Experiments and Simulations", *Biochimica et Biophysica Acta (BBA) - Biomembranes*, vol. 1858, no. 10, pp. 2451–2467, 2016.

[86] A. Fick, "Über Diffusion", *Annalen Der Physik*, vol. 170, no. 1, pp. 59–86, 1855.

[87] R. Brown, "XXVII. A Brief Account of Microscopical Observations Made in the Months of June, July and August 1827, on the Particles Contained in the Pollen of Plants; and on the General Existence of Active Molecules in Organic and Inorganic Bodies", *Philosophical Magazine Series 2*, vol. 4, no. 21, pp. 161–173, 1828.

[88] A. Einstein, "Über die von der Molekularkinetischen Theorie der Wärme Geforderte Bewegung von in Ruhenden Flüssigkeiten Suspendierten Teilchen", *Annalen Der Physik*, vol. 322, no. 8, pp. 549–560, 1905.

[89] M. Von Smoluchowski, "Zur Kinetischen Theorie Der Brownschen Molekularbewegung Und Der Suspensionen", *Annalen Der Physik*, vol. 326, no. 14, pp. 756–780, 1906.

[90] J. Perrin, "Mouvement Brownien Et Réalité Moléculaire", in *Annales de Chimie et de Physique*, vol. 18, 1909, pp. 5–104.

[91] Y. He, S. Burov, R. Metzler, and E. Barkai, "Random Time-Scale Invariant Diffusion and Transport Coefficients", *Physical Review Letters*, vol. 101, no. 5, p. 058 101, 2008.

[92] M. H. Cohen and D. Turnbull, "Molecular Transport in Liquids and Glasses", *The Journal of Chemical Physics*, vol. 31, no. 5, pp. 1164–1169, 1959.

[93] H. Eyring, "The Activated Complex in Chemical Reactions", *The Journal of Chemical Physics*, vol. 3, no. 2, pp. 107–115, 1935.

[94] P. Macedo and T. Litovitz, "On the Relative Roles of Free Volume and Activation Energy in the Viscosity of Liquids", *The Journal of Chemical Physics*, vol. 42, no. 1, pp. 245–256, 1965.

[95] J. E. MacCarthy and J. J. Kozak, "Lateral Diffusion in Fluid Systems", *The Journal of Chemical Physics*, vol. 77, no. 4, pp. 2214–2216, 1982.

[96] H.-J. Galla, W. Hartmann, U. Theilen, and E. Sackmann, "On Two-Dimensional Passive Random Walk in Lipid Bilayers and Fluid Pathways in Biomembranes", *The Journal of Membrane Biology*, vol. 48, no. 3, pp. 215–236, 1979.

[97] W. L. Vaz, R. M. Clegg, and D. Hallmann, "Translational Diffusion of Lipids in Liquid Crystalline Phase Phosphatidylcholine Multibilayers. A Comparison of Experiment with Theory", *Biochemistry*, vol. 24, no. 3, pp. 781–786, 1985.

[98] T. O'Leary, "Lateral Diffusion of Lipids in Complex Biological Membranes", *Proceedings of the National Academy of Sciences of the United States of America*, vol. 84, no. 2, pp. 429–433, 1987.

[99] M. Gudmand, M. Fidorra, T. Bjørnholm, and T. Heimburg, "Diffusion and Partitioning of Fluorescent Lipid Probes in Phospholipid Monolayers", *Biophysical Journal*, vol. 96, no. 11, pp. 4598–4609, 2009.

[100] E. Falck, M. Patra, M. Karttunen, M. T. Hyvönen, and I. Vattulainen, "Lessons of Slicing Membranes: Interplay of Packing, Free Area, and Lateral Diffusion in Phospholipid/Cholesterol Bilayers", *Biophysical Journal*, vol. 87, no. 2, pp. 1076–1091, 2004.

[101] E. Falck, P. Michael, M. Karttunen, M. T. Hyvönen, and I. Vattulainen, "Response to Comment by Almeida *et al.*: Free Area Theories for Lipid Bilayers—predictive or Not?", *Biophysical Journal*, vol. 89, no. 1, pp. 745–752, 2005.

[102] T. Apajalahti, P. Niemelä, P. N. Govindan, M. S. Miettinen, E. Salonen, S.-J. Marrink, and I. Vattulainen, "Concerted Diffusion of Lipids in Raft-like Membranes", *Faraday Discussions*, vol. 144, pp. 411–430, 2010.

[103] C. Armstrong, M. Trapp, J. Peters, T. Seydel, and M. Rheinstädter, "Short Range Ballistic Motion in Fluid Lipid Bilayers Studied by Quasi-Elastic Neutron Scattering", *Soft Matter*, vol. 7, no. 18, pp. 8358–8362, 2011.

[104] S. Busch, C. Smuda, L. C. Pardo, and T. Unruh, "Molecular Mechanism of Long-Range Diffusion in Phospholipid Membranes Studied by Quasielastic Neutron Scattering", *Journal of the American Chemical Society*, vol. 132, no. 10, pp. 3232–3233, 2010.

[105] B. Hughes, B. Pailthorpe, and L. White, "The Translational and Rotational Drag on a Cylinder Moving in a Membrane", *Journal of Fluid Mechanics*, vol. 110, pp. 349–372, 1981.

[106] E. P. Petrov and P. Schwille, "Translational Diffusion in Lipid Membranes beyond the Saffman-Delbrück Approximation", *Biophysical Journal*, vol. 94, no. 5, pp. L41–L43, 2008.

[107] W. L. Vaz and H. Dieter, "Experimental Evidence against the Applicability of the Saffman-Delbrück Model to the Translational Diffusion of Lipids in Phosphatidylcholine Bilayer Membranes", *FEBS Letters*, vol. 152, no. 2, pp. 287–290, 1983.

[108] B. A. Camley, M. G. Lerner, R. W. Pastor, and F. L. Brown, "Strong Influence of Periodic Boundary Conditions on Lateral Diffusion in Lipid Bilayer Membranes", *The Journal of Chemical Physics*, vol. 143, no. 24, p. 243 113, 2015.

[109] S. Ramadurai, A. Holt, V. Krasnikov, G. van den Bogaart, J. A. Killian, and B. Poolman, "Lateral Diffusion of Membrane Proteins", *Journal of the American Chemical Society*, vol. 131, no. 35, pp. 12 650–12 656, 2009.

[110] K. Weiß, A. Neef, Q. Van, S. Kramer, I. Gregor, and J. Enderlein, "Quantifying the Diffusion of Membrane Proteins and Peptides in Black Lipid Membranes with 2-Focus Fluorescence Correlation Spectroscopy", *Biophysical Journal*, vol. 105, no. 2, pp. 455–462, 2013.

[111] F. Oswald, A. Varadarajan, H. Lill, E. J. Peterman, and Y. J. Bollen, "MreB-Dependent Organization of the *E. Coli* Cytoplasmic Membrane Controls Membrane Protein Diffusion", *Biophysical Journal*, vol. 110, no. 5, pp. 1139–1149, 2016.

[112] C. C. Lee and N. O. Petersen, "The Lateral Diffusion of Selectively Aggregated Peptides in Giant Unilamellar Vesicles", *Biophysical Journal*, vol. 84, no. 3, pp. 1756–1764, 2003.

[113] G. Guigas and M. Weiss, "Size-Dependent Diffusion of Membrane Inclusions", *Biophysical Journal*, vol. 91, no. 7, pp. 2393–2398, 2006.

[114] G. Guigas and M. Weiss, "Influence of Hydrophobic Mismatching on Membrane Protein Diffusion", *Biophysical Journal*, vol. 95, no. 3, pp. L25–L27, 2008.

[115] J. E. Goose and M. S. Sansom, "Reduced Lateral Mobility of Lipids and Proteins in Crowded Membranes", *PLoS Computational Biology*, vol. 9, no. 4, e1003033, 2013.

[116] Y. Gambin, R. Lopez-Esparza, M. Reffay, E. Sierecki, N. Gov, M. Genest, R. Hodges, and W. Urbach, "Lateral Mobility of Proteins in Liquid Membranes Revisited", *Proceedings of the National Academy of Sciences of the United States of America*, vol. 103, no. 7, pp. 2098–2102, 2006.

[117] A. Naji, A. J. Levine, and P. A. Pincus, "Corrections to the Saffman-Delbrück Mobility for Membrane Bound Proteins", *Biophysical Journal*, vol. 93, no. 11, pp. L49–L51, 2007.

[118] B. A. Camley and F. L. Brown, "Contributions to Membrane-Embedded-Protein Diffusion beyond Hydrodynamic Theories", *Physical Review E*, vol. 85, no. 6, p. 061 921, 2012.

[119] G. Viswanathan, E. Raposo, and M. Da Luz, "Lévy Flights and Superdiffusion in the Context of Biological Encounters and Random Searches", *Physics of Life Reviews*, vol. 5, no. 3, pp. 133–150, 2008.

[120] M. Javanainen, H. Hammaren, L. Monticelli, J.-H. Jeon, M. S. Miettinen, H. Martinez-Seara, R. Metzler, and I. Vattulainen, "Anomalous and Normal Diffusion of Proteins and Lipids in Crowded Lipid Membranes", *Faraday Discussions*, vol. 161, pp. 397–417, 2013.

[121] B. B. Mandelbrot and J. W. Van Ness, "Fractional Brownian Motions, Fractional Noises and Applications", *SIAM Review*, vol. 10, no. 4, pp. 422–437, 1968.

[122] E. Lutz, "Fractional Langevin Equation", *Physical Review E*, vol. 64, no. 5, p. 051 106, 2001.

[123] J.-H. Jeon and R. Metzler, "Fractional Brownian Motion and Motion Governed by the Fractional Langevin Equation in Confined Geometries", *Physical Review E*, vol. 81, no. 2, p. 021 103, 2010.

[124] S. Burov, J.-H. Jeon, R. Metzler, and E. Barkai, "Single Particle Tracking in Systems Showing Anomalous Diffusion: The Role of Weak Ergodicity Breaking", *Physical Chemistry Chemical Physics*, vol. 13, no. 5, pp. 1800–1812, 2011.

[125] Z. Al-Rekabi and S. Contera, "Multifrequency AFM Reveals Lipid Membrane Mechanical Properties and the Effect of Cholesterol in Modulating Viscoelasticity", *Proceedings of the National Academy of Sciences of the United States of America*, vol. 115, no. 11, pp. 2658–2663, 2018.

[126] E. W. Montroll, "Random Walks on Lattices. III. Calculation of First-Passage Times with Application to Exciton Trapping on Photosynthetic Units", *Journal of Mathematical Physics*, vol. 10, no. 4, pp. 753–765, 1969.

[127] H. Scher and E. W. Montroll, "Anomalous Transit-Time Dispersion in Amorphous Solids", *Physical Review B*, vol. 12, no. 6, p. 2455, 1975.

[128] J. H. Schulz, E. Barkai, and R. Metzler, "Aging Effects and Population Splitting in Single-Particle Trajectory Averages", *Physical Review Letters*, vol. 110, no. 2, p. 020 602, 2013.

[129] A. V. Weigel, B. Simon, M. M. Tamkun, and D. Krapf, "Ergodic and Nonergodic Processes Coexist in the Plasma Membrane as Observed by Single-Molecule Tracking", *Proceedings of the National Academy of Sciences of the United States of America*, vol. 108, no. 16, pp. 6438–6443, 2011.

[130] M. Goiko, J. R. De Bruyn, and B. Heit, "Short-Lived Cages Restrict Protein Diffusion in the Plasma Membrane", *Scientific Reports*, vol. 6, p. 34 987, 2016.

[131] M. Goiko, J. R. de Bruyn, and B. Heit, "Membrane Diffusion Occurs by a Continuous-Time Random Walk Sustained by Vesicular Trafficking", *Biophysical Journal*, vol. 114, no. 12, pp. 2887–2899, 2018.

[132] B. O'Shaughnessy and I. Procaccia, "Diffusion on Fractals", *Physical Review A*, vol. 32, no. 5, p. 3073, 1985.

[133] P. Massignan, C. Manzo, J. Torreno-Pina, M. García-Parajo, M. Lewenstein, and G. Lapeyre Jr, "Nonergodic Subdiffusion from Brownian Motion in an Inhomogeneous Medium", *Physical Review Letters*, vol. 112, no. 15, p. 150 603, 2014.

[134] C. Manzo, J. A. Torreno-Pina, P. Massignan, G. J. Lapeyre Jr, M. Lewenstein, and M. F. G. Parajo, "Weak Ergodicity Breaking of Receptor Motion in Living Cells Stemming from Random Diffusivity", *Physical Review X*, vol. 5, no. 1, p. 011 021, 2015.

[135] A. Weron, K. Burnecki, E. J. Akin, L. Solé, M. Balcerek, M. M. Tamkun, and D. Krapf, "Ergodicity Breaking on the Neuronal Surface Emerges From Random Switching Between Diffusive States", *Scientific Reports*, vol. 7, no. 1, p. 5404, 2017.

[136] M. V. Chubynsky and G. W. Slater, "Diffusing Diffusivity: A Model for Anomalous, yet Brownian, Diffusion", *Physical Review Letters*, vol. 113, no. 9, p. 098 302, 2014.

[137] A. V. Chechkin, F. Seno, R. Metzler, and I. M. Sokolov, "Brownian yet Non-Gaussian Diffusion: From Superstatistics to Subordination of Diffusing Diffusivities", *Physical Review X*, vol. 7, no. 2, p. 021 002, 2017.

[138] S. K. Ghosh, A. G. Cherstvy, D. S. Grebenkov, and R. Metzler, "Anomalous, Non-Gaussian Tracer Diffusion in Crowded Two-Dimensional Environments", *New Journal of Physics*, vol. 18, no. 1, p. 013 027, 2016.

[139] D. Axelrod, D. Koppel, J. Schlessinger, E. Elson, and W. W. Webb, "Mobility Measurement by Analysis of Fluorescence Photobleaching Recovery Kinetics", *Biophysical Journal*, vol. 16, no. 9, pp. 1055–1069, 1976.

[140] Y. Chen, B. C. Lagerholm, B. Yang, and K. Jacobson, "Methods to Measure the Lateral Diffusion of Membrane Lipids and Proteins", *Methods*, vol. 39, no. 2, pp. 147–153, 2006.

[141] T. J. Feder, I. Brust-Mascher, J. P. Slattery, B. Baird, and W. W. Webb, "Constrained Diffusion or Immobile Fraction on Cell Surfaces: A New Interpretation", *Biophysical Journal*, vol. 70, no. 6, pp. 2767–2773, 1996.

[142] F. Höfling and T. Franosch, "Anomalous Transport in the Crowded World of Biological Cells", *Reports on Progress in Physics*, vol. 76, no. 4, p. 046 602, 2013.

[143] A. Lubelski and J. Klafter, "Fluorescence Recovery after Photobleaching: The Case of Anomalous Diffusion", *Biophysical Journal*, vol. 94, no. 12, pp. 4646–4653, 2008.

[144] D. Magde, E. Elson, and W. W. Webb, "Thermodynamic Fluctuations in a Reacting System—Measurement by Fluorescence Correlation Spectroscopy", *Physical Review Letters*, vol. 29, no. 11, p. 705, 1972.

[145] L. Wawrezinieck, H. Rigneault, D. Marguet, and P.-F. Lenne, "Fluorescence Correlation Spectroscopy Diffusion Laws to Probe the Submicron Cell Membrane Organization", *Biophysical Journal*, vol. 89, no. 6, pp. 4029–4042, 2005.

[146] S. W. Hell and J. Wichmann, "Breaking the Diffraction Resolution Limit by Stimulated Emission: Stimulated-Emission-Depletion Fluorescence Microscopy", *Optics Letters*, vol. 19, no. 11, pp. 780–782, 1994.

[147] L. Kastrup, H. Blom, C. Eggeling, and S. W. Hell, "Fluorescence Fluctuation Spectroscopy in Subdiffraction Focal Volumes", *Physical Review Letters*, vol. 94, no. 17, p. 178 104, 2005.

[148] G. Vicidomini, G. Moneron, K. Y. Han, V. Westphal, H. Ta, M. Reuss, J. Engelhardt, C. Eggeling, and S. W. Hell, "Sharper Low-Power STED Nanoscopy by Time Gating", *Nature Methods*, vol. 8, no. 7, pp. 571–573, 2011.

[149] A. Honigmann, V. Mueller, H. Ta, A. Schoenle, E. Sezgin, S. W. Hell, and C. Eggeling, "Scanning STED-FCS Reveals Spatiotemporal Heterogeneity of Lipid Interaction in the Plasma Membrane of Living Cells", *Nature Communications*, vol. 5, 2014.

[150] P. Muehlschlegel, H.-J. Eisler, O. J. Martin, B. Hecht, and D. Pohl, "Resonant Optical Antennas", *Science*, vol. 308, no. 5728, pp. 1607–1609, 2005.

[151] P. M. Winkler, R. Regmi, V. Flauraud, J. Brugger, H. Rigneault, J. Wenger, and M. F. García-Parajo, "Transient Nanoscopic Phase Separation in Biological Lipid Membranes Resolved by Planar Plasmonic Antennas", *ACS Nano*, vol. 11, no. 7, pp. 7241–7250, 2017.

[152] C. Manzo and M. F. Garcia-Parajo, "A Review of Progress in Single Particle Tracking: From Methods to Biophysical Insights", *Reports on Progress in Physics*, vol. 78, no. 12, p. 124 601, 2015.

[153] A. Sergé, N. Bertaux, H. Rigneault, and D. Marguet, "Dynamic Multiple-Target Tracing to Probe Spatiotemporal Cartography of Cell Membranes", *Nature Methods*, vol. 5, no. 8, pp. 687–694, 2008.

[154] K. Lindfors, T. Kalkbrenner, P. Stoller, and V. Sandoghdar, "Detection and Spectroscopy of Gold Nanoparticles Using Supercontinuum White Light Confocal Microscopy", *Physical Review Letters*, vol. 93, no. 3, p. 037 401, 2004.

[155] J. Ortega Arroyo, J. Andrecka, K. Spillane, N. Billington, Y. Takagi, J. Sellers, and P. Kukura, "Label-Free, All-Optical Detection, Imaging, and Tracking of a Single Protein", *Nano Letters*, vol. 14, no. 4, pp. 2065–2070, 2014.

[156] S. Spindler, J. Ehrig, K. König, T. Nowak, M. Piliarik, H. E. Stein, R. W. Taylor, E. Garanger, S. Lecommandoux, and I. D. Alves, "Visualization of Lipids and Proteins at High Spatial and Temporal Resolution Via Interferometric Scattering (iSCAT) Microscopy", *Journal of Physics D: Applied Physics*, vol. 49, no. 27, p. 274 002, 2016.

[157] H.-M. Wu, Y.-H. Lin, T.-C. Yen, and C.-L. Hsieh, "Nanoscopic Substructures of Raft-Mimetic Liquid-Ordered Membrane Domains Revealed by High-Speed Single-Particle Tracking", *Scientific Reports*, vol. 6, p. 20 542, 2016.

[158] D. Axelrod, "Cell-Substrate Contacts Illuminated by Total Internal Reflection Fluorescence.", *The Journal of Cell Biology*, vol. 89, no. 1, pp. 141–145, 1981.

[159] L. Guo, J. Y. Har, J. Sankaran, Y. Hong, B. Kannan, and T. Wohland, "Molecular Diffusion Measurement in Lipid Bilayers over Wide Concentration Ranges: A Comparative Study", *ChemPhysChem*, vol. 9, no. 5, pp. 721–728, 2008.

[160] W. Pfeiffer, T. Henkel, E. Sackmann, W. Knoll, and D. Richter, "Local Dynamics of Lipid Bilayers Studied by Incoherent Quasi-Elastic Neutron Scattering", *Europhysics Letters*, vol. 8, no. 2, p. 201, 1989.

[161] J. P. Embs, F. Juranyi, and R. Hempelmann, "Introduction to Quasielastic Neutron Scattering", *Zeitschrift Für Physikalische Chemie*, vol. 224, no. 1–2, pp. 5–32, 2010.

[162] P. M. Macdonald, Q. Saleem, A. Lai, and H. H. Morales, "NMR Methods for Measuring Lateral Diffusion in Membranes", *Chemistry and Physics of Lipids*, vol. 166, pp. 31–44, 2013.

[163] J. E. Tanner, "Use of the Stimulated Echo in NMR Diffusion Studies", *The Journal of Chemical Physics*, vol. 52, no. 5, pp. 2523–2526, 1970.

[164] M. Bloom, E. Burnell, M. Valic, and G. Weeks, "Nuclear Magnetic Resonance Line Shapes in Lipid Bi-Layer Model Membranes", *Chemistry and Physics of Lipids*, vol. 14, no. 2, pp. 107–112, 1975.

[165] H. A. Scheidt, D. Huster, and K. Gawrisch, "Diffusion of Cholesterol and Its Precursors in Lipid Membranes Studied by ^{1}H Pulsed Field Gradient Magic Angle Spinning NMR", *Biophysical Journal*, vol. 89, no. 4, pp. 2504–2512, 2005.

[166] G. Binnig, C. F. Quate, and C. Gerber, "Atomic Force Microscope", *Physical Review Letters*, vol. 56, no. 9, p. 930, 1986.

[167] D. J. Müller, A. Engel, U. Matthey, T. Meier, P. Dimroth, and K. Suda, "Observing Membrane Protein Diffusion at Subnanometer Resolution", *Journal of Molecular Biology*, vol. 327, no. 5, pp. 925–930, 2003.

[168] I. Casuso, J. Khao, M. Chami, P. Paul-Gilloteaux, M. Husain, J.-P. Duneau, H. Stahlberg, J. N. Sturgis, and S. Scheuring, "Characterization of the Motion of Membrane Proteins Using High-Speed Atomic Force Microscopy", *Nature Nanotechnology*, vol. 7, no. 8, pp. 525–529, 2012.

[169] I. Munguira, I. Casuso, H. Takahashi, F. Rico, A. Miyagi, M. Chami, and S. Scheuring, "Glasslike Membrane Protein Diffusion in a Crowded Membrane", *ACS Nano*, vol. 10, no. 2, pp. 2584–2590, 2016.

[170] M. Chavent, T. Reddy, J. Goose, A. C. E. Dahl, J. E. Stone, B. Jobard, and M. S. Sansom, "Methodologies for the Analysis of Instantaneous Lipid Diffusion in MD Simulations of Large Membrane Systems", *Faraday Discussions*, vol. 169, pp. 455–475, 2014.

[171] A. P. Lyubartsev and A. L. Rabinovich, "Force Field Development for Lipid Membrane Simulations", *Biochimica et Biophysica Acta (BBA) - Biomembranes*, vol. 1858, no. 10, pp. 2483–2497, 2016.

[172] M. J. Robertson, J. Tirado-Rives, and W. L. Jorgensen, "Improved Peptide and Protein Torsional Energetics with the OPLS-AA Force Field", *Journal of Chemical Theory and Computation*, vol. 11, no. 7, pp. 3499–3509, 2015.

[173] A. Maciejewski, M. Pasenkiewicz-Gierula, O. Cramariuc, I. Vattulainen, and T. Rog, "Refined OPLS All-Atom Force Field for Saturated Phosphatidylcholine Bilayers at Full Hydration", *The Journal of Physical Chemistry B*, vol. 118, no. 17, pp. 4571–4581, 2014.

[174] D. P. Tieleman, J. L. MacCallum, W. L. Ash, C. Kandt, Z. Xu, and L. Monticelli, "Membrane Protein Simulations with a United-Atom Lipid and All-Atom Protein Model: Lipid–Protein Interactions, Side Chain Transfer Free Energies and Model Proteins", *Journal of Physics: Condensed Matter*, vol. 18, no. 28, S1221–S1234, 2006.

[175] O. Berger, O. Edholm, and F. Jähnig, "Molecular Dynamics Simulations of a Fluid Bilayer of Dipalmitoylphosphatidylcholine at Full Hydration, Constant Pressure, and Constant Temperature", *Biophysical Journal*, vol. 72, no. 5, pp. 2002–2013, 1997.

[176] M. Manna, M. Niemelä, J. Tynkkynen, M. Javanainen, W. Kulig, D. J. Müller, T. Rog, and I. Vattulainen, "Mechanism of Allosteric Regulation of β2-Adrenergic Receptor by Cholesterol", *eLife*, vol. 5, e18432, 2016.

[177] K. Pluhackova, S. A. Kirsch, J. Han, L. Sun, Z. Jiang, T. Unruh, and R. A. Böckmann, "A Critical Comparison of Biomembrane Force Fields: Structure and Dynamics of Model DMPC, POPC, and POPE Bilayers", *The Journal of Physical Chemistry B*, vol. 120, no. 16, pp. 3888–3903, 2016.

[178] A. Sandoval-Perez, K. Pluhackova, and R. A. Böckmann, "Critical Comparison of Biomembrane Force Fields: Protein–Lipid Interactions at the Membrane Interface", *Journal of Chemical Theory and Computation*, vol. 13, no. 5, pp. 2310–2321, 2017.

[179] S. Rauscher, V. Gapsys, M. J. Gajda, M. Zweckstetter, B. L. de Groot, and H. Grubmüller, "Structural Ensembles of Intrinsically Disordered Proteins Depend Strongly on Force Field: A Comparison to Experiment", *Journal of Chemical Theory and Computation*, vol. 11, no. 11, pp. 5513–5524, 2015.

[180] M. Javanainen, A. Lamberg, L. Cwiklik, I. Vattulainen, and O. S. Ollila, "Atomistic Model for Nearly Quantitative Simulations of Langmuir Monolayers", *Langmuir*, vol. 34, no. 7, pp. 2565–2572, 2018.

[181] A. Catte, M. Girych, M. Javanainen, C. Loison, J. Melcr, M. S. Miettinen, L. Monticelli, J. Määttä, V. S. Oganesyan, O. S. Ollila, J. Tynkkynen, and S. Vilov, "Molecular Electrometer and Binding of Cations to Phospholipid

Bilayers", *Physical Chemistry Chemical Physics*, vol. 18, no. 47, pp. 32 560–32 569, 2016.

[182] A. Botan, F. Favela-Rosales, P. F. Fuchs, M. Javanainen, M. Kanduč, W. Kulig, A. Lamberg, C. Loison, A. Lyubartsev, M. S. Miettinen, L. Monticelli, J. Määttä, O. S. Ollila, M. Retegan, T. Róg, H. Santuz, and J. Tynkkynen, "Toward Atomistic Resolution Structure of Phosphatidylcholine Headgroup and Glycerol Backbone at Different Ambient Conditions", *The Journal of Physical Chemistry B*, vol. 119, no. 49, pp. 15 075–15 088, 2015.

[183] C. Kutzner, S. Páll, M. Fechner, A. Esztermann, B. L. de Groot, and H. Grubmüller, "Best Bang for Your Buck: GPI Nodes for Gromacs Biomolecular Simulations", *Journal of Computational Chemistry*, vol. 36, no. 26, pp. 1990–2008, 2015.

[184] M. J. Abraham, T. Murtola, R. Schulz, S. Páll, J. C. Smith, B. Hess, and E. Lindahl, "GROMACS: High Performance Molecular Simulations through Multi-Level Parallelism from Laptops to Supercomputers", *SoftwareX*, vol. 1, pp. 19–25, 2015.

[185] S. Riniker, J. R. Allison, and W. F. van Gunsteren, "On Developing Coarse-Grained Models for Biomolecular Simulation: A Review", *Physical Chemistry Chemical Physics*, vol. 14, no. 36, pp. 12 423–12 430, 2012.

[186] S. J. Marrink and D. P. Tieleman, "Perspective on the Martini Model", *Chemical Society Reviews*, vol. 42, no. 16, pp. 6801–6822, 2013.

[187] S. J. Marrink, H. J. Risselada, S. Yefimov, D. P. Tieleman, and A. H. De Vries, "The Martini Force Field: Coarse Grained Model for Biomolecular Simulations", *The Journal of Physical Chemistry B*, vol. 111, no. 27, pp. 7812–7824, 2007.

[188] M. Javanainen, H. Martinez-Seara, R. Metzler, and I. Vattulainen, "Diffusion of Integral Membrane Proteins in Protein-Rich Membranes", *The Journal of Physical Chemistry Letters*, vol. 8, no. 17, pp. 4308–4313, 2017.

[189] R. Guixà-González, M. Javanainen, M. Gómez-Soler, B. Cordobilla, J. C. Domingo, F. Sanz, M. Pastor, F. Ciruela, H. Martinez-Seara, and J. Selent, "Membrane Omega-3 Fatty Acids Modulate the Oligomerisation Kinetics of Adenosine A_{2A} and Dopamine D_2 Receptors", *Scientific Reports*, vol. 6, p. 19 839, 2016.

[190] S. J. Marrink, A. H. De Vries, and A. E. Mark, "Coarse Grained Model for Semiquantitative Lipid Simulations", *The Journal of Physical Chemistry B*, vol. 108, no. 2, pp. 750–760, 2004.

[191] P. J. Bond and M. S. Sansom, "Insertion and Assembly of Membrane Proteins via Simulation", *Journal of the American Chemical Society*, vol. 128, no. 8, pp. 2697–2704, 2006.

[192] P. J. Bond, J. Holyoake, A. Ivetac, S. Khalid, and M. S. Sansom, "Coarse-Grained Molecular Dynamics Simulations of Membrane Proteins and Peptides", *Journal of Structural Biology*, vol. 157, no. 3, pp. 593–605, 2007.

[193] L. Monticelli, S. K. Kandasamy, X. Periole, R. G. Larson, D. P. Tieleman, and S.-J. Marrink, "The Martini Coarse-Grained Force Field: Extension to Proteins", *Journal of Chemical Theory and Computation*, vol. 4, no. 5, pp. 819–834, 2008.

[194] D. H. de Jong, G. Singh, W. D. Bennett, C. Arnarez, T. A. Wassenaar, L. V. Schafer, X. Periole, D. P. Tieleman, and S. J. Marrink, "Improved Parameters for the Martini Coarse-Grained Protein Force Field", *Journal of Chemical Theory and Computation*, vol. 9, no. 1, pp. 687–697, 2012.

[195] T. A. Wassenaar, H. I. Ingólfsson, R. A. Böckmann, D. P. Tieleman, and S. J. Marrink, "Computational Lipidomics with Insane: A Versatile Tool for Generating Custom Membranes for Molecular Simulations", *Journal of Chemical Theory and Computation*, vol. 11, no. 5, pp. 2144–2155, 2015.

[196] C. Arnarez, J. J. Uusitalo, M. F. Masman, H. I. Ingólfsson, D. H. de Jong, M. N. Melo, X. Periole, A. H. de Vries, and S. J. Marrink, "Dry Martini, a Coarse-Grained Force Field for Lipid Membrane Simulations with Implicit Solvent", *Journal of Chemical Theory and Computation*, vol. 11, no. 1, pp. 260–275, 2014.

[197] A. C. Stark, C. T. Andrews, and A. H. Elcock, "Toward Optimized Potential Functions for Protein–Protein Interactions in Aqueous Solutions: Osmotic Second Virial Coefficient Calculations Using the Martini Coarse-Grained Force Field", *Journal of Chemical Theory and Computation*, vol. 9, no. 9, pp. 4176–4185, 2013.

[198] M. Javanainen, H. Martinez-Seara, and I. Vattulainen, "Excessive Aggregation of Membrane Proteins in the Martini Model", *PLoS One*, vol. 12, no. 11, e0187936, 2017.

[199] T. A. Wassenaar, K. Pluhackova, R. A. Böckmann, S. J. Marrink, and D. P. Tieleman, "Going Backward: A Flexible Geometric Approach to Reverse Transformation from Coarse Grained to Atomistic Models", *Journal of Chemical Theory and Computation*, vol. 10, no. 2, pp. 676–690, 2014.

[200] A. R. Leach, *Molecular Modelling: Principles and Applications*. Pearson, 2001, ISBN: 0582382106.

[201] D. Frenkel and B. Smit, *Understanding Molecular Simulation: From Algorithms to Applications*. Academic Press, 2001, ISBN: 0122673514.

[202] E. Rougier, A. Munjiza, and N. John, "Numerical Comparison of Some Explicit Time Integration Schemes Used in DEM, FEM/DEM and Molecular Dynamics", *International Journal for Numerical Methods in Engineering*, vol. 61, no. 6, pp. 856–879, 2004.

[203] W. Humphrey, A. Dalke, and K. Schulten, "VMD: Visual Molecular Dynamics", *Journal of Molecular Graphics*, vol. 14, no. 1, pp. 33–38, 1996.

[204] N. Michaud-Agrawal, E. J. Denning, T. B. Woolf, and O. Beckstein, "MDAnalysis: A Toolkit for the Analysis of Molecular Dynamics Simulations", *Journal of Computational Chemistry*, vol. 32, no. 10, pp. 2319–2327, 2011.

[205] G. A. Tribello, M. Bonomi, D. Branduardi, C. Camilloni, and G. Bussi, "PLUMED 2: New Feathers for an Old Bird", *Computer Physics Communications*, vol. 185, no. 2, pp. 604–613, 2014.

[206] M. R. Shirts, D. L. Mobley, J. D. Chodera, and V. S. Pande, "Accurate and Efficient Corrections for Missing Dispersion Interactions in Molecular Simulations", *The Journal of Physical Chemistry B*, vol. 111, no. 45, pp. 13 052–13 063, 2007.

[207] T. Darden, D. York, and L. Pedersen, "Particle Mesh Ewald: An N·log (N) Method for Ewald Sums in Large Systems", *The Journal of Chemical Physics*, vol. 98, no. 12, pp. 10 089–10 092, 1993.

[208] U. Essmann, L. Perera, M. L. Berkowitz, T. Darden, H. Lee, and L. G. Pedersen, "A Smooth Particle Mesh Ewald Method", *The Journal of Chemical Physics*, vol. 103, no. 19, pp. 8577–8593, 1995.

[209] S. Páll and B. Hess, "A Flexible Algorithm for Calculating Pair Interactions on SIMD Architectures", *Computer Physics Communications*, vol. 184, no. 12, pp. 2641–2650, 2013.

[210] J. Delhommelle and P. Millié, "Inadequacy of the Lorentz-Berthelot Combining Rules for Accurate Predictions of Equilibrium Properties by Molecular Simulation", *Molecular Physics*, vol. 99, no. 8, pp. 619–625, 2001.

[211] M. A. Lomize, A. L. Lomize, I. D. Pogozheva, and H. I. Mosberg, "OPM: Orientations of Proteins in Membranes Database", *Bioinformatics*, vol. 22, no. 5, pp. 623–625, 2006.

[212] P. J. Stansfeld, J. E. Goose, M. Caffrey, E. P. Carpenter, J. L. Parker, S. Newstead, and M. S. Sansom, "MemProtMD: Automated Insertion of Membrane Protein Structures into Explicit Lipid Membranes", *Structure*, vol. 23, no. 7, pp. 1350–1361, 2015.

[213] E. L. Wu, X. Cheng, S. Jo, H. Rui, K. C. Song, E. M. Dávila-Contreras, Y. Qi, J. Lee, V. Monje-Galvan, R. M. Venable, J. B. Klauda, and W. Im, "CHARMM-GUI Membrane Builder toward Realistic Biological Membrane Simulations", *Journal of Computational Chemistry*, vol. 35, no. 27, pp. 1997–2004, 2014.

[214] Y. Qi, H. I. Ingólfsson, X. Cheng, J. Lee, S. J. Marrink, and W. Im, "CHARMM-GUI Martini Maker for Coarse-Grained Simulations with the Martini Force Field", *Journal of Chemical Theory and Computation*, vol. 11, no. 9, pp. 4486–4494, 2015.

[215] J. Lee, X. Cheng, J. M. Swails, M. S. Yeom, P. K. Eastman, J. A. Lemkul, S. Wei, J. Buckner, J. C. Jeong, Y. Qi, S. Jo, V. S. Pande, D. A. Case, L. Brooks Charles, A. D. MacKerell, J. B. Klauda, and W. Im, "CHARMM-GUI Input Generator for NAMD, Gromacs, Amber, OpenMM, and CHARMM/OpenMM Simulations Using the CHARMM36 Additive Force Field", *Journal of Chemical Theory and Computation*, vol. 12, no. 1, pp. 405–413, 2015.

[216] M. Javanainen and H. Martinez-Seara, "Efficient Preparation and Analysis of Membrane and Membrane Protein Systems", *Biochimica et Biophysica Acta (BBA) - Biomembranes*, vol. 1858, no. 10, pp. 2468–2482, 2016.

[217] J. Wong-ekkabut and M. Karttunen, "The Good, the Bad and the User in Soft Matter Simulations", *Biochimica et Biophysica Acta (BBA) - Biomembranes*, vol. 1858, no. 10, pp. 2529–2538, 2016.

[218] E. V. Bocharov, M. L. Mayzel, P. E. Volynsky, M. V. Goncharuk, Y. S. Ermolyuk, A. A. Schulga, E. O. Artemenko, R. G. Efremov, and A. S. Arseniev, "Spatial Structure and pH-Dependent Conformational Diversity of Dimeric

Transmembrane Domain of the Receptor Tyrosine Kinase EphA1", *Journal of Biological Chemistry*, vol. 283, no. 43, pp. 29 385–29 395, 2008.

[219] E. V. Bocharov, D. M. Lesovoy, K. V. Pavlov, Y. E. Pustovalova, O. V. Bocharova, and A. S. Arseniev, "Alternative Packing of EGFR Transmembrane Domain Suggests that Protein–Lipid Interactions Underlie Signal Conduction across Membrane", *Biochimica et Biophysica Acta (BBA) - Biomembranes*, vol. 1858, no. 6, pp. 1254–1261, 2016.

[220] L. Chen, M. Merzlyakov, T. Cohen, Y. Shai, and K. Hristova, "Energetics of ErbB1 Transmembrane Domain Dimerization in Lipid Bilayers", *Biophysical Journal*, vol. 96, no. 11, pp. 4622–4630, 2009.

[221] E. O. Artemenko, N. S. Egorova, A. S. Arseniev, and A. V. Feofanov, "Transmembrane Domain of EphA1 Receptor Forms Dimers in Membrane-like Environment", *Biochimica et Biophysica Acta (BBA) - Biomembranes*, vol. 1778, no. 10, pp. 2361–2367, 2008.

[222] M. Höltje, T. Förster, B. Brandt, T. Engels, W. von Rybinski, and H.-D. Höltje, "Molecular Dynamics Simulations of Stratum Corneum Lipid Models: Fatty Acids and Cholesterol", *Biochimica et Biophysica Acta (BBA) - Biomembranes*, vol. 1511, no. 1, pp. 156–167, 2001.

[223] W. L. Jorgensen, J. Chandrasekhar, J. D. Madura, R. W. Impey, and M. L. Klein, "Comparison of Simple Potential Functions for Simulating Liquid Water", *The Journal of Chemical Physics*, vol. 79, no. 2, pp. 926–935, 1983.

[224] M. Javanainen, L. Monticelli, J. B. de la Serna, and I. Vattulainen, "Free Volume Theory Applied to Lateral Diffusion in Langmuir Monolayers: Atomistic Simulations for a Protein-Free Model of Lung Surfactant", *Langmuir*, vol. 26, no. 19, pp. 15 436–15 444, 2010.

[225] H. M. Berman, J. Westbrook, Z. Feng, G. Gilliland, T. N. Bhat, H. Weissig, I. N. Shindyalov, and P. E. Bourne, "The Protein Data Bank, 1999–", in *International Tables for Crystallography Volume F: Crystallography of biological macromolecules*, Springer, 2006, pp. 675–684.

[226] A. Šali and T. L. Blundell, "Comparative Protein Modelling by Satisfaction of Spatial Restraints", *Journal of Molecular Biology*, vol. 234, no. 3, pp. 779–815, 1993.

[227] X. Periole, M. Cavalli, S.-J. Marrink, and M. A. Ceruso, "Combining an Elastic Network with a Coarse-Grained Molecular Force Field: Structure, Dynamics, and Intermolecular Recognition", *Journal of Chemical Theory and Computation*, vol. 5, no. 9, pp. 2531–2543, 2009.

[228] M. G. Wolf, M. Hoefling, C. Aponte-Santamaría, H. Grubmüller, and G. Groenhof, "g_membed: Efficient Insertion of a Membrane Protein into an Equilibrated Lipid Bilayer with Minimal Perturbation", *Journal of Computational Chemistry*, vol. 31, no. 11, pp. 2169–2174, 2010.

[229] T. H. Schmidt and C. Kandt, "Lambada and Inflategro2: Efficient Membrane Alignment and Insertion of Membrane Proteins for Molecular Dynamics Simulations", *Journal of Chemical Information and Modeling*, vol. 52, no. 10, pp. 2657–2669, 2012.

[230] R. Staritzbichler, C. Anselmi, L. R. Forrest, and J. D. Faraldo-Gómez, "Griffin: A Versatile Methodology for Optimization of Protein–Lipid Interfaces for Membrane Protein Simulations", *Journal of Chemical Theory and Computation*, vol. 7, no. 4, pp. 1167–1176, 2011.

[231] C. Kandt, W. L. Ash, and D. P. Tieleman, "Setting up and Running Molecular Dynamics Simulations of Membrane Proteins", *Methods*, vol. 41, no. 4, pp. 475–488, 2007.

[232] L. Martínez, R. Andrade, E. G. Birgin, and J. M. Martínez, "Packmol: A Package for Building Initial Configurations for Molecular Dynamics Simulations", *Journal of Computational Chemistry*, vol. 30, no. 13, pp. 2157–2164, 2009.

[233] E. Jefferys, Z. A. Sands, J. Shi, M. S. Sansom, and P. W. Fowler, "Alchembed: A Computational Method for Incorporating Multiple Proteins into Complex Lipid Geometries", *Journal of Chemical Theory and Computation*, vol. 11, no. 6, pp. 2743–2754, 2015.

[234] H. Koldsø and M. S. Sansom, "Organization and Dynamics of Receptor Proteins in a Plasma Membrane", *Journal of the American Chemical Society*, vol. 137, no. 46, pp. 14 694–14 704, 2015.

[235] J. M. Johnston and M. Filizola, "Differential Stability of the Crystallographic Interfaces of Mu-and Kappa-Opioid Receptors", *PLoS One*, vol. 9, no. 2, e90694, 2014.

[236] M. Chavent, A. P. Chetwynd, P. J. Stansfeld, and M. S. Sansom, "Dimerization of the EphA1 Receptor Tyrosine Kinase Transmembrane Domain: Insights into the Mechanism of Receptor Activation", *Biochemistry*, vol. 53, no. 42, pp. 6641–6652, 2014.

[237] M. Lelimousin, V. Limongelli, and M. S. Sansom, "Conformational Changes in the Epidermal Growth Factor Receptor: Role of the Transmembrane Domain Investigated by Coarse-Grained Metadynamics Free Energy Calculations", *Journal of the American Chemical Society*, vol. 138, no. 33, pp. 10 611–10 622, 2016.

[238] J. Michalowsky, L. V. Schäfer, C. Holm, and J. Smiatek, "A Refined Polarizable Water Model for the Coarse-Grained Martini Force Field with Long-Range Electrostatic Interactions", *The Journal of Chemical Physics*, vol. 146, no. 5, p. 054 501, 2017.

[239] A. Filippov, G. Orädd, and G. Lindblom, "The Effect of Cholesterol on the Lateral Diffusion of Phospholipids in Oriented Bilayers", *Biophysical Journal*, vol. 84, no. 5, pp. 3079–3086, 2003.

[240] S. Stachura and G. R. Kneller, "Anomalous Lateral Diffusion in Lipid Bilayers Observed by Molecular Dynamics Simulations with Atomistic and Coarse-Grained Force Fields", *Molecular Simulation*, vol. 40, no. 1–3, pp. 245–250, 2014.

[241] E. Flenner, J. Das, M. C. Rheinstädter, and I. Kosztin, "Subdiffusion and Lateral Diffusion Coefficient of Lipid Atoms and Molecules in Phospholipid Bilayers", *Physical Review E*, vol. 79, no. 1, p. 011 907, 2009.

[242] G. Kneller, K. Baczynski, and M. Pasenkiewicz-Gierula, "Communication: Consistent Picture of Lateral Subdiffusion in Lipid Bilayers: Molecular Dynamics Simulation and Exact Results", *Journal of Chemical Physics*, vol. 135, no. 14, p. 141 105, 2011.

[243] E. Bakalis, S. Höfinger, A. Venturini, and F. Zerbetto, "Crossover of Two Power Laws in the Anomalous Diffusion of a Two Lipid Membrane", *The Journal of Chemical Physics*, vol. 142, no. 21, p. 215 102, 2015.

[244] Y. Oh, J. Kim, A. Yethiraj, and B. J. Sung, "Swing Motion as a Diffusion Mechanism of Lipid Bilayers in a Gel Phase", *Physical Review E*, vol. 93, no. 1, p. 012 409, 2016.

[245] N. Shafique, K. E. Kennedy, J. F. Douglas, and F. W. Starr, "Quantifying the Heterogeneous Dynamics of a Simulated Dipalmitoylphosphatidylcholine (DPPC) Membrane", *The Journal of Physical Chemistry B*, vol. 120, no. 23, pp. 5172–5182, 2016.

[246] G. Lindblom and G. Orädd, "Lipid Lateral Diffusion and Membrane Heterogeneity", *Biochimica et Biophysica Acta (BBA) - Biomembranes*, vol. 1788, no. 1, pp. 234–244, 2009.

[247] K. M. Spillane, J. Ortega-Arroyo, G. de Wit, C. Eggeling, H. Ewers, M. I. Wallace, and P. Kukura, "High-Speed Single-Particle Tracking of GM1 in Model Membranes Reveals Anomalous Diffusion Due to Interleaflet Coupling and Molecular Pinning", *Nano Letters*, vol. 14, no. 9, pp. 5390–5397, 2014.

[248] A. L. Duncan, T. Reddy, H. Koldsø, J. Hélie, P. W. Fowler, M. Chavent, and M. S. Sansom, "Protein Crowding and Lipid Complexity Influence the Nanoscale Dynamic Organization of Ion Channels in Cell Membranes", *Scientific Reports*, vol. 7, no. 1, p. 16 647, 2017.

[249] J.-H. Jeon, M. Javanainen, H. Martinez-Seara, R. Metzler, and I. Vattulainen, "Protein Crowding in Lipid Bilayers Gives Rise to Non-Gaussian Anomalous Lateral Diffusion of Phospholipids and Proteins", *Physical Review X*, vol. 6, no. 2, p. 021 006, 2016.

[250] M. Weiss, H. Hashimoto, and T. Nilsson, "Anomalous Protein Diffusion in Living Cells as Seen by Fluorescence Correlation Spectroscopy", *Biophysical Journal*, vol. 84, no. 6, pp. 4043–4052, 2003.

[251] S. J. Sahl, M. Leutenegger, M. Hilbert, S. W. Hell, and C. Eggeling, "Fast Molecular Tracking Maps Nanoscale Dynamics of Plasma Membrane Lipids", *Proceedings of the National Academy of Sciences of the United States of America*, vol. 107, no. 15, pp. 6829–6834, 2010.

[252] M. Triantafilou, S. Morath, A. Mackie, T. Hartung, and K. Triantafilou, "Lateral Diffusion of Toll-Like Receptors Reveals That They are Transiently Confined Within Lipid Rafts on the Plasma Membrane", *Journal of Cell Science*, vol. 117, no. 17, pp. 4007–4014, 2004.

[253] T. Fujiwara, K. Ritchie, H. Murakoshi, K. Jacobson, and A. Kusumi, "Phospholipids Undergo Hop Diffusion in Compartmentalized Cell Membrane", *The Journal of Cell Biology*, vol. 157, no. 6, pp. 1071–1082, 2002.

[254] K. Suzuki, K. Ritchie, E. Kajikawa, T. Fujiwara, and A. Kusumi, "Rapid Hop Diffusion of a G-Protein-Coupled Receptor in the Plasma Membrane as Revealed by Single-Molecule Techniques", *Biophysical Journal*, vol. 88, no. 5, pp. 3659–3680, 2005.

[255] H. Koldsø, T. Reddy, P. W. Fowler, A. L. Duncan, and M. S. Sansom, "Membrane Compartmentalization Reducing the Mobility of Lipids and Proteins within a Model Plasma Membrane", *The Journal of Physical Chemistry B*, vol. 120, no. 34, pp. 8873–8881, 2016.

[256] S. Sadegh, J. L. Higgins, P. C. Mannion, M. M. Tamkun, and D. Krapf, "Plasma Membrane is Compartmentalized by a Self-Similar Cortical Actin Meshwork", *Physical Review X*, vol. 7, no. 1, p. 011 031, 2017.

[257] T. K. Fujiwara, K. Iwasawa, Z. Kalay, T. A. Tsunoyama, Y. Watanabe, Y. M. Umemura, H. Murakoshi, K. G. Suzuki, Y. L. Nemoto, N. Morone, and A. Kusumi, "Confined Diffusion of Transmembrane Proteins and Lipids Induced by the Same Actin Meshwork Lining the Plasma Membrane", *Molecular Biology of the Cell*, vol. 27, no. 7, pp. 1101–1119, 2016.

[258] S. K. Saka, A. Honigmann, C. Eggeling, S. W. Hell, T. Lang, and S. O. Rizzoli, "Multi-Protein Assemblies Underlie the Mesoscale Organization of the Plasma Membrane", *Nature Communications*, vol. 5, p. 4509, 2014.

[259] H. Yin and A. D. Flynn, "Drugging Membrane Protein Interactions", *Annual Review of Biomedical Engineering*, vol. 18, no. 1, pp. 51–76, 2016.

[260] S. R. George, B. F. O'Dowd, and S. P. Lee, "G-Protein-Coupled Receptor Oligomerization and its Potential for Drug Discovery", *Nature Reviews Drug Discovery*, vol. 1, no. 10, pp. 808–820, 2002.

ORIGINAL PUBLICATIONS

I

UNIVERSAL METHOD FOR EMBEDDING PROTEINS INTO COMPLEX LIPID BILAYERS FOR MOLECULAR DYNAMICS SIMULATIONS

by
Matti Javanainen, 2014
Journal of Chemical Theory and Computation vol 10, 2577–2582,
DOI: 10.1021/ct500046e

JCTC Journal of Chemical Theory and Computation

Article

pubs.acs.org/JCTC

Universal Method for Embedding Proteins into Complex Lipid Bilayers for Molecular Dynamics Simulations

Matti Javanainen*

Tampere University of Technology, Tampere, Finland

Supporting Information

ABSTRACT: The growing interest toward membrane protein simulations calls for a universal and efficient protocol for embedding multiple proteins simultaneously into asymmetric many-component lipid membranes. To this end, here, we present a new and simple technique based on pushing proteins into a lipid membrane from its side by applying a high lateral pressure on the system. This approach is compatible with most (if not all) simulation software packages, and it is independent of external program codes. Most importantly, our protocol does not alter the lipid composition or the transmembrane lipid distribution of the host bilayer membrane. It can be employed with both atomistic and coarse-grained models, and it allows multiple proteins to be embedded into a membrane at the same time. It is shown that the protein structure is unaffected by the pressure applied to the system during the procedure, and the simulation resources required for protein insertion are shown to be modest, regarding both atomistic and coarse-grained simulation models.

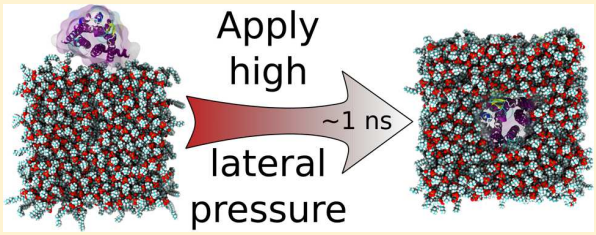

1. INTRODUCTION

During the last two decades, it has become more and more clear that a large fraction of the functions of cells is based on the interplay of membrane proteins and lipids. In many cases, lipids influence the stability of membrane proteins or even modulate their conformation and function.[1−4] This, in part, has become evident from the three-dimensional (3D) crystal structures of membrane proteins that have revealed lipids to be an integral component of protein structure,[5,6] suggesting that there are binding sites for specific lipids. There are also proteins whose function is known to be modulated by specific lipids,[7] even if lipid binding sites seem to be absent. Furthermore, membrane-mediated interactions can also have a role to play in protein activation, as has been highlighted for proteins that are sensitive to membrane elasticity, lateral stress, and membrane curvature.[8]

The current view for membrane protein function is captured by the lipid raft paradigm,[9] which states that there are nanoscale functional units composed of membrane proteins and lipids, and when these match, the function may emerge. The condition for matching the protein(s) with specific lipids relates to both the lateral distribution of lipids around the protein(s), as well as the asymmetric transmembrane lipid distributions,[10−12] since they both can contribute to protein activation. Since they both deal with nanoscale phenomena, the understanding of the structure of lipid raftlike units has remained quite limited.

Molecular simulations are largely the method of choice for unraveling nanoscale phenomena, since they can provide one with almost unlimited accuracy to understand the properties of lipid membranes and lipid−protein complexes. In this context, the progress during the last 2−3 decades has been substantial, as the focus of molecular simulations in membrane systems has shifted from pure lipid systems[13−17] to complex lipid−protein units.[18−25] Meanwhile, studies of multicomponent lipid membranes and their effects on membrane proteins[26] have become increasingly popular, and particular attention has been paid to proteins partitioning into rafts.[27,28] In addition, consideration of asymmetric transmembrane lipid distributions has also become more accurate in simulation studies.[29−33] Important to the progress in the field is also the increase in available computational power and the increasing pace at which new structures for membrane proteins are being determined.[34] Overall, one can summarize that the chances to describe biological membranes in a realistic manner have improved quite dramatically.

However, while computational simulations of membrane proteins have become one of the mainstream areas of membrane biophysics, the methodology for constructing initial structures for these simulations is not well-established. Numerous membrane protein insertion methods have been suggested, but they all suffer from shortcomings (see below for details). Most importantly, many methods involve the removal of lipids from a lipid membrane, therefore altering its lipid composition and lipids' transmembrane distributions upon protein insertion. This can be a serious problem, since, for practical reasons, the size of the studied system should be optimized to the smallest reasonable level in order to access longest possible simulation times. This implies that the removal of even a few lipids might result in significant deviations from the desired lipid distributions, which might alter the desired

Received: January 19, 2014
Published: May 1, 2014

transmembrane symmetry/asymmetry. This, in turn, as explained above, may change the behavior of proteins, since the specific interplay of proteins with their neighboring lipids may be compromised.

In this context, we briefly discuss the previously suggested methods for membrane protein insertion into lipid membranes. For a more thorough report of the available approaches, see the review by Kandt et al.[35]

In the two very earliest attempts to study membrane proteins embedded in a lipid bilayer, the membrane was built around the protein.[36,37] This approach is currently implemented, to the best of our knowledge, only in the CHARMM-GUI,[38,39] which provides an intuitive and highly automatized tool for building heterogeneous membranes around proteins. However, it is restricted to be employed with the CHARMM force field and with the lipid types available in the CHARMM library.

Another method involves the insertion of a protein in a void generated by the removal of overlapping lipid molecules. This is the most straightforward approach available. It can be employed by either deleting all conflicting lipids upon protein insertion, or by allowing some overlap, which is then eliminated during energy minimization.[40] This procedure alters the lipid composition because of the removal of lipids that collide with the protein. In addition, because of the large number of lipid conformations available, the void space resulting from lipid removal might be quite substantial, therefore requiring long re-equilibration. An example of this method can be achieved in GROMACS[41] using the tool GENBOX, which will "solvate" any membrane protein in a provided membrane with the removal of overlapping lipid molecules.

This conceptually simple method has evolved to include various more advanced modifications, too. In general they involve some sort of external forces that facilitate the formation of the void into which the protein is embedded. The simplest approach includes an additional simulation during which a cylindrical repulsive force is applied around the void created by the removal of lipids, thereby enlarging it to a suitable size.[42] In a yet more advanced method, the repulsive forces are not exerted in a cylindrical shape, yet they follow the shape of the protein.[43] First, colliding lipids are removed based on their headgroup locations. The repulsive forces on other surrounding lipid atoms are applied based on the shape of the solvent accessible surface (SAS) of the protein. This approach is available as a GROMACS-compatible tool MAKE_HOLE (also called MDRUN_HOLE). In addition to the issues related to the removal of lipids, this approach relies heavily on the MD engine resulting in code portability problems, and it requires the SAS calculations to be performed usually by third-party software. So far, it has only been implemented in some outdated GROMACS versions. The CHARMM-GUI[38] offers pre-equilibrated membrane patches with cylindrical holes of multiple sizes in them. However, the available bilayers are currently limited to two sizes and only homogeneous bilayers with a few lipid types are available.

A much more refined method is provided by GRIFFIN (GRId-based Force Field INput).[44] In this approach, a void is again generated by the removal of lipids. This is followed by an optimization of the protein/lipid interface based on forces provided by the GRIFFIN software aiming to mimic the presence of the protein. The strength of this method is clearly in being compatible with hollow (i.e., doughnut-like) proteins that can encapsulate lipids in the void at their center. However, GRIFFIN is an external software with multiple dependencies and it needs to be compiled prior to execution. In addition, it is currently limited to being used together with GROMACS or NAMD software packages.

The GROMACS simulation package currently includes a G_MEMBED tool[45] for protein insertion into lipid membranes. In this approach, a small void is generated by lipid removal, followed by inserting a squeezed version of the protein into the membrane. This is followed by inflating the protein back to its real size during which the surrounding lipid molecules are pushed back from the volume occupied eventually by the protein. The largest shortcoming of this approach, as in all methods listed above, is the necessary lipid removal step, which changes the lipid composition of the host bilayer. In addition, the method is currently available exclusively in the GROMACS package, preventing its universal adaptation.

Another clever approach available, InflateGRO,[35] begins with the expansion of the host bilayer by scaling its coordinates. This is followed by insertion of the protein by removal of the colliding lipids and the subsequent stepwise compression and energy minimization steps. This method was recently updated to InflateGRO2, a fully automatized and improved version of the tool.[46] Even though it is commended because of its minimal requirement for manual intervention, the approach also involves lipid removal and it requires external, file-format-dependent tools, making it currently compatible only with the GROMACS package. In the InflateGRO tool, the compression step is supposed to be terminated as the area per lipid matches that of the protein-free bilayer, a quantity quite tedious to estimate for a protein−lipid system. This is overcome in InflateGRO2. However, whereas the previous version allows for embedding of doughnut-shaped proteins encapsulating lipids, this is no longer supported in the updated one. It was also noted that employing the tool results in a loss of membrane hydration.[45]

Allowing the lipid bilayer to spontaneously form around the protein has also been suggested.[35] This is well within the reach of current computational resources, yet again the requirement of desired symmetric or asymmetric lipid composition of the leaflets renders it obsolete.

Here, we present a new approach to membrane protein embedding that is based on pushing the protein into the lipid membrane from one side, followed by relaxation of the membrane area back to equilibrium. Our method does not involve the removal of lipid molecules from the host membrane and it can be employed with both atomistic and coarse-grained approaches, as described below. Most importantly, it can be used with any simulation packages without further modifications or need of external tools, provided that they support semi-isotropic pressure coupling and absolute position restraints, which are standards in all commonly employed simulation packages. In addition, multiple proteins can be embedded at once, which is important since studies involving protein oligomerization and protein crowding effects are becoming increasingly common.[23]

2. EMBEDDING PROTOCOL

The new suggested protein embedding protocol consists of the following steps: (1) placement of the lipid membrane and the protein in the same simulation box; (2) inclusion of required restraints; (3) simulation with applied lateral pressure ("push simulation"); and (4) recovery of the system from the applied lateral pressure ("relaxation simulation").

2.1. Placement of the Lipid Membrane and the Protein in the Same Simulation Box. The protein is positioned next to the membrane in its plane and at such a height that its hydrophobic residues match the hydrophobic core of the membrane (see Figure 1). This manual preparation

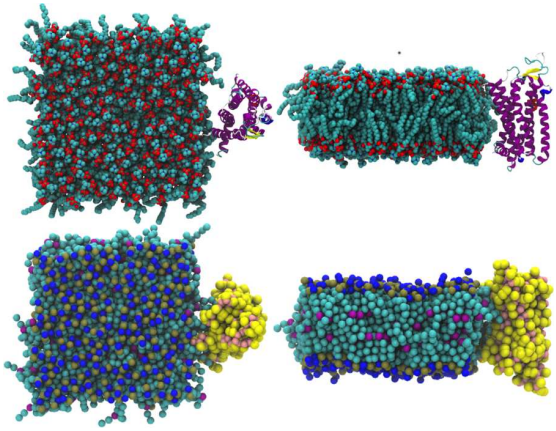

Figure 1. Positioning of a protein next to a lipid bilayer prior to inclusion of lateral pressure in step 1 of the embedding protocol. The positioning is shown for an atomistic system (top row) as well as a coarse-grained system (bottom row). For details of the systems, see discussion in the text. Protein in the coarse-grained system is shown as yellow and pink spheres, whereas in the atomistic system it is depicted with the colors corresponding to its secondary structure. Nitrogen and phosphorus atoms (choline and phosphate groups in the coarse-grained representation) are shown in blue and brown, respectively. Oxygen atoms in the atomistic system are shown in red. All carbon atoms in atomistic system as well as hydrocarbon tails in coarse-grained system are shown in cyan with the coarse-grained beads including the double bond colored purple. Hydrogen atoms and water are not shown for clarity. Snapshots were rendered with the aid of the Tachyon ray tracer[51] supplied with the VMD software.[47]

task can be easily performed by either using graphical tools such as VMD[47] or PyMol,[48] or by employing command line tools supplied with the MD package, e.g., EDITCONF in GROMACS[41] or TRANSLATE in AmberTools.[49] At the same time, the box is enlarged in such a way that the protein fits in it without collisions with the membrane. If the box is made a square in the membrane plane, it will maintain its shape through the process as a semi-isotropic pressure bath is employed. However, the embedding process is accelerated if the length of the simulation box is only increased in the dimension necessary for including the protein. Note also for more-complex purposes that multiple proteins can be embedded at once and their intermolecular distance can be adjusted by altering their initial positioning in the vacuum space next to the bilayer patch. In the case of identical proteins, this is also achieved by single insertion followed by replicating the obtained system. The bilayer employed here can either be hydrated or not. In addition, a pre-equilibrated bilayer as well as its rough approximation from any membrane builder can be employed.

2.2. Inclusion of Required Restraints. During the pushing of the protein into the bilayer, its secondary and ternary structures should remain intact. Therefore, all the atoms of the protein are kept in place by position restraints, which, in many cases, are automatically generated as the protein topology is created. Based on our tests (see below), a force constant of 10 000 kJ mol^{-1} nm^{-2} is adequate for this purpose when using a harmonic potential for the restraints. Other restraining methods are equally acceptable, provided that no structural changes in the protein are observed. In addition, the lipid molecules should not be allowed to escape from the membrane plane to the vacuum created in step 1. Accordingly, one atom of their headgroup (such as a nitrogen atom in the case of a phospholipid with a choline headgroup) is restrained in the direction normal to the membrane plane. In rare occasions when the lipid tails flip toward the vacuum space, the terminal groups of these tails can also be restrained in the direction normal to the membrane plane. This also prevents the tails, in a pre-equilibrated bilayer, from straightening up and beginning to form a gel phase upon the application of pressure. If solvent is present in the system, restraining it (i.e., oxygen atom for water) in the normal direction will accelerate equilibration, since the solvent molecules are not required to escape the hydrophobic membrane core into which they might get trapped without applying these restraints.

2.3. Simulation with Applied Lateral Pressure ("Push Simulation"). The energy of the constructed system is minimized. The system is then simulated with a large lateral pressure with all restraints active. The Berendsen barostat[50] is the natural choice for pressure coupling, because it takes the system to equilibrium rapidly and monotonously. Based on our sample cases (see below), 1000 bar should be adequate for both atomistic and coarse-grained systems. In our example systems, the protein is swallowed by the bilayer in approximately a nanosecond in both atomistic and coarse-grained systems. At this moment, the vacuum space has disappeared around the bilayer and the decrease of the box edge length slows down substantially. These two criteria can be employed to select the end state of the push simulation. The effects of the extended push simulation on the subsequent system relaxation are discussed in the Supporting Information (SI).

2.4. Recovery of the System from the Applied Lateral Pressure ("Relaxation Simulation"). After the protein is surrounded by lipids, another simulation is performed in which the system is allowed to relax to recover the tensionless state of the membrane. In this simulation, only the protein restraints are active. The lateral pressure is simply set to its standard value and the system is simulated until its lateral area is stabilized. In our test cases (see below), this took a few nanoseconds for both atomistic and coarse-grained systems. The validity of these short relaxation simulations is verified in the SI. However, the length of this simulation is expected to be dependent on the system. The equilibration of the area should be checked prior to advancing to the following steps (see below).

The purpose of the relaxation step is to compensate for the effects of the lateral pressure on the membrane. This does not include the relaxation of the protein structure, relative to its environment, which must be performed afterward. Since the removal of protein restraints (often performed during multiple steps) is a standard protocol necessary in all protein insertion methodologies, it will not be discussed here. However, an example on the effect of the relaxation simulation duration on protein structure upon removal of the restraints in given in the SI.

3. EXAMPLE SYSTEMS USED TO DEMONSTRATE THE PRINCIPLE

The proposed approach is applied to three model systems. The embedding of an adenosine A_{2A} receptor (Protein Data Bank[52]

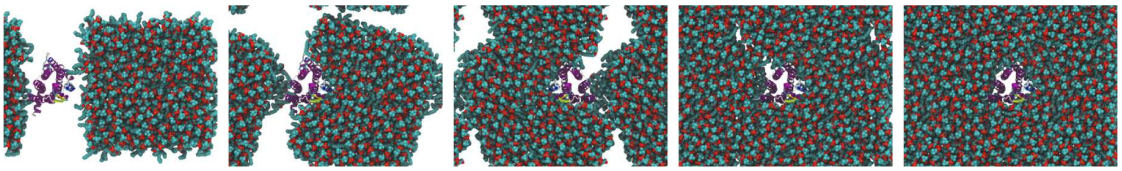

Figure 2. Snapshots presenting the atomistic single-protein insertion process at time steps of 0, 250, 500, 750, and 1000 ps. Coloring is as described in Figure 1.

record 3EML) into a lipid bilayer formed of 288 POPC (1-palmitoyl,2-oleoyl-*sn*-glycero-3-phosphocholine) lipid molecules is considered, employing both atomistic OPLS[53,54] and coarse-grained MARTINI[55,56] approaches using GROMACS. In the atomistic case, we also consider the embedding of two A_{2A} receptors at once. The simulation parameters of these sample cases are made as identical as possible. Water molecules were included in all simulations, even though, in most situations, the speed boost obtained by initially removing them might be greatly beneficial. In addition, the considered host bilayers were adequately pre-equilibrated, even though this is by no means necessary for the insertion process. Upon placing the protein next to the host membrane, the box was made square in both cases.

3.1. Atomistic System. Prior to protein insertion, the atomistic lipid bilayer was constructed and adequately hydrated with either 45 or 60 water molecules per lipid to be used in embedding one and two proteins, respectively. The membranes were then sufficiently equilibrated. Ten (10) Cl^- ions were included per protein to neutralize protein charges. The atomistic insertion and relaxation simulations were performed for 1 and 2 ns, respectively. The simulation parameters for the insertion of one and two proteins were identical. A time step of 2 fs was employed. The nitrogen atom and the terminal carbon atoms of the lipid tails were restrained along the normal of the membrane with a force constant of 10 000 kJ mol^{-1} nm^{-2}. Heavy atoms (non-hydrogen) of the protein were restrained in all three dimensions with a force constant of 10 000 kJ mol^{-1} nm^{-2}. The cutoff radii for both Lennard-Jones and electrostatic interactions were set to 1 nm, beyond which the Particle-Mesh Ewald[57] approach was employed for the latter. A neighbor list of 1 nm was updated every 10 steps. The temperature was kept constant at 310 K with the Berendsen thermostat[50] with a coupling time constant of 0.5 ps. The entire system was coupled together. The pressure was controlled semi-isotropically through the Berendsen barostat,[50] with a coupling time of 20 ps. During protein insertion, the lateral pressure (in the membrane plane) was set to 1000 bar, whereas a value of 1 bar was employed during relaxation simulation. The pressure in the direction of the bilayer normal was always set to 1 bar. A standard workstation computer was able to run the two simulations (without GPU acceleration) within 2 and 4 h, respectively.

3.2. Coarse-Grained System. The protein employed in the atomistic simulations was coarse-grained with the Martinize script. The secondary structure was obtained from the DSSP[58] tool and supplied as an input for the script. A POPC bilayer was constructed and equilibrated with adequate hydration of 45 water molecules per lipid, resulting in a total of 3240 water beads. After including the protein, 10 chlorides were added as counterions for the protein charges.

A simulation time step of 10 fs was employed and the insertion and relaxation simulations were run for 1 and 2 ns, respectively. The choline bead as well as the last beads of the hydrocarbon tails were restrained in the direction normal to the membrane plane with a force constant of 10 000 kJ mol^{-1} nm^{-2}. All protein beads were restrained by a force constant of 10 000 kJ mol^{-1} nm^{-2}. A standard shift approach was employed for nonbonded interactions. Electrostatic and Lennard-Jones interactions were shifted to zero between 0 to 1.2 and 0.9 to 1.2 nm, respectively. A neighbor list with a radius of 1.2 nm was updated every 10 steps. The Berendsen thermostat and barostat[50] were employed for maximal stability and quick relaxation with coupling times of 0.5 and 20 ps, respectively. The reference temperature was set to 310 K, and the entire system was coupled together. Semi-isotropic scaling was employed for the barostat. The reference pressure in the membrane plane was set to 1000 and 1 bar in the insertion and relaxation simulations, respectively, whereas normal to the membrane, a value of 1 bar was employed in both simulations. With this standard setup, the simulated time scales (1−2 ns) were reachable within ∼1 min on a regular desktop workstation.

Based on our tests, the key parameter affecting the stability of the insertion simulation is the coupling time constant of the barostat. Whereas employing 20 ps resulted in a stable simulation in all the cases considered here, increasing this value might be required in some rare cases. This will naturally slightly increase the time needed for the vacuum space to disappear from the simulation box.

3.3. Results Show That the Principle Works. The push simulation is visualized in Figure 2. Additional data are given as a video presentation in the SI. The time evolution of the box edge in both push and relaxation simulations is shown in Figure 3 for both sample cases. Solid lines show data from the push step, whereas the dashed lines refer to relaxation simulations. Black lines stand for the coarse-grained system, whereas blue and red curves show data for the atomistic system in the case of embedding one or two proteins, respectively. The data clearly indicate that very short simulations of ∼1 ns are adequate in

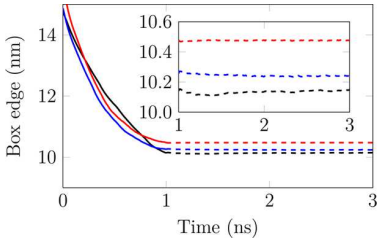

Figure 3. Time evolution of the simulation box edge during protein insertion (solid lines) and relaxation (dashed lines) steps in coarse-grained (black) and atomistic (red and blue) systems. Data for insertion of one and two proteins in an atomistic system are shown in blue and red, respectively. The box edge time evolution during the relaxation simulation is shown in the inset with more detail.

pushing a protein into the bilayer in both atomistic and coarse-grained descriptions of this considered system. This is also clear from the videos provided in the SI. The determination of the suitable end state is trivial either by visually observing the system or by considering the saturation of the box size.

The bilayer itself is not compressed to a large extent, which is indicated by the rapid recovery of the membrane size as the excessive lateral pressure is removed (dashed lines in Figure 3). This is also evident from the time evolution of the box size during much longer relaxation simulations (see the SI). No lipid flip-flops or gel domain formation were observed during the simulations, because of the restraints.

It must be emphasized that the lengths of the simulations employed in the example cases presented in this paper are only guidelines. The proper disappearance of the vacuum space during the push simulation and the area equilibration during the relaxation simulation should always be verified as the required simulation length might vary from one system to another.

The protein structure was basically unaffected by the lateral pressure during the insertion simulations, as can be seen from the root-mean-square deviation (RMSD) of the proteins presented in Figure 4. Dashed lines show the RMSD of proteins under vacuum with the same restraints applied. The small values obtained and the minor increase caused by the lateral pressure in comparison to the vacuum simulations suggest that the chosen force constant of 10 000 kJ mol^{-1} nm^{-2} is sufficient to preserve the secondary structure of the protein during insertion.

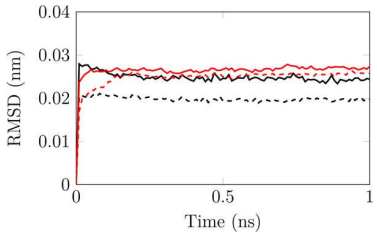

Figure 4. Root-mean-square deviation (RMSD) of protein atoms as a function of time during insertion simulations (solid lines). The RMSD under vacuum is also shown for comparison (dashed lines). Red and black lines show data for atomistic (insertion of one protein) and coarse-grained systems, respectively.

4. CONCLUSIONS

In this article, we have presented a new approach for embedding proteins into lipid membranes. The approach is, in multiple ways, superior to various other methods suggested and employed earlier. It is independent of the employed simulation software and does not rely heavily on software or scripts. It can be employed with all force fields by simply running two fairly short simulations. First, the protein is pushed into the host lipid bilayer by applying a large lateral pressure to the system. This is followed by a quick relaxation simulation, which is essentially required in all protein insertion simulations. No removal of lipids is involved and, therefore, the lipid composition and the transmembrane lipid distribution of the host bilayer are preserved during the insertion process. The suggested approach also allows the simultaneous insertion of multiple proteins. In addition to the examples presented here, the method has been successfully adapted in numerous ongoing studies on various GPCRs, using both atomistic and coarse-grained models.

There are also some downsides of the suggested methodology. First, the required computation time is slightly increased, yet this is compensated for by the lower demand for human effort or input. Based on our tests on atomistic and coarse-grained models, the required equilibration times involved with our method are of the order of a few nanoseconds. Moreover, the area of the host membrane is adequately stabilized during this short period. Therefore, the time scale required by the suggested method is comparable to other existing methods when the required equilibration after protein insertion is considered. In addition, the time requirements of our method pose no challenge for a modern workstation, even in the atomistic system, and the situation is even better with coarse-grained models as simulations in the nanosecond regime require ∼1 min of real time on a standard workstation computer. In addition, considering that the microsecond regime for membrane protein simulations has been available for quite some time[59] and that this time scale is required for proper convergence of these simulations,[60] the imposed requirement is considered acceptable already with the computing power presently available. Second, for the time being, the insertion of conical proteins or doughnut-shaped proteins encapsulating lipids requires some additional manual input. These complicated cases are discussed in the SI.

■ ASSOCIATED CONTENT

Supporting Information

Videos showing the embedding process in the atomistic system. Examination on the effect of the durations of the pushing and relaxation simulations on the system equilibration. The capability of the membrane to host an unrestrained protein after a short relaxation simulation is verified. Discussion on the possible ways to insert conical and doughnut-shaped proteins. This material is available free of charge via the Internet at http://pubs.acs.org/.

■ AUTHOR INFORMATION

Corresponding Author

*Tel.: +358 (0)40 1981185. Fax: +358 (0)3 31153015. E-mail: matti.javanainen@tut.fi.

Notes

The authors declare no competing financial interest.

■ ACKNOWLEDGMENTS

The author is grateful to Ilpo Vattulainen, Hector Martinez-Seara Monné, and Tomasz Róg for fruitful discussions and support and for the colleagues for eagerly employing the methodology on various systems. The author also thanks CSC−IT Center for Science for computational resources and the Finnish Doctoral Programme in Computational Sciences (FICS) for funding.

■ REFERENCES

(1) Lee, A. G. *Biochim. Biophys. Acta, Biomembr.* **2004**, *1666*, 62−87.
(2) Oates, J.; Watts, A. *Curr. Opin. Struct. Biol.* **2011**, *21*, 802−807.
(3) Jafurulla, M.; Chattopadhyay, A. *Curr. Med. Chem.* **2013**, *20*, 47−55.
(4) Phillips, R.; Ursell, T.; Wiggins, P.; Sens, P. *Nature* **2009**, *459*, 379−385.
(5) Solmaz, S. R. N.; Hunte, C. *J. Biol. Chem.* **2008**, *283*, 17542−17549.

(6) Hanson, M. A.; Cherezov, V.; Griffith, M. T.; Roth, C. B.; Jaakola, V.-P.; Chien, E. Y. T.; Velasquez, J.; Kuhn, P.; Stevens, R. C. *Structure* **2008**, *16*, 897−905.
(7) Coskun, U.; Simons, K. *Structure* **2011**, *19*, 1543−1548.
(8) McIntosh, T. J.; Simon, S. A. *Annu. Rev. Biophys. Biomol. Struct.* **2006**, *35*, 177.
(9) Lingwood, D.; Simons, K. *Science* **2010**, *327*, 46−50.
(10) Bretscher, M. S. *Nature (London), New Biol.* **1972**, *236*, 11.
(11) Verhoven, B.; Schlegel, R.; Williamson, P. *J. Exp. Med.* **1995**, *182*, 1597−1601.
(12) van Meer, G. *Cold Spring Harbor Perspect. Biol.* **2011**, *3*, a004671.
(13) Feller, S. E. *Curr. Opin. Colloid Interface Sci.* **2000**, *5*, 217−223.
(14) Pastor, R. W. *Curr. Opin. Struct. Biol.* **1994**, *4*, 486−492.
(15) Tieleman, D. P.; Marrink, S.-J.; Berendsen, H. J. C. *Biochim. Biophys. Acta, Rev. Biomembr.* **1997**, *1331*, 235−270.
(16) Merz, K. M., Jr. *Curr. Opin. Struct. Biol.* **1997**, *7*, 511−517.
(17) Pandit, S. A.; Scott, H. L. *Biochim. Biophys. Acta, Biomembr.* **2009**, *1788*, 136−148.
(18) Lindahl, E.; Sansom, M. S. *Curr. Opin. Struct. Biol.* **2008**, *18*, 425−431.
(19) Gumbart, J.; Wang, Y.; Aksimentiev, A.; Tajkhorshid, E.; Schulten, K. *Curr. Opin. Struct. Biol.* **2005**, *15*, 423−431.
(20) Bond, P. J.; Holyoake, J.; Ivetac, A.; Khalid, S.; Sansom, M. S. *J. Struct. Biol.* **2007**, *157*, 593−605.
(21) Roux, B.; Schulten, K. *Structure* **2004**, *12*, 1343−1351.
(22) Ash, W. L.; Zlomislic, M. R.; Oloo, E. O.; Tieleman, D. P. *Biochim. Biophys. Acta, Biomembr.* **2004**, *1666*, 158−189.
(23) Grossfield, A. *Biochim. Biophys. Acta, Biomembr.* **2011**, *1808*, 1868−1878.
(24) Vattulainen, I.; Rog, T. *Cold Spring Harbor Perspect. Biol.* **2011**, *3*, a004655.
(25) Niemela, P. S.; Miettinen, M.; Monticelli, L.; Hammaren, H.; Bjelkmar, P.; Murtola, T.; Lindahl, E.; Vattulainen, I. *J. Am. Chem. Soc.* **2010**, *132*, 7574−7575.
(26) Sadiq, S. K.; Guixà-González, R.; Dainese, E.; Pastor, M.; De Fabritiis, G.; Selent, J. *Curr. Med. Chem.* **2013**, *20*, 22−38.
(27) Berkowitz, M. L. *Biochim. Biophys. Acta, Biomembr.* **2009**, *1788*, 86−96.
(28) Chini, B.; Parenti, M. *J. Mol. Endocrinol.* **2004**, *32*, 325−338.
(29) Polley, A.; Vemparala, S.; Rao, M. *J. Phys. Chem. B* **2012**, *116*, 13403−13410.
(30) López Cascales, J. J.; Otero, T. F.; Smith, B. D.; Gonzalez, C.; Marquez, M. *J. Phys. Chem. B* **2006**, *110*, 2358−2363.
(31) Gurtovenko, A. A.; Vattulainen, I. *J. Phys. Chem. B* **2008**, *112*, 4629−4634.
(32) Gurtovenko, A. A.; Vattulainen, I. *J. Phys. Chem. B* **2008**, *112*, 1953−1962.
(33) Gurtovenko, A. A.; Vattulainen, I. *J. Am. Chem. Soc.* **2007**, *129*, 5358−5359.
(34) Bill, R. M.; Henderson, P. J.; Iwata, S.; Kunji, E. R.; Michel, H.; Neutze, R.; Newstead, S.; Poolman, B.; Tate, C. G.; Vogel, H. *Nat. Biotechnol.* **2011**, *29*, 335−340.
(35) Kandt, C.; Ash, W. L.; Peter Tieleman, D. *Methods* **2007**, *41*, 475−488.
(36) Edholm, O.; Berger, O.; Jähnig, F. *J. Mol. Biol.* **1995**, *250*, 94−111.
(37) Woolf, T. B.; Roux, B. *Proc. Natl. Acad. Sci. U.S.A.* **1994**, *91*, 11631−11635.
(38) Jo, S.; Kim, T.; Im, W. *PLoS One* **2007**, *2*, e880.
(39) Jo, S.; Lim, J. B.; Klauda, J. B.; Im, W. *Biophys. J.* **2009**, *97*, 50−58.
(40) Tieleman, D.; Berendsen, H. *Biophys. J.* **1998**, *74*, 2786−2801.
(41) Hess, B.; Kutzner, C.; van der Spoel, D.; Lindahl, E. *J. Chem. Theory Comput.* **2008**, *4*, 435−447.
(42) Shen, L.; Bassolino, D.; Stouch, T. *Biophys. J.* **1997**, *73*, 3−20.
(43) Faraldo-Gómez, J. D.; Smith, G. R.; Sansom, M. S. *Eur. Biophys. J.* **2002**, *31*, 217−227.
(44) Staritzbichler, R.; Anselmi, C.; Forrest, L. R.; Faraldo-Gómez, J. D. *J. Chem. Theory Comput.* **2011**, *7*, 1167−1176.
(45) Wolf, M. G.; Hoefling, M.; Aponte-Santamara, C.; Grubmüller, H.; Groenhof, G. *J. Comput. Chem.* **2010**, *31*, 2169−2174.
(46) Schmidt, T. H.; Kandt, C. *J. Chem. Inf. Model.* **2012**, *52*, 2657−2669.
(47) Humphrey, W.; Dalke, A.; Schulten, K. *J. Mol. Graphics* **1996**, *14*, 33−38.
(48) Schrödinger, LLC. *The PyMOL Molecular Graphics System, Version 1.3r1*; unpublished work, 2010.
(49) Case, D. A.; Cheatham, T. E.; Darden, T.; Gohlke, H.; Luo, R.; Merz, K. M.; Onufriev, A.; Simmerling, C.; Wang, B.; Woods, R. J. *J. Comput. Chem.* **2005**, *26*, 1668−1688.
(50) Berendsen, H. J. C.; Postma, J. P. M.; van Gunsteren, W. F.; DiNola, A.; Haak, J. R. *J. Chem. Phys.* **1984**, *81*, 3684.
(51) Stone, J. *Tachyon Parallel/Multiprocessor Ray Tracing System*, Available via the Internet at http://jedi.ks.uiuc.edu/~johns/raytracer/, 1998.
(52) Berman, H. M.; Westbrook, J.; Feng, Z.; Gilliland, G.; Bhat, T. N.; Weissig, H.; Shindyalov, I. N.; Bourne, P. E. *Nucleic Acids Res.* **2000**, *28*, 235−242.
(53) Jorgensen, W. L.; Maxwell, D. S.; Tirado-Rives, J. *J. Am. Chem. Soc.* **1996**, *118*, 11225−11236.
(54) Kaminski, G. A.; Friesner, R. A.; Tirado-Rives, J.; Jorgensen, W. L. *J. Phys. Chem. B* **2001**, *105*, 6474−6487.
(55) Marrink, S. J.; Risselada, H. J.; Yefimov, S.; Tieleman, D. P.; de Vries, A. H. *J. Phys. Chem. B* **2007**, *111*, 7812−7824.
(56) Monticelli, L.; Kandasamy, S. K.; Periole, X.; Larson, R. G.; Tieleman, D. P.; Marrink, S.-J. *J. Chem. Theory Comput.* **2008**, *4*, 819−834.
(57) Darden, T.; York, D.; Pedersen, L. *J. Chem. Phys.* **1993**, *98*, 10089.
(58) Kabsch, W.; Sander, C. *Biopolymers* **1983**, *22*, 2577−2637.
(59) Khelashvili, G.; Grossfield, A.; Feller, S. E.; Pitman, M. C.; Weinstein, H. *Proteins: Struct., Funct., Bioinf.* **2009**, *76*, 403−417.
(60) Grossfield, A.; Feller, S. E.; Pitman, M. C. *Proteins: Struct., Funct., Bioinf.* **2007**, *67*, 31−40.

II

EXCESSIVE AGGREGATION OF MEMBRANE PROTEINS IN THE MARTINI MODEL

by
Matti Javanainen, Hector Martinez-Seara Monne, and Ilpo Vattulainen, 2017
PLoS One vol 12, e0187936,
DOI: 10.1371/journal.pone.0187936

PLOS ONE

RESEARCH ARTICLE

Excessive aggregation of membrane proteins in the Martini model

Matti Javanainen[1,2], **Hector Martinez-Seara**[1,3]*, **Ilpo Vattulainen**[1,2,4]*

1 Laboratory of Physics, Tampere University of Technology, Tampere, Finland, **2** Department of Physics, University of Helsinki, Helsinki, Finland, **3** Institute of Organic Chemistry and Biochemistry, Czech Academy of Sciences, Prague, Czech Republic, **4** Memphys - Center for Biomembrane Physics

* hseara@gmail.com (HMS); ilpo.vattulainen@helsinki.fi (IV)

Citation: Javanainen M, Martinez-Seara H, Vattulainen I (2017) Excessive aggregation of membrane proteins in the Martini model. PLoS ONE 12(11): e0187936. https://doi.org/10.1371/journal.pone.0187936

Editor: Elena Papaleo, Danish Cancer Society Research Center, DENMARK

Received: August 15, 2017

Accepted: October 27, 2017

Published: November 13, 2017

Data Availability Statement: All data discussed in this work are openly available from www.zenodo.org under Creative Commons Attribution 4.0 license: Umbrella Sampling Simulations of TM Domain Dimerization (DOI:10.5281/zenodo.1019733); Simulations of Spontaneous TM Domain Dimer Formation (DOI:10.5281/zenodo.1009183).

Funding: MJ, HMS, and IV thank the Academy of Finland (Centre of Excellence program (grant no. 307415)) and the European Research Council (Advanced Grant CROWDED-PRO-LIPIDS (grant

Abstract

The coarse-grained Martini model is employed extensively to study membrane protein oligomerization. While this approach is exceptionally promising given its computational efficiency, it is alarming that a significant fraction of these studies demonstrate unrealistic protein clusters, whose formation is essentially an irreversible process. This suggests that the protein–protein interactions are exaggerated in the Martini model. If this held true, then it would limit the applicability of Martini to study multi-protein complexes, as the rapidly clustering proteins would not be able to properly sample the correct dimerization conformations. In this work we first demonstrate the excessive protein aggregation by comparing the dimerization free energies of helical transmembrane peptides obtained with the Martini model to those determined from FRET experiments. Second, we show that the predictions provided by the Martini model for the structures of transmembrane domain dimers are in poor agreement with the corresponding structures resolved using NMR. Next, we demonstrate that the first issue can be overcome by slightly scaling down the Martini protein–protein interactions in a manner, which does not interfere with the other Martini interaction parameters. By preventing excessive, irreversible, and non-selective aggregation of membrane proteins, this approach renders the consideration of lateral dynamics and protein–lipid interactions in crowded membranes by the Martini model more realistic. However, this adjusted model does not lead to an improvement in the predicted dimer structures. This implicates that the poor agreement between the Martini model and NMR structures cannot be cured by simply uniformly reducing the interactions between all protein beads. Instead, a careful amino-acid specific adjustment of the protein–protein interactions is likely required.

Introduction

Aggregation of proteins has severe implications for health. For instance, G protein-coupled receptors (GPCRs) form complex functional oligomers that act as drug targets in membranes [1, 2]. Also, the aggregation of misfolded proteins is considered to be the cause of numerous neurodegenerative conditions such as Alzheimer's disease [3]. Without doubt, there is a need to understand how and why proteins arrange themselves into oligomers.

no. 290974)) for financial support. HMS thanks the Czech Science Foundation (grant no. P208/12/G016).

Competing interests: The authors have declared that no competing interests exist.

The molecular dynamics (MD) simulation technique has been applied quite extensively to study the oligomerization and aggregation of membrane proteins including GPCRs [4–11] (see also the extensive review by Periole [12]) as well as members of other membrane protein classes [13, 14]. Quite a few studies have also focused on the lateral diffusion dynamics in protein-rich membranes [15–18]. The most ambitious MD simulations have studied the assembly of respiratory chain supercomplexes [19] and the complete influenza A virion, whose surface is crowded with proteins [20].

All of these studies have used the coarse-grained (CG) Martini model [21–23] or its relatives [24] to probe time and length scales that are beyond the reach of fully atomistic simulations. Especially the Martini model has become very popular in the biomolecular simulation community due to its large library of molecule types, efficiency, as well as availability of high-quality simulation and analysis tools [25–30]. Martini has been parametrized [21] to contain a fairly limited set of bead types, each describing a group of 2–4 heavy atoms. This guarantees speed, simplicity, and transferability, while it also provides an adequate level of chemical specificity for many applications. Notably, the Lennard-Jones (LJ) interactions between the 18 bead types are described by a total of 9 interaction levels with the interaction strength ϵ ranging from 2.0 to 5.6 kJ/mol, and the interaction distance parameter σ having either a value of 0.62 (super repulsive type) or 0.47 nm (all other types). Additional "small" beads used in rings are described with $\sigma = 0.43$ nm together with ϵ that is reduced by 25% of the normal values. The original Martini model [21] also contains a limited set of bonded parameters. The masses are set to either 72 amu or 45 amu ("small types"), and partial charges exist as multiples of 1 e.

The bead types used in the Martini model were selected to provide liquid state conditions at room temperature and also to reproduce the partitioning coefficients of selected solutes between water and organic solvents [21]. Similarly, the Martini protein model [22] was parametrized using the same bead types, though the originally limited bonded interactions were expanded to provide correct geometries for the different amino acids and protein secondary structures. The performance of the parametrization was assessed based on the partitioning of amino acids between water and cyclohexane [22]. The protein force field was later fine-tuned based on the partitioning free energy between water and decane [23]. Even though numerous other checks were performed at both stages of the parametrization—including the evaluation of some amino acid dimerization free energies—[22, 23] the strength of protein–protein interactions—which cannot be predicted from those of individual amino acids—was actually not validated against experimental data [31].

This issue was brought up recently as Stark *et al.* [32] showed that interactions between water-soluble proteins in the Martini model are pronounced, leading to precipitation at concentrations much below the solubility limit [23]. By using the second osmotic virial coefficient as the target experimental value, Stark *et al.* [32] showed that it can be reproduced if the Lennard-Jones interaction strength between protein beads is drastically weakened [32]. In the same spirit, dimerization free energies calculated for membrane proteins and peptides indicate a very strong tendency for dimerization [11, 12, 33–38] as exemplified by the dimerization free energies of about −150 kJ/mol and −160 kJ/mol reported for outer membrane protein F (OmpF) [38] and κ-opioid receptor (KOPr) [11], respectively. Even though free energies cannot be directly linked to dimerization kinetics, it is obvious that such strong affinities indicate irreversible binding.

Förster resonance energy transfer (FRET) enables the calculation of dimerization free energies in simple model liposomes [39] as well as in liposomes constructed from mammalian plasma membrane extracts [40]. FRET provides association constants, which can be converted to dimerization free energy values allowing direct comparison of simulation with experiment. Still, it must be kept in mind that the values provided by FRET are obtained indirectly and are

certainly not free of uncertainties. Notably, a dimer is defined as a state in which the fluorescent labels attached to the monomers—residing outside the membrane—are reasonably close to each other. Despite these limitations, FRET can be considered to be the most reasonable technique to provide dimerization free energies of membrane proteins in lipid membranes.

Consistent experimental dimerization data exist for certain protein types, allowing a straightforward comparison to simulations. The transmembrane (TM) domains of proteins in the receptor tyrosine kinase (RTK) class are a prime example. To begin with, FRET reported a value of −10.5 kJ/mol for the TM segment of an ErbB1 receptor in a DLPC bilayer [41]. Meanwhile, a Martini simulation of this dimer in a DPPC bilayer provided a much larger value of −25.5 kJ/mol [42], and a recent study with a Martini-derived force field on a ErbB1 homology model in a DPPC bilayer reported a value of −38 ± 3 kJ/mol [43]. The dimerization free energy of another RTK TM segment, the Ephrin type-A receptor 1 (EphA1), was measured by FRET to be −15.4 kJ/mol in a DMPC bilayer [44]. Meanwhile, Martini simulation provided a substantially larger value of −60 kJ/mol in a DPPC bilayer [34]. Even though simulation data do not exist for the fibroblast growth factor receptor 3 (FGRF3) that is also a member of the RTK class, experiments in POPC liposomes reported dimerization free energies between −11.3 kJ/mol and −12.6 kJ/mol even when mutations are present [45–48]. Concluding, a number of results for the RTK TM domains point to dimerization free energies in the ballpark of −10 to −15 kJ/mol, while Martini simulations consistently provide too stable dimers with dimerization free energies ranging between −25 and −60 kJ/mol. While there is still room for speculation since the computational setups do not usually match the experimental ones, the significant discrepancy between experiment and Martini model predictions gives rise to concern.

The disagreement is not always this evident. For example, FRET experiments reported Glycophorin A (GpA) dimerization free energies in the range of −(13–17) kJ/mol in various cell membranes [40, 49], while Martini simulations in model bilayers provided much larger values of −26 kJ/mol, −35 kJ/mol, and −40 kJ/mol [50–52]. However, experiments performed using a steric trap obtained values of −50.6 kJ/mol for GpA in a POPC membrane [53], while values of −31.6 kJ/mol [54] and −31.4 kJ/mol [55] were measured by a GALLEX assay in *E. coli* inner membranes.

Similarly, the dimerization free energy of the WALP23 peptide was calculated from a Martini simulation in a DOPC membrane to be −20 kJ/mol [56], while values of −12.2 ± 2 kJ/mol [57] and −15 kJ/mol [58] were measured in DOPC and DLiPC bilayers, respectively. These values can also be compared to those measured for the structurally similar $(AALALAA)_3$ peptide, for which a value of −12.7 ± 0.4 kJ/mol was obtained with FRET [59]. On the other hand, the dimerization free energy of these $(AALALAA)_3$ peptides was seen to be well reproduced with Martini but not with an atomistic force field [31]. Interestingly, a study comparing Martini with several atomistic force fields indicates that the atomistic force fields usually display lower dimerization free energies and some even underestimate them in comparison to experiments. [31]

The large scatter of the above listed experimental values that depend on the experimental technique and setup complicates comparison to simulations. However, most of the listed evidence points towards Martini predicting too strong dimerization. This is a potentially severe issue, since too large dimerization free energies lead to several problems: 1. Extracting information on the lateral diffusion in realistic crowded-like conditions is compromised due to pronounced aggregation, which unrealistically confines the diffusion of proteins as well as lipids. 2. Resolving favorable lipid–protein interactions in membranes with multiple proteins is undermined as the affinity of proteins for the lipid binding sites is higher than that of lipids. 3. Studying protein–protein dimerization interfaces becomes incomplete even in exceedingly

long Martini simulations as proteins aggregate upon first contact and do not properly sample all possible configurations.

In this work, we show that the dimerization free energies obtained using the non-polarizable and polarizable variants of Martini for TM segments of RTKs are substantially larger than those measured in FRET experiments. We also show that the agreement between the simulation-based structures of spontaneously formed TM segment dimers and the structures resolved using NMR leaves a lot of room for improvement. We attempt to improve the situation of the non-polarizable Martini model by downscaling the protein–protein interactions without affecting other carefully parametrized parts of the Martini model. We find that the modification suggested by Stark *et al.* [32] (downscaling of the protein–protein LJ ϵ parameter by 60%) is too drastic to resolve the excessive binding issue found with membrane proteins. On the other hand, applying this modification to only parts of the protein residing in the water phase does not reduce the dimerization energies sufficiently. Meanwhile, when we apply a milder (10%) and uniform reduction in all protein–protein interactions, we find the dimerization free energies of TM segments to closely match experimental data, allowing for studies on membrane dynamics and protein–lipid interactions. However, the simulation structures of spontaneously formed dimers of transmembrane peptides are not improved, which calls for a more careful amino acid specific adjustment of the interaction levels.

Materials and methods

Umbrella sampling simulations

We consider RTK TM domain dimerization as a representative case for studying protein–protein interaction. This choice is made for two reasons. First, a large amount of experimental data exists for this protein class. Many TM domain dimer structures have been resolved by NMR and hence this information can be exploited to validate that the most favorable dimerization interface is studied in the simulations. Second, despite their flexibility, the convergence is more likely with TM domains formed by single helices rather than with more complex proteins, such as those composed of multiple helices or beta barrels.

The EphA1 dimer (PDB [60] entry 2K1L [61]) was embedded [27] in a lipid bilayer comprised of 400 DLPC molecules (indistinguishable from DMPC in Martini). The system was hydrated by 12.5 water beads (corresponding to 50 water molecules) per lipid out of which 10% were presented by the antifreeze type water beads. A physiological salt concentration of 150 mM of NaCl was included to the system (in addition to counter ions) to match the setup employed in experiments [44]. See Fig 1 for selected snapshots of the system.

In addition, a dimer of ErbB1 TM domains (PDB [60] entry 2M0B [62]) was embedded into an identical DLPC bilayer. The only difference to the EphA1 system described above, in addition to the protein, was that the NaCl concentration was higher at 500 mM in order to match the experimental setup [41].

The systems were first simulated for 50 ns with restraints on the dimer, so that the membrane was able to adapt to the newly included dimer. The restraints were then released and the system was simulated for another 50 ns. Next, using the lateral distance between the centers of mass (COMs) of the TM domains as the reaction coordinate, the peptides were pulled apart to generate initial structures for umbrella sampling windows. In these initial structures, the COM distance varied between 0.6 and 5.0 nm with a spacing of 0.2 nm.

The non-polarizable Martini model version 2.2 was employed [23] in the simulations together with the suggested "New-RF" simulation parameter set. [63] More concretely, the reaction field electrostatics and Lennard-Jones potentials were shifted to zero at the cut-off distance of 1.1 nm. A dielectric constant of 15 was employed up to the cut-off length, after which

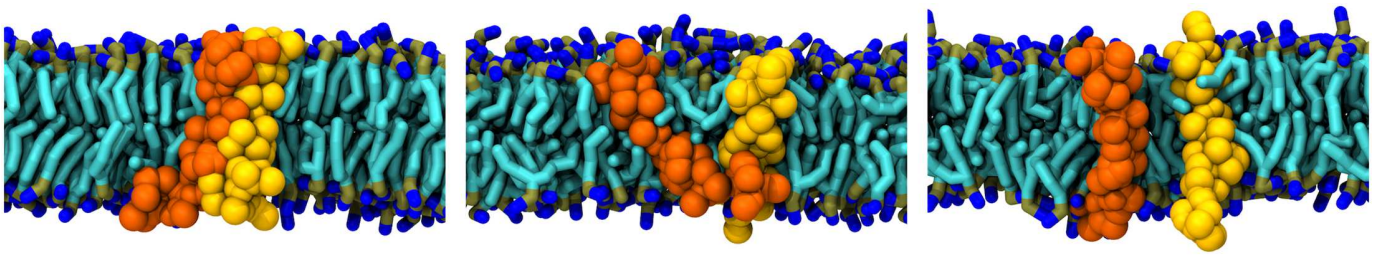

Fig 1. Selected snapshots of transmembrane domain dimerization. Examples of conformations at different COM–COM distances (from top to the bottom: 1.2, 2.0, and 2.4 nm) from the umbrella sampling simulations (COM stands for the center of mass). Here, the U-0.1 scaling method is employed (see below). Chains of lipids (DLPC) are shown in cyan, phosphate beads in brown, and choline beads in blue. Peptides (EphA1) are shown in yellow and orange. Water, antifreeze particles, and ions have been omitted from the images.

https://doi.org/10.1371/journal.pone.0187936.g001

it was given a value of infinity. The Verlet cut-off scheme was employed with parameters defined by Gromacs. Temperatures of the dimer, the lipids, and the solvent were separately kept constant at 303 K with the stochastic velocity rescaling thermostat [64], while pressure was maintained semi-isotropically at 1 bar using the Parrinello–Rahman barostat [65] with a time constant of 12 ps and a compressibility of 3×10^{-4} bar^{-1}. Additionally, as a reference we repeated the umbrella sampling simulations for the EphA1 dimer with the older set of suggested simulation parameters, referred to as "Common" (for details, see Ref. [63]), as well as using the recently updated polarizable parameters [66, 67], combined with the "New-RF" simulation parameters (with a dielectric constant of 2.5) [63]. In all simulations, the elastic network [68] with default options, *i.e.* a force constant of 500 kJ mol^{-1} nm^{-2} and an upper cut-off of 0.9 nm were employed for the TM domains.

For the umbrella sampling, the lateral distance of the COMs of the two TM segments was restrained with a harmonic spring with a constant of 400 kJ mol^{-1} nm^{-2}, which provided a suitable overlap in the umbrella histograms. The selected umbrella windows (see Results) were each simulated for 10 μs with a time step of 20 fs, and the first 50 ns of each window was discarded from analyses. The COM–COM distances were stored every 10 time steps (200 fs). Potential of mean force (PMF) profiles, estimating the free energy profile of dimerization ($G(r)$) were extracted using the `g_wham` tool [69]. The same tool was used to estimate the error bars in the PMF profiles using 100 bootstrap samples. All simulations were performed with the Gromacs version 5.0.x [70].

The dimerization free energy ΔG_{DIM} calculated from FRET experiments corresponds to the probability of the TM segments being in any bound state, *i.e.* the depth of the well in the free energy profile cannot be directly compared to experiment. Rather, an average needs to be calculated using [50]

$$\Delta G_{\mathrm{DIM}} = -RT \ln (K_{\mathrm{a}}), \tag{1}$$

where

$$K_{\mathrm{a}} = \pi \int_0^{r_{\mathrm{max}}} r \exp\left(-\frac{G(r)}{RT}\right) \mathrm{d}r. \tag{2}$$

Here, K_{a} is the association constant, R the gas constant, T the temperature, and $G(r)$ the free energy change (with respect to the chosen zero-level) at a COM–COM distance r. The usual standard state used in FRET experiments [40], 1 nm^2 per receptor, is also adapted here. The $G(r)$ profiles are shifted to zero at a COM–COM distace of 2.75 nm. Most profiles have reached a plateau at this arbitrarily chosen distance. The integration limit (r_{max}) is set to 2.0 nm. The

r_{max} value is larger than the used cutoff lengths, and the increase of r_{max} above 2.0 nm has an insignificant effect on the obtained ΔG_{DIM} value. The error in the ΔG_{DIM} values is the standard deviation of the individual values extracted from the 100 bootstrapped $G(r)$ samples.

Spontaneous dimer formation

We also evaluated the ability of the Martini model to predict the structures of TM domain dimers. For this purpose, we considered TM domains that are known to dimerize [71]. Notably, to this end we chose 1) Glycophorin A dimer (PDB entry 1AFO [72]), 2) integrin αIIbβ3 heterodimer (PDB entry 2K9J [73]), 3) BNIP3 TM domain dimer (PDB entry 2KA1 [74]), 4) T cell receptor signaling module $\zeta\zeta$ (PDB entry 2HAC [75]), and 5) DAP12 signaling subunit dimer (PDB entry 2L34 [76]). As initial simulation structures, the peptides in the dimer structures were separated by $\sim$4 nm and coarse-grained using the `martinize` tool, and embedded in a DLPC bilayer with `insane` [27]. The bilayers consisted of $\sim$400 lipids and were hydrated by $\sim$6000 water beads, out of which 10% was presented with the antifreeze type. About 150 mM of NaCl was added to the water phase together with counter ions.

The assembled systems were first equilibrated for 50 ns with position restraints applied to the protein beads, after which 10 μs simulations for generating initial structures for the production simulations were performed for each system. During these simulations, the distance between the COMs of the peptides was kept at $\sim$4 nm with a harmonic potential with a spring constant of 400 kJ mol^{-1} nm^{-2}. Next, a total of 10 structures were extracted at 1 μs intervals, and employed as independent replicas with different initial structures. The 10 replica simulations were run with both unscaled Martini parameters as well as with the U-0.1 scaling strategy (see below). Therefore, the total number of these unbiased simulations was 5 (dimer structures) × 2 (scaled vs. unscaled) × 10 (replicas). Each of these simulations was run for 40 μs with the "New-RF" simulation parameters (see above), resulting in a total of 4 ms of simulation time.

The quality of the dimeric structures from these unbiased simulations was evaluated from the last 20 μs of simulations using three criteria: root-mean-square deviation (RMSD) of the backbone beads from the coarse-grained NMR structures of the dimer, the deviation of the dimer crossing angles from their values extracted from the coarse-grained NMR structures, and the deviations in the number of inter-peptide contacts (defined with a cut-off of 0.8 nm) between the backbone beads in the coarse-grained NMR structure. The dimer crossing angles were calculated as the mean angles between the principal moments of inertia of the peptides calculated using a single value decomposition of the backbone beads of the residues defining the contact helices (See S1 Table in Supporting Information (SI)).

Order of oligomerization

We evaluated whether EphA1 and ErbB1 form dimers, as observed in experiments [41, 44], or higher order oligomers. To this end, we began with the structures extracted from the umbrella sampling windows with the lateral protein–protein distance equal to $\sim$3 nm. We then replicated this system in the membrane plane four-fold (2 × 2). The systems containing a total of 8 monomers were simulated using both unscaled Martini parameters and the U-0.1 scaling strategy (see below) for 40 μs. The "New-RF" simulation parameters were again used (see above). The center of mass trajectories of the peptides were created with `g_traj` and analyzed with the tool `g_clustsize`. We used a cut-off of 2.5 nm for the clusters, as the radial distribution functions for the peptide COMs converged to zero at approximately this distance.

Adjustment of protein–protein interaction levels

We consider two ways to scale down the LJ interactions among proteins in order to lower the dimerization free energies to a level observed in FRET experiments. These two approaches are described below. In Martini, the LJ interaction parameters are not calculated from combination rules but are instead tabulated as explained in the interaction matrix shown in the original Martini publication [21]. Therefore, the ϵ parameters considered here refer to the interaction parameters of two protein beads (i, j, often denoted $\epsilon_{i,j}$) instead of the LJ parameter of a single bead.

Approach U: Uniform scaling applied to all beads. The Lennard-Jones interactions between all protein beads are here reduced by scaling down ϵ with a fixed scaling parameter α ($\alpha = 0.1$ for a reduction of 10%, etc.). This method is identical (despite the reversed definition of α) to that presented by Stark *et al.* [32] The scaled ϵ-parameter ϵ_{scaled} calculated from the original value $\epsilon_{\text{original}}$ is

$$\epsilon_{\text{scaled}} = \epsilon_{\text{repulsive}} + (1 - \alpha)(\epsilon_{\text{original}} - \epsilon_{\text{repulsive}}), \quad (3)$$

where $\epsilon_{\text{repulsive}}$ corresponds to the weakest (repulsive) interaction in the Martini model (2 kJ/mol). Notably, in this method the values of ϵ are never smaller than 2 kJ/mol, which leads to a smaller spread of ϵ values and hence to less chemical specificity upon increasing α. Unlike in the original work in the aqueous phase, we scale down the protein–protein interactions involving all bead types, including P4, Qa, and Qd. In this paper, the scaled results using this method will be labeled "U-α" with "U" standing for uniform scaling.

Approach W: Scaling applied to water-contacting beads. Motivated by the good agreement with experiment based on scaling protein–protein interactions in water-soluble proteins by 60% ($\alpha = 0.6$) [32], in this approach we scale down the protein–protein interactions of only those beads in membrane proteins that are mostly in contact with water (see details below). The interactions among these beads are adjusted following the approach "U" described above. The results obtained using this method will be labeled "W-α" with "W" standing for water.

The beads to which the scaling was applied were determined as follows: First, the dimer was simulated for 1 μs, and the contacts between each residue with water and lipids were counted after a 50 ns equilibration period. Second, the sesidues that had more contacts with water than with lipids (defined by a cut-off of 0.6 nm) were assigned new particle types, whose mutual interactions were scaled as in the "U" approach. The interactions between scaled and unscaled protein beads remained as in standard Martini.

Results and discussion

Dimerization free energies suggested by Martini are excessive

Using the EphA1 and ErbB1 dimer systems, we evaluated the ability of the Martini model to capture the dimerization free energies of TM domains. Fig 2 depicts the free energy profiles (PMFs) calculated for the EphA1 and the ErbB1 dimer using either the non-polarizable ("Non-Polar.") or the polarizable ("Pol.") Martini model. The use of "Common" simulation parameters instead of the "New-RF" ones is indicated by an asterisk (*). All curves have been shifted to realize convergence to zero at a COM–COM distance of 2.75 nm. The values extracted from these profiles using Eqs (2) and (1) are shown in Table 1.

Using FRET, Artemenko *et al.* [44] measured a dimerization free energy of $\Delta G_{\text{DIM}} = -15.4 \pm 0.5$ kJ/mol for the EphA1 TM domains in DMPC liposomes at 303 K [44], *i.e.* in a setup matching our computational one. They also verified that EphA1 TM segments form dimers and not higher order oligomers. On the other hand, earlier Martini simulations of

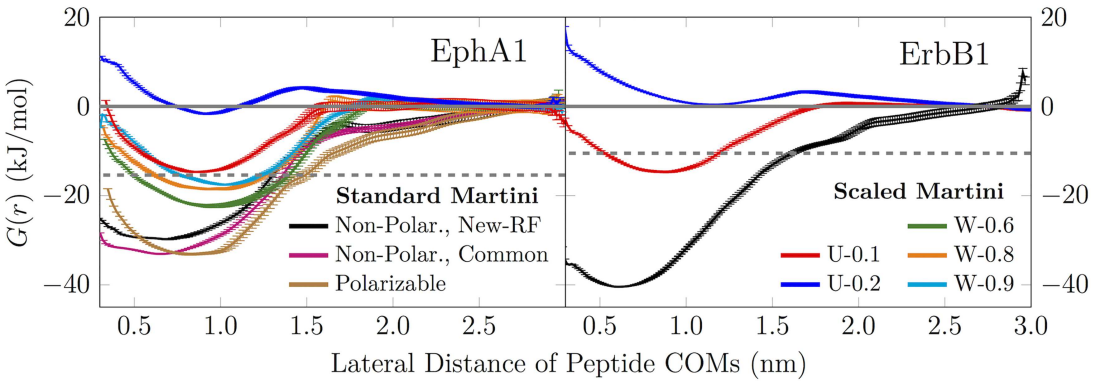

Fig 2. Dimerization free energy profiles of transmembrane domains. Free energy profiles of EphA1 and ErbB1 TM domain dimerization using either unmodified Martini or the "U" and "W" scaling strategies. The solid gray line at a value of zero is to guide the eye. The dashed gray line shows the experimental value for ΔG_{DIM}. Note that the common legend is split between the two panels.

https://doi.org/10.1371/journal.pone.0187936.g002

EphA1 in a DPPC membrane at 323 K provided a drastically different value of −60 ± 2 kJ/mol for the depth of the well in the free energy profile [34].

As shown in Table 1, both the non-polarizable and polarizable Martini models provide values that are drastically higher than the ones obtained from experiments. The non-polarizable Martini provides a value of −29.9 ± 1.0 kJ/mol that is approximately twice the experimental value. Importantly, the choice of simulation parameters ("New-RF" vs. "Common") has a small effect on the value: the dimerization free energy is slightly larger with the latter parameter set likely due to the longer cutoffs for non-bonded interactions. In addition, the polarizable Martini force field also provides very similar results suggesting that it also suffers from protein–protein overbinding. In all these simulations with an unscaled Martini model (non-polarizable or polarizable), the free energy profiles calculated do not fully reach a plateau even at an

Table 1. Transmembrane domain dimerization free energies.

	EphA1	ErbB1
Experimental [41, 44]	−15.4 ± 0.5	−10.5 ± 0.4
Non-Polar. Martini	−29.9 ± 1.0	−39.5 ± 1.0
Non-Polar. Martini*	−32.9 ± 0.5	–
Polar. Martini	−33.5 ± 1.0	–
Scaled U-0.1	−15.2 ± 1.0	−15.3 ± 0.3
Scaled U-0.2	NA	NA
Scaled W-0.6	−23.2 ± 0.8	–
Scaled W-0.8	−19.6 ± 1.4	–
Scaled W-0.9	−18.4 ± 0.4	–
Prev. Studies [34, 42, 43]	−60 ± 2	−25.5 ± 0.6 −38 ± 3

EphA1 and ErbB1 TM domain dimerization free energies ΔG_{DIM} (in kJ/mol) calculated from Eqs (2) and (1). In two cases, the dimer does not represent the minimum free energy state and hence ΔG_{DIM} values cannot be extracted (NA (not available)). The systems marked with "–" were not simulated. The system simulated with the "Common" parameter set instead of the "New-RF" (see Ref. [63]) setup is denoted with *. Standard and polarizable versions of Martini are denoted by "Non-Polar." and "Polar.", respectively.

https://doi.org/10.1371/journal.pone.0187936.t001

inter-protein distance of 3 nm. The protein–protein interactions are so strong that the monomers tilt to maintain any interaction at such large distances, resulting in a monotonous profile.

As to the ErbB1 dimer, FRET measurements by Chen *et al.* [41] in DLPC liposomes (with 500 mM NaCl) for ΔG_{DIM} of the TM domains provided −10.5 ± 0.5 kJ/mol. In these experiments, it was again verified that no higher order oligomers were formed. Notably, two independent FRET techniques were employed, and both of them provided almost identical ΔG_{DIM} values. A recent metadynamics study using the non-polarizable Martini model, on the other hand, provided a much larger value of ΔG_{DIM} = −38 ± 3 kJ/mol in a DPPC bilayer [43]. This value was obtained by a thorough sampling of the two-dimensional free energy surface (COM–COM separation and crossing angle). Additionally, an earlier Monte Carlo study using the Martini model in a DPPC bilayer at 323 K provided a value of ΔG_{DIM} = −25.5 ± 0.6 kJ/mol [42].

The value reported by Lelimousin *et al.* [43] (ΔG_{DIM} = −38 ± 3 kJ/mol) is in excellent agreement with the value we obtained here with the standard Martini model (ΔG_{DIM} = −39.5 ± 1.0 kJ/mol). This suggests that the two-dimensional sampling technique is likely not necessary when the structure of the dimer is readily available from experiments, as is the case with the two TM domains used as examples in this work.

Similarly as for the EphA1 dimer, our free energy profiles converge at unusually large inter-protein distances indicating that the monomers try to remain in contact by tilting toward each other. Indeed, as shown in S1 Fig for the ErbB1 dimer using the non-polarizable Martini (see the SI), the peptides show a systematic tilting at large inter-protein distances.

The experiments for EphA1 and ErbB1 dimerization [41, 44] suggested that neither of these peptides forms higher order oligomers. Using unscaled Martini, we observed that EphA1 rapidly forms two tetramers, while ErbB1 oligomerizes slower but eventually assembles into an octamer. The time evolution of the average size of the oligomers is shown on the left in S3 Fig, and the histogram of the oligomer sizes during the last 10 μs of the simulation on the right in S3 Fig.

Martini cannot predict dimer structures correctly

We also evaluated the ability of the non-polarizable Martini model to predict the structures of five dimers of TM domains, resolved by NMR (see Methods). This provides an alternate comparison between simulation and experiment to the free energies presented in the previous section.

The COM–COM distance of the two peptides is shown in S2 Fig (see the SI), while a careful structural comparison between spontaneously formed dimers and the NMR structures is summarized in Fig 3.

The distances shown in S2 Fig (see the SI) indicate that all observed TM domains form dimers in a few microseconds, as expected. Fig 3 shows that simulations with the standard (non-polarizable) Martini are not able to predict the structures of spontaneously formed dimers correctly. In this figure, the simulation structure coinciding perfectly with the NMR structure would be a purple dot located at the origin. While it is difficult to decide how large deviations from the perfect match are acceptable, we have chosen to highlight in green (Fig 3) a deviation of 10˚ (crossing angle) and 1 nm (RMSD) that we consider to be reasonable. This choice should help in assessing how well the simulation results agree with experimental data. Importantly, our data clearly show that the number of inter-peptide contacts in the dimer is often severely overestimated for the standard Martini, in line with the excessive dimerization free energies. Interestingly, for the 2L34 dimer, all replicas using the standard Martini fall in the same point in the graph, while other dimers show larger scatter of the replicas indicating a more diverse set of molecular conformations. This might result from the irreversible dimerization of the peptides upon first contact.

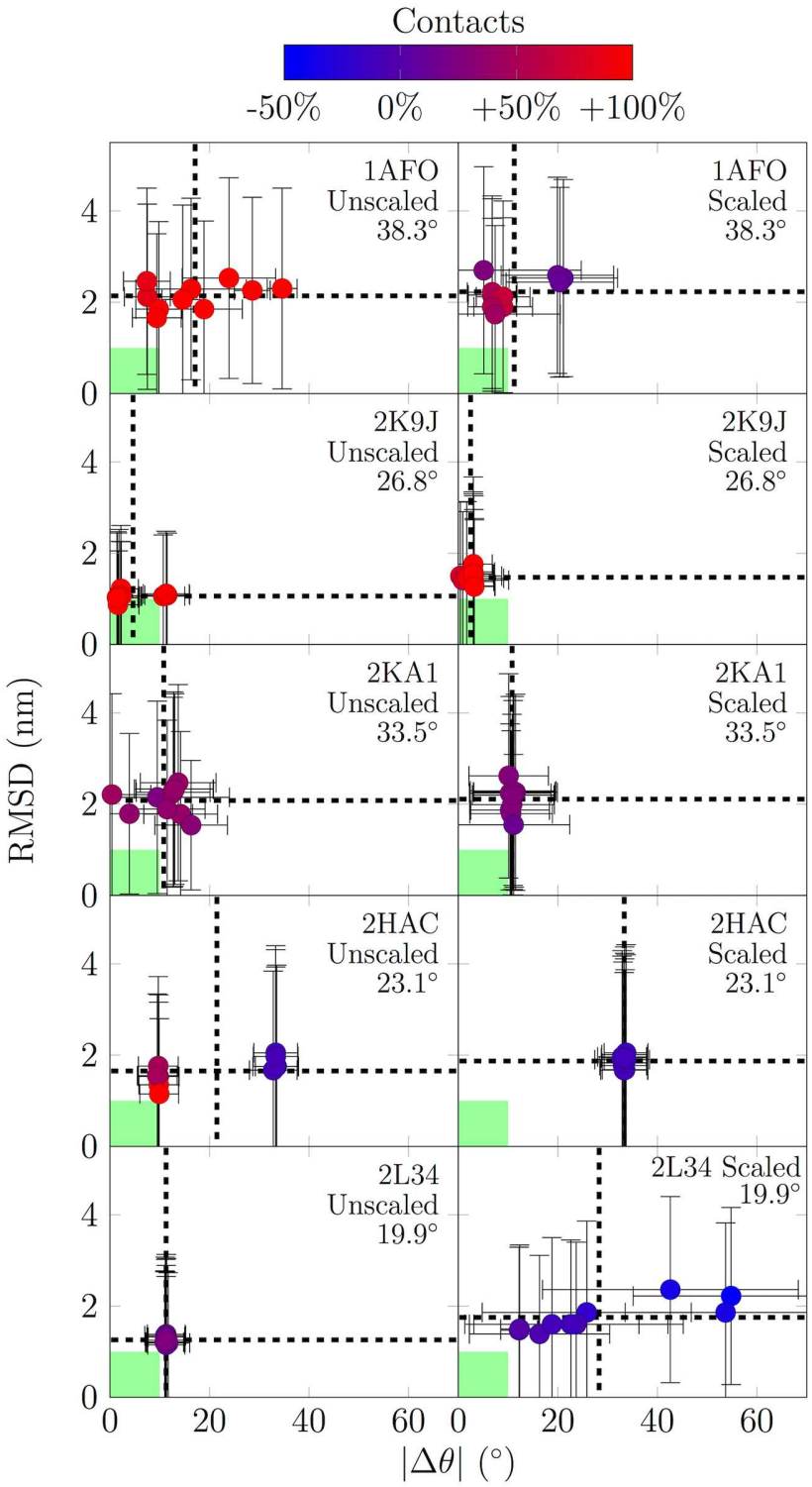

Fig 3. Deviation of the spontaneously formed dimer structures from their NMR structures. Data is shown for both the standard (non-polarizable) Martini and the U-0.1 scaling. The root-mean-square deviation (RMSD) is shown on the *y* axis, and the absolute value of the deviation of the dimer crossing angle on the *x* axis. The coloring shows the deviation in the number of backbone bead contacts (cutoff of 0.8 nm). Therefore, an optimal result would be a purple dot (correct number of contacts) at the origin (RMSD equal to 0 nm and

with the correct dimer crossing angle). As a rule of thumb, to guide the eye, the acceptable region (deviations up to 10° and 1 nm considered to be acceptable) is highlighted in green. In each graph, data are shown for 10 replica simulations. Each replica is depicted with a marker with error bars showing standard deviation, while the mean over replicas is highlighted by the dashed lines. The crossing angle of the NMR structure is given for each dimer in degrees. Data are extracted from the last 20 μs of the simulations.

https://doi.org/10.1371/journal.pone.0187936.g003

Still our approach of projecting the dimer structures onto three collective variables does not provide a full picture of the quality of the structures. To provide a more intuitive comparison between simulation and experiment, the final structures of all replicas of the spontaneous dimerization simulations are shown together with the corresponding NMR structures in Fig 4. Here, the structures are aligned to the NMR structure based on an RMSD fit of the dimerization motif of the first (in PDB) peptide, shown in yellow [71]. This motif is highlighted by purple spheres and the obtained fitted replicas are depicted in gray. The other (not RMSD-aligned) peptide from NMR is shown in green. Finally, the position of the not RMSD-aligned peptides from the replicas is shown with colors from a spectrum of red-white-blue. This representation allows a straightforward evaluation of the spontaneously formed dimers by simply comparing the location of the second peptide observed in simulations (red-white-blue) with its location in the NMR structure (green).

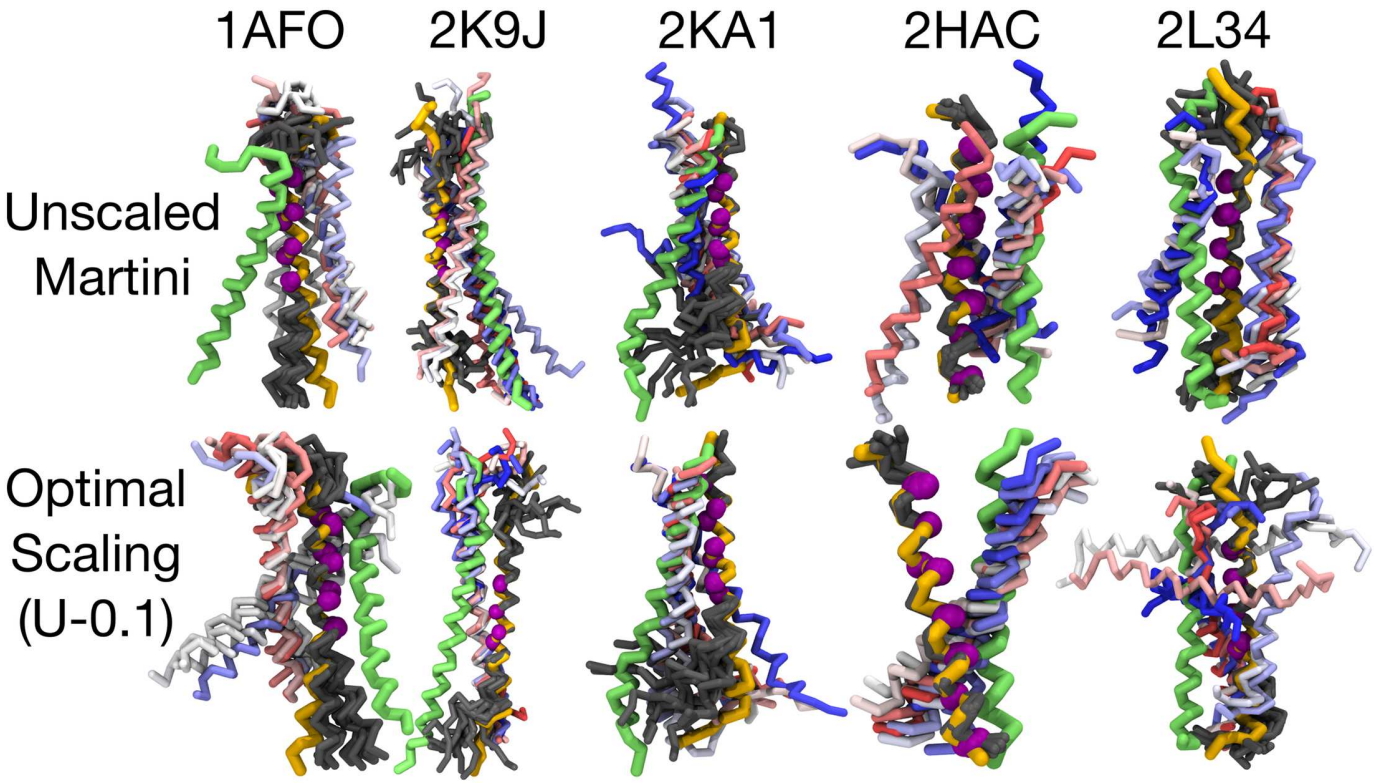

Fig 4. Final structures of the 10 validation replica simulations. Shown here are the structures for both standard (non-polarizable) Martini and the best scaling strategy resolved in this work (U-0.1). The two peptides in the NMR structure are shown in yellow (first peptide) and green (second peptide). The dimerization motif (see Ref. [71]) of the first peptide is additionally highlighted in purple. The dimer structures based on the simulations are depicted in a manner, where the first peptides of the replicas (all shown in gray) are RMSD-aligned at the dimerization motif (purple) on the first peptide of the NMR structure (yellow). The reader should here concentrate on the second peptide structures (not aligned) given by the 10 replica simulations that are depicted by a spectrum of red-white-blue. If there is good agreement between simulation and NMR, the structures of the second peptide (red-white-blue) should coincide with the second peptide in the NMR structure (green).

https://doi.org/10.1371/journal.pone.0187936.g004

It is evident that in most cases the simulations are unable to predict the experimentally resolved dimer conformation, supporting the poor agreement between simulation and experiment suggested by Fig 3. The standard Martini often predicts conformations in which peptides are parallel to each other to maximize the number of inter-peptide contacts. In cases like 1AFO, the dimers form at the wrong interface. This is evident from the positioning of the second peptide in the NMR structures (shown in green) on the other side of the first peptide (shown in yellow) for all the replicas (shown in red-white-blue). For 2K9J, there is some overlap with the simulation replicas and the NMR structure. However, this agreement does not occur at the dimerization site. Instead, the peptides are almost parallel, resulting in too many inter-peptide contacts (see also Fig 3). For 2KA1, there is again some overlap at a correct site. However, for 2HAC, Martini shows multiple conformations indicating irreversible binding upon first contact. Finally, for 2L34, the conformations are again mutually inconsistent among the replicas.

While these results are not very encouraging, we must point out that the dimerization free energies calculated earlier are not affected by the poor prediction of dimer configurations, as the dimer configurations were obtained directly from structures resolved with NMR. It must be kept in mind, though, that the crossing angle deviation, RMSD, and the deviation in the number of inter-peptide backbone contacts were compared to the NMR structure, which is not always determined in a bilayer environment.

Performance of the scaling approaches

Having demonstrated the poor agreement between the standard Martini and experimental results, we move on to evaluate whether the issues can be corrected by scaling down the protein–protein interactions. As a first test, for the EphA1 dimer, we attempted the "W-0.6" fix, *i.e.* scaling down the interactions among the beads in contact with water. This approach was based on the promising results obtained by Stark *et al.* on water-soluble proteins [32]. This approach provided a value of −23.2 ± 0.8 kJ/mol, which is ∼50% too high compared to experimental results. Even further reduction of the interactions among the water-touching residues (W-0.8 or W-0.9) does not reduce the value of ΔG_{DIM} to the experimental value (see Table 1), providing concrete evidence that also the hydrophobic residues need to be scaled. Even if this strong scaling had provided good agreement with the experiment, it would have removed all chemical specificity from the model, since for example at $\alpha = 0.9$ the most repulsive and the most attractive interactions are separated by only ∼0.4 kJ/mol (2.0 vs. 2.36 kJ/mol).

Next, we applied the uniform scaling approach ("U") to the EphA1 dimer. We first scaled the LJ ϵ values using scaling factors α in the range of 0.1–0.9 with a spacing of 0.1 (see Eq (3)). After 250 ns of free energy (umbrella sampling) simulations per window, the obviously wrong values of α in each strategy were discarded, and the simulations were continued to 10 μs per window using only the most promising candidates (U-0.1 and U-0.2). Also, the number of simulated windows was limited at this point, as only the windows that were required to reach the convergence of free energy profiles were extended to 10 μs. Depending on the scaling approach and the dimer, this plateau was reached at 2.6–3.6 nm.

As shown in Table 1, the best agreement with experiment with the EphA1 dimer is obtained with the U-0.1 approach, *i.e.* when the protein–protein interactions among all protein beads are reduced by 10%. This approach gives a value of −15.2 ± 1.0 kJ/mol, which is consistent, within error margins, with the value obtained from experiment. Using stronger scaling ($\alpha >$ 0.1) leads to unstable dimerization as the minimum in the free energy profile vanishes.

Applying the U-0.1 approach to the ErbB1 dimer, we obtained a value of −15.3 ± 0.3 kJ/mol, *i.e.* the dimer is somewhat too stable in the simulation but the dimerization free energy is

still sufficiently low for reversible binding that allows sampling of different dimerization interfaces (see Table 1). Meanwhile, stronger scaling did not lead to a stable dimer. This hints that a uniform approach is not sufficient, but a more careful amino-acid specific adjustment of the protein–protein interactions might be required.

Next, we verified that the U-0.1 scaling approach is gentle enough to not result in the unfolding of proteins. The S1 File (see the SI) demonstrates that protein structures are stable also with the scaling.

Having established U-0.1 as the most promising scaling approach, we evaluated its performance in predicting the structures of the spontaneously forming dimers as well as the level of oligomerization. These are tasks for which the standard Martini was shown above to be not optimal. As shown in S3 Fig, using the U-0.1 scaling, the eight ErbB1 monomers form one tetramer and two dimers, which is a clear improvement over the octamer observed for standard Martini. For EphA1, on the other hand, the performance was not improved by the U-0.1 scaling, and two tetramers were observed. It is not possible to ensure that the clustering process has reached equilibrium in our simulations. However, it is unlikely that the formed oligomers would decrease in size if the simulations were extended further. Equilibrium oligomer sizes are overestimated for both models. However, we observe several promising unbinding events with the scaled model, which suggests that the scaling takes the behavior of the system in the correct direction.

Moving on to the structures of spontaneously formed dimers, as shown in S2 Fig, the dimers form spontaneously even when the protein–protein interactions are reduced, however the formation of dimers takes more time when the U-0.1 scaling is employed. This allows the dimers to sample dimerization interfaces before a stable dimer is formed. Even one brief dissociation event is observed for the 2K9J dimer with the U-0.1 scaling.

Unfortunately, as shown in Fig 4, the agreement with experiment is not improved systematically with the U-0.1 scaling, and as with the standard Martini, all replicas fall outside the region highlighted in green. The scaled Martini model provides mutually consistent behavior among the replicas for most of the dimers (2K9J, 2KA1, and 2HAC). However, the only decent agreement with experiment is observed for 2HAC, for which all replicas show substantial overlap with the NMR structure. However, the deviations grow towards the bottom part of the structure resulting in a substantial deviation in the tilt angle (see Fig 3).

At this point, it is clear that the properties discussed here seem to be very sensitive to the scaling parameters. As an example, free energies of dimerization can change by multiple dozen kilojoules per mole upon a decrease of only 10% in the Lennard-Jones interactions. Similarly, this small decrease affects the structures of dimers quite drastically as shown in Fig 3. Based on these observations, any scaling scheme should be always adapted with care, and its validity should be evaluated by comparison with experiment.

The U-0.1 scaling should benefit studies on membrane dynamics as it prevents excessive and unrealistic clustering. It should also help proteins sample protein dimerization interfaces before actually forming a dimer. One would also assume that a uniform scaling would not affect the preference of the protein dimerization interfaces. However, the proper sampling of dimerization interfaces of membrane proteins such as GPCRs requires substantial effort and simulation time [7, 28, 35, 43]. Since such a thorough study is beyond the scope of this work, the validity of the scaling approach in predicting protein dimerization interfaces remains to be studied.

With the apparent limitations in the ability of the standard Martini model to describe protein–protein interactions, and considering that our two approaches to adjust the interaction levels also fail in predicting the correct dimerization interfaces, the obvious question is how the situation could be improved. Our results show that the reduction in protein–protein

interactions required for membrane proteins to reproduce experimental dimerization free energies (10%) is much smaller than for water-soluble proteins (60% [32]). Importantly, the amino acid content in these two kinds of proteins is very different, suggesting that an amino acid specific scaling strategy, even though being very laborious and beyond the scope of this work, could provide an approach applicable to a wide range of protein types. Notably, such a technique would be especially crucial for studies involving full-length membrane proteins where ectodomains and cytosolic regions are largely exposed to interactions with water, while the TM domains are mainly in a hydrophobic environment. Currently, however, such amino acid specific scaling is also limited by the lack of quantitative experimental data for validation, covering both membrane proteins and water soluble proteins, let alone proteins with segments inside and outside the membrane.

Membrane lipids also play a key role in the oligomerization of membrane proteins. A recent study by Castillo *et. al* showed that a large hydrophobic mismatch can stabilize a dimer substantially [56]. Furthermore, the role of membrane lipids in altering the rate and the interface of receptor oligomerization were also recently demonstrated by computer simulations [7, 77]. In the free energy calculations described in this work, the role of lipids was accounted for; the membrane compositions followed those used in the respective experiments, and the correct dimerization interfaces were sampled as the conformations were derived from the dimer structure resolved by NMR. Also, the changes in ΔG_{DIM} due to hydrophobic mismatch [56] were smaller than the observed deviations between experiments and Martini and cannot therefore explain their poor mutual agreement. Furthermore, in our recent work [7] we observed that scaling down protein–protein interactions decreased the rate of oligomerization systematically for two different lipid compositions pointing out to a general trend that cannot be explained by the choice of lipids.

Coarse-grained simulations lack many details provided by their atomistic counterparts. Notably, in addition to van der Waals forces and steric repulsion, entropic effects and hydrogen bonding are also captured in the LJ potential in the coarse-grained scheme. Therefore, in order to resolve the nature of protein–protein and protein–lipid interactions in detail, the fine-graining of the simulated structures to atomistic resolution, followed by further simulation, is recommended. Fortunately, the recent developments in resolution transformation tools (`martinize` and `backward` [29]) provide easy access to such effective multiscale simulations. In these simulations, it is of crucial importance that the interactions are reasonably similar at the used resolutions. Otherwise efficient CG simulations might take the system to an unfavorable state—such as a tightly bound protein aggregate or a protein with its lipid binding sites covered by other proteins—from which the united-atom or all-atom simulations cannot escape.

Conclusions

Membrane protein dimerization free energies calculated using the coarse-grained Martini model [21–23] are often much larger than the corresponding experimental values by tens of kilojoules per mole. If dimerization free energies in simulation models are too large, or even excessive, they can result in instantaneous, nonselective, and irreversible binding, thereby leading to formation of unrealistic protein oligomers or superaggregates. This further complicates the interpretation of simulation data for dimerization interfaces: if the binding between two proteins is disproportionately strong and fast, then the dimerization interface predicted by coarse-grained simulations may be wrong. Also, the aggregates resulting from excessively large dimerization free energies may give rise to unrealistically pronounced confinement effects for lipids and proteins diffusing in the membrane plane, thereby impairing the lateral dynamics of

membrane systems. All these issues complicate the interpretation of experimental data with the aid of molecular dynamics simulations based on the coarse-grained Martini force field.

In this work, we attempted to improve this situation by scaling the interaction between the membrane proteins. The results based on this strategy are partly encouraging. We found that only a small reduction of approximately 10% in the LJ interactions is required to bring the dimerization free energies of RTK TM domains to the same ballpark with values obtained from FRET experiments. This signals that the Martini parametrization together with its simple combination rules gets impressively close to optimal values in a task that the Martini model was never parametrized for. Meanwhile, the small reduction in the LJ interactions did not improve agreement between the structures of spontaneously formed dimers found in simulations and those resolved from NMR, and the degree of oligomerization was still too large as compared to experiments.

Martini has also occasionally been able to predict the most favorable dimer structures [35, 43], even though their absolute binding energies are not in line with experiment. In this case, the slight and universal decrease of protein–protein interactions will likely not affect the relative affinities of the interfaces, yet it will allow the proteins to sample more conformations until they find the optimal orientation. However, this remains to be confirmed in future studies.

To conclude, our study brings about an issue in the description of protein–protein interactions in the Martini model. We consider that our work sets a promising basis for further studies to design a more accurate parametrization strategy based on, *e.g.*, amino acid specific scaling of protein–protein interactions. In the meantime, the scaled version of Martini, as discussed in this paper, can be used to improve studies on membrane dynamics and protein–lipid interactions. However, in all cases a careful comparison of simulation predictions with biochemical experiments must be performed whenever possible.

Supporting information

S1 Table. Dimer reference crossing angles. Residues used for the calculation of dimeric crossing angles. Pept-1 and Pept-2 show the two peptides consituting the dimers. The indicated residues from both peptides (numbering starting from 1) were used in the calculation; the crossing angle is defined as the angle between the principal moments of inertia of the backbone beads of the indicated residues. The angle extracted from the PDB structures is indicated by "Ang-PDB", while that calculated in this work is labeled "Ang-Exp.". Note that we omit the handedness and only show positive crossing angle values.
(XLSX)

S1 Fig. Monomer tilt angles. Tilt angles of ErpB1 monomers with respect to the membrane normal as a function of COM–COM separation (COM stands for the centre of mass). The systematic increase of the angle, seen in the unscaled Martini model (red and black curves), is due to the strong protein–protein interaction: when the peptides are separated, they tilt in order to keep the termini at one end in contact with each other.
(PDF)

S2 Fig. Peptide–peptide distances. Distance between the peptide COMs as a function of simulation time in the unbiased simulations. Data are shown for the 10 repeats done for each system, and the insets show the data for the last 20 μs in more detail.
(PDF)

S3 Fig. Order of oligomerization. A) The time evolution of the average oligomer size of EphA1 and ErbB1 peptides. B) The histogram of the oligomer sizes during the last 10 μs of the

simulation.
(PDF)

S1 File. Stability of BtuB membrane protein with the U-0.1 scaling. Details of a simulation of a BtuB membrane protein. Stability analysis comparing the results between the normal (unscaled) Martini model and the U-0.1 scaling.
(PDF)

Acknowledgments

We acknowledge Leija Lahtinen for her help in the early stages of the project. CSC—IT Center for Science (Espoo, Finland) is acknowledged for computing resources.

Author Contributions

Conceptualization: Matti Javanainen, Hector Martinez-Seara, Ilpo Vattulainen.

Data curation: Matti Javanainen, Hector Martinez-Seara.

Formal analysis: Matti Javanainen, Hector Martinez-Seara.

Funding acquisition: Hector Martinez-Seara, Ilpo Vattulainen.

Investigation: Matti Javanainen, Hector Martinez-Seara.

Methodology: Matti Javanainen, Hector Martinez-Seara.

Project administration: Hector Martinez-Seara, Ilpo Vattulainen.

Resources: Matti Javanainen, Ilpo Vattulainen.

Supervision: Hector Martinez-Seara, Ilpo Vattulainen.

Validation: Matti Javanainen, Hector Martinez-Seara.

Visualization: Matti Javanainen.

Writing – original draft: Matti Javanainen, Hector Martinez-Seara.

Writing – review & editing: Matti Javanainen, Hector Martinez-Seara, Ilpo Vattulainen.

References

1. Ferré S, Casadó V, Devi LA, Filizola M, Jockers R, Lohse MJ, et al. G Protein–Coupled Receptor Oligomerization Revisited: Functional and Pharmacological Perspectives. Pharmacol Rev. 2014; 66(2):413–434. https://doi.org/10.1124/pr.113.008052 PMID: 24515647
2. Gomes I, Ayoub MA, Fujita W, Jaeger WC, Pfleger KD, Devi LA. G Protein-Coupled Receptor Heteromers. Annu Rev Pharmacol Toxicol. 2016; 56:403–425. https://doi.org/10.1146/annurev-pharmtox-011613-135952 PMID: 26514203
3. Haass C, Selkoe DJ. Soluble Protein Oligomers in Neurodegeneration: Lessons From the Alzheimer's Amyloid β-Peptide. Nat Rev Mol Cell Biol. 2007; 8(2):101–112. https://doi.org/10.1038/nrm2101 PMID: 17245412
4. Ghosh A, Sonavane U, Joshi R. Multiscale Modelling to Understand the Self-Assembly Mechanism of Human β2-Adrenergic Receptor in Lipid Bilayer. Computat Biol Chem. 2014; 48:29–39. https://doi.org/10.1016/j.compbiolchem.2013.11.002
5. Mondal S, Johnston JM, Wang H, Khelashvili G, Filizola M, Weinstein H. Membrane Driven Spatial Organization of GPCRs. Sci Rep. 2013; 3:2909. https://doi.org/10.1038/srep02909 PMID: 24105260
6. Periole X, Huber T, Marrink SJ, Sakmar TP. G Protein-Coupled Receptors Self-Assemble in Dynamics Simulations of Model Bilayers. J Am Chem Soc. 2007; 129(33):10126–10132. https://doi.org/10.1021/ja0706246 PMID: 17658882

7. Guixà-González R, Javanainen M, Gómez-Soler M, Cordobilla B, Domingo JC, Sanz F, et al. Membrane Omega-3 Fatty Acids Modulate the Oligomerisation Kinetics of Adenosine A_{2A} and Dopamine D_2 Receptors. Sci Rep. 2016; 6. https://doi.org/10.1038/srep19839 PMID: 26796668
8. Provasi D, Boz MB, Johnston JM, Filizola M. Preferred Supramolecular Organization and Dimer Interfaces of Opioid Receptors From Simulated Self-Association. PLoS Comput Biol. 2015; 11(3): e1004148. https://doi.org/10.1371/journal.pcbi.1004148 PMID: 25822938
9. Koldsø H, Sansom MS. Organization and Dynamics of Receptor Proteins in a Plasma Membrane. J Am Chem Soc. 2015; 137(46):14694–14704. https://doi.org/10.1021/jacs.5b08048 PMID: 26517394
10. Johnston JM, Aburi M, Provasi D, Bortolato A, Urizar E, Lambert NA, et al. Making Structural Sense of Dimerization Interfaces of Delta Opioid Receptor Homodimers. Biochemistry. 2011; 50(10):1682–1690. https://doi.org/10.1021/bi101474v PMID: 21261298
11. Johnston JM, Filizola M. Differential Stability of the Crystallographic Interfaces of Mu-And Kappa-Opioid Receptors. PLoS One. 2014; 9(2):e90694. https://doi.org/10.1371/journal.pone.0090694 PMID: 24651466
12. Periole X. Interplay of G Protein-Coupled Receptors With the Membrane: Insights From Supra-Atomic Coarse Grain Molecular Dynamics Simulations. Chem Rev. 2016; 117(1):156–185. https://doi.org/10.1021/acs.chemrev.6b00344 PMID: 28073248
13. Parton DL, Klingelhoefer JW, Sansom MS. Aggregation of Model Membrane Proteins, Modulated by Hydrophobic Mismatch, Membrane Curvature, and Protein Class. Biophys J. 2011; 101(3):691–699. https://doi.org/10.1016/j.bpj.2011.06.048 PMID: 21806937
14. Rassam P, Copeland NA, Birkholz O, Tóth C, Chavent M, Duncan AL, et al. Supramolecular Assemblies Underpin Turnover of Outer Membrane Proteins in Bacteria. Nature. 2015; 523(7560):333–336. https://doi.org/10.1038/nature14461 PMID: 26061769
15. Javanainen M, Hammaren H, Monticelli L, Jeon JH, Miettinen MS, Martinez-Seara H, et al. Anomalous and Normal Diffusion of Proteins and Lipids in Crowded Lipid Membranes. Faraday Disc. 2013; 161:397–417. https://doi.org/10.1039/C2FD20085F
16. Jeon JH, Javanainen M, Martinez-Seara H, Metzler R, Vattulainen I. Protein Crowding in Lipid Bilayers Gives Rise to Non-Gaussian Anomalous Lateral Diffusion of Phospholipids and Proteins. Phys Rev X. 2016; 6(2):021006.
17. Goose JE, Sansom MS. Reduced Lateral Mobility of Lipids and Proteins in Crowded Membranes. PLoS Comput Biol. 2013; 9(4):e1003033. https://doi.org/10.1371/journal.pcbi.1003033 PMID: 23592975
18. Chavent M, Reddy T, Goose J, Dahl ACE, Stone JE, Jobard B, et al. Methodologies for the Analysis of Instantaneous Lipid Diffusion in MD Simulations of Large Membrane Systems. Faraday Disc. 2014; 169:455–475. https://doi.org/10.1039/C3FD00145H
19. Arnarez C, Marrink S, Periole X. Molecular Mechanism of Cardiolipin-Mediated Assembly of Respiratory Chain Supercomplexes. Chem Sci. 2016; 7:4435–4443. https://doi.org/10.1039/C5SC04664E
20. Reddy T, Shorthouse D, Parton DL, Jefferys E, Fowler PW, Chavent M, et al. Nothing to Sneeze At: A Dynamic and Integrative Computational Model of an Influenza a Virion. Structure. 2015; 23(3):584–597. https://doi.org/10.1016/j.str.2014.12.019 PMID: 25703376
21. Marrink SJ, Risselada HJ, Yefimov S, Tieleman DP, De Vries AH. The MARTINI Force Field: Coarse Grained Model for Biomolecular Simulations. J Phys Chem B. 2007; 111(27):7812–7824. https://doi.org/10.1021/jp071097f PMID: 17569554
22. Monticelli L, Kandasamy SK, Periole X, Larson RG, Tieleman DP, Marrink SJ. The MARTINI Coarse-Grained Force Field: Extension to Proteins. J Chem Theory Comput. 2008; 4(5):819–834. https://doi.org/10.1021/ct700324x PMID: 26621095
23. de Jong DH, Singh G, Bennett WD, Arnarez C, Wassenaar TA, Schäfer LV, et al. Improved Parameters for the Martini Coarse-Grained Protein Force Field. J Chem Theory Comput. 2012; 9(1):687–697. https://doi.org/10.1021/ct300646g PMID: 26589065
24. Bond PJ, Sansom MS. Insertion and Assembly of Membrane Proteins via Simulation. J Am Chem Soc. 2006; 128(8):2697–2704. https://doi.org/10.1021/ja0569104 PMID: 16492056
25. Stansfeld PJ, Goose JE, Caffrey M, Carpenter EP, Parker JL, Newstead S, et al. MemProtMD: Automated Insertion of Membrane Protein Structures Into Explicit Lipid Membranes. Structure. 2015; 23 (7):1350–1361. https://doi.org/10.1016/j.str.2015.05.006 PMID: 26073602
26. Qi Y, Ingólfsson HI, Cheng X, Lee J, Marrink SJ, Im W. CHARMM-GUI Martini Maker for Coarse-Grained Simulations With the Martini Force Field. J Chem Theory Comput. 2015; 11(9):4486–4494. https://doi.org/10.1021/acs.jctc.5b00513 PMID: 26575938
27. Wassenaar TA, Ingólfsson HI, Böckmann RA, Tieleman DP, Marrink SJ. Computational Lipidomics With insane: A Versatile Tool for Generating Custom Membranes for Molecular Simulations. J Chem Theory Comput. 2015; 11(5):2144–2155. https://doi.org/10.1021/acs.jctc.5b00209 PMID: 26574417

28. Wassenaar TA, Pluhackova K, Moussatova A, Sengupta D, Marrink SJ, Tieleman DP, et al. High-Throughput Simulations of Dimer and Trimer Assembly of Membrane Proteins. The DAFT Approach. J Chem Theory Comput. 2015; 11(5):2278–2291. https://doi.org/10.1021/ct5010092 PMID: 26574426

29. Wassenaar TA, Pluhackova K, Böckmann RA, Marrink SJ, Tieleman DP. Going Backward: A Flexible Geometric Approach to Reverse Transformation From Coarse Grained to Atomistic Models. J Chem Theory Comput. 2014; 10(2):676–690. https://doi.org/10.1021/ct400617g PMID: 26580045

30. Javanainen M, Martinez-Seara H. Efficient Preparation and Analysis of Membrane and Membrane Protein Systems. Biochim Biophys Acta. 2016; 1858(10):2468–2482. https://doi.org/10.1016/j.bbamem.2016.02.036 PMID: 26947184

31. Nishizawa M, Nishizawa K. Potential of Mean Force Analysis of the Self-Association of Leucine-Rich Transmembrane α-Helices: Difference Between Atomistic and Coarse-Grained Simulations. J Chem Phys. 2014; 141(7):075101. https://doi.org/10.1063/1.4891932 PMID: 25149815

32. Stark AC, Andrews CT, Elcock AH. Toward Optimized Potential Functions for Protein–Protein Interactions in Aqueous Solutions: Osmotic Second Virial Coefficient Calculations Using the Martini Coarse-Grained Force Field. J Chem Theory Comput. 2013; 9(9):4176–4185. https://doi.org/10.1021/ct400008p

33. Dunton TA, Goose JE, Gavaghan DJ, Sansom MS, Osborne JM. The Free Energy Landscape of Dimerization of a Membrane Protein, NanC. PLoS Comput Biol. 2014; 10(1):e1003417. https://doi.org/10.1371/journal.pcbi.1003417 PMID: 24415929

34. Chavent M, Chetwynd AP, Stansfeld PJ, Sansom MS. Dimerization of the EphA1 Receptor Tyrosine Kinase Transmembrane Domain: Insights Into the Mechanism of Receptor Activation. Biochemistry. 2014; 53(42):6641–6652. https://doi.org/10.1021/bi500800x PMID: 25286141

35. Periole X, Knepp AM, Sakmar TP, Marrink SJ, Huber T. Structural Determinants of the Supramolecular Organization of G Protein-Coupled Receptors in Bilayers. J Am Chem Soc. 2012; 134(26):10959–10965. https://doi.org/10.1021/ja303286e PMID: 22679925

36. Johnston JM, Wang H, Provasi D, Filizola M. Assessing the Relative Stability of Dimer Interfaces in G Protein-Coupled Receptors. PLoS Comput Biol. 2012; 8(8):e1002649. https://doi.org/10.1371/journal.pcbi.1002649 PMID: 22916005

37. Provasi D, Johnston JM, Filizola M. Lessons From Free Energy Simulations of δ-Opioid Receptor Homodimers Involving the Fourth Transmembrane Helix. Biochemistry. 2010; 49(31):6771–6776. https://doi.org/10.1021/bi100686t PMID: 20617813

38. Casuso I, Khao J, Chami M, Paul-Gilloteaux P, Husain M, Duneau JP, et al. Characterization of the Motion of Membrane Proteins Using High-Speed Atomic Force Microscopy. Nat Nanotech. 2012; 7(8):525–529. https://doi.org/10.1038/nnano.2012.109

39. You M, Li E, Wimley WC, Hristova K. Förster Resonance Energy Transfer in Liposomes: Measurements of Transmembrane Helix Dimerization in the Native Bilayer Environment. Anal Biochem. 2005; 340(1):154–164. https://doi.org/10.1016/j.ab.2005.01.035 PMID: 15802141

40. Chen L, Novicky L, Merzlyakov M, Hristov T, Hristova K. Measuring the Energetics of Membrane Protein Dimerization in Mammalian Membranes. J Am Chem Soc. 2010; 132(10):3628–3635. https://doi.org/10.1021/ja910692u PMID: 20158179

41. Chen L, Merzlyakov M, Cohen T, Shai Y, Hristova K. Energetics of ErbB1 Transmembrane Domain Dimerization in Lipid Bilayers. Biophys J. 2009; 96(11):4622–4630. https://doi.org/10.1016/j.bpj.2009.03.004 PMID: 19486684

42. Prakash A, Janosi L, Doxastakis M. Self-Association of Models of Transmembrane Domains of ErbB Receptors in a Lipid Bilayer. Biophys J. 2010; 99(11):3657–3665. https://doi.org/10.1016/j.bpj.2010.10.023 PMID: 21112290

43. Lelimousin M, Limongelli V, Sansom MS. Conformational Changes in the Epidermal Growth Factor Receptor: Role of the Transmembrane Domain Investigated by Coarse-Grained Metadynamics Free Energy Calculations. J Am Chem Soc. 2016; 138:10611–10622. https://doi.org/10.1021/jacs.6b05602 PMID: 27459426

44. Artemenko EO, Egorova NS, Arseniev AS, Feofanov AV. Transmembrane Domain of EphA1 Receptor Forms Dimers in Membrane-Like Environment. Biochim Biophys Acta. 2008; 1778(10):2361–2367. https://doi.org/10.1016/j.bbamem.2008.06.003 PMID: 18590698

45. Li E, You M, Hristova K. FGFR3 Dimer Stabilization Due to a Single Amino Acid Pathogenic Mutation. J Mol Biol. 2006; 356(3):600–612. https://doi.org/10.1016/j.jmb.2005.11.077 PMID: 16384584

46. Li E, You M, Hristova K. Sodium Dodecyl Sulfate-Polyacrylamide Gel Electrophoresis and Förster Resonance Energy Transfer Suggest Weak Interactions Between Fibroblast Growth Factor Receptor 3 (FGFR3) Transmembrane Domains in the Absence of Extracellular Domains and Ligands. Biochemistry. 2005; 44(1):352–360. https://doi.org/10.1021/bi048480k PMID: 15628877

47. Merzlyakov M, Chen L, Hristova K. Studies of Receptor Tyrosine Kinase Transmembrane Domain Interactions: The EmEx-FRET Method. J Membr Biol. 2007; 215(2–3):93–103. https://doi.org/10.1007/s00232-007-9009-0 PMID: 17565424

48. You M, Li E, Hristova K. The Achondroplasia Mutation Does Not Alter the Dimerization Energetics of the Fibroblast Growth Factor Receptor 3 Transmembrane Domain. Biochemistry. 2006; 45(17):5551–5556. https://doi.org/10.1021/bi060113g PMID: 16634636

49. Sarabipour S, Hristova K. Glycophorin a Transmembrane Domain Dimerization in Plasma Membrane Vesicles Derived From CHO, HEK 293T, and A431 Cells. Biochim Biophys Acta. 2013; 1828(8):1829–1833. https://doi.org/10.1016/j.bbamem.2013.03.022 PMID: 23562404

50. Sengupta D, Marrink SJ. Lipid-Mediated Interactions Tune the Association of Glycophorin a Helix and Its Disruptive Mutants in Membranes. Phys Chem Chem Phys. 2010; 12(40):12987–12996. https://doi.org/10.1039/c0cp00101e PMID: 20733990

51. Janosi L, Prakash A, Doxastakis M. Lipid-Modulated Sequence-Specific Association of Glycophorin a in Membranes. Biophys J. 2010; 99(1):284–292. https://doi.org/10.1016/j.bpj.2010.04.005 PMID: 20655857

52. Domański J, Hedger G, Best RB, Stansfeld PJ, Sansom MS. Convergence and Sampling in Determining Free Energy Landscapes for Membrane Protein Association. J Phys Chem B. 2017; 121(15):3364–3375. https://doi.org/10.1021/acs.jpcb.6b08445 PMID: 27807980

53. Hong H, Blois TM, Cao Z, Bowie JU. Method to Measure Strong Protein–Protein Interactions in Lipid Bilayers Using a Steric Trap. Proc Natl Acad Sci USA. 2010; 107(46):19802–19807. https://doi.org/10.1073/pnas.1010348107 PMID: 21041662

54. Nash A, Notman R, Dixon AM. De Novo Design of Transmembrane Helix–Helix Interactions and Measurement of Stability in a Biological Membrane. Biochim Biophys Acta. 2015; 1848(5):1248–1257. https://doi.org/10.1016/j.bbamem.2015.02.020 PMID: 25732028

55. Finger C, Volkmer T, Prodöhl A, Otzen DE, Engelman DM, Schneider D. The Stability of Transmembrane Helix Interactions Measured in a Biological Membrane. J Mol Biol. 2006; 358(5):1221–1228. https://doi.org/10.1016/j.jmb.2006.02.065 PMID: 16574146

56. Castillo N, Monticelli L, Barnoud J, Tieleman DP. Free Energy of WALP23 Dimer Association in DMPC, DPPC, and DOPC Bilayers. Chem Phys Lipids. 2013; 169:95–105. https://doi.org/10.1016/j.chemphyslip.2013.02.001 PMID: 23415670

57. Schäfer LV, de Jong DH, Holt A, Rzepiela AJ, de Vries AH, Poolman B, et al. Lipid Packing Drives the Segregation of Transmembrane Helices Into Disordered Lipid Domains in Model Membranes. Proc Natl Acad Sci USA. 2011; 108(4):1343–1348. https://doi.org/10.1073/pnas.1009362108 PMID: 21205902

58. Ash WL. Helix-Helix Interactions in Membrane Proteins Probed With Computer Simulations. University of Calgary; 2009.

59. Yano Y, Matsuzaki K. Measurement of Thermodynamic Parameters for Hydrophobic Mismatch 1: Self-Association of a Transmembrane Helix. Biochemistry. 2006; 45(10):3370–3378. https://doi.org/10.1021/bi052286w PMID: 16519531

60. Berman HM, Westbrook J, Feng Z, Gilliland G, Bhat TN, Weissig H, et al. The Protein Data Bank. Nucl Acids Res. 2000; 28(1):235–242. https://doi.org/10.1093/nar/28.1.235 PMID: 10592235

61. Bocharov EV, Mayzel ML, Volynsky PE, Goncharuk MV, Ermolyuk YS, Schulga AA, et al. Spatial Structure and pH-Dependent Conformational Diversity of Dimeric Transmembrane Domain of the Receptor Tyrosine Kinase EphA1. J Biol Chem. 2008; 283(43):29385–29395. https://doi.org/10.1074/jbc.M803089200 PMID: 18728013

62. Bocharov EV, Lesovoy DM, Pavlov KV, Pustovalova YE, Bocharova OV, Arseniev AS. Alternative Packing of EGFR Transmembrane Domain Suggests That Protein–Lipid Interactions Underlie Signal Conduction Across Membrane. Biochim Biophys Acta. 2016; 1858(6):1254–1261. https://doi.org/10.1016/j.bbamem.2016.02.023 PMID: 26903218

63. de Jong DH, Baoukina S, Ingólfsson HI, Marrink SJ. Martini Straight: Boosting Performance Using a Shorter Cutoff and GPUs. Comput Phys Commun. 2016; 199:1–7. https://doi.org/10.1016/j.cpc.2015.09.014

64. Bussi G, Donadio D, Parrinello M. Canonical Sampling Through Velocity Rescaling. J Chem Phys. 2007; 126(1):014101. https://doi.org/10.1063/1.2408420 PMID: 17212484

65. Parrinello M, Rahman A. Polymorphic Transitions in Single Crystals: A New Molecular Dynamics Method. J Appl Phys. 1981; 52(12):7182–7190. https://doi.org/10.1063/1.328693

66. Yesylevskyy SO, Schäfer LV, Sengupta D, Marrink SJ. Polarizable Water Model for the Coarse-Grained MARTINI Force Field. PLoS Comput Biol. 2010; 6(6):e1000810. https://doi.org/10.1371/journal.pcbi.1000810 PMID: 20548957

67. Michalowsky J, Schäfer LV, Holm C, Smiatek J. A Refined Polarizable Water Model for the Coarse-Grained MARTINI Force Field With Long-Range Electrostatic Interactions. J Chem Phys. 2017; 146 (5):054501. https://doi.org/10.1063/1.4974833 PMID: 28178817

68. Periole X, Cavalli M, Marrink SJ, Ceruso MA. Combining an Elastic Network With a Coarse-Grained Molecular Force Field: Structure, Dynamics, and Intermolecular Recognition. J Chem Theory Comput. 2009; 5(9):2531–2543. https://doi.org/10.1021/ct9002114 PMID: 26616630

69. Hub JS, De Groot BL, Van Der Spoel D. g_wham—a Free Weighted Histogram Analysis Implementation Including Robust Error and Autocorrelation Estimates. J Chem Theory Comput. 2010; 6(12):3713–3720. https://doi.org/10.1021/ct100494z

70. Abraham MJ, Murtola T, Schulz R, Páll S, Smith JC, Hess B, et al. GROMACS: High Performance Molecular Simulations Through Multi-Level Parallelism From Laptops to Supercomputers. SoftwareX. 2015; 1:19–25. https://doi.org/10.1016/j.softx.2015.06.001

71. Cymer F, Veerappan A, Schneider D. Transmembrane Helix–Helix Interactions Are Modulated by the Sequence Context and by Lipid Bilayer Properties. Biochim Biophys Acta. 2012; 1818(4):963–973. https://doi.org/10.1016/j.bbamem.2011.07.035 PMID: 21827736

72. MacKenzie KR, Prestegard JH, Engelman DM. A Transmembrane Helix Dimer: Structure and Implications. Science. 1997; 276(5309):131–133. https://doi.org/10.1126/science.276.5309.131 PMID: 9082985

73. Lau TL, Kim C, Ginsberg MH, Ulmer TS. The Structure of the Integrin αIIbβ3 Transmembrane Complex Explains Integrin Transmembrane Signalling. EMBO J. 2009; 28(9):1351–1361. https://doi.org/10.1038/emboj.2009.63 PMID: 19279667

74. Sulistijo ES, MacKenzie KR. Structural Basis for Dimerization of the BNIP3 Transmembrane Domain. Biochemistry. 2009; 48(23):5106–5120. https://doi.org/10.1021/bi802245u PMID: 19415897

75. Call ME, Schnell JR, Xu C, Lutz RA, Chou JJ, Wucherpfennig KW. The Structure of the $\zeta\zeta$ Transmembrane Dimer Reveals Features Essential for Its Assembly With the T Cell Receptor. Cell. 2006; 127 (2):355–368. https://doi.org/10.1016/j.cell.2006.08.044 PMID: 17055436

76. Call ME, Wucherpfennig KW, Chou JJ. The Structural Basis for Intramembrane Assembly of an Activating Immunoreceptor Complex. Nat Immunol. 2010; 11(11):1023–1029. https://doi.org/10.1038/ni.1943 PMID: 20890284

77. Prasanna X, Chattopadhyay A, Sengupta D. Cholesterol Modulates the Dimer Interface of the β_2-Adrenergic Receptor via Cholesterol Occupancy Sites. Biophys J. 2014; 106(6):1290–1300. https://doi.org/10.1016/j.bpj.2014.02.002 PMID: 24655504

III

FREE VOLUME THEORY APPLIED TO LATERAL DIFFUSION IN LANGMUIR MONOLAYERS: ATOMISTIC SIMULATIONS FOR A PROTEIN-FREE MODEL OF LUNG SURFACTANT

by
Matti Javanainen, Luca Monticelli, Jorge Bernardino de la Serna, and Ilpo Vattulainen, 2010
Langmuir vol 26, 15436–15444,
DOI: 10.1021/la102454m

Langmuir
Article
pubs.acs.org/Langmuir

Free Volume Theory Applied to Lateral Diffusion in Langmuir Monolayers: Atomistic Simulations for a Protein-Free Model of Lung Surfactant

Matti Javanainen,[†] Luca Monticelli,[†,‡,§,∥] Jorge Bernardino de la Serna,[⊥] and Ilpo Vattulainen*[,†,‡,⊥]

[†]*Department of Physics, Tampere University of Technology, P.O. Box 692, FI-33101 Tampere, Finland,* [‡]*Department of Applied Physics, Aalto University School of Science and Technology, Finland,* [§]*INSERM, UMR-S665, DSIMB 75015 Paris, France,* [∥]*Universite' Paris Diderot - Paris 7, UFR Life Sciences, Paris, France, and* [⊥]*MEMPHYS - Center for Biomembrane Physics, University of Southern Denmark, Odense, Denmark*

Received June 16, 2010. Revised Manuscript Received August 19, 2010

We hereby present a study on lateral diffusion of lipids in Langmuir monolayers. We apply atomistic molecular dynamics simulations to a model system whose composition is consistent with protein-free lung surfactant. Our main focus is on the assessment of the validity of the free volume theory for lateral diffusion and on the interpretation of the cross-sectional area and activation energy parameters appearing in the theory. We find that the diffusion results can be fitted to the description given by the free volume theory, but the interpretation of its parameters is not straightforward. While the cross-sectional area appears to be related to the hard-core cross-sectional area of a lipid, its role in the lateral diffusion process is unclear. Also, the activation energy derived using the free volume theory is different from the activation energy found through Arrhenius analysis, and its physical interpretation remains elusive. Finally, we find that lipid diffusion does not occur via rapid single-particle "jumps". Instead, lipids move in a concerted manner as loosely defined transient clusters, as observed earlier for lipid bilayers.

I. Introduction

The significance of lipid monolayers in life sciences has been overshadowed by the major body of research done on lipid bilayers,[1,2] which are an integral component of cell membranes and a number of other biological entities. Yet, the biological significance of lipid monolayers in, e.g., lung surfactant and human lens membranes is paramount.[2−4] Moreover, Langmuir monolayers are used in a variety of technological applications that range from proteins functioning in supported lipid films to applications in electronic devices.[3,4]

Living matter is in constant motion, driven by thermal fluctuations giving rise to diffusion of molecules. In lipid monolayers, this motion is manifested as lateral diffusion in the plane of a membrane, playing a role in a variety of phenomena such as domain formation, ordering phenomena in membranes covering the eye, and nonequilibrium dynamics of lipids in lung surfactant during the respiratory cycle. Lung surfactant dynamics is particularly important for human health. Lung surfactant is a surface-active mixture of phospholipids, cholesterol, and proteins that create a unique and highly dynamic film separating air and liquids at the alveolar cell surface. Normal lung function requires surfactant that reduces the surface tension to near-zero values. Insufficiently low surface tension at the air−liquid interface (arising, for example, as a consequence of acute inflammation) leads to respiratory distress syndrome. As this condition can be fatal, understanding the lateral dynamics of the lung surfactant lipid components is an issue of medical relevance.

Given these examples, it is somewhat surprising how poorly the diffusion of lipids is understood. While a number of studies have quantified typical lipid diffusion coefficients that characterize the pace of lipid motion in the monolayer plane,[5−8] the mechanism by which lipids migrate along these soft interfaces has remained unknown. Moreover, while monolayers are an example of soft matter driven by thermal fluctuations, the importance of collective density fluctuations in lipid diffusion has not been clarified in monolayers. Overall, the theoretical understanding of lipid diffusion in monolayers is limited.

For lipid bilayers, the understanding of lateral lipid dynamics is somewhat more advanced. It has been proposed that the free volume theory[9] can be used to describe lateral diffusion in lipid bilayers.[10] The free volume theory assumes that lipids diffuse via thermally activated, lateral displacements or "jumps"; these "jumps" occur as often as there is a large enough free volume pocket adjacent to the lipid. Assuming that this idea holds, the lateral diffusion of lipids can be described with an activation barrier and the close-packed cross-sectional area of a lipid in the bilayer plane.

Recently, concerns about the validity of the free volume theory for describing lipid and membrane dynamics have been brought about.[11−15] These largely stem from the fact that the free volume theory was originally developed for colloid-like systems.[9] While

*Corresponding author. E-mail: Ilpo.Vattulainen@tut.fi.

(1) Yeagle, P. L. *The Structure of Biological Membranes*, 2nd ed.; CRC Press: Boca Raton, FL, 2005.
(2) Mouritsen, O. G. *Lige−As a Matter of Fat*; Springer-Verlag: Berlin, 2005.
(3) Petty, M. C. *Langmuir-Blodgett Films: An Introduction*; Cambridge University Press: Cambridge, 1996.
(4) Brockman, H. *Curr. Opin. Struct. Biol.* **1999**, *9*, 438–443.
(5) Gudmand, M.; Fidorra, M.; Bjornholm, T.; Heimburg, T. *Biophys. J.* **2009**, *96*, 4598–4609.
(6) Forstner, M. B.; Kas, J.; Martin, D. *Langmuir* **2001**, *17*, 567–570.
(7) Caruso, F.; Grieser, F.; Thistlethwaite, P. J.; Almgren, M. *Biophys. J.* **1993**, *65*, 2493–2503.
(8) Ke, P. C.; Naumann, C. A. *Langmuir* **2001**, *17*, 5076–5081.
(9) Cohen, M. H.; Turnbull, D. *J. Chem. Phys.* **1959**, *31*, 1164.
(10) Almeida, P. F. F.; Vaz, W. L. C.; Thompson, T. E. *Biochemistry* **1992**, *31*, 6739–6747.
(11) Bemporad, D.; Luttmann, C.; Essex, J. W. *Biophys. J.* **2004**, *87*, 1–13.
(12) Marrink, S. J.; Sok, R. M.; Berendsen, H. J. C. *J. Chem. Phys.* **1996**, *104*, 9090–9099.
(13) Xiang, T.-X. *J. Chem. Phys.* **1998**, *109*, 7876–7884.
(14) Xiang, T.-X. *J. Phys. Chem. B* **1999**, *103*, 385–394.
(15) Falck, E.; Patra, M.; Karttunen, M.; Hyvönen, M. T.; Vattulainen, I. *Biophys. J.* **2005**, *89*, 745–752.

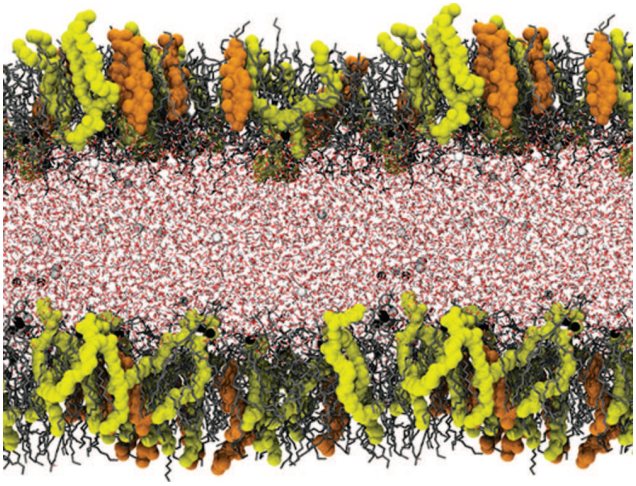

Figure 1. Snapshot of the system with $\langle A \rangle = 56$ Å^2 per lipid using two replicas in the membrane plane. Vacuum slabs below and above the system have been omitted. DPPC and POPC are colored in gray and are shown using the licourice scheme. POPG is colored in yellow and cholesterol in orange, and they both are rendered with the surface scheme. Sodium (white) and chloride (black) ions are shown by the van der Waals scheme. Water is rendered by licourice with hydrogen in white and oxygen in red.

the assumptions made in deriving the free volume theory were justified in systems composed of hard spheres, it is not obvious that they are also appropriate for lipid diffusion, since the cross-sectional area of lipids is not constant[16] and diffusion likely does not take place as single-particle "jumps".[17−19] Instead, recent simulation studies have shown that the diffusion of lipids in fluid bilayers takes place through concerted lipid motions, where tens or possibly hundreds of lipids move in concert as loosely defined clusters,[17,18] and that the lifetime of these dynamically correlated lipid clusters is of the order of a microsecond.[18] Recent quasi-elastic neutron scattering experiments have confirmed the existence of concerted lipid motions in lipid bilayers.[19]

In this article, our objective is to shed light on the diffusion properties of lipids in monolayers. Particular attention is paid to the free volume theory, with an objective to clarify whether it describes lipid diffusion data in monolayers and how the parameters appearing in the free volume theory should be interpreted. For this purpose, we consider the lateral diffusion of lipids in Langmuir monolayers through atomistic molecular dynamics simulations for a model system whose composition is consistent with protein-free lung surfactant. We find that the free volume theory fits the lateral diffusion data reasonably well, but the interpretation of the parameters appearing in the free volume theory is nontrivial.

The article is organized as follows. In section II we describe the models and methods employed in this work. Section III deals with how the lateral diffusion coefficient is defined and also introduces the free volume theory and its assumptions. The simulation results are presented in section IV and discussed in section V, concluding remarks closing the article in section VI.

II. Models and Methods

To model protein-free lung surfactant through atomistic molecular dynamics (MD) simulations, we considered systems composed of two monolayers separated by a water slab (see Figure 1). Each monolayer consisted of 100 lipid molecules with the composition of 60 mol % dipalmitoylphosphatidylcholine (DPPC), 20 mol % palmitoyloleoylphosphatidylcholine (POPC), 10 mol % palmitoyloleoylphosphatidylglycerol (POPG), and 10 mol % cholesterol. These values are consistent with the relative content of saturated, unsaturated, charged, and neutral lipid components observed in lung surfactant.[20,21] The systems were fully hydrated with 7235 water molecules. The systems included 20 sodium counterions to compensate for the negative charges in POPG headgroup and a concentration of 150 mM NaCl.

The simulations were performed in the NVT ensemble, constraining the monolayer area to a fixed value. Periodic boundary conditions were applied in all three directions. For initial configurations, we first constructed a random lipid distribution that was confined to a regular grid. The system structure obtained in this fashion was simulated with a varying monolayer area to generate initial configurations for seven systems with molecular areas (the total area of the monolayer divided by the number of molecules in the monolayer) ranging from $\langle A \rangle = 44$ to 68 Å^2 with a step of 4 Å^2. Larger and smaller systems were also built, but they either underwent pore formation or were unable to relax to a planar configuration during the simulation and are thus not discussed in this work.

The force fields used for lipids followed the Berger description,[22] which is often combined with the SPC (or SPC/E) model for water. Here we used instead the TIP3P model since the Lennard-Jones parameters in the Berger model are based on OPLS-UA, which is often used together with the TIP3P water model. For a pure DPPC monolayer we calculated its dynamic properties with both SPC and TIP3P water models and found essentially no difference. For cholesterol, we used the description of Holtje et al.[23] Salt and counterions were described by the GROMACS force field. In the simulations, temperature was kept at 310 K with the Nose−Hoover thermostat[24] using a time constant of 0.5 ps. Electrostatic interactions were calculated using the particle mesh Ewald (PME) method.[25] Interactions in the reciprocal space were calculated using a fourth-order B-spline interpolation, and the grid spacing was ∼0.12 nm. A cutoff of 1 nm was employed for Lennard-Jones interactions. The neighbor list with a radius of 1 nm was updated every 10 steps. All bonds were constrained using LINCS.[26,27] The simulations were performed with the GROMACS 4 simulation package[28] using a time step of 2 fs.

In all simulations, the systems were simulated for 260 ns. Equilibration was monitored by considering the time dependence of the total energy, which stabilized after about 75 ns. Yet, we consider this time scale to be too short for true equilibration. It is known that the adsorption and desorption events of monovalent ions at the lipid−water interface are slow processes and may slow

(16) Falck, E.; Patra, M.; Karttunen, M.; Hyvonen, M. T.; Vattulainen, I. *Biophys. J.* **2004**, *87*, 1076.
(17) Falck, E.; Rog, T.; Karttunen, M.; Vattulainen, I. *J. Am. Chem. Soc.* **2008**, *130*, 44.
(18) Apajalahti, T.; Niemelä, P.; Govindan, P. N.; Miettinen, M. S.; Salonen, E.; Marrink, S. J.; Vattulainen, I. *Faraday Discuss.* **2010**, *144*, 411–430.
(19) Busch, S.; Smuda, C.; Pardo, L. C.; Unruh, T. *J. Am. Chem. Soc.* **2010**, *132*, 3232–3233.
(20) Goerke, J. *Biochim. Biophys. Acta* **1998**, *1408*, 79–89.
(21) Gregory, T. J.; Longmore, W. J.; Moxley, M. A.; Whitsett, J. A.; Reed, C. R.; Fowler, A. A.; et al. *J. Clin. Invest.* **1991**, *88*, 1976.
(22) Berger, O.; Edholm, O.; Jähnig, F. *Biophys. J.* **1997**, *72*, 2002–2013.
(23) Holtje, M.; Forster, T.; Brandt, B.; Engels, T.; von Rybinski, W.; Holtje, H.-D. *Biochim. Biophys. Acta* **2001**, *1511*, 156–167.
(24) Evans, D. J.; Holian, B. L. *J. Chem. Phys.* **1985**, *83*, 4069.
(25) Darden, T.; York, D.; Pedersen, L. *J. Chem. Phys.* **1993**, *98*, 10089.
(26) Hess, B.; Bekker, H.; Berendsen, H. J. C.; Fraaije, J. *J. Comput. Chem.* **1997**, *18*, 1463–1472.
(27) Hess, B. *J. Chem. Theory Comput.* **2008**, *4*, 116–122.
(28) Hess, B.; Kutzner, C.; van der Spoel, D.; Lindahl, E. *J. Chem. Theory Comput.* **2008**, *4*, 435–447.

down equilibration to the 100 ns time scale.[29] Further, it is worth stressing that here we deal with a four-component system where the mixing of lipids through lateral diffusion has to be accounted for. Assuming a typical lateral diffusion coefficient of $D = 1 \times 10^{-7}$ cm^2/s, and considering diffusion in the plane of the membrane over a length scale of $L \approx 2.4$ nm (roughly three molecular diameters in the plane of the monolayer), the time scale for local mixing would be $t = L^2/(4D) \approx 120$ ns. Consequently, to avoid significant concerns with respect to mixing of lipids in this many-component system, we considered the first 180 ns of the simulation as the equilibration period and used the last 80 ns of the trajectory for analysis. We emphasize that the simulation time scale is short compared to time scales associated with domain formation. If the lipid composition with a given surface pressure corresponded to a different domain structure, that would not be seen in the simulations. This is currently a general limitation for atomistic membrane simulations.

The above studies at 310 K were complemented with further simulations to consider the temperature dependence of lateral diffusion using the Arrhenius description for this transport coefficient:

$$D = D_0 \exp(-E_{\mathrm{Arrh}}/k_{\mathrm{B}}T) \tag{1}$$

where D_0 is a constant assumed not to depend on T, or its temperature dependence is presumed to be weak. To find the barrier E_{Arrh}, we carried out simulations with the molecular areas of 48 and 68 Å^2 at 292, 301, 320, and 330 K, in addition to the above-described simulations at 310 K. The initial structures in these simulations corresponded to the final structures (after 260 ns) at 310 K for each given area. The simulations were run for at least 100 ns, allowing the systems to equilibrate for 20 ns and using the rest of the trajectory for analysis.

For comparison with the area parameter given by the free volume theory (see next section), we determined the average close-packed cross-sectional area of the lipids using the alternative technique discussed by Falck et al.[16] For each of the lipid types, we computed the average hard-core cross-sectional area profile as slices across the monolayer. As the procedure is described in ref 16 in detail, here we present only the essential features. We map each system configuration on several cubic three-dimensional grids as follows. If a grid point lies within the hard-core radius r_{HC} of an atom belonging to (say) cholesterol molecule, this point is considered occupied, and otherwise empty, on a grid keeping account of cholesterol molecules. Grid points within hard-core radii of atoms belonging to POPC, in turn, will be occupied on a grid characterizing the POPC molecules, and so forth for each molecule and ion type in the system. The hard-core radius r_{HC} has been chosen to be determined by the distance at which the Lennard-Jones interaction of the atomtype with itself equals 10 $k_{\mathrm{B}}T$. The grid spacing was fixed to 0.05 nm in all three dimensions. The grids found in this fashion can be used to view given slices of the monolayers, as they show cross sections of DPPC, other lipids, water (and ions) as well as patches of free area. An illustration of the analysis for the occupied and free-volume regions inside a membrane is given in Figure 8 of ref 16, which also depicts that the above approach has a certain resemblance to tomography. From the grids constructed, we compute total area profiles for the various molecular species, that is, average total areas occupied by the molecules as functions of the distance from the middle of the water phase. In addition, we can calculate free area (volume) profiles, i.e., the amount of free area (volume) (space not occupied by any molecule or ion) as a function of the distance from the middle of the water phase. Summarizing, the analysis averages over the lipids in a membrane and provides an average "hard-core" or close-packed shape of the lipids. Also, it yields the profile of the average free volume across a membrane.

Finally, we wish to mention that in this article we focus on the lateral dynamics in this model system. As for structural aspects, the pressure−area isotherm has been found to be in reasonable agreement with previous studies for simpler model systems,[30] though a direct comparison is not possible. The results concerning the structural properties will be discussed elsewhere (Javanainen et al., work in progress).

III. Formulation of Lateral Diffusion and Free Volume Theory

A. Definition of Lateral Diffusion Coefficient. Diffusion of single particles is often described in terms of the mean-squared displacement

$$\mathrm{MSD}(t) \equiv \langle [\mathbf{r}_i(t + t') - \mathbf{r}_i(t')]^2 \rangle \tag{2}$$

where $\mathbf{r}(t)$ is the position of the particle i at time t. The angle brackets denote averaging over all particles of a given type as well as averaging over all time origins t'. The diffusion coefficient D describing the stochastic motion of a particle in a random-walk-like manner is then defined as

$$D \equiv \lim_{t \to \infty} \frac{1}{2dt} \mathrm{MSD}(t) \tag{3}$$

where d is the dimensionality of diffusion. For lateral diffusion $d = 2$. In order to have a well-defined diffusion coefficient, one must find $\mathrm{MSD}(t) \sim t^{\alpha}$ with $\alpha = 1$. This condition is satisfied at long times. Meanwhile, at short times the diffusion is subdiffusive, and the motion along the membrane normal direction also plays a role via protrusions and undulations[31] which imply that lipid motion is not truly two-dimensional.

In simulations of membrane systems, the membrane position may fluctuate with respect to the water phase. Consequently, the motion of individual lipids has to be computed with respect to the motion of the membrane's center of mass.[32]

B. Brief Overview of Free Volume Theories. Free volume theory, presented in 1959 by Cohen and Turnbull,[9] is a model for describing diffusion in a liquid environment. It was originally developed for colloids, more specifically for hard spheres, but it has later been further developed and extended to describe diffusion also in lipid membranes.[10,33−37]

The free volume theory suggests that diffusion occurs via jumps[33−35] where the diffusing particle moves in a short period of time a distance close to its own size. The theory connects the diffusion coefficient with the average free volume available for the

(29) Böckmann, R. A.; Hac, A.; Heimburg, T.; Grubmüller, H. *Biophys. J.* **2003**, *85*, 1647–1655.
(30) Baoukina, S.; Monticelli, L.; Marrink, S. J.; Tieleman, D. P. *Langmuir* **2007**, *23*, 12617–12623.
(31) Sum, A. K.; Faller, R.; de Pablo, J. J. *Biophys. J.* **2003**, *85*, 2830–2844.
(32) Patra, M.; Karttunen, M.; Hyvonen, M. T.; Falck, E.; Lindqvist, P.; Vattulainen, I. *Biophys. J.* **2003**, *84*, 3636–3645.
(33) Galla, H.-J.; Hartmann, W.; Theilen, U.; Sackmann, E. *J. Membr. Biol.* **1979**, *48*, 215–236.
(34) MacCarthy, J. E.; Kozak, J. J. *J. Chem. Phys.* **1982**, *77*, 2214–2216.
(35) O'Leary, T. J. *Proc. Natl. Acad. Sci. U.S.A.* **1987**, *84*, 429–433.
(36) Macedo, P. B.; Litovitz, T. A. *J. Chem. Phys.* **1965**, *42*, 245.
(37) Vaz, W. L. C.; Clegg, R. M.; Hallmann, D. *Biochemistry* **1985**, *24*, 781–786.

diffusing particle to undergo diffusive motion. The relation is given as

$$D = A \exp(-\gamma v^*/v_f) \quad (4)$$

where v_f is the free volume available and v^* is called critical volume, that is, it represents the minimum volume of the void required for the jump. The parameter A is a constant, and γ is a numerical factor which accounts for possible overlap of free volume ($0.5 < \gamma < 1$).[9]

The free volume theory was further developed by Macedo et al.,[36] who proposed that free energy should also be taken into account for a diffusive jump to overcome possible energetic barriers. The equation for the diffusion coefficient is then written as

$$D = D' p(v) p(E) \quad (5)$$

where $p(v)$ is the probability for finding a sufficiently large void next to the diffusing particle and $p(E)$ represents the probability that the diffusing particle has enough free energy to release itself from the interactions with neighboring molecules. The expression $p(E)$ follows the Boltzmann distribution, and D' is a constant.

More recent studies have extended the free volume theory to describe diffusion in lipid bilayers.[10,33−35,37] As there are quite a few slightly different versions of the free volume theory, we focus here on one of the most recent ones.[10] It is also worth pointing out that, as in lipid bilayers one deals with diffusion in two dimensions, it is common to speak about the free area theory where the quantity of interest are area fluctuations in the plane of a lipid membrane. Another relevant remark is that while the free volume in a membrane is distributed in small pieces, its total amount inside a membrane is rather substantial.[38,39] It has been found, for example, that there is sufficient free volume around the water−membrane interfacial region to enable fast rotations of non-native molecules such as fluorescent probes.[40,41]

Almeida et al.[10] applied the free volume theory to lipids in a planar membrane. They assumed that the problem is essentially two-dimensional, and therefore the critical volume can be replaced with a critical area parameter a^*. For diffusion in a plane, a^* describes the area above which lateral diffusion becomes possible. Following the results of MacCarthy and Kozak,[34] Almeida et al. considered that $\gamma a^* = a_0$, where a_0 is now the cross-sectional close-packed area of the lipid. The expression they used is thus given as

$$D = \frac{\delta}{2\sqrt{2}} \sqrt{\frac{k_B T}{m}} \exp\left[\frac{-a_0}{a(T) - a_0} - \frac{E_a}{k_B T}\right] \quad (6)$$

where δ is the distance between cages, k_B the Boltzmann constant, $a(T)$ the area per lipid at temperature T, and E_a the activation energy of a diffusion jump. The theory considers lipids as homogeneous rods that all span the same height in the membrane. The lipids rattle in a cage formed by the surrounding lipids until they are able to jump a distance close to their own size to the neighboring cage. The jump is assumed to happen at thermal speed (corresponding to thermal energy),[10] meaning that for a lipid it would take of the order of 10 ps to move the distance of about 1 nm. By noticing that δ in a tight-packed cubic lattice is just the square root of the area per lipid and by plugging the numerical values of the constants into eq 6, one obtains a useable formula for the diffusion coefficient

$$D = 3.224 \times 10^{-5} \sqrt{\frac{T a(T)}{M}} \exp\left[\frac{-a_0}{a(T) - a_0} - \frac{E_a}{k_B T}\right] \quad (7)$$

where M is the molar mass given in units of g/mol. The values for the areas are given in Å^2.

When the free volume theory is applied in practice, the measured lateral diffusion data is fitted to the above description, yielding the close-packed cross-sectional area of a lipid a_0 and the activation energy E_a.

C. Assumptions in Free Volume Theory for Lateral Diffusion. For the discussion in this article, it is useful to consider the limitations of the current free volume theories for lateral diffusion. The main assumptions of the free volume model of Almeida et al.[10] are as follows:[15] (1) For describing diffusion in membranes, a lipid is considered as a hard rod with a well-defined close-packed area a_0, which is independent of temperature and composition of the membrane. (2) Diffusion proceeds via jumps. During a jump, a whole lipid moves a distance close to its own diameter in a short interval of time. (3) A lipid may jump when it is given a patch of free area larger than a_0 next to it. (4) Changes in free volume (area) distribution occur faster (on a much faster time scale) than the translational motion of lipids and do not require local free energy. (5) The lipid needs to overcome an activation barrier, i.e., break loose from the interactions with its nearest neighbors. This requires an activation energy E_a. The activation energy also incorporates the interactions with the aqueous phase. The validity of some of these assumptions has been questioned in the literature. We summarize here the issues related to three of these assumptions, namely the cross-sectional area, the activation barrier, and the diffusion mechanism.

While the free volume theory regards membranes as homogeneous in the direction of the membrane normal, they are actually heterogeneous.[12,16,42] The average close-packed area of a phospholipid and the average free area per lipid vary considerably along the membrane normal.[11,12,16,39,43,44] Also, this close-packed area profile and free area distribution change with lipid composition[16] and are likely to be temperature dependent, too. For the reasons above, the assumption of a well-defined and constant cross-sectional area of a lipid seems not well justified for lipid membranes.

The activation energy E_a describes the barrier needed to break loose from the interactions with the lipid's nearest neighbors. This view is largely similar to the interpretation of the effective activation barrier E_{Arrh} extracted from the very commonly used Arrhenius description. Given this idea, are these two activation barriers related? More generally, how should E_a be interpreted in terms of the interactions in a membrane?

The free volume theory assumes that particle motion takes place via "jumps".[33−35] While this is possible for hard-sphere systems like colloids, it is not clear whether this assumption is appropriate for lipids in membranes. Simulation studies by Essmann and Berkowitz,[45] Moore et al.,[46] and Voth et al.[47]

(38) Sane, P.; Salonen, E.; Falck, E.; Repakova, J.; Tuomisto, F.; Holopainen, J. M.; Vattulainen, I. *J. Phys. Chem. B* **2009**, *113*, 1810–1812.
(39) Falck, E.; Patra, M.; Karttunen, M.; Hyvonen, M. T.; Vattulainen, I. *J. Chem. Phys.* **2004**, *121*, 12676–12689.
(40) Repakova, J.; Capkova, P.; Holopainen, J. M.; Vattulainen, I. *J. Phys. Chem. B* **2004**, *108*, 13438–13448.
(41) Gullapalli, R. R.; Demirei, M. C.; Butler, P. J. *Phys. Chem. Chem. Phys.* **2008**, *10*, 3548–3560.
(42) Marrink, S. J.; Berendsen, H. J. C. *J. Phys. Chem.* **1994**, *98*, 4155–4168.
(43) Alinchenko, M. G.; Anikeenko, A. V.; Medvedev, N. N.; Voloshin, V. P.; Mezei, M.; Jedlovszky, P. *J. Phys. Chem. B* **2004**, *108*, 19056–19067.
(44) Kupiainen, M.; Falck, E.; Ollila, S.; Niemela, P.; Gurtovenko, A. A.; Hyvonen, M. T.; Patra, M.; Karttunen, M.; Vattulainen, I. *J. Comput. Theor. Nanosci.* **2005**, *2*, 401–413.
(45) Essmann, U.; Berkowitz, M. L. *Biophys. J.* **1999**, *76*, 2081–2089.
(46) Moore, P. B.; Lopez, C. F.; Klein, M. L. *Biophys. J.* **2001**, *81*, 2484–2494.
(47) Ayton, G. S.; Voth, G. A. *Biophys. J.* **2004**, *87*, 3299.

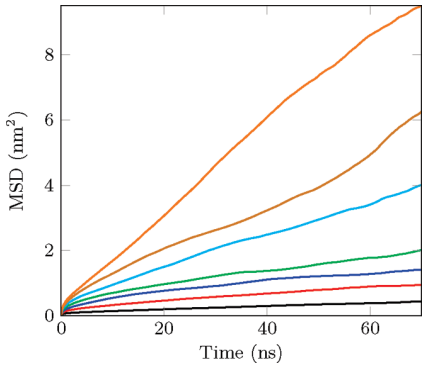

Figure 2. Mean-squared displacement data for DPPC. The different curves stand for an area of 44 Å^2 (black), 48 Å^2 (red), 52 Å^2 (blue), 56 Å^2 (green), 60 Å^2 (cyan), 64 Å^2 (brown), and 68 Å^2 (orange).

Table 1. Long-Time Diffusion Coefficients for the Lipids (in Units of 1×10^{-7} cm^2/s)[a]

A/lipid (Å^2)	$D_{average}$	D_{DPPC}	D_{POPC}	D_{POPG}	$D_{cholesterol}$
44	0.146	0.143	0.142	0.177	0.117
48	0.386	0.378	0.367	0.363	0.582
52	0.697	0.649	0.805	0.560	1.014
56	0.740	0.687	0.858	0.596	1.069
60	1.312	1.258	1.278	1.039	2.523
64	1.777	1.702	1.862	1.370	3.040
68	2.838	2.760	2.978	2.286	4.137

[a] The error bars are less than 10%. They were calculated by estimating the maximum error, which was determined by the difference of the diffusion coefficients in the x and y directions (on the monolayer plane).

suggest that jumps do not dominate lateral diffusion in bilayers but instead collective fluctuations[47] are prevalent. Simulations by Falck et al.[17] and Apajalahti et al.[18] also provided evidence for concerted lipid motions, where lipids move as transient lipid clusters. The same view has been given by recent experimental data.[19] Considering these results, if there are no jumps, then how should the area parameter a_0 and the activation energy E_a be interpreted?

In the rest of this paper we try to answer the questions above. In particular, we investigate the physical interpretation for the area parameter and the activation barrier, and we also consider the mechanism of lipid diffusion. Lipid monolayers provide interesting test systems for studying the free volume theory since the total area of the system can be varied systematically and in a controlled way, both in experiments and in simulations.

IV. Results

A. Free Volume Theory Fitted to Lateral Diffusion Data.

The mean-squared displacement of DPPC with varying area per molecule is shown in Figure 2. The regime of normal diffusion where MSD(t) $\sim t^1$ emerges at times of about 10−20 ns, depending on the area per lipid. The diffusion coefficients determined from the long-time limit of the mean-squared displacement are given in Table 1. The results indicate that the diffusion coefficients for all lipid types increase for increasing area per molecule, as expected.

The diffusion coefficients were fitted to eq 7. Here, the activation energy of a diffusion jump (E_a), one of the parameters in the free volume theory, was considered to be independent of the compression state of the system. The area of a cholesterol molecule was fixed to a value of 30 Å^2. This assumption seems reasonable because cholesterol has a smooth and rigid structure, with a well-defined cross-sectional area.[16] Under these conditions,

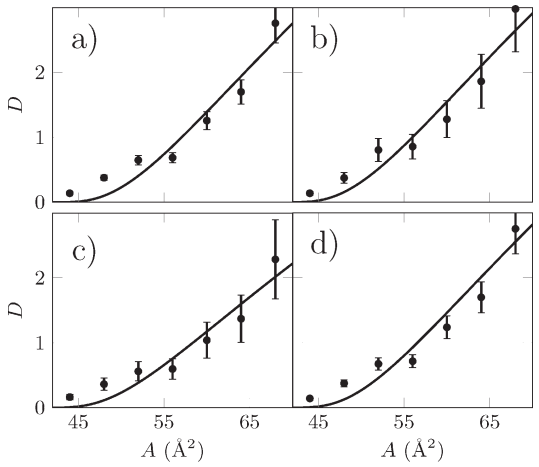

Figure 3. Free volume theory fits (full line) to the calculated diffusion coefficients (crosses): (a) DPPC, (b) POPC, (c) POPG, and (d) average over all phospholipids. Diffusion coefficients are given in units of 10^{-7} cm^2/s.

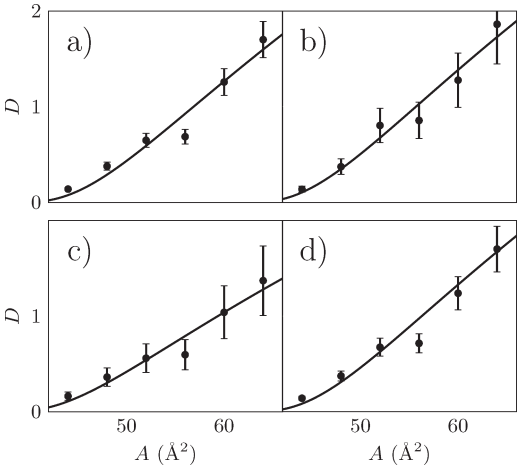

Figure 4. Free volume theory fits (full line) to the calculated diffusion coefficients (crosses), without the data for the largest system (A = 68 Å^2): (a) DPPC, (b) POPC, (c) POPG, and (d) average over all all phospholipids. Diffusion coefficients are given in units of 10^{-7} cm^2/s.

the fitting process allowed us to extract the two parameters that are central to the free volume theory, namely a_0 and E_a. Additional studies with cholesterol's cross-sectional area different from 30 Å^2 (between 25 and 35 Å^2) indicated that this had only a marginal effect on the results below: the activation barrier remained unchanged and a_0 varied less than 0.5 Å^2.

The fitting procedure was first performed on the data of all seven systems, resulting in the fit shown in Figure 3. It is clear that the data and the free volume theory do not match particularly well in this case. Especially the data of the system with the largest area per molecule deviates from the description of the free area theory. This is expected since the system with the largest area indicated formation of membrane pores, which speed up diffusion compared to a defect-free monolayer. For this reason we also performed another fit leaving out the most expanded monolayer. Fits obtained in this manner were found to follow the diffusion data better (see Figure 4).

The parameters extracted from both fits (a_0, E_a) are given in Table 2. The area parameter is about 35 Å^2, and the activation

Table 2. Parameters Obtained through Fitting to the Free Volume Theory

	all points		largest area left out	
lipid	a_0 (Å^2)	E_a (kJ/mol)	a_0 (Å^2)	E_a (kJ/mol)
DPPC	40.11	13.37	35.95	14.74
POPC	39.21	13.33	35.38	14.59
POPG	39.32	14.03	34.47	15.55
phospholipids	39.70	14.21	35.84	15.47

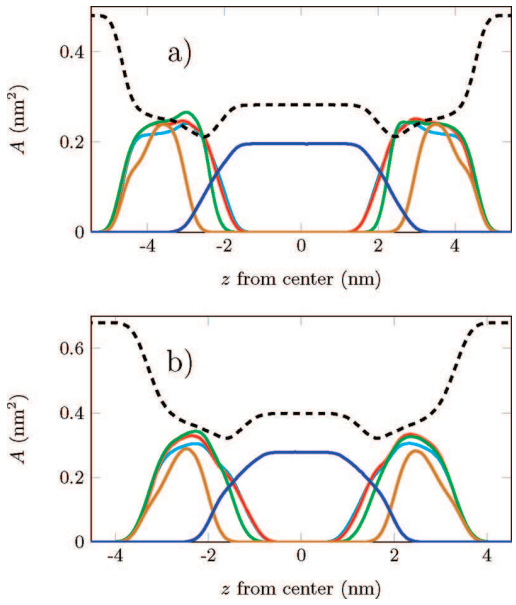

Figure 5. Close-packed cross-sectional area profiles for the lipids as functions of distance from the middle of the water phase: (a) $\langle A \rangle = 48$ Å^2 and (b) $\langle A \rangle = 68$ Å^2. Color codes are as follows: water (dark blue), POPC (red), DPPC (light blue), POPG (green), cholesterol (brown), free volume (dashed black). Note that here results are shown for the two different monolayers facing the water phase (see Figure 1). The minor differences in the almost symmetric profiles (with respect to $z = 0$) indicate that the errors are of the order of a few percent.

barrier is ~15 kJ/mol. There is only minor variation among the parameter values for the different lipid types.

B. Cross-Sectional Closed-Packed Area Profile of Lipids. The cross-sectional area of lipids in a membrane is conceptually difficult to define, unless one considers rigid molecules such as cholesterol, or very ordered phases such as the gel state. The difficulty arises from the highly flexible conformations of phospholipid acyl chains. The conformations of individual phospholipids change rapidly in time, and the distribution of possible conformations is very broad.

To get more insight into this issue, we determined the average close-packed cross-sectional area of the lipids using the technique discussed by Falck et al.[16] (see Models and Methods). The results in Figure 5 show that the cross-sectional area is not constant but varies rather strongly along membrane normal direction. The cross-sectional area is the largest close to the headgroup region, as the packing of lipids is the highest in this part of the membrane. As we need some operational definition for the close-packed area, we decide to consider the largest values of the area profiles in Figure 5 and use them as the close-packed cross-sectional area for the lipids discussed here.

Figure 5 shows that the close-packed cross-sectional area of cholesterol is about 0.25 Å^2 at $\langle A \rangle = 48$ Å^2 and about 0.30 Å^2 at

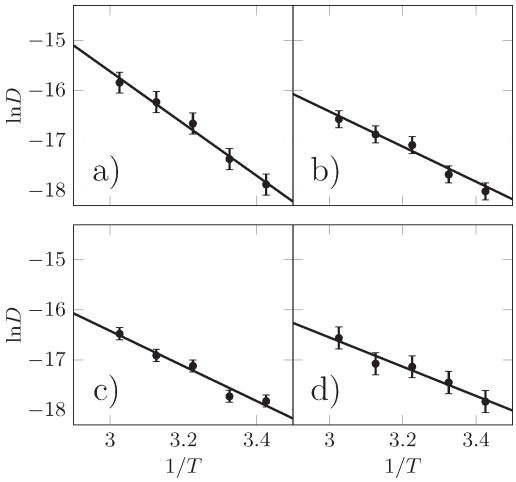

Figure 6. Arrhenius equation fits to the calculated diffusion data for the system with $A = 48$ Å^2/lipid. Inverse temperatures are given in units of 10^{-3} K^{-1}. (a) Cholesterol, (b) DPPC, (c) POPC, and (d) POPG.

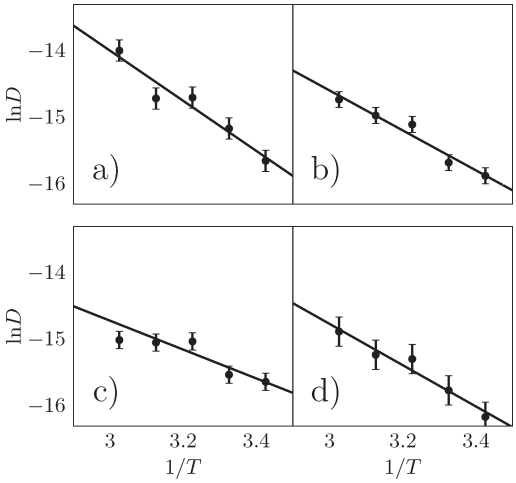

Figure 7. Arrhenius equation fits to the calculated diffusion data for the system with $A = 68$ Å^2/lipid. Inverse temperatures are given in units of 10^{-3} K^{-1}. (a) Cholesterol, (b) DPPC, (c) POPC, and (d) POPG.

$\langle A \rangle = 68$ Å^2. The figure of 0.25 Å^2 found in the highly compressed case is consistent with the steric profile measured by Rothman and Engelman, who found the cross-sectional area of cholesterol to have a plateau around 25 Å^2.[48] This confirms that the present analysis is valid, providing insight for the close-packed cross-sectional area profile. For other lipids, the cross-sectional areas are larger, as expected, and range between 0.25 and 0.28 Å^2 at $\langle A \rangle = 48$ Å^2 and between 0.32 and 0.35 Å^2 at $\langle A \rangle = 68$ Å^2. The close-packed cross-sectional areas are smallest for cholesterol and increase in the order of DPPC, POPC, and POPG.

C. Activation Barrier and Diffusion Mechanism. The interpretation of the activation barrier E_a in the free volume theory also calls for attention. To better understand its nature, we compared its value to the diffusion barrier determined from the Arrhenius analysis. The results in Figures 6 and 7 highlight that the Arrhenius form describes the temperature dependence of lateral diffusion well over the given temperature window.

(48) Rothman, J. E.; Engelman, D. M. *Nat. New Biol.* **1972**, *237*, 42–44.

Table 3. Arrhenius Barriers (kJ/mol) for the Two Different Systems with Area per Lipid of 48 and 68 Å^2

lipid	48 Å^2	68 Å^2
all	30.76	23.65
cholesterol	43.34	31.31
DPPC	30.66	24.95
POPC	29.18	18.04
POPG	24.29	25.79

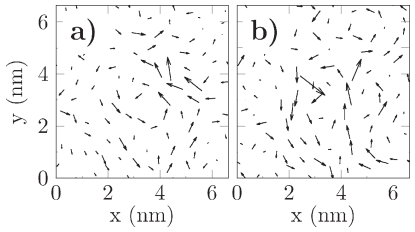

Figure 8. Diffusion patterns for a system with an area per molecule equal to 40 Å^2. The displacements are shown with respect to the same initial structure. The given positions are in units of nanometers. The displacement time intervals are (a) 20 ns and (b) 40 ns.

Table 3 shows that the Arrhenius barriers found through this analysis are about 30 kJ/mol at 48 Å^2 and 24 kJ/mol at 68 Å^2.

One of the underlying assumptions in the free volume theory for lipid diffusion is that lipids migrate in terms of "jumps" from one cage to another. We considered this aspect by following the motions of all the lipids in the studied systems. During these analyses, we found no indication for single-particle "jumps", where a lipid would have rapidly moved a distance comparable to its own size, while other lipids around it would have remained in their own cages.

A pictorial representation of lipid diffusion is given in Figure 8, showing in-plane lateral displacements for time intervals of 20 and 40 ns. The cooperative nature of lipid diffusion at this length scale is evident. Lipids diffuse in a concerted manner as loosely defined dynamic clusters. The motion gives rise to diffusion patterns which closely resemble those observed in fluid single-component and many-component lipid bilayers.[17,18]

V. Discussion

A. Diffusion Coefficients. The values of diffusion coefficients shown in Table 1 are in line with earlier simulations and experiments. Baoukina et al. have calculated the diffusion coefficients for a coarse-grained single-component (DPPC) monolayer in the liquid-expanded (LE) and liquid-condensed (LC) phases at 300 K.[30] They found values of $(2.4 \pm 0.1) \times 10^{-7}$ and $(3.3 \pm 0.1) \times 10^{-7}$ cm^2/s with areas per molecule of 57 and 63 Å^2, respectively. Our present results indicate diffusion coefficients about 2−3 times smaller. The discrepancy is minor and can be explained by the difference in the composition between the simulated systems. Indeed, the present systems contain cholesterol, which is known to slow down diffusion. In fluidlike two-component bilayers the slowing down has been observed to take place by a factor of about 2−3,[10,49] while in membranes whose composition is consistent with pulmonary surfactant, de la Serna et al. found cholesterol to slow down diffusion by about 10−15%.[50]

Comparison to Langmuir monolayer experiments is more difficult to carry out. Diffusion in Langmuir monolayers is often measured using lipid-linked probe particles whose sizes range from about 30 to 100 nm,[6] and they inevitably have some role to play in the dynamics of the tagged lipid. Another common concern is the collective drift of a monolayer, which complicates the analysis of diffusion. Forstner et al.[6] made a considerable effort to rule out many of such undesired effects in a study of lateral diffusion for a DMPC monolayer at room temperature. They found a diffusion coefficient of about 1×10^{-8} cm^2/s for a wide range of surface pressures from about 1 to 30 mN/m. This diffusion coefficient is considerably smaller than the ones we have observed. However, it is not clear why the diffusion coefficients found in ref 6 do not depend on the area per molecule, as one would expect. Gudmand et al. have very recently used fluorescence correlation spectroscopy to measure lateral diffusion in a DMPC monolayer at 295 K.[5] They found[5] $D \approx 4 \times 10^{-7}$ cm^2/s at 70 Å^2, about 2.5×10^{-7} cm^2/s at 60 Å^2, and 1.5×10^{-7} cm^2/s at 55 Å^2. These are roughly 2 times larger than our results, but considering the presence of cholesterol in our monolayer, the agreement seems very reasonable. Remarkably, lateral diffusion coefficients found in those experiments increase monotonously with increasing surface area (i.e., decreasing surface pressure), in line with our observations.

B. Free Volume Theory Fits Diffusion Data. The fits shown in Figures 3 and 4 indicate that the free volume theory can be used to describe the diffusion data, if one concentrates on the condensed phase at high surface pressure. Deviations from the theory are evident at the lowest surface pressure, which is characterized by formation of pores. Clearly the inherent assumptions in the free volume theory are broken in those conditions, as larger free volume regions emerge and facilitate diffusion. This topic was recently discussed by Falck et al. in the context of lipid bilayers.[15] Merkel et al. did lipid monolayer experiments and also concluded[51] that the free volume theory was not valid in the regime where the monolayer was in the gas phase characterized by considerable pores in the membrane. In a more recent study by Gudmand et al.,[5] the authors studied a DMPC Langmuir monolayer for areas per molecule from about 50 to 95 Å^2. They observed their data to fit the free volume theory well.

We notice that the formation of pores in monolayer simulations at relatively small surface areas is an artifact due to the unrealistic surface tension of a simulated water−vapor interface. At 25 °C the surface tension of water is ∼72 mN/m, while the TIP3P water model yields only about 48 mN/m (with simulation conditions as specified in the Models and Methods section). As a result, the energy cost of a water−vapor interface is underestimated by the model. This, in turn, allows the formation of pores in the lipid monolayer. Another consequence of this artifact is the underestimation of the total surface tension at the interfaces. Despite these limitations, the properties and the behavior of lipid monolayers in simulations are realistic as long as the simulated systems do not have water−vapor interfaces.

C. Cross-Sectional Area in Free Volume Theory. The cross-sectional area and activation energy obtained from our simulations (see Table 2) are very similar for all phosholipids in our system, so we focus here on DPPC as an example. The cross-sectional area a_0 is found to be 36.0 Å^2, and the activation energy turns out to be 14.7 kJ/mol. How realistic are these numbers, and how do they compare to the other measures we have determined by the other analysis techniques?

The value we obtained for DPPC's cross-sectional close-packed area parameter $a_0 = 36.0$ Å^2 is seemingly realistic, but are there means to validate it? According to the free volume theory, the critical area $a^* = a_0/\gamma$ should describe the smallest

(49) Filippov, A.; Oradd, G.; Lindblom, G. *Biophys. J.* **2003**, *84*, 3079–3086.
(50) de la Serna, J. B.; Oradd, G.; Bagatolli, L. A.; Simonsen, A. C.; Marsh, D.; Lindblom, G.; Perez-Gil, J. *Biophys. J.* **2009**, *97*, 1381–1389.
(51) Merkel, R.; Sackmann, E. *J. Phys. Chem.* **1994**, *98*, 4428–4442.

possible area that renders a diffusion jump possible. Given that values of γ range between 0.5 and 1,[9] the critical area a^* would be 36−72 Å^2. Intuitively, this value should be almost identical to the area per lipid in the gel phase, where lipids diffuse but do so very slowly due to the very small amount of free volume. For DPPC the area per lipid in the gel phase has been found to be 47.2 ± 0.5 and 47.9 Å^2,[52,53] suggesting that a^* and hence also a_0 are realistic.

More insight is given by the analysis we carried out using the technique discussed by Falck et al.[16] For DPPC, the average close-packed cross-sectional area is about 25 Å^2 in the highly compressed system ($\langle A \rangle$ = 48 Å^2) and about 32 Å^2 in the fluid monolayer ($\langle A \rangle$ = 68 Å^2). In the case of $\langle A \rangle$ = 68 Å^2, the results for DPPC are in good agreement with those in ref 16 for a DPPC−cholesterol bilayer with a small cholesterol concentration.

As the free volume theory assumes lipids to be like rods with a well-defined shape, and with a constant a_0 that does not depend on surface pressure, the logical choice is to compare the smallest close-packed cross-sectional area with a_0. The result in this highly compressed case, 25 Å^2, is somewhat smaller than the value given by the fit to the free volume theory, 36.0 Å^2. The difference between the two may be even larger, as the value we have used for the close-packed cross-sectional area is the maximum in the area profile (see Figure 5). Nonetheless, given the uncertainty in fitting, and the fact that the analysis is based on averaging over the specific shapes of individual lipids, this number is in reasonable agreement with the value of 36.0 Å^2 that results from the free volume theory fit.

For other phospholipids, the results and conclusions are essentially similar to those found for DPPC. The largest areas are found for POPG, which yields a closed-packed cross-sectional area of about 28 Å^2 at $\langle A \rangle$ = 48 Å^2 and about 35 Å^2 at $\langle A \rangle$ = 68 Å^2. The fit of the POPG diffusion data to the free volume theory yields a_0 = 34.5 Å^2.

The results indicate that the cross-sectional area a_0 obtained by fitting D (using the free volume theory) is approximately similar to the cross-sectional area calculated directly from the simulation data, although the agreement is not quantitative. The differences are about 5−40%. Given the uncertainties in the fitting procedure, the agreement is reasonable.

D. Activation Barrier in Free Volume Theory. How about the interpretation of the activation energy E_a? We compared the values of E_a obtained via the free volume theory (Table 2) with the Arrhenius diffusion barriers E_{Arrh} (Table 3), obtained by analyzing simulations at different temperatures. The Arrhenius description can generally be applied to different kinds of activated processes, including lateral diffusion in lipid membranes.[33,49,54−56]

We find that E_a depends only weakly on the type of lipid, the largest differences being about 7%. For Arrhenius barriers the differences between the lipids are more considerable, the largest ones being about 80%.

Let us first consider the Arrhenius barriers since comparison to experimental data is then easier to make. Overall for all the lipids, the results are consistent with typical Arrhenius diffusion barriers of about 27−31 kJ/mol measured by NMR in fluid single-component lipid bilayers in the same temperature range.[49] The figures we found for E_{Arrh} also seem reasonable: 18−31 kJ/mol correspond to about 7−13 k_BT at physiological temperature. For comparison, hydrogen bonds are typically about 5−8 k_BT, and as they are one of the most common interaction types in lipid−water systems, the Arrhenius barrier values seem appropriate.

The largest Arrhenius barrier is found for cholesterol, characterizing that its rate of change is the largest among the lipids considered for increasing T. The Arrhenius barriers further increase as the membrane becomes more packed. This is also consistent with experiments, as Filippov et al. found for cholesterol-rich PC membranes Arrhenius diffusion barriers of about 31−64 kJ/mol,[49] where the largest values were observed in densely packed cholesterol−sphingomyelin systems.

The Arrhenius barriers are higher (by a factor of about 2) than the activation barriers predicted by the free volume theory. In the context of lipid bilayers, Falck et al. also found substantial discrepancies between the Arrhenius diffusion barrier and the activation energy associated with the free volume theory.[15]

The Arrhenius barrier is an average over a distribution of instantaneous activation barriers. The barrier found via the Arrhenius analysis is expected to reflect some effective energy barrier related to the rate limiting step in the diffusion process. It is tempting to assume that the interpretation of E_a in the free volume theory is the same, but apparently this is not the case. Currently, we are unaware of other physical variables describing the thermally activated nature of diffusion that could provide an interpretation for E_a. The physical meaning of the activation energy in the free volume theory remains therefore unclear.

E. Diffusion Mechanism. Finally, let us discuss the diffusion mechanism. When the free volume theory is applied to describe diffusion in lipid bilayers and monolayers, it is rather commonly assumed that the diffusion of lipids takes place as "jumps",[33−35] where the particle moves a distance of its own size rapidly at thermal speed:[10] a lipid rattles for long times in its cage, where it is surrounded by other molecules, and only occasionally it undergoes a rapid jump over a distance of its own linear size in the membrane plane from one cage to another. In our analysis, we did not observe any of such jumps. Instead, the simulation results indicate the diffusion of lipids to take place through concerted lipid movements with tens of lipids moving in unison as loosely defined lipid clusters. These observations are largely similar to those found in lipid bilayers,[17,18,57] and recent quasi-elastic neutron scattering experiments for lipid bilayers are also consistent with this view.[19]

This observation enforces one to reconsider the interpretation and the role of a_0 in the diffusion process. Diffusion of lipids takes place in terms of transient lipid clusters where the cluster diffuses as a whole, and the diffusion of lipids cannot be described as rapid motion of single lipids in a slowly changing environment. Therefore, given that there are no true single-particle displacements that would require local free area pockets of the same size as a_0, the role of the single-particle close-packed cross-sectional area in the lateral diffusion process is unclear.

VI. Concluding Remarks

In this article, we have considered lateral diffusion of lipids in a protein-free model for the lung surfactant. In particular, we have studied the validity of the free volume theory for diffusion in Langmuir monolayers and the interpretation of its parameters.

The applicability of the free volume theory has been discussed previously for lipid bilayers[15,58] and to some extent also for

(52) Sun, W.; Suter, R. M.; Knewtson, M. A.; Worthington, C. R.; Tristram-Nagle, S.; Zhang, R.; Nagle, J. F. *Phys. Rev. E* **1994**, *49*, 4665–4676.
(53) Tristram-Nagle, S.; Zhang, R.; Suter, R. M.; Worthington, C. R.; Sun, W. J.; Nagle, J. F. *Biophys. J.* **1993**, *64*, 1097–1109.
(54) Filippov, A.; Oradd, G.; Lindblom, G. *Langmuir* **2003**, *19*, 6397–6400.
(55) Cullis, P. R. *FEBS Lett.* **1976**, *70*, 223–228.
(56) Shin, Y.-K.; Freed, J. H. *Biophys. J.* **1989**, *55*, 537–550.
(57) Roark, M.; Feller, S. E. *J. Phys. Chem. B* **2009**, *113*, 13229–13234.
(58) Almeida, P. F. F.; Vaz, W. L. C.; Thompson, T. E. *Biophys. J.* **2005**, *88*(6), 4434–4438.

experimental studies of monolayers.[5] With the present study we considered its validity for lipid monolayers in the liquid-condensed and liquid-expanded phases. We found that the free volume theory describes the diffusion data reasonably well, if one concentrates on the highly packed phases. Deviations from the theory are evident in the loosely packed systems characterized by membrane pores, which inevitably facilitate and speed up diffusion. This finding implies that the free volume theory is not particularly useful for describing diffusion in the gas phase. However, even in closely packed phases, there is reason to ask what can we learn from the free volume theory, assuming that it describes realistically the diffusion process. Our present results indicate that the parameters extracted from the fits of the diffusion data to the free volume theory are not easy to interpret.

The values we obtained for the critical area $a^* = a_0/\gamma$ are consistent with the area per lipid in the gel phase. However, this view has to be taken with caution, since the numerical correction factor γ accounting for possible overlap of free volume ranges from 0.5 to 1, and hence also a^* embraces a broad distribution of areas from 36 to 72 Å^2. A more direct comparison of a_0 with the "hard-core" cross-sectional area profile[16] showed that a_0 differs from the hard-core size of a lipid, the quantitative difference being about 5−40%. Given the uncertainty in fitting and analysis, this difference is acceptable. The cross-sectional area parameter a_0 thus may have potential for describing the close-packed size of a lipid.

The interpretation of the activation energy E_a in the free volume theory is more problematic. A careful comparison to the Arrhenius diffusion barrier showed that the activation barrier of the free volume theory and the Arrhenius diffusion barrier are not directly related. While the free volume theory yields $E_a \approx 15$ kJ/mol, the Arrhenius analysis gives $E_{Arrh} \approx 25$ kJ/mol for DPPC and POPG. Moreover, while the activation barriers E_a are almost identical for all the four lipid types we have considered, the Arrhenius diffusion barriers range from 18 to 43 kJ/mol. We conclude that the physical meaning of the activation energy in the free volume theory is unclear.

Another point that has been part of the free volume theory since its derivation for colloidal systems is the assumption of diffusion taking place through jumps. While this assumption of jumplike motions is typically not mentioned in the extensions of free volume theories for membranes, it is unavoidably part of them. Our results for lipid monolayers have shown that, instead of single-particle jumps from one cage to another, lipids diffuse in terms of concerted motions where numerous lipids move in concert as a dynamical cluster. Clearly, there is reason to consider revising the free volume theory to account for this collective mechanism.

Summarizing, the present results are in line with previous studies,[5,10,51] showing that the free volume theory can be parametrized to describe lateral diffusion data for lipids, at least approximately. The more difficult task is to interpret the parameters in a physically meaningful way. There is clearly work to be done to clarify the remaining issues and to develop novel theoretical descriptions that also account for the concerted nature of diffusion.

Acknowledgment. We thank the Academy of Finland Center of Excellence program (M.J., L.M., I.V.), the Danish National Research Foundation (J.B.S.), and the Lundbeck Foundation (J.B.S.) for support. The CSC−IT Centre for Science in Finland and the HorseShoe cluster in Odense, Denmark, are thanked for computing resources.

IV

DIFFUSION OF INTEGRAL MEMBRANE PROTEINS IN PROTEIN-RICH MEMBRANES

by
Matti Javanainen, Hector Martinez-Seara Monne, Ralf Metzler, and Ilpo Vattulainen, 2017
Journal of Physical Chemistry Letters vol 8, 4308–4313,
DOI: 10.1021/acs.jpclett.7b01758

THE JOURNAL OF PHYSICAL CHEMISTRY Letters

Letter

pubs.acs.org/JPCL

Diffusion of Integral Membrane Proteins in Protein-Rich Membranes

Matti Javanainen,[†,‡] Hector Martinez-Seara,[†,¶] Ralf Metzler,[§] and Ilpo Vattulainen*[,†,‡,∥]

[†]Laboratory of Physics, Tampere University of Technology, 33101 Tampere, Finland

[‡]Department of Physics, University of Helsinki, 00014 Helsinki, Finland

[¶]Institute of Organic Chemistry and Biochemistry of the Czech Academy of Sciences, 166 10 Prague, Czech Republic

[§]Institute for Physics and Astronomy, University of Potsdam, 14476 Potsdam-Golm, Germany

[∥]MEMPHYS - Centre for Biomembrane Physics, University of Southern Denmark, 5230 Odense, Denmark

Supporting Information

ABSTRACT: The lateral diffusion of embedded proteins along lipid membranes in protein-poor conditions has been successfully described in terms of the Saffman−Delbrück (SD) model, which predicts that the protein diffusion coefficient D is weakly dependent on its radius R as $D \propto \ln(1/R)$. However, instead of being protein-poor, native cell membranes are extremely crowded with proteins. On the basis of extensive molecular simulations, we here demonstrate that protein crowding of the membrane at physiological levels leads to deviations from the SD relation and to the emergence of a stronger Stokes-like dependence $D \propto 1/R$. We propose that this $1/R$ law mainly arises due to geometrical factors: smaller proteins are able to avoid confinement effects much better than their larger counterparts. The results highlight that the lateral dynamics in the crowded setting found in native membranes is radically different from protein-poor conditions and plays a significant role in formation of functional multiprotein complexes.

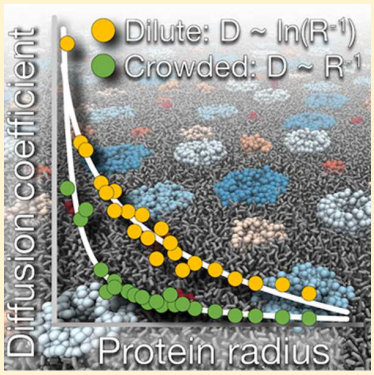

In living biological cells, the plasma membrane hosts numerous integral proteins. Together with membrane lipids and other macromolecules, they are thermally driven to diffuse[1,2] along the plasma membrane to form functional protein oligomers[3,4] and lipid−protein assemblies[5,6] involved in, for example, metabolism, recognition, and signaling.

In this context, the major challenge is to understand protein diffusion under the crowding of proteins. Membranes of living biological cells are highly heterogeneous, partitioned, and extremely rich in proteins,[7−10] with typical lipid/protein ratios ranging between 50 and 200.[11,12] The average in-plane distance between membrane proteins is just a few nanometers, implying that the proteins are in constant interplay colliding with one another. However, how this dynamical interplay induced by protein crowding influences membrane protein diffusion remains poorly understood.

It is known that crowding, together with other phenomena occurring in the membranes of living cells, leads to complex effects,[13,14] but their characterization in the nanoscale has turned out to be difficult. Molecular simulations would be an excellent approach or even the method of choice to explore this challenging topic, but surprisingly, quite little has been done until now. Simulations[15,16] have revealed the emergence of crowding-induced anomalous diffusion[13,14] in lipid membranes, complementing earlier Monte Carlo simulations with immobile objects[17] and clarifying the interpretation of fluorescence correlation spectroscopy experiments[18] that originally confirmed anomalous diffusion to take place in lipid bilayer systems. Besides this, simulations have largely just supported the experimental observations[19] that diffusion slows down for increasing crowding.[15,20,21] As to recent progress on the experimental side, modern atomic force microscopy, single-particle tracking, and a variety of super-resolution microscopy techniques are able to detect, for example, heterogeneity, anomalous diffusion, and nonergodicity in the motion of membrane proteins.[22−24] These techniques have potential to generate breakthrough insight on how functional protein complexes form in native membranes through diffusion and oligomerization. Planning and interpretation of these experiments is difficult, though, given the lack of theoretical understanding of how membrane protein diffusion takes place under protein-rich conditions.

Meanwhile, in the protein-poor limit, the diffusion of proteins is fairly well understood.[1,19] Experimental data have provided compelling evidence that for a membrane protein of lateral radius R, the protein diffusion coefficient D scales logarithmically as $D \propto \ln(1/R)$. This logarithmic dependence has been observed for a variety of membrane proteins[1,25−27] and aggregated peptides.[28] Computer simulations of proteins in protein-poor conditions also support this relation,[20,29] even in the presence of hydrophobic mismatch.[30] While deviations from this relation have also been reported,[31−33] they have been suggested to result from local membrane deformations[34] or experimental setups.[25]

Received: July 8, 2017
Accepted: August 19, 2017
Published: August 19, 2017

DOI: 10.1021/acs.jpclett.7b01758
J. Phys. Chem. Lett. 2017, 8, 4308−4313

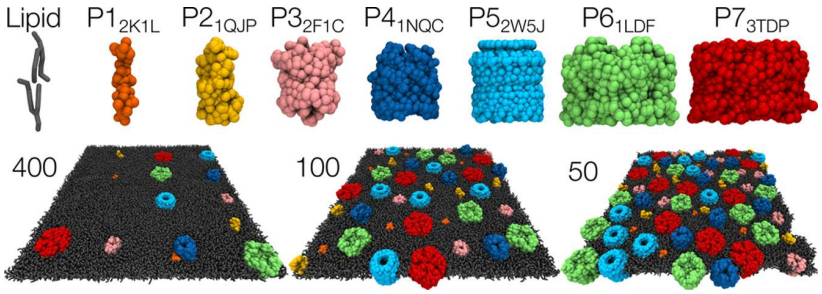

Figure 1. Top: Transmembrane proteins in the polydisperse coarse-grained simulations, labeled P1−P7; the subscript is the PDB identifier (Tables S1 and S2 in the Supporting Information). Two DPPC lipids, making up the bilayer, are also shown to scale. Bottom: Examples of the simulated polydisperse CG membranes with a varying lipid/protein ratio of 400, 100, and 50 lipids per protein per leaflet (left to right). The rightmost system has also appeared in ref 13.

Theoretically, the logarithmic dependence of D on R is predicted by the Saffman−Delbrück (SD) model derived for protein-poor conditions. The SD model links the diffusion coefficient of a protein with the physical properties of the lipid membrane and the surrounding solvent[35,36]

$$D_{\mathrm{SD}} = \frac{k_{\mathrm{B}}T}{4\pi\mu_{\mathrm{m}}h} \times \left[\ln\left(\frac{h\mu_{\mathrm{m}}}{\mu_{\mathrm{f}}R}\right) - \gamma\right] \tag{1}$$

where μ_{m} and μ_{f} are the viscosities of the membrane and the surrounding solvent (typically water), h is the hydrophobic thickness of the membrane, and $\gamma \approx 0.5772$ is the Euler−Mascheroni constant. The SD model treats the lipid bilayer as a continuum liquid, thus failing to describe the diffusion of membrane lipids[37] unless the interleaflet friction is considered.[38] The SD model should be valid for membrane inclusions smaller than the SD length $L_{\mathrm{SD}} = h\mu_{\mathrm{m}}/(2\mu_{\mathrm{f}})$ with a typical value of ∼100 nm.[39] This holds for membrane proteins, but for diffusing objects larger than L_{SD}, the SD model was extended and a Stokes-like dependence $D \propto 1/R$ was found.[39,40] This relation successfully describes domain diffusion in monolayer experiments,[41,42] computer simulations on large inclusions,[29] and diffusion in viscous membranes.[43] However, interpretation of the parameters, such as R, in the SD model is not obvious,[44] and fits to data measured in living cells provide nonphysical values for them.[27] Still, the SD model is consistent with extensive experimental data for the logarithmic dependence on R and hence widely accepted under dilute conditions.

However, given the assumptions made in deriving the SD model for infinitely dilute protein concentrations, can one assume its applicability to biologically relevant membrane systems characterized by protein crowding? If not, then the central questions are, what is the size dependence $D(R)$ replacing the SD law, and for what physical reasons?

In this work, we tackle these outstanding questions by molecular dynamics (MD) simulations. Previous MD studies have addressed the effects of crowding and highlighted decreased diffusivities,[15,20,21] an extended subdiffusion regime,[15,16,20] and deviations from Gaussian statistics.[16] Despite all of the experimental and computational efforts, however, no studies have attempted to probe the validity of the SD model in crowded membranes or found rigorous descriptions for $D(R)$ in the protein-rich limit.

On the basis of the present work on membranes hosting a polydisperse set of proteins, we find that in dilute conditions we reproduce the SD-like weak $D \propto \ln(1/R)$ dependence. However, protein crowding at physiological levels is here shown to result in a crossover to a significantly more pronounced Stokes-like $D \propto 1/R$ relation. We argue that this $1/R$ law mainly arises due to geometrical factors: smaller proteins are able to avoid confinement effects much better than their larger counterparts. This claim is in full agreement with our additional simulations of crowded membranes with a monodisperse protein population and with simulations of a 2D Lennard-Jones (2DLJ) liquid.

To elucidate the effect of protein crowding on the $D(R)$ relationship, we performed MD simulations using two very different models. First, we simulated extensive membranes in the coarse-grained (CG) scheme[45−47] using the Martini model. These membranes contained a polydisperse mixture of seven transmembrane proteins with effective radii between 1 and 4.5 nm, thus mimicking realistic conditions to a satisfactory extent. In each of the simulated five membranes, with lipid/protein ratios equal to 50, 75, 100, 200, and 400 per leaflet, the relative concentrations of the seven protein types were equal. These proteins, chosen to have minimal extramembrane domains and a cylindrical shape, are shown in Figure 1, along with examples of simulated membrane systems. The protein−protein interactions were slightly reduced, resulting in realistic transient oligomerization. Additionally, we used this Martini model to simulate crowded membranes with a monodisperse set of proteins and a lipid/protein ratio of 50 per leaflet. Here, in addition to the proteins shown in Figure 1, the simulations also included two other small proteins (see section S1.4). Second, we simulated 2DLJ fluids with 15 circular inclusions of different radii. The free LJ particle/inclusion ratio varied between 300 and 1000, which provides similar protein/inclusion area coverages as the CG Martini systems. Details on the CG and 2DLJ models and simulations are provided in sections S1.1−S1.4.

The simulations of polydisperse CG models were run for 100 μs each, which allowed reliable extraction of D in the microsecond regime, where diffusion is no longer anomalous but normal[15,16] (section S2.2). The extracted lipid and protein D are shown as a function of the lipid/protein ratio in the top panel of Figure 2. The effect of crowding is somewhat nonlinear, in agreement with earlier works.[15,48] In particular, the effect of crowding on the D's of the smallest proteins and the lipids is most severe. The diffusion coefficients measured for each individual protein reveal fairly small scatter around the mean, indicating that no proteins are immobilized by, for example, extensive aggregation or confinement (section S2.6), except for the $P2_{1QJP}$; see below.

DOI: 10.1021/acs.jpclett.7b01758
J. Phys. Chem. Lett. 2017, 8, 4308−4313

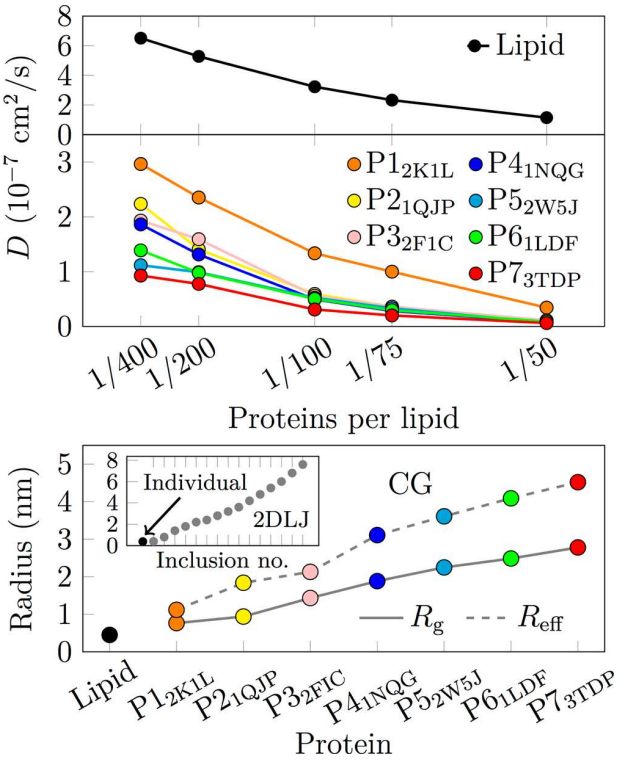

Figure 2. Top: Lipid and protein diffusivities from polydisperse CG simulations. Note that the x axis is linear in protein/lipid values.[15] Bottom: Gyration radii and effective radii of the proteins extracted from single-protein simulations. Inset: size distribution in the 2DLJ system. Coloring as in Figure 1.

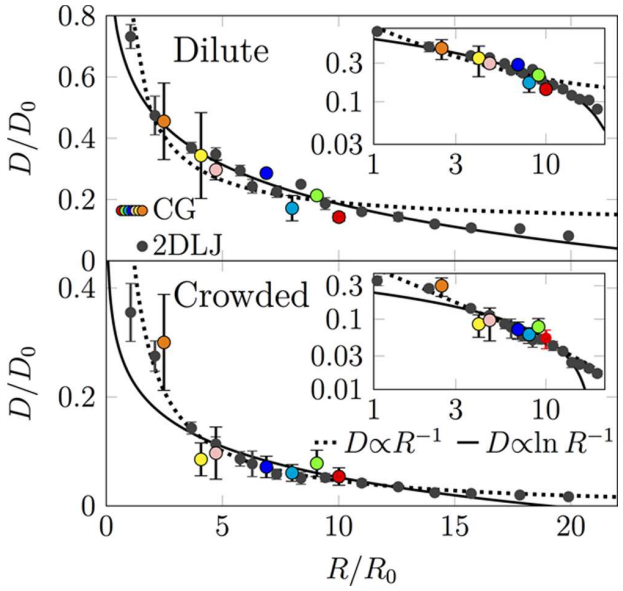

Figure 3. Diffusion coefficients versus protein/inclusion size of the polydisperse CG membrane and 2DLJ models shown in dimensionless units. Unscaled data are shown in sections S2.3 and S2.5. In the dilute case, the data fully agree with the SD model, whereas in the crowded case, the $1/R$ dependence of the diffusivity is evident. Coloring as in Figure 1.

It is established that the radius of a diffusing protein is not simply that of the bare protein alone but includes a shell of lipids moving together with the protein.[44,49] We estimated these effective radii R_{eff} from average lipid displacements in the vicinity of the protein in single-protein simulations (sections S1.2 and S2.1). Protein R_{eff} as well as their bare gyration radii R_g are shown in the bottom panel of Figure 2. R_{eff} values exhibit a systematic increase as a function of R_g. Superimposing the lipid displacement profiles reveals that the thickness of the lipid shell is approximately 1.5 lipid layers thick and independent of the size of the protein as well as of the lipid/protein ratio (see section S2.1).

Figure 3 depicts the protein diffusion coefficient as a function of R_{eff}. Fits of the logarithmic SD-like (eq 1) and the Stokes-like behavior ($D = k_BT\lambda(4\pi\mu_m hR)^{-1} + c$ with characteristic length λ) are shown in Figures 3 and S9. The value of constant c was insignificant. It is evident that at low protein concentrations the data follow $D \propto \ln(1/R)$, in line with previous studies. However, at higher protein concentrations, $D(R)$ becomes increasingly Stokes-like. This observation is independent of the definition of the protein radius (section S2.3), even though R_{eff} provides slightly better fits. The change from the SD-like to the Stokes-like behavior upon crowding is evident on the double-logarithmic scale (insets of Figures 3 and S9). Importantly, these conclusions for the crossover from the logarithmic SD-like to the Stokes-like behavior hold for the polydisperse CG Martini model and also for the 2DLJ model. Further, under protein crowding, the Stokes-like behavior is observed also in monodisperse CG systems (see section S2.9). As an exception to the general trend, the diffusion coefficients calculated for the second smallest protein ($P2_{1QJP}$) do not follow the observed tendencies in most of the systems due to its tendency to aggregate with the largest protein ($P7_{3TDP}$) (see section S2.4), which serves as a reminder that simplified theoretical models cannot account for specific interactions in biological systems. Yet, in monodisperse crowded CG systems (section S2.9), $P2_{1QJP}$ diffuses freely in the absence of $P7_{3TDP}$ and hence follows the $D \propto 1/R$ behavior. Overall, the observation of the Stokes-like behavior for crowded membranes is our first main result.

Setting the hydrophobic thickness of the membrane to $h = 4$ nm[50] and the water viscosity to $\mu_f = 0.7$ mPa s[51] and using R_{eff}, we extract 2.7 mPa s for the membrane viscosity μ_m from fits to the SD model (eq 1) for the most dilute system. This agrees favorably with 3 mPa s measured for a pure DPPC bilayer,[50] suggesting that the $D \propto \ln(1/R)$ dependence arises from an underlying SD-like relationship.

Our extensive CG simulations already provide compelling evidence that at high protein crowding, corresponding to physiological conditions (section S2.8), the $D \propto \ln(1/R)$ relation gets replaced by the $D \propto 1/R$ one. We also considered a 2DLJ model that contains no coupling between the diffusion plane and the surrounding solvent. This model successfully reproduced the key features of membrane dynamics in our earlier work.[16,52] Remarkably, the change in the dependence of $D(R)$ from SD to Stokes-like behavior is also convincingly reproduced by the 2DLJ systems; see Figure 3 (and section S2.5).

The extracted μ_m from the dilute CG simulations gives $L_{SD} \approx 7.7$ nm. The SD model assumes that the diffusing proteins have radii smaller and interprotein distances larger than L_{SD} and that the host membrane and the surrounding solvent are infinite. Otherwise, the finite size of the simulation system might affect its dynamic properties.[38] The observation that $D \propto \ln(1/R)$ is observed in our state-of-the-art simulations, which only partly

DOI: 10.1021/acs.jpclett.7b01758
J. Phys. Chem. Lett. 2017, 8, 4308−4313

fulfill these requirements,[39] suggests that the regime where the relation holds is actually broader than what is expected based on the SD model. Alternatively, the $D \propto \ln(1/R)$ law might result from another underlying and unresolved mechanism, supported by similar behavior of the 2DLJ simulations without membrane−solvent coupling. The observation of the $D \propto \ln(1/R)$ relation in conditions where SD is not expected to hold is our second main result.

Figure 3 combines data from the polydisperse CG (colored dots) and the 2DLJ simulations (black dots) for the dilute (top, 400 lipids per protein, 1000 free LJ particles per inclusion) and crowded (bottom, 50 lipids per protein, 300 free LJ particles per inclusion) cases using dimensionless units (both diffusivities and radii are divided by the corresponding values of a lipid or a single LJ particle (see section S1.5)). While the compared systems do not have exactly the same protein/lipid or inclusion/free LJ particle ratios nor the same surface coverage of proteins/inclusions, this normalization reveals the striking similarity of the functional relationship between diffusion coefficients and radii in these two fundamentally different systems. The data for the dilute systems are well fitted by the $D \propto \ln(1/R)$ model. The crowded case does not follow this SD-like dependence but is instead described accurately by the Stokes-like $1/R$ law. This full *quantitative* consistency of the $D(R)$ behavior between the CG and the 2DLJ models is our third main result.

What is the physical origin of the observed change in the functional form of $D(R)$? Protein crowding increases membrane viscosity, which results in an increase of the SD length and hence should expand the validity of the SD model. However, we instead find that the SD model no longer describes diffusion in the crowded regime. The presence of other proteins violates the basic assumption in the SD model of a single protein embedded in an isotropic continuum liquid. Could interprotein interactions and aggregation lead to smaller effective protein mobilities and thus effect deviations from the SD law? This effect is excluded as due to the specifics of our model setup (sections S1.1 and S1.3) no significant aggregation between proteins or inclusions was observed, except for the aforementioned $P2_{1QJP}$−$P7_{3TDP}$ interaction (see section S2.4). Crowding may also alter the protein and lipid dynamics due to confinement, and proteins mutually act as moving obstacles. It was recently found that proteins need to escape their confinement to properly sample the membrane plane and reach the normal diffusion regime.[15] This escape probability is directly proportional to the protein cross section and hence radius. In the crowded systems, the smallest proteins are able to travel longer distances by slipping through small openings between proteins that are impenetrable for larger proteins. This is visualized in section S2.7 showing 35 μs long trajectories of each of the protein types in the most crowded system. The trajectory of the smallest protein shows both localized rattling motion and rapid movement across longer distances. These spurts correspond to events where the small protein slips through an opening between the larger proteins.

The hypothesis that geometric confinement is responsible for the crossover from $D \propto \ln(1/R)$ behavior to the $1/R$ law is further supported by the 2DLJ simulations, in which the diffusion of disk-shaped inclusions of different radii undergoes an identical transition, as demonstrated *quantitatively* in Figure 3. Also, given that the 2DLJ system is void of any hydrodynamic interactions with the solvent, it is obvious that the change in $D(R)$ must arise from geometric factors: The embedded disks act as obstacles and give rise to confinement effects. Because hydrodynamics is not predominant for this system, the dynamics are likely mostly affected by collisions, which can effectively be modeled by the 2D Enskog theory.[53] While this theory was derived for fairly dilute conditions, it interestingly suggests a $1/R$ dependence of the collision rates on the particle radius.

Does the observed change in the $D(R)$ dependence have any biological relevance? Proteins occupy at least 20% of the surface area of a red blood cell membrane.[11] This corresponds to between 100 and 200 lipids per protein. On the basis of data for lateral protein concentration in the rod outer segment and in the baby hamster kidney cell membranes, an estimate of 50 lipids per protein has been made.[12] In the present work, we found that the crossover from the SD law to the Stokes-like regime takes place at about 200−300 lipids per protein (section S2.8). Therefore, in cell membranes exceptionally crowded with proteins, the diffusion takes place in a regime characterized by Stokes-like scaling $D \propto 1/R$.

Hence, in the crowded case, there is an order of magnitude difference between the diffusion coefficients of the smallest proteins and protein complexes that can be as large as 10 nm, such as the nuclear pore complex. Under crowding, large protein complexes are essentially immobile but interact with small proteins that diffuse rapidly and aggregate with the complex to render them functional. The dynamics in the crowded setting is therefore radically different from protein-poor conditions, where the diffusion of proteins is largely independent of their size, as highlighted by the SD law.

We demonstrated that the $D \propto \ln(1/R)$ relation akin to the celebrated SD model fails to describe protein diffusion under protein crowding. Such conditions favor the diffusion of smaller proteins that are able to escape geometric confinement. Remarkably, this behavior is reproduced in a simple 2DLJ fluid, providing compelling support for the hypothesis that the observed crossover from $D \propto \ln(1/R)$ to $D \propto 1/R$ in crowded membranes is mainly affected by geometric constraints and thus the ability of a given protein to escape confinement. Importantly, the change from the SD-like to the Stokes-like behavior occurs at protein concentrations that are relevant for cellular membranes.[11,12] This suggests that while the SD model has been successful in describing diffusion coefficients in dilute model systems, it should be applied to more realistic biological membranes with extreme care.

■ ASSOCIATED CONTENT

Supporting Information

The Supporting Information is available free of charge on the ACS Publications website at DOI: 10.1021/acs.jpclett.7b01758.

Details on the employed models, the setup of the simulations, and additional results (PDF)

■ AUTHOR INFORMATION

Corresponding Author

*E-mail: ilpo.vattulainen@helsinki.fi.

ORCID

Matti Javanainen: 0000-0003-4858-364X

Ilpo Vattulainen: 0000-0001-7408-3214

Notes

The authors declare no competing financial interest.

DOI: 10.1021/acs.jpclett.7b01758
J. Phys. Chem. Lett. 2017, 8, 4308−4313

Simulation data and all the files required to reproduce or extend the simulations of the polydisperse coarse-grained systems are available at DOI: 10.5281/zenodo.846428.

■ ACKNOWLEDGMENTS

We thank CSC−IT Center for Science for computational resources. The Academy of Finland (Centre of Excellence program (Grant No. 307415)), the European Research Council (Advanced Grant CROWDED-PRO-LIPIDS (Grant No. 290974)), and the Czech Science Foundation (Grant No. 208/12/G016) are thanked for financial support.

■ REFERENCES

(1) Vaz, W. L.; Goodsaid-Zalduondo, F.; Jacobson, K. Lateral Diffusion of Lipids and Proteins in Bilayer Membranes. *FEBS Lett.* **1984**, *174*, 199−207.
(2) Mika, J. T.; Poolman, B. Macromolecule Diffusion and Confinement in Prokaryotic Cells. *Curr. Opin. Biotechnol.* **2011**, *22*, 117−126.
(3) Kasai, R. S.; Kusumi, A. Single-Molecule Imaging Revealed Dynamic GPCR Dimerization. *Curr. Opin. Cell Biol.* **2014**, *27*, 78−86.
(4) Gahbauer, S.; Böckmann, R. A. Membrane-Mediated Oligomerization of G Protein Coupled Receptors and Its Implications for GPCR Function. *Front. Physiol.* **2016**, *7*, 494.
(5) Laganowsky, A.; Reading, E.; Allison, T. M.; Ulmschneider, M. B.; Degiacomi, M. T.; Baldwin, A. J.; Robinson, C. V. Membrane Proteins Bind Lipids Selectively to Modulate Their Structure and Function. *Nature* **2014**, *510*, 172−175.
(6) Barrera, N. P.; Zhou, M.; Robinson, C. V. The Role of Lipids in Defining Membrane Protein Interactions: Insights from Mass Spectrometry. *Trends Cell Biol.* **2013**, *23*, 1−8.
(7) Dix, J. A.; Verkman, A. Crowding Effects on Diffusion in Solutions and Cells. *Annu. Rev. Biophys.* **2008**, *37*, 247−263.
(8) Kusumi, A.; Nakada, C.; Ritchie, K.; Murase, K.; Suzuki, K.; Murakoshi, H.; Kasai, R. S.; Kondo, J.; Fujiwara, T. Paradigm Shift of the Plasma Membrane Concept from the Two-Dimensional Continuum Fluid to the Partitioned Fluid: High-Speed Single-Molecule Tracking of Membrane Molecules. *Annu. Rev. Biophys. Biomol. Struct.* **2005**, *34*, 351−378.
(9) Engelman, D. M. Membranes Are More Mosaic Than Fluid. *Nature* **2005**, *438*, 578−580.
(10) Zhou, H.-X.; Rivas, G.; Minton, A. P. Macromolecular Crowding and Confinement: Biochemical, Biophysical, and Potential Physiological Consequences. *Annu. Rev. Biophys.* **2008**, *37*, 375−397.
(11) Dupuy, A. D.; Engelman, D. M. Protein Area Occupancy at the Center of the Red Blood Cell Membrane. *Proc. Natl. Acad. Sci. U. S. A.* **2008**, *105*, 2848−2852.
(12) Jacobson, K.; Mouritsen, O. G.; Anderson, R. G. Lipid Rafts: At a Crossroad Between Cell Biology and Physics. *Nat. Cell Biol.* **2007**, *9*, 7−14.
(13) Metzler, R.; Jeon, J.-H.; Cherstvy, A. Non-Brownian Diffusion in Lipid Membranes: Experiments and Simulations. *Biochim. Biophys. Acta, Biomembr.* **2016**, *1858*, 2451−2467.
(14) Guigas, G.; Weiss, M. Effects of Protein Crowding on Membrane Systems. *Biochim. Biophys. Acta, Biomembr.* **2016**, *1858*, 2441−2450.
(15) Javanainen, M.; Hammaren, H.; Monticelli, L.; Jeon, J.-H.; Miettinen, M. S.; Martinez-Seara, H.; Metzler, R.; Vattulainen, I. Anomalous and Normal Diffusion of Proteins and Lipids in Crowded Lipid Membranes. *Faraday Discuss.* **2013**, *161*, 397−417.
(16) Jeon, J.; Javanainen, M.; Martinez-Seara, H.; Metzler, R.; Vattulainen, I. Protein Crowding in Lipid Bilayers Gives Rise to Non-Gaussian Anomalous Lateral Diffusion of Phospholipids and Proteins. *Phys. Rev. X* **2016**, *6*, 021006.
(17) Saxton, M. J. Anomalous Diffusion Due to Obstacles: A Monte Carlo Study. *Biophys. J.* **1994**, *66*, 394−401.
(18) Horton, M. R.; Höfling, F.; Rädler, J. O.; Franosch, T. Development of Anomalous Diffusion Among Crowding Proteins. *Soft Matter* **2010**, *6*, 2648−2656.
(19) Peters, R.; Cherry, R. J. Lateral and Rotational Diffusion of Bacteriorhodopsin in Lipid Bilayers: Experimental Test of the Saffman-Delbrück Equations. *Proc. Natl. Acad. Sci. U. S. A.* **1982**, *79*, 4317−4321.
(20) Goose, J. E.; Sansom, M. S. Reduced Lateral Mobility of Lipids and Proteins in Crowded Membranes. *PLoS Comput. Biol.* **2013**, *9*, e1003033.
(21) Guigas, G.; Weiss, M. Membrane Protein Mobility Depends on the Length of Extra-Membrane Domains and on the Protein Concentration. *Soft Matter* **2015**, *11*, 33−37.
(22) Casuso, I.; Khao, J.; Chami, M.; Paul-Gilloteaux, P.; Husain, M.; Duneau, J.-P.; Stahlberg, H.; Sturgis, J. N.; Scheuring, S. Characterization of the Motion of Membrane Proteins Using High-Speed Atomic Force Microscopy. *Nat. Nanotechnol.* **2012**, *7*, 525−529.
(23) Weigel, A. V.; Simon, B.; Tamkun, M. M.; Krapf, D. Ergodic and Nonergodic Processes Coexist in the Plasma Membrane as Observed by Single-Molecule Tracking. *Proc. Natl. Acad. Sci. U. S. A.* **2011**, *108*, 6438−6443.
(24) Manzo, C.; Torreno-Pina, J. A.; Massignan, P.; Lapeyre, G. J., Jr; Lewenstein, M.; Garcia Parajo, M. F. Weak Ergodicity Breaking of Receptor Motion in Living Cells Stemming from Random Diffusivity. *Phys. Rev. X* **2015**, *5*, 011021.
(25) Ramadurai, S.; Holt, A.; Krasnikov, V.; van den Bogaart, G.; Killian, J. A.; Poolman, B. Lateral Diffusion of Membrane Proteins. *J. Am. Chem. Soc.* **2009**, *131*, 12650−12656.
(26) Weiß, K.; Neef, A.; Van, Q.; Kramer, S.; Gregor, I.; Enderlein, J. Quantifying the Diffusion of Membrane Proteins and Peptides in Black Lipid Membranes with 2-Focus Fluorescence Correlation Spectroscopy. *Biophys. J.* **2013**, *105*, 455−462.
(27) Oswald, F.; Varadarajan, A.; Lill, H.; Peterman, E. J.; Bollen, Y. J. MreB-Dependent Organization of the E. Coli Cytoplasmic Membrane Controls Membrane Protein Diffusion. *Biophys. J.* **2016**, *110*, 1139−1149.
(28) Lee, C. C.; Petersen, N. O. The Lateral Diffusion of Selectively Aggregated Peptides in Giant Unilamellar Vesicles. *Biophys. J.* **2003**, *84*, 1756−1764.
(29) Guigas, G.; Weiss, M. Size-Dependent Diffusion of Membrane Inclusions. *Biophys. J.* **2006**, *91*, 2393−2398.
(30) Guigas, G.; Weiss, M. Influence of Hydrophobic Mismatching on Membrane Protein Diffusion. *Biophys. J.* **2008**, *95*, L25−L27.
(31) Gambin, Y.; Lopez-Esparza, R.; Reffay, M.; Sierecki, E.; Gov, N.; Genest, M.; Hodges, R.; Urbach, W. Lateral Mobility of Proteins in Liquid Membranes Revisited. *Proc. Natl. Acad. Sci. U. S. A.* **2006**, *103*, 2098−2102.
(32) Kriegsmann, J.; Gregor, I.; von der Hocht, I.; Klare, J.; Engelhard, M.; Enderlein, J.; Fitter, J. Translational Diffusion and Interaction of a Photoreceptor and Its Cognate Transducer Observed in Giant Unilamellar Vesicles by Using Dual-Focus FCS. *ChemBioChem* **2009**, *10*, 1823−1829.
(33) Harb, F.; Sarkis, J.; Ferte, N.; Tinland, B. Beyond Saffman-Delbruck Approximation: A New Regime for 2D Diffusion of α-Hemolysin Complexes in Supported Lipid Bilayer. *Eur. Phys. J. E: Soft Matter Biol. Phys.* **2012**, *35*, 1−9.
(34) Naji, A.; Levine, A. J.; Pincus, P. A. Corrections to the Saffman-Delbrück Mobility for Membrane Bound Proteins. *Biophys. J.* **2007**, *93*, L49−L51.
(35) Saffman, P.; Delbrück, M. Brownian Motion in Biological Membranes. *Proc. Natl. Acad. Sci. U. S. A.* **1975**, *72*, 3111−3113.
(36) Saffman, P. Brownian Motion in Thin Sheets of Viscous Fluid. *J. Fluid Mech.* **1976**, *73*, 593−602.
(37) Vaz, W. L.; Dieter, H. Experimental Evidence Against the Applicability of the Saffman-Delbrück Model to the Translational Diffusion of Lipids in Phosphatidylcholine Bilayer Membranes. *FEBS Lett.* **1983**, *152*, 287−290.

DOI: 10.1021/acs.jpclett.7b01758
J. Phys. Chem. Lett. 2017, 8, 4308−4313

(38) Camley, B. A.; Lerner, M. G.; Pastor, R. W.; Brown, F. L. Strong Influence of Periodic Boundary Conditions on Lateral Diffusion in Lipid Bilayer Membranes. *J. Chem. Phys.* **2015**, *143*, 243113.
(39) Petrov, E. P.; Schwille, P. Translational Diffusion in Lipid Membranes Beyond the Saffman-Delbrück Approximation. *Biophys. J.* **2008**, *94*, L41−L43.
(40) Hughes, B.; Pailthorpe, B.; White, L. The Translational and Rotational Drag on a Cylinder Moving in a Membrane. *J. Fluid Mech.* **1981**, *110*, 349−372.
(41) Klingler, J. F.; McConnell, H. M. Brownian Motion and Fluid Mechanics of Lipid Monolayer Domains. *J. Phys. Chem.* **1993**, *97*, 6096−6100.
(42) Wilke, N.; Maggio, B. The Influence of Domain Crowding on the Lateral Diffusion of Ceramide-Enriched Domains in a Sphingomyelin Monolayer. *J. Phys. Chem. B* **2009**, *113*, 12844−12851.
(43) Cicuta, P.; Keller, S. L.; Veatch, S. L. Diffusion of Liquid Domains in Lipid Bilayer Membranes. *J. Phys. Chem. B* **2007**, *111*, 3328−3331.
(44) Niemelä, P. S.; Miettinen, M. S.; Monticelli, L.; Hammaren, H.; Bjelkmar, P.; Murtola, T.; Lindahl, E.; Vattulainen, I. Membrane Proteins Diffuse as Dynamic Complexes with Lipids. *J. Am. Chem. Soc.* **2010**, *132*, 7574−7575.
(45) Marrink, S. J.; Risselada, H. J.; Yefimov, S.; Tieleman, D. P.; De Vries, A. H. The MARTINI Force Field: Coarse Grained Model for Biomolecular Simulations. *J. Phys. Chem. B* **2007**, *111*, 7812−7824.
(46) Monticelli, L.; Kandasamy, S. K.; Periole, X.; Larson, R. G.; Tieleman, D. P.; Marrink, S.-J. The MARTINI Coarse-Grained Force Field: Extension to Proteins. *J. Chem. Theory Comput.* **2008**, *4*, 819−834.
(47) de Jong, D. H.; Singh, G.; Bennett, W. D.; Arnarez, C.; Wassenaar, T. A.; Schäfer, L. V.; Periole, X.; Tieleman, D. P.; Marrink, S. J. Improved Parameters for the Martini Coarse-Grained Protein Force Field. *J. Chem. Theory Comput.* **2013**, *9*, 687−697.
(48) Saxton, M. J. Lateral Diffusion in an Archipelago. The Effect of Mobile Obstacles. *Biophys. J.* **1987**, *52*, 989−997.
(49) Camley, B. A.; Brown, F. L. Contributions to Membrane-Embedded-Protein Diffusion Beyond Hydrodynamic Theories. *Phys. Rev. E* **2012**, *85*, 061921.
(50) Den Otter, W.; Shkulipa, S. Intermonolayer Friction and Surface Shear Viscosity of Lipid Bilayer Membranes. *Biophys. J.* **2007**, *93*, 423−433.
(51) Fuhrmans, M.; Sanders, B. P.; Marrink, S.-J.; de Vries, A. H. Effects of Bundling on the Properties of the SPC Water Model. *Theor. Chem. Acc.* **2010**, *125*, 335−344.
(52) Jeon, J.-H.; Monne, H. M.-S.; Javanainen, M.; Metzler, R. Anomalous Diffusion of Phospholipids and Cholesterols in a Lipid Bilayer and Its Origins. *Phys. Rev. Lett.* **2012**, *109*, 188103.
(53) Gass, D. M. Enskog Theory for a Rigid Disk Fluid. *J. Chem. Phys.* **1971**, *54*, 1898−1902.

DOI: 10.1021/acs.jpclett.7b01758
J. Phys. Chem. Lett. 2017, 8, 4308−4313

V

ANOMALOUS AND NORMAL DIFFUSION OF PROTEINS AND LIPIDS IN CROWDED LIPID MEMBRANES

by
Matti Javanainen, Henrik Hammaren, Luca Monticelli, Jae-Hyung Jeon, Markus S. Miettinen, Hector Martinez-Seara Monne, Ralf Metzler, and Ilpo Vattulainen, 2013
Faraday Discussions vol 161, 397–417,
DOI: 10.1039/c2fd20085f

Anomalous and normal diffusion of proteins and lipids in crowded lipid membranes

Matti Javanainen,[a] Henrik Hammaren,[a] Luca Monticelli,[b] Jae-Hyung Jeon,[a] Markus S. Miettinen,[c] Hector Martinez-Seara,[a] Ralf Metzler[ad] and Ilpo Vattulainen*[ae]

Received 27th April 2012, Accepted 1st June 2012
DOI: 10.1039/c2fd20085f

Lateral diffusion plays a crucial role in numerous processes that take place in cell membranes, yet it is quite poorly understood in native membranes characterized by, *e.g.*, domain formation and large concentration of proteins. In this article, we use atomistic and coarse-grained simulations to consider how packing of membranes and crowding with proteins affect the lateral dynamics of lipids and membrane proteins. We find that both packing and protein crowding have a profound effect on lateral diffusion, slowing it down. Anomalous diffusion is observed to be an inherent property in both protein-free and protein-rich membranes, and the time scales of anomalous diffusion and the exponent associated with anomalous diffusion are found to strongly depend on packing and crowding. Crowding with proteins also has a striking effect on the decay rate of dynamical correlations associated with lateral single-particle motion, as the transition from anomalous to normal diffusion is found to take place at macroscopic time scales: while in protein-poor conditions normal diffusion is typically observed in hundreds of nanoseconds, in protein-rich conditions the onset of normal diffusion is tens of microseconds, and in the most crowded systems as large as milliseconds. The computational challenge which results from these time scales is not easy to deal with, not even in coarse-grained simulations. We also briefly discuss the physical limits of protein motion. Our results suggest that protein concentration is anything but constant in the plane of cell membranes. Instead, it is strongly dependent on proteins' preference for aggregation.

1 Introduction

Lateral diffusion of lipids and proteins[1,2] is one of the most significant dynamic processes in cell membranes, as it governs a variety of phenomena such as formation of membrane protein complexes and self-assembly of functional nano-scale membrane domains known as lipid rafts.[3] Understanding how these complex processes take place in native cell membranes under biologically relevant conditions

[a]*Department of Physics, Tampere University of Technology, P.O. Box 692, FI–33101 Tampere, Finland. E-mail: ilpo.vattulainen@tut.fi*
[b]*INSERM, UMR-S665, DSIMB 75015, Université Paris Diderot - Paris 7, UFR Life Sciences, Paris, France*
[c]*Fachbereich Physik, Freie Universität Berlin, 14195 Berlin, Germany*
[d]*Institute for Physics & Astronomy, University of Potsdam, Karl-Liebknecht-Strasse 24/25, D-14476 Potsdam-Golm, Germany*
[e]*MEMPHYS Center for Biomembrane Physics, University of Southern Denmark, Odense, Denmark*

is key to unlocking many of the cellular functions. In this work, we focus on one of the central issues in this context, that is, the effects of lipid packing and protein crowding on lipid and protein diffusion.

In cell membranes, their local surface density depends quite substantially on lipid composition. Membrane regions rich in polyunsaturated lipids are loosely packed, while in cholesterol and sphingolipid rich regions the packing of lipids is much tighter.[4–6] Especially the latter situation is appealing since the concept of lipid rafts is largely based on the interplay of cholesterol and sphingolipids that are abundant in these highly ordered and packed domains. Considering the heterogeneity of cell membranes and the spatially varying membrane density in the membrane plane, there is reason to expect that lateral diffusion also depends on lipid packing. Experiments on model membranes support this view.[7,8]

Meanwhile, given that in native membranes the (molar) ratio of proteins and lipids has been suggested[9,10] to vary roughly between 1 : 50 and 1 : 100, it is obvious that membranes in living cells can be crowded with proteins.[11] What does this mean in practice? Assuming a typical phospholipid whose area per lipid is 0.64 nm^2 and an alpha-helical transmembrane peptide/protein whose diameter is 3 nm, then for a protein-to-lipid number ratio of 1 : 50, the average distance between the proteins' surfaces is about 3.2 nm. This suggests that in membranes crowded with proteins, membrane-mediated protein–protein interactions may play decisive roles in lateral diffusion.

Packing and crowding may also play a role in the nature of diffusion, since in other biological contexts, such as in the cytoplasm of living cells it has been found that diffusion of individual molecules at "short" time scales is anomalous[12,13] (also called subdiffusion), with the average mean-squared displacement scaling as a power-law t^{α} in time t with an anomalous scaling exponent $\alpha < 1$.[14] Similar behavior has been suggested very recently for membrane channels in plasma membranes of human kidney cells.[15] At long times, if molecular motion is not confined to a certain region, one expects a random walk-like normal diffusion with $\alpha = 1$.

While most of the discussion relates to normal diffusion occurring at long times and large length scales, the concept and the biological relevance of crowding-induced anomalous diffusion have recently received increased attention, opening up new vistas for interesting implications. In the cytoplasm of living cells anomalous diffusion of tracers such as labelled messenger RNA,[12] lipid granules,[13] or chromosomal loci[16] have been observed on time scales of tens of seconds, in accordance with control experiments in dense dextran[17] or protein solutions.[18] At longer times this anomalous motion is of the type of viscoelastic subdiffusion. As found by Golding and Cox[12] as well as Guigas and Weiss,[19] viscoelastic subdiffusion leads to increased recurrence of the position coordinate and may lead to increased local reaction rates of diffusing reactants. Anomalous diffusion may also lead to dynamical localisation, as argued for chromosomal separation in eukaryotes from measurements of the telomere motion,[20] with similar consequences for the membrane channels investigated in ref. 15. Finally, anomalous diffusion would strongly influence the dynamics of surface-bulk exchange.[21,22]

As far as membrane proteins and lipids are concerned, the current understanding of their lateral diffusion is almost completely based on considerations in rather idealized conditions compared to a real biological environment, as the issues due to, *e.g.*, crowding, have not been clarified. Nonetheless, recent progress has provided a great deal of new insight into the mechanisms and physical laws associated with lipid and protein motion under protein-poor conditions. For instance, atomistic simulations recently showed[23] that the so-called free-volume theories[24–26] often used to interpret lipid diffusion data are incomplete, as they do not account for the proper diffusion mechanism of lipids. Unlike assumed earlier, the mechanism by which lipids diffuse in the plane of a membrane turned out to be a concerted one, based on tens of lipids moving in unison as loosely defined dynamical clusters.[23,27] These predictions based on simulations were recently verified by quasi-elastic neutron scattering

experiments.[28] Also, it has been found that not only lipid diffusion but also protein motion is based on concerted effects, as atomistic as well as coarse-grained simulations have highlighted membrane proteins to diffuse as dynamical clusters together with about 100 lipids around them,[29] the size of the complex being much larger than the size of the protein itself. As the current paradigm of membrane protein diffusion in protein-poor membranes is based on the Saffman–Delbrück model,[30] which describes the protein diffusion coefficient in terms of physical parameters such as protein size, even the understanding of lateral diffusion in protein-poor conditions is an important goal.

However, when more complex situations have been considered, experiments have shown that in native cell membranes the diffusion of proteins and lipids can be distinctly different compared to simplified model systems.[31–36] One of the striking findings is that if identical proteins undergo lateral diffusion in the membranes of seemingly identical cells, the diffusion coefficients determined for individual proteins in different regions of a membrane may be quite different, differing by a factor of five.[33] This conclusion seems to hold true regardless of the fact that the motion of the proteins has been followed up to macroscopic time scales. Meanwhile, diffusion of lipids can also be quite complex. Recent super-resolution microscopy studies of living cells have shown that the motion of lipids can be slowed down significantly on time scales of the order of milliseconds and length scales of tens of nanometers,[34] suggesting that there are unknown mechanisms to confine diffusion of specific lipid types.

While these two examples are just suggestive, they highlight the complexity of molecular motion in membrane systems. There are many factors that can affect how rapidly molecules diffuse in membranes, and it is quite plausible that many of them contribute at the same time. First, the roles of the actin and cytoskeleton networks are often important, as they create domains that confine molecular motion.[35] Specific lipid–protein and protein–protein interactions can also contribute, slowing down diffusion through complex formation. Lipids in the vicinity of membrane proteins are known to diffuse much more slowly compared to lipids far from proteins.[29] Furthermore, it is clear that crowding can have an influence on lateral molecular motion, since with large enough protein concentrations the motion of lipids and proteins will be blocked.[32,37,38] Overall, one can conclude that the complexity of native cell membranes renders studies of protein and lipid diffusion quite difficult, and care is warranted when the results are being interpreted.

The main objective of this work is to shed light on the implications of crowding on the dynamics of lipids and membrane proteins. This broad topic embraces considerations of how lateral diffusion coefficients depend on crowding of proteins and molecular packing of lipids, and how the time scales of anomalous diffusion and its exponent relate to crowded conditions. For lipids, anomalous diffusion has been identified in previous studies,[39–41] but its biological significance has remained unclear. As for membrane proteins, recent simulations have identified anomalous diffusion to be an intrinsic property of protein motion under crowding,[38] though its biological relevance is not understood.

Here we have considered these topics from two complementary viewpoints. First, we have elucidated crowding in the sense of *packing* through atomistic simulations of protein-free lipid monolayers, with a purpose to understand how membrane density affects lipid dynamics in the membrane plane. In a biological context, this is a relevant question, *e.g.*, during the respiratory cycle during which the monolayer-like lung surfactant is first expanded and then compressed. Second, we investigated how *crowding of membrane proteins* affects lateral dynamics in tensionless lipid bilayers. This topic is biologically highly relevant since—as mentioned above—native cell membranes are rich in proteins.

We have found that anomalous diffusion is an inherent property in both protein-free and protein-rich membranes, and that the time scales of anomalous diffusion and the anomalous diffusion exponents of lipids and proteins strongly depend on

packing/crowding. Strikingly, while in protein-poor conditions normal diffusion is observed in hundreds of nanoseconds, in protein-rich (crowded) conditions the onset of normal diffusion takes place in tens of microseconds, and in the most crowded systems quite likely on time scales that are no less than milliseconds. Given that the time scales associated with normal diffusion are so long, this matter has to be accounted for in analysis of diffusion data, and especially in simulations where the time scale problem is very severe even with coarse-grained simulation models. Moving on, we also discuss physical limits of protein motion, paying attention to the optimal protein concentration where protein diffusion would be fast enough to enable sufficiently rapid motion over large length scales and also promote protein–protein collisions needed for protein complex formation.

2 Methodology

2.1 Langmuir monolayers

We used atomistic molecular dynamics (MD) simulations to consider seven Langmuir monolayer systems with a mean molecular area ranging from 44 Å^2 to 68 Å^2, with a uniform spacing of 4 Å^2. With this range of compression, the monolayer states cover liquid condensed to liquid expanded phases. Further compression was found to result in monolayer buckling, while further expansion induced formation of holes.

The studied systems consisted of two monolayers separated by a water slab and a thick vacuum region to separate the monolayers from one another (see Fig. 1 for snapshots of individual monolayers in the systems). The monolayers contained 100 lipid molecules each, with the composition of 60 mol% dipalmitoylphosphatidylcholine (DPPC), 20 mol% palmitoyloleoylphosphatidylcholine (POPC), 10 mol% palmitoyloleoylphosphatidylglycerol (POPG), and 10 mol% cholesterol, in

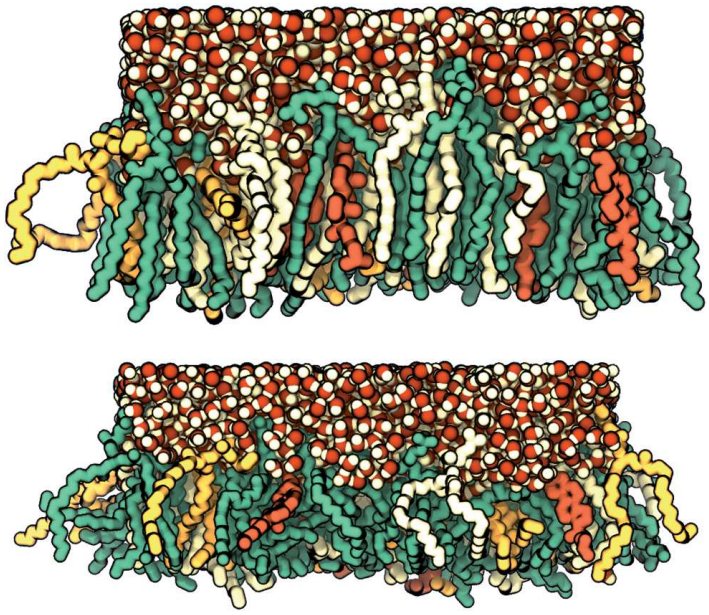

Fig. 1 Snapshots of the monolayer systems at a water–air interface at two different compressions: a fairly compressed system with $\langle A \rangle = 48$ Å^2 is shown above and a system with a lower surface pressure and $\langle A \rangle = 64$ Å^2 is depicted below. Lipids are drawn in the liquorice scheme with DPPC presented in green, POPC in white, POPG in yellow, and cholesterol in orange. Water is shown using the van der Waals scheme. For clarity, lipids on the sides have not been truncated but there are still periodic boundaries on both sides. Snapshots have been rendered with VMD.

agreement with experimental measurements on the human lung surfactant.[42] Extensive hydration was achieved with 7235 water molecules. A concentration of 150 mMol of NaCl was included in order to mimic physiological conditions. Additional sodium ions were added to neutralize the negative charges in POPG head groups. Two systems with mean molecular areas equal to 48 $Å^2$ and 64 $Å^2$ are represented in Fig. 1, showing clearly the difference in the ordering of their tails.

As described in our earlier work,[43] the force fields used for lipids followed the Berger description,[44] for cholesterol we used the description of Holtje *et al.*,[45] and for water we used the TIP3P model.[46] Salt and counterions were described by the GROMACS force field.

All simulations were conducted using the GROMACS simulation package.[47] The leap-frog integrator was employed in all simulations with a time step of 2 fs. NVT conditions were applied with temperature kept constant at 310 K with the Nosé–Hoover thermostat[48] with a time constant of 0.5 ps. Electrostatics were handled with the PME algorithm[49] of the order of 4. The cut-off used between real and inverse space calculations was 1 nm. The Lennard-Jones potential was cut-off at 1 nm and the neighbor list for the long-range interactions with a radius of 1 nm was updated every 10 steps. All bonds were constrained with LINCS[50] of the order of 4. Further details of the simulation model and protocol can be found from ref. 43.

Three sets of simulations were performed with different sampling frequencies in order to obtain information of lipid motion over a wide range of time scales from tens of femtoseconds to hundreds of nanoseconds. The shortest simulations were ran for 500 ps with data collected every 10 fs. The values for the second set were 10 ns and 100 fs, respectively. Finally, all the systems were simulated for at least 100 ns with coordinates saved every 10 ps. As the regime of normal diffusion was not achieved even after 100 ns, the simulations of the limiting cases of the most expanded and the most compressed systems were further extended to 660 ns and 610 ns, respectively. Data corresponding to the first 10% of the trajectories were discarded in all analyses.

2.2 Membrane proteins in lipid bilayers

To consider the joint lateral diffusion of proteins and lipids in membranes, we used coarse-grained (CG) models for two different one-component lipid bilayers to host membrane proteins. The first set of bilayers was composed of dilinoleoylphosphatidylcholine (DLPC) lipids, while the second one was comprised of dipalmitoylphosphatidylcholine (DPPC) lipids. These bilayers were simulated with a varying number of NaK channel (2AHY) proteins embedded in the membranes. The starting structures consisted of proteins positioned in a grid in the membrane plane.

The choice of these lipids and proteins was based on careful testing that concluded their properties to be distinctly different with respect to protein aggregation. In DLPC bilayers, NaK channels were found to avoid aggregation due to the minor hydrophobic mismatch between the proteins and the lipid bilayer. In DPPC bilayers, the situation was completely different, as NaK proteins were observed to prefer forming aggregates due to their larger hydrophobic mismatch. Therefore, the choice of lipids and proteins in our models is not based on their biological relevance but instead is just pragmatic: with these choices we can model two different scenarios, one preferring protein aggregation (DPPC) and another avoiding it (DLPC). In this spirit, the DPPC and DLPC systems are from here on referred to as aggregating (A) and non-aggregating (NA), respectively. Snapshots of chosen systems in the end of simulations are shown in Fig. 2.

Both systems were studied with multiple protein-to-lipid ratios (1 : 50, 1 : 75, 1 : 100, 1 : 150, and 1 : 200 in each leaflet, see Table 1) to consider diffusion at different levels of crowding. In addition, systems with a single protein embedded in a bilayer were also considered to describe dilute (protein-poor) conditions that we here denote as a protein-to-lipid ratio as 1 : infinity. The simulated systems

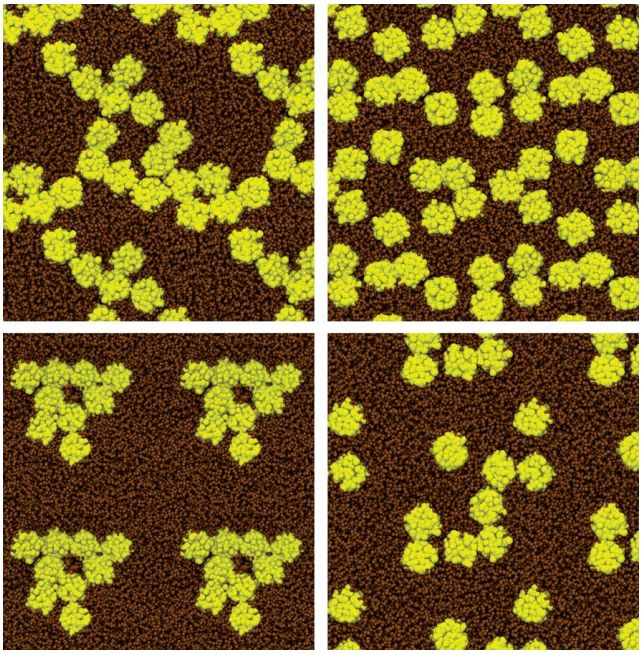

Fig. 2 Snapshots of protein–lipid systems with selected protein-to-lipid ratios. The aggregating DPPC system (A) is shown on the left hand side and the non-aggregating DLPC (NA) system on the right. The upper images show the system with a protein-to-lipid ratio of 1 : 50 in each leaflet, and the lower ones the case with the protein-to-lipid ratio of 1 : 100 per leaflet. In each case, the simulated system has been repeated four times (2 × 2) with periodic boundary conditions to better visualize large-scale ordering. Snapshots correspond to the end of each respective simulation. Proteins are colored in yellow and lipids in brown. Pictures have been rendered with VMD.

Table 1 Details of the simulated protein–lipid systems. "A" stands for aggregating, "NA" for non-aggregating, and "INF" stands for infinity. The number of proteins refers to the total number in the bilayer. The number of lipids in the 1 : INF system is 2045 (DPPC) or 3000 (DLPC)

DPPC (A)						
Protein-to-lipid ratio	1 : 50	1 : 75	1 : 100	1 : 150	1 : 200	1 : INF
No. of proteins	16	16	9	9	4	1
Size in *x*/*y* (nm)	27.4	31.3	26.1	30.9	23.4	25.1
Size in *z* (nm)	9.5	9.3	9.5	9.3	9.6	9.4
DLPC (NA)						
Protein-to-lipid ratio	1 : 50	1 : 75	1 : 100	1 : 150	1 : 200	1 : INF
No. of proteins	16	16	9	9	4	1
Size in *x*/*y* (nm)	27.2	31.2	26.1	30.7	23.3	30.1
Size in *z* (nm)	9.3	9.4	9.2	9.3	9.2	9.1

contained one, four, nine, or sixteen proteins depending on the protein-to-lipid ratio. For comparison with experimental studies, the surface area covered by proteins was in the different DPPC–NaK systems as follows: 2.4% (1 : infinity), 11% (1 : 200), 15% (1 : 150), 21% (1 : 100), 27% (1 : 75), and 34% (1 : 50). The system dimensions ranged between 23 and 31 nm along the bilayer (*xy*-plane). The thickness of the system along membrane normal direction (*z*) was about 10 nm. These values are listed in Table 1.

The molecules were modelled with a CG force field derived from MARTINI[51–53] and modified for membrane peptides and proteins.[54] The starting structure of the

protein was also based on the earlier work discussed elsewhere.[54] The simulations were carried out using the GROMACS simulation package.[47] The A-systems were simulated for 26 μs and the NA-systems for 10 μs. Data were collected every 100 ps. The time step was fixed to 40 fs in all simulations. Data corresponding to the first microsecond of simulation were discarded in all diffusion analysis to account for equilibration. Below, the time scales reported for the CG models are the real simulation times without a commonly used scaling factor of four[51–53] that is used to account for the faster dynamics in CG models compared to atomistic ones. However, the diffusion coefficients reported below have been scaled by this factor.

The electrostatics were handled by potentials shifted to zero in the interval from 0 to 1.2 nm. The Lennard-Jones interactions were shifted in between 0.9 and 1.2 nm. Neighbor lists with a radius of 1.2 nm were updated every 10 steps. NPT ensemble was adapted and pressure was held constant at 1 bar with the Parrinello–Rahman barostat[55] with a time constant of 4 ps and compressibility of 4×10^{-5} bar^{-1}. The x and y directions were coupled together and z separately. The system was also coupled to a heat bath at 310 K produced by the Nosé–Hoover thermostat[48] with a time constant of 1 ps. No constraints were applied to the bonds.

2.3 Mean-squared displacement

The mean-squared displacement (MSD) curves act as a starting point for the diffusion analysis. The MSD can be calculated as

$$\mathrm{MSD}(t) = \langle [\mathbf{r}_i(t + t') - \mathbf{r}_i(t')]^2 \rangle, \quad (1)$$

where $\mathbf{r}_i(t)$ is the location of the examined particle i at time t. Angular brackets denote averaging over both time and the set of examined particles. Lateral diffusion coefficient describing the pace of motion in the xy (membrane) plane is obtained from the MSD as

$$D_L = \lim_{t \to \infty} \frac{\mathrm{MSD}(t)}{4t}. \quad (2)$$

The MSD in eqn (1) is based on a time average taken over the time series $\mathbf{r}(t)$ of the lipid motion. While viscoelastic subdiffusion is ergodic in the sense that in the limit of long measurement times the ensemble average and the time average of the MSD are identical for free motion[56–58] (in contrast to anomalous diffusion with scale-free waiting time distributions[59] as observed in ref. 15), for finite measurement times the amplitude of the time averaged MSD fluctuates around the ergodic value.[57] A smooth curve may be obtained by averaging the time averaged MSD over individual trajectories. Further, it is important to mention that the long-time limit in eqn (2) means that D_L should be determined from the region where $\mathrm{MSD}(t) \sim t^{\alpha}$ with $\alpha = 1$.

In Langmuir monolayers, the MSD curves were computed for the 90 phospholipid molecules in each monolayer (diffusion of cholesterol was not included in the analysis). The two monolayers in each system (separated by vacuum) were considered independently, and the motion of the centre of mass (COM) of the examined monolayer was discarded before the analysis. This choice was made to avoid possible issues, which could arise from the motion of the leaflet as a whole,[60,61] and therefore, in practice, the motion of each lipid's COM was determined with respect to the center of mass of the monolayer in which the given lipid resides. Data used in further analysis were based on an average of MSD results of the two monolayers.

In protein–bilayer systems, the integral proteins anchor the leaflets to one another, and hence the possible motion of the two bilayer leaflet COMs (compared to each other) is expected to be much slower compared to membrane protein-free systems. Given this, in bilayer systems we first removed the COM motion of the membrane

(by accounting for all lipids and proteins, but not water) and then determined the displacements of particles' COM to compute the MSDs.

2.4 Exponent associated with mean-squared displacement

We assume the mean-squared displacement to scale as a power-law in time as follows:

$$\mathrm{MSD}(t) \sim t^{\alpha}, \tag{3}$$

where $\alpha = \alpha(t)$ is the time-dependent anomalous diffusion exponent. By definition, the exponent can be obtained as the slope of log(MSD) *versus* log(t). In practice, the MSD data are first translated to a logarithmic scale. However, as particle locations are sampled at constant time intervals in our simulations, the data obtained are not uniformly spaced in the logarithmic description. To fix this issue for further analysis, a smoothing spline was fitted to the log–log data and the spline was sampled at constant intervals in the logarithmic scale. This fitting procedure also smoothed roughness in the data which occurs when data saved from different sets of simulations with different saving frequencies overlap.

The time dependence of α was calculated by fitting a straight line to a moving window containing 20 data points (represented in a log–log scale) both backward and forward of the examined moment of time. This interval corresponds to 0.41 time units in logarithmic scale with a base of 10.

In a further step the anomalous motion should be scrutinised through additional, complementary analysis tools to diagnose precisely the nature of the stochastic motion of lipids and proteins. For instance, one may analyse moment ratios,[62] the velocity autocorrelation,[57] or apply the p-variation method.[63] The results of analysis based on these tools will be discussed elsewhere.

3 Results

3.1 Diffusion in Langmuir monolayers

The MSD curves obtained from the longest simulations are shown in Fig. 3. The data of the most compressed and the most expanded systems have been calculated from the whole trajectory (>600 ns), resulting in better statistical quality compared to the other cases where simulations lasted for 100 ns. Still, in all cases the MSD data are fairly smooth.

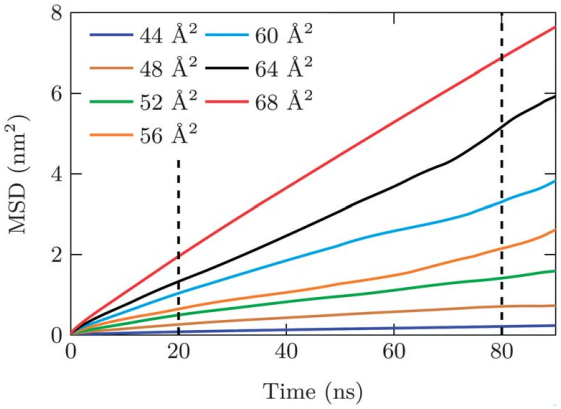

Fig. 3 MSD curves of phospholipids in the monolayer systems, with colors corresponding to different compression states. Dashed lines show the time range used in fitting eqn (2) to the data.

The data in Fig. 3 bring about a very important point which one should pay attention to in all the discussion below. That is, the MSDs in Fig. 3 are *seemingly linear in time*, therefore supporting the idea that one could use eqn (2) to determine the diffusion coefficient. However, as the data and the discussion below show, this is not the case. Nonetheless, for the time being, let us assume that the assumption of MSD(t) $\sim$ t^1 holds. Possible issues related to the calculation of the diffusion coefficient when the exponent is less than one will be addressed and discussed later in the Discussion.

The diffusion coefficients obtained from fitting eqn (2) to the MSD data are shown in Fig. 4. The diffusion coefficients are consistent with the expected behavior that lipid dynamics are faster the looser the packing in a monolayer. The diffusion coefficients are also in agreement with experimentally and computationally measured values for lipid diffusion in monolayers, if the effect of cholesterol is taken into account (see discussion in ref. 43). Notably, even in the most packed system (44 Å^2) the diffusion coefficient is several orders of magnitude larger compared to diffusion in the gel (solid-like) phase, where diffusion coefficients in lipid bilayers are[1] of the order of 10^{-16}–10^{-11} cm^2 s^{-1}, highlighting that all systems considered here are fluid.

3.2 Self-assembly of membrane proteins in bilayers

Before considering lateral diffusion in lipid bilayers with membrane proteins, it is crucial to have well-defined systems that have equilibrated. To this end, the aggregation tendency of membrane proteins was investigated by calculating the number of close contacts between proteins during the simulations. The calculation was performed every 100 ns, analyzing the first 10 μs of all systems. Two proteins were considered to be in close contact if the distance between their centres of mass in the xy-plane was smaller than 1.7 times the initial maximum distance between the beads of a protein and its COM. While protein radius is not easy to define, according to our benchmarks on the validity of the chosen criterion, the chosen value was found to best describe the limit at which there is a contact between two proteins. The calculated aggregation maps are shown in Fig. 5.

The results (Fig. 5) confirm the conclusion which was readily hinted by Fig. 2: proteins in A-systems start to form aggregates already after a few hundred nanoseconds and almost all proteins become connected to each other during the first microsecond. The clusters of proteins are also stable in the A-system. This result also supports our choice to discard the first microsecond of simulation data from the analysis as the formation of protein aggregates takes about a microsecond.

In the NA-system, proteins tend to stay unconnected for up to microseconds and some of them remain separated from other proteins during the whole 10 μs

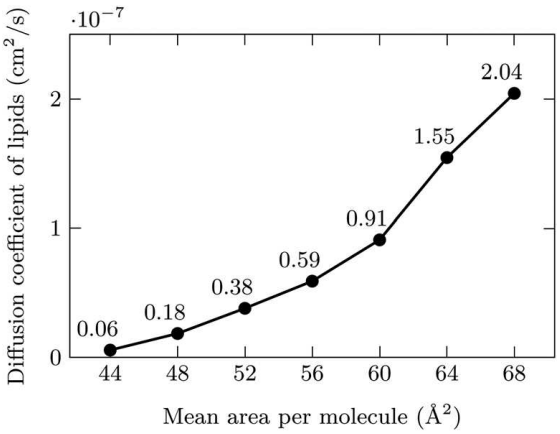

Fig. 4 Diffusion coefficients of phospholipids in Langmuir monolayer systems as a function of mean area per molecule.

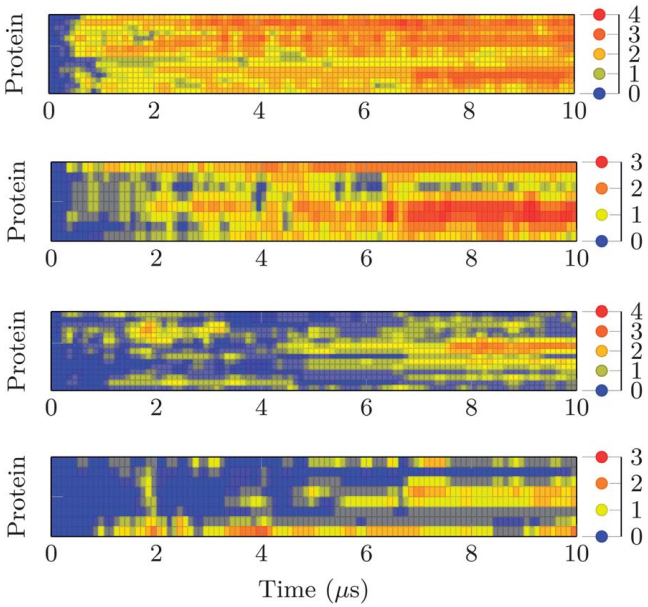

Fig. 5 The number of close contacts that each protein has with other proteins. The two upper figures show the behavior in the aggregating DPPC system (A) with protein-to-lipid ratios of 1 : 75 (top) and 1 : 100 (second from top). The two lower plots show the number of close contacts in the non-aggregating DLPC system (NA) with similar protein-to-lipid ratios of 1 : 75 (second from bottom) and 1 : 100 (bottom). Note that the color bars are scaled differently in systems with a different total number of proteins.

simulation. The aggregates in the NA-system are also able to break apart once they are formed.

The difference in protein behavior between the two lipid–protein systems, and especially the time it takes to form aggregates, cannot be explained by the speed of lateral dynamics. The proteins in DLPC (NA) membranes have higher diffusion coefficients compared to the DPPC (A) membranes (data to be shown below), thus in the NA-systems the proteins meet other proteins on time scales shorter than those in the A-systems. Yet, the aggregates form faster in the A-systems, which confirms the higher aggregation tendency of proteins in the DPPC bilayer.

3.3 Diffusion in aggregating (A) protein system

With the first microsecond of data discarded, a total of 25 μs of simulation time was considered for MSD calculation of the aggregating NaK–DPPC system. The MSD curves for lipids are shown in Fig. 6 and for proteins in Fig. 7.

Fig. 6 suggests that the dynamics of lipids are faster in the less crowded systems, as expected. Diffusion slows down even for minor protein concentrations, and this effect is the stronger the larger is the concentration of proteins.

The effect of crowding on protein motion is even more dramatic than in the case of lipids, see Fig. 7. The system with a protein-to-lipid ratio of 1 : 200 shows a drastic slowing down of diffusion.

The lipid diffusion coefficients determined from the MSD curves with different levels of crowding are listed in Fig. 8. The diffusion coefficients decrease almost linearly with increasing protein-to-lipid ratio. The decrease arises in part from the effect of blocking: as the protein content increases, there is less space for lipid motion, slowing down diffusion. Confinement of lipids in cages formed by proteins strengthens this effect (see Fig. 2), and it is likely that lipid–protein interactions play a role, too. In experiments, in line with our data, proteins have been found to cause a significant reduction in lateral diffusion rate of phospholipids in the plane of membranes.[8]

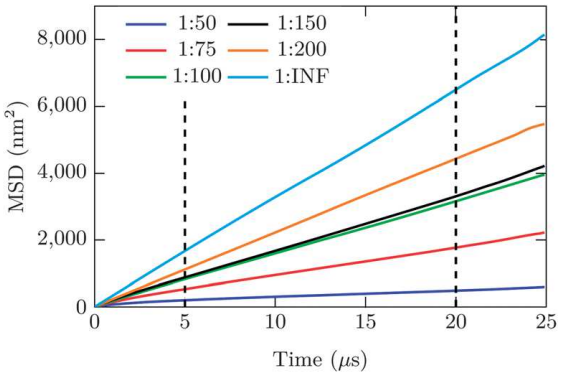

Fig. 6 MSD curves of lipids in the DPPC (A) systems with different protein-to-lipid ratios. Dashed lines show the time range used in fitting eqn (2) to the data.

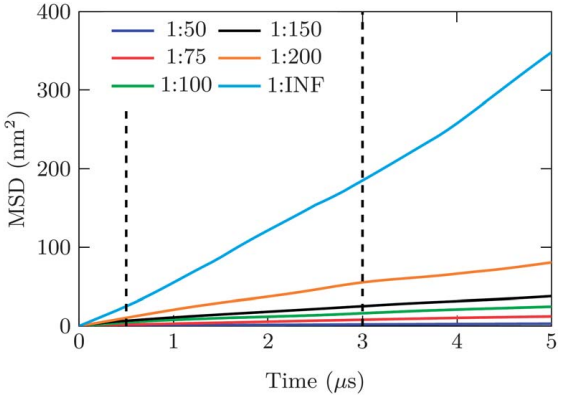

Fig. 7 MSD curves of proteins in the DPPC (A) systems. The time range used for fitting eqn (2) is shown with a pair of dashed lines.

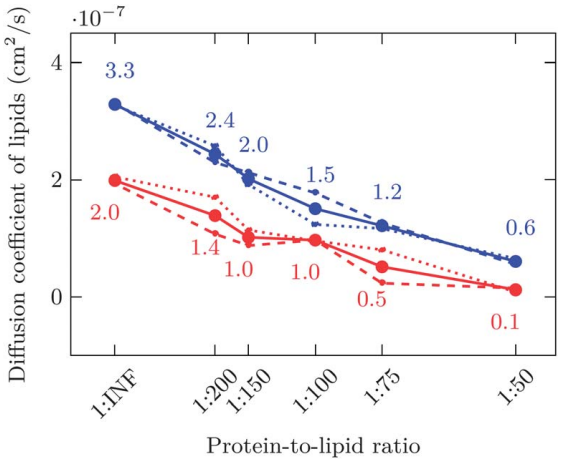

Fig. 8 Diffusion coefficients of lipids in membranes with different protein-to-lipid ratios: data for DPPC (red) and DLPC (blue). INF stands for infinity. The diffusion coefficients in x and y directions have been drawn with dashed and dotted lines of the same color, respectively, full curve being the average.

The values for the diffusion coefficient in x and y directions were also calculated in order to examine the possible anisotropic effects of wall-like structures formed by protein aggregation. These coefficients are also shown in Fig. 8. Not surprisingly,

in some systems lateral diffusion is not uniform in both directions in the plane. These differences in x and y directions may also in part be due to finite size effects. However, the differences are relatively small.

The diffusion of proteins is even more affected by crowding, see Fig. 9. First, for the aggregating proteins, the dependence of protein diffusion coefficient on protein-to-lipid ratio is stronger than linear. Second, its values span two orders of magnitude in the case of the DPPC (A) system. A seemingly minor increase in protein content from 1 : infinity to 1 : 200 slows diffusion down by a factor of four. In the most crowded DPPC–NaK system protein motion has virtually stopped, which is described by a very low value of the diffusion coefficient (about 1×10^{-10} cm^2 s^{-1}). When the diffusion coefficients of lipids and proteins are compared to each other, the diffusion of proteins is slower by a factor of 5 (protein-poor) to 30 (protein-rich conditions).

If the diffusion of membrane proteins could be described in terms of hard disks moving on a plane, then the protein diffusion coefficient would decrease linearly for increasing area fraction covered by proteins.[64] Based on Fig. 9, this behavior holds approximately well at small protein-to-lipid ratios but breaks down around 1 : 150, where protein clustering becomes evident. Clearly, aggregation of proteins plays a profound role in protein diffusion under crowding, and theoretical work to describe this behavior would be welcome.

Experiments have shown quite generally that the lateral diffusion coefficient of membrane proteins decreases for increasing protein concentration,[32,37,65] in agreement with our data.

3.4 Diffusion in non-aggregating (NA) protein systems

The analysis on the non-aggregating protein–DLPC system was performed similarly as on the aggregating protein–DPPC system. The diffusion coefficients are depicted in Fig. 8 and 9.

Diffusion coefficients of lipids in the non-aggregating systems are 1.5 to 5 times higher than the values in the aggregating DPPC membranes. In the limit of small protein concentration (1 : infinity), aggregation of proteins cannot affect lipid diffusion, thus the main reason why DLPC and DPPC diffuse at a different pace in this limit is the different viscosity (or alternatively a different membrane fluidity described also by a different average area per lipid) of these lipid bilayers. If changes in membrane viscosities are assumed to be similar in DPPC and DLPC bilayers with

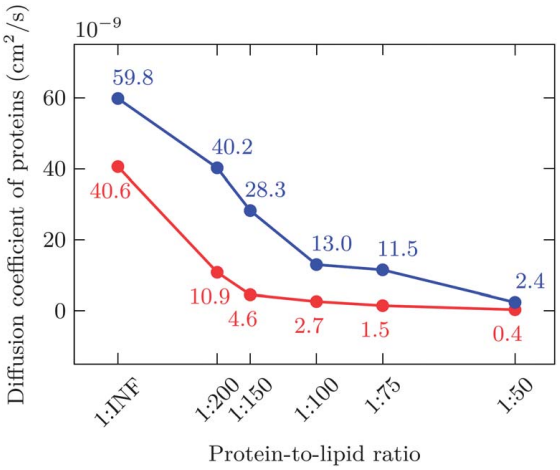

Fig. 9 Diffusion coefficients of NaK channel proteins in membranes with different protein-to-lipid ratios. Curves show lateral diffusion coefficients in DPPC (red) and DLPC membranes (blue). INF stands for infinity.

increasing protein density, then in the 1 : 50 ratio, the diffusion of DPPC is slowed down by a factor of 3.6 compared to DLPC, and this difference is due to protein aggregation.

Protein diffusion in the DPPC system is slowed down by a factor of 1.5 to 10 compared to DLPC, as the protein-to-lipid ratio is increased from 1 : infinity to 1 : 50, respectively. Again in the dilute protein system, the difference in protein diffusion coefficients is due to different membrane viscosities in the DLPC and DPPC bilayers. The remaining part is due to aggregation, or changes in membrane viscosity associated with aggregation.

3.5 Anomalous diffusion exponent

3.5.1 Langmuir monolayer systems. As data on lipid diffusion in Langmuir monolayers were collected in multiple simulations with different data saving intervals, it was first combined for the log–log plots. The smoothed data, spanning almost 8 orders of magnitude, are shown in Fig. 10.

We can readily find three different regimes in Fig. 10. First, there is a regime corresponding to superdiffusive ballistic motion at very short time scales. In this regime, the exponent $\alpha = 2$. Anomalous diffusion follows after a transition period and is characterized by an exponent smaller than one. Finally, at long times, one finds a transition towards normal diffusion characterized by an exponent $\alpha = 1$.

For further analysis, let us focus on how α behaves in time, see Fig. 11. It is readily seen that the level of compression has a profound effect on the nature of diffusive motion. At very short times the behavior in the monolayers subject to different packing conditions is similar, characterizing ballistic motion. However, the curves describing different packing conditions start to separate from each other in a time scale of hundreds of femtoseconds.

Subsequently, superdiffusion changes into subdiffusion in about 1 picosecond, and one finds a plateau consistent with subdiffusion with an exponent that is approximately constant over several orders of magnitude in time, starting between 1 and 10 picoseconds. The subdiffusion exponents of the most compressed and the most expanded systems were found to be quite low: 0.30 and 0.57, respectively. The tighter the packing, the smaller the exponent.

After the subdiffusive regime, the exponents start to grow, expected to level off at a value of one, thus describing normal random walk like diffusion at long times. In the most expanded system the long-time regime was almost reached during the simulations, and one can estimate that the onset of normal diffusion (τ_{onset}) in this case is

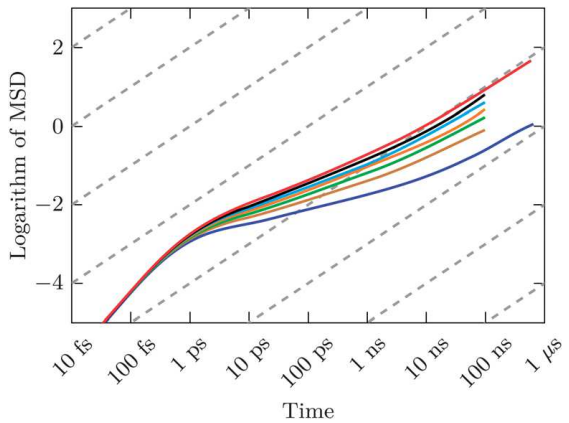

Fig. 10 Mean-squared displacements of lipids in Langmuir monolayers shown on a log–log scale. The dashed gray lines show normal diffusion behavior with $\alpha = 1$. Color code used in the curves is as follows: 44 Å^2 (blue), 48 Å^2 (brown), 52 Å^2 (green), 56 Å^2 (orange), 60 Å^2 (cyan), 64 Å^2 (black), and 68 Å^2 (red).

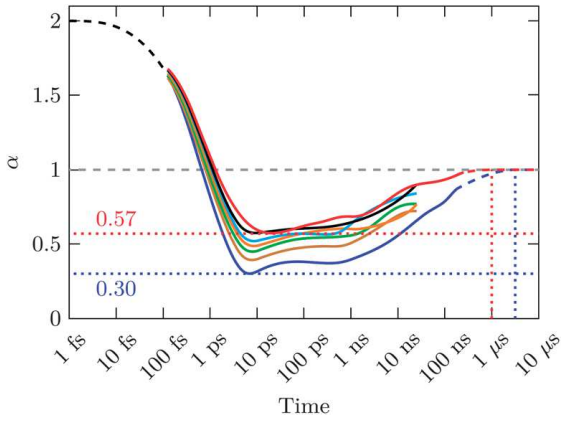

Fig. 11 Time evolution of the exponent α associated with the mean-squared displacement of lipids in Langmuir monolayers. Color code used in the curves is as follows: 44 Å^2 (blue), 48 Å^2 (brown), 52 Å^2 (green), 56 Å^2 (orange), 60 Å^2 (cyan), 64 Å^2 (black), and 68 Å^2 (red). Dashed black line shows the expected extrapolation to ballistic behaviour ($\alpha = 2$), and the dashed red and blue lines show extrapolation to normal diffusion ($\alpha = 1$) at long times. Dotted red and blue lines guide the eye to the estimated time scales in which normal diffusion is reached, and also to the subdiffusion exponent. Dashed gray line shows the normal diffusion exponent. Error bars (considering the standard error of the mean) in the value of α are very small at short times (± 0.01) and increase slightly at longer times (± 0.03).

close to 1 microsecond. Other, more compressed systems are expected to behave similarly but less rapidly, and our best educated guess based on the data in Fig. 11 suggests that the onset of normal diffusion ranges in these cases from about 1 to 10 microseconds.

3.5.2 Aggregating protein systems. For the DPPC system with protein aggregation, the time evolution of α for lipid motion is shown in Fig. 12. The corresponding curve for protein diffusion is depicted in Fig. 13.

We stress that the data in this case have been collected at fairly long intervals of 100 picoseconds in order to focus on the long-time motion. Therefore, a plateau associated with subdiffusion is not included in Fig. 12 and 13 (compared to Fig. 11). It would appear at short times (<1 ns) if data of particle positions had been saved more frequently.

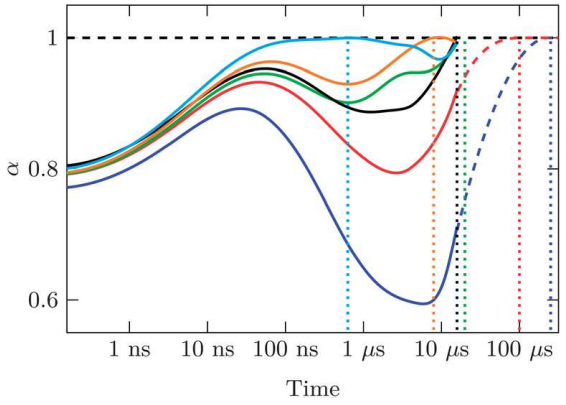

Fig. 12 Exponent characterizing lipid motion in the aggregating DPPC systems. Curves are colored as follows: 1 : 50 (blue), 1 : 75 (red), 1 : 100 (green), 1 : 150 (black), 1 : 200 (orange), and 1 : infinity (cyan). Error bars (considering the standard error of the mean) in the value of α are the smallest at short times (<0.01) and increase up to about ± 0.01 at 3 μs. Extrapolations at the longest times (shown by dashed lines) are based on a conservative estimate of $\alpha(t)$ between about 10–20 μs.

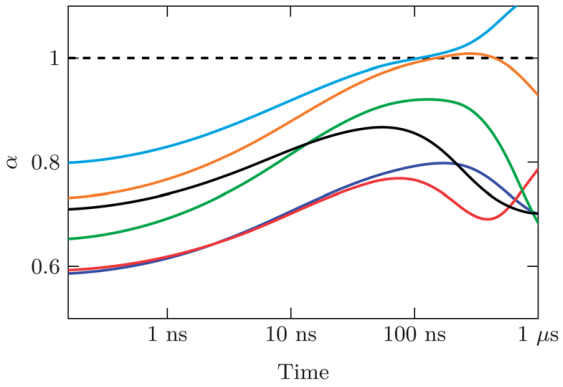

Fig. 13 Exponent characterizing protein motion in the aggregating DPPC systems. Curves are colored as follows: 1 : 50 (blue), 1 : 75 (red), 1 : 100 (green), 1 : 150 (black), 1 : 200 (orange), and 1:infinity (cyan). Error bars are about ±0.01 at short times and about ±0.02 at the longest times.

Let us first focus on lipid motion (Fig. 12). At times of the order of 1–100 ns, the exponent in every case increases towards one, reflecting a tendency to aim for random walk like motion. In the most dilute system with just a single membrane protein, the regime of normal diffusion is indeed reached in about 100 ns. However, in other systems where crowding of proteins becomes more prominent, the exponent falls down and reaches a minimum at 1–10 μs, the exponent being the smaller the more crowded the membrane is, and the time at which the minimum is observed increasing for increasing crowding. We discuss this in more detail below.

The collisions of lipids with proteins become more and more frequent for increasing protein concentration, giving rise to dynamical correlations in lipid motion, which in turn is manifested as anomalous diffusion ($\alpha < 1$) where the motion of lipids has a memory. We find that the anomalous diffusion exponent decreases for increasing protein concentration, in agreement with experiments by Horton *et al.*[66] At very long times the lipids will undergo a random walk characterized by $\alpha = 1$, and therefore one can expect the curves in Fig. 12 to eventually recover to a value of one. How long this takes is not clear, though. The data in Fig. 12 suggest that for intermediate crowding (1 : 200, 1 : 150, 1 : 100) normal diffusion would be observed at times of the order of 10 μs. For the most crowded systems (1 : 75, 1 : 50), the time scale of reaching normal diffusion is considerably larger, and our best educated guess based on interpolation of the data is that normal diffusion would be observed at times of the order of 100 μs or even milliseconds.

Let us come back to Fig. 12 and discuss why the anomalous diffusion exponent decreases at intermediate times. The data below (Fig. 16) for the non-aggregated lipid–protein system do not highlight a similar major decrease in α, thus the drop in the exponent cannot be due to lipid–protein collisions as such. Instead, it turned out that the decrease in α is largely due to lipids whose motion is confined due to proteins around them. As Fig. 2 shows, there are membrane regions where the lipids are surrounded by proteins from all possible directions, confining their motion to a limited part of the membrane. This is illustrated in Fig. 14, which shows a trajectory of a single tagged lipid during a 25 μs simulation. The motion of the lipid is clearly restricted, allowing it to access only part of the membrane surface. If the confinement would continue over a period longer than the simulation time, then MSD would converge to a constant value, implying that one would have a situation where $\mathrm{MSD}(t) \sim t^0$. The data in Fig. 12 suggest that the waiting time of lipids to escape confined regions is large, but it is smaller than the simulation time. This is also supported by the data in Fig. 15, which depicts time-averaged MSDs of all lipids in the DPPC system one by one, and, more importantly, the distribution of the single-particle-based anomalous diffusion exponents at times of 10 ns and 1 μs. The

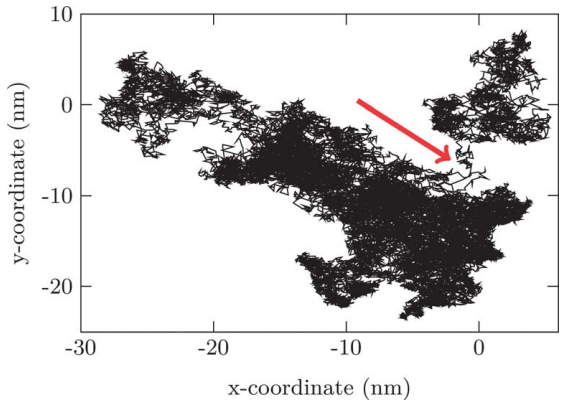

Fig. 14 Trajectory of a single tagged lipid in the DPPC–NaK system with a protein-to-lipid ratio of 1 : 50 over a simulation time of 25 μs. Note confinement of the lipid into restricted areas. The red arrow shows how the lipid escapes from one region, ending up in another, moving through a narrow channel between the two.

distribution of α in both cases is quite broad, but importantly in the latter case (at 1 μs) there are no or just a few exponents close to zero but there are exponents equal to one. In other words, the data indicate that while there are few lipids whose motion is almost non-existent due to the caging effect of proteins, the confinement of lipids is temporary. Also, at times of the order of a microsecond there are individual lipids undergoing free random walk like diffusion.

In the case of protein motion, Fig. 13 demonstrates that the conclusions based on lipid motion are largely valid also for protein motion. The main differences are the smaller exponent values in protein motion, and the time scales that seem to be longer for proteins compared to lipids. That is, normal diffusion is recovered in non-crowded systems in about one microsecond, but in the highly crowded cases the time required for accessing the normal diffusion regime is likely larger than in the case of lipid motion.

3.5.3 Non-aggregating protein systems. In the non-aggregating DLPC–protein systems, the time evolution of α for lipids is shown in Fig. 16. As it shows, the nature of lipid diffusion in the non-aggregating protein system is somewhat different compared to that of the aggregating DPPC system. Unlike in the DPPC–NaK system (Fig. 12), here the dip in the exponent α is much less evident. Instead, there

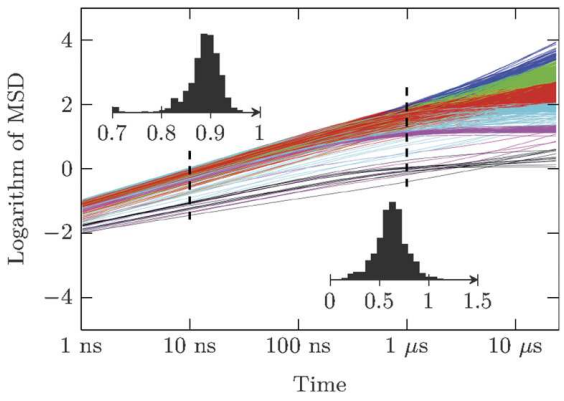

Fig. 15 MSDs shown separately for each lipid in the DPPC–NaK system with a protein-to-lipid ratio of 1 : 50. Also shown in insets are the distributions of anomalous diffusion exponents at two different times (10 ns and 1 μs) to demonstrate their width and approximate Gaussian profile.

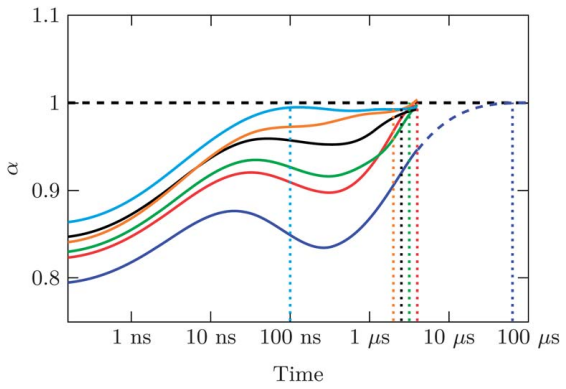

Fig. 16 Exponents determined from running fits for the MSD of lipids in non-aggregating DLPC–protein systems. Curves are colored as in earlier plots: 1 : 50 (blue), 1 : 75 (red), 1 : 100 (green), 1 : 150 (black), 1 : 200 (orange), and 1 : infinity (cyan). Normal diffusion behavior with $\alpha = 1$ is shown with a gray dashed line. Error bars are as in Fig. 12. Extrapolation at long times (shown by a dashed line) in the 1 : 50 case is based on a conservative estimate of $\alpha(t)$ between 1–5 μs.

is almost a plateau covering about one order of magnitude in time from a few tens of nanoseconds to a few hundred nanoseconds. The plateau is a common feature in all non-aggregating systems. The system with a single protein (1 : infinity) finds the normal diffusion regime in about 100 ns, whereas in the multi-protein systems the diffusion becomes normal with $\alpha = 1$ at much longer times. Even minor crowding (1 : 200) increases the onset of normal diffusion to about 1 μs. In more crowded systems it is more difficult to estimate how long it takes to get to the normal diffusion regime, but, again based on an educated guess, it ranges roughly between 10 and 100 microseconds.

Importantly, in the dilute case (1 : infinity) the time dependence of α in the aggregating and non-aggregating systems is almost identical (see Fig. 12 and 16). The differences between the DLPC–protein and DPPC–protein systems under crowding are therefore not due to different dynamics of the lipid molecules but rather result from alterations caused by the aggregation tendency of the proteins. Furthermore, also important to stress is that atomistic Langmuir monolayer simulations and coarse-grained lipid bilayer models are largely consistent with each other: in Langmuir monolayers with an area per lipid comparable to tensionless lipid bilayers (60–68 Å^2), normal diffusion is accessed in 100–1000 ns, which is also the case in coarse-

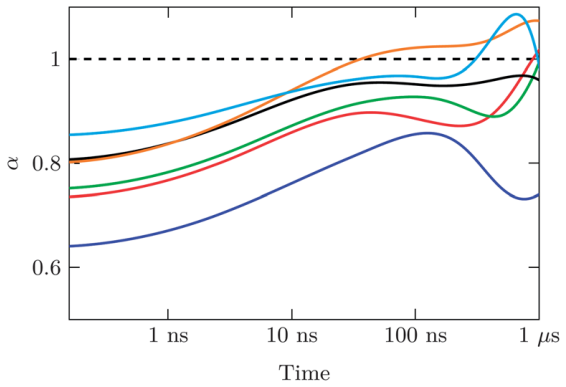

Fig. 17 Exponents determined from running fits for the MSD of proteins in non-aggregating DLPC–protein systems. Curves are colored as in earlier plots: 1 : 50 (blue), 1 : 75 (red), 1 : 100 (green), 1 : 150 (black), 1 : 200 (orange), and 1 : infinity (cyan). Normal diffusion behavior with $\alpha = 1$ is shown with a gray dashed line. Error bars are as in Fig. 13.

grained model studies. The time scales predicted by the coarse-grained models are therefore in the right ballpark (regarding the order of magnitude).

The plots for protein motion, see Fig. 17, show slightly different behavior compared to the aggregating system (Fig. 13). The diffusion exponents α for DLPC–protein membranes are larger than in the case of the aggregating DPPC system and they reach $\alpha = 1$ to some extent faster.

4 Discussion and conclusions

Cell membranes modulate or even govern a variety of cellular functions. The key molecules either responsible or at least involved in these functions are lipids and membrane proteins. To understand their full role in cellular functions, one has to understand the principles that control their lateral dynamics as the formation of functional nanoscale membrane domains (with a specific set of proteins and lipids) is based on lateral diffusion. However, while this dynamical process has been paid a great deal of attention to, most of the previous studies have been based on rather idealized conditions where the complexity of native membranes has not been taken into account. One of the great challenges in this spirit is to understand the effects of crowding on lipid and protein diffusion.

Here we have considered this topic from two complementary viewpoints, elucidating the effects of lipid packing through considerations of Langmuir monolayers, as well as the effects of protein crowding in lipid bilayers.

Simulations of Langmuir monolayers in the absence of proteins indicated that the motion of lipids is to do with quite substantial memory effects manifested as anomalous diffusion that persist over a broad range of time. We observed that the anomalous diffusion exponent depends on the packing of the monolayer; increasing packing leading to smaller exponent. In the same spirit, also the transition from anomalous to normal diffusion was found to depend on how strongly the lipids are packed, as increasing packing increases the onset of normal (random walk like) diffusion. What is quite stunning is the magnitude of the characteristic time needed to cross over from anomalous to normal diffusion (τ_{onset}). Even in fluid monolayers where packing of lipids is low (like in the liquid-expanded phase), τ_{onset} was found to be several hundred nanoseconds, and in the most compact monolayers of the order of microseconds.

In simulations of lipid bilayers the objective was to further our understanding of proteins' role in lateral diffusion, when proteins either aggregate or stay apart from each other. We observed the influence of protein crowding on lateral diffusion to be strong. Increasing protein concentration slowed down both lipid and protein diffusion, the slowing down being as large as a factor of 10 for lipids and 20–100 for proteins. Recent simulation results by Domanski *et al.* are consistent with this picture.[38] We also explored the extent to which protein crowding can affect τ_{onset}, thereby slowing down lateral dynamics. The observed effects associated with anomalous diffusion demonstrated the roles of blocking (entropy) and protein self-organization (aggregation). The system that promoted protein aggregation expressed the strongest effects manifested as lipid and protein confinement, complemented by the largest values we observed for τ_{onset}.

All simulated scenarios point to the fact that in systems that are highly packed or crowded with proteins, the time it takes to access the regime of normal diffusion is large. In protein-poor systems this ranges from 100 to 1000 ns. In protein-rich systems with significant crowding, τ_{onset} can be of the order of milliseconds. Experiments using biotinylated avidin lipid anchors as a crowding agent suggest[66] that τ_{onset} could actually be much larger, of the order of 100 ms. Is this a potential problem? In simulations it is, since availability of computer resources needed to access millisecond simulations are not common. If one wanted to explore lipid and/or protein diffusion in native-like membranes with a significant concentration of proteins, one should carry out simulations that last for several milliseconds.

Shorter simulations would not provide quantitatively reliable data for normal diffusion. This stems from the fact that the definition of the lateral diffusion coefficient is valid only in the limit of long times (see eqn (2)) for random walk like diffusion, when $\alpha = 1$. If $\alpha < 1$, as in anomalous diffusion, the diffusion coefficient is not well defined. This is the case, *e.g.*, when the simulation time is less than τ_{onset}. In practice the simulation time should however be considerably longer, at least $10 \times \tau_{onset}$, to gather decent statistics for MSD up to times that are much longer than the onset of normal diffusion τ_{onset}.

The above implies that the reader should consider our data for diffusion coefficients with reservation, too. Despite our best efforts and quite substantial computer resources, even the longest of our simulations covered less than 30 microseconds. Therefore, at least the diffusion coefficients of the most crowded protein systems (1 : 50, 1 : 75, and 1 : 100) studied in this work are questionable. Quite likely they are qualitatively in order, but quantitatively they are certainly compromised since in those cases we were not able to gauge the times where $\alpha = 1$.

What is even more stunning are the conclusions of our atomistic Langmuir monolayer simulations, which set the minimal standard for atomistic simulations of lipid diffusion in fluid membranes: the simulations should last at least for 1000 ns. This is not good news given that the simulation time scale of typical atomistic MD simulations of lipid membranes is currently of the order of 100 ns. Of course, one can use such data for consideration of lateral diffusion, and one can extract the diffusion coefficient too, but one should keep in mind that the quantity obtained in this manner will be an effective one, describing subdiffusive behavior instead of long-time (hydrodynamic) normal diffusion. The comparison of subdiffusive data determined from simulations with long-time scale diffusion data measured in experiments would also be problematic, and comparison of trends would then be more meaningful instead of comparing just quantitative numbers.

Quite unfortunately, the above scenario is yet the optimistic one, if one considers the challenge to simulate long enough times. The above discussed views hold as long as the lipids and proteins diffuse in a well-defined membrane domain. If the membrane is characterized by formation of domains with different properties, or if there is a need to consider diffusion in a membrane coupled to an actin-based membrane skeleton, then one has to account for effects of domain boundaries that typically slow down diffusion from one domain to another. The hydrodynamic long-time diffusion would then take place at times much larger than those associated with diffusion inside a single membrane domain. It is quite plausible that if one wanted to consider lateral diffusion of proteins in heterogeneous membranes with considerable domain formation, including the effects of actin-based confinement, then the true normal diffusion in the hydrodynamic long-time limit would be observed only in simulations of the order of seconds or minutes. While these time scales are just an educated guess, they highlight the size of the challenge.

Finally, let us briefly discuss physical limits of protein motion. Following the ideas of Dill *et al.*, is there an optimal concentration of membrane proteins that would maximize the speed of biochemical reactions?[67] On the one hand, protein diffusion should then be fast enough to enable sufficiently rapid motion over large length scales. This idea would be best fulfilled in protein-poor membranes. On the other hand, the optimal conditions should also promote protein–protein collisions needed for protein complex formation, and this idea in turn would favor crowding. Using hard sphere models for proteins in cytosol, Dill *et al.* predicted that the optimal protein volume concentration would be 19%, compared to 20% observed in cells.[67] In 2D membranes the validity of the hard disk model is less obvious, but what is obvious is that the protein concentration cannot be too high, since otherwise protein diffusion would become too slow as the data in Fig. 9 also demonstrate. Actually, what is striking in Fig. 9 is the slowing down of diffusion in the aggregating DPPC–NaK system, where protein diffusion slows down rather steeply down to a protein-to-lipid ratio of 1 : 150. This corresponds to an area fraction of 15%

occupied by the proteins. Similar diffusion in the non-aggregated DLPC–NaK system is observed with the protein-to-lipid ratio of 1 : 50, corresponding to a protein area fraction of 34%. If cells want to maximize their membrane protein diffusion without sacrificing chances for biochemical reactions (in terms of protein complex formation), then our data suggest that protein concentration is anything but constant in the membrane plane but is strongly dependent on proteins' preference for aggregation.

Acknowledgements

We acknowledge Mark Sansom and Phillip Stansfeld for sharing their membrane protein models. We wish to thank CSC – IT Centre for Science (Espoo, Finland) for computing resources. The Academy of Finland and the European Research Council (project 290974 CROWDED-PRO-LIPIDS) is acknowledged for financial support.

References

1 P. F. F. Almeida and W. L. C. Vaz, *Handbook of Biological Physics*, Elsevier, Amsterdam, 1995, ch. 6, pp. 305–357.
2 I. Vattulainen and O. G. Mouritsen, *Diffusion in condensed matter: Methods, materials, models*, Springer-Verlag, Berlin, 2nd edn, 2005, pp. 471–509.
3 D. Lingwood and K. Simons, *Science*, 2010, **327**, 46–50.
4 E. Falck, M. Patra, M. Karttunen, M. T. Hyvonen and I. Vattulainen, *Biophys. J.*, 2004, **87**, 1076–1091.
5 P. S. Niemela, S. Ollila, M. T. Hyvonen, M. Karttunen and I. Vattulainen, *PLoS Comput. Biol.*, 2007, **3**, 304–312.
6 S. Ollila, M. T. Hyvonen and I. Vattulainen, *J. Phys. Chem. B*, 2007, **111**, 3139–3150.
7 A. Filippov, G. Oradd and G. Lindblom, *Biophys. J.*, 2007, **93**, 3182–3190.
8 J. B. de la Serna, G. Oradd, L. A. Bagatolli, A. C. Simonsen, D. Marsh, G. Lindblom and J. Perez-Gil, *Biophys. J.*, 2009, **97**, 1381–1389.
9 A. D. Dupuy and D. M. Engelman, *Proc. Natl. Acad. Sci. U. S. A.*, 2008, **105**, 2848.
10 K. Jacobson, O. G. Mouritsen and R. G. W. Anderson, *Nat. Cell Biol.*, 2007, **9**, 7.
11 T. A. Ryan, J. Myers, D. Holowska, B. Baird and W. W. Webb, *Science*, 1988, **239**, 61–64.
12 I. Golding and E. C. Cox, *Phys. Rev. Lett.*, 2006, **96**, 098102.
13 J.-H. Jeon, V. Tejedor, S. Burov, E. Barkai, C. Selhuber-Unkel, K. Berg-Sorensen, L. Oddershede and R. Metzler, *Phys. Rev. Lett.*, 2011, **106**, 048103.
14 R. Metzler and J. Klafter, *Phys. Rep.*, 2000, **339**, 1.
15 A. V. Weigel, B. Simon, M. M. Tamkun and D. Krapf, *Proc. Natl. Acad. Sci. U. S. A.*, 2011, **108**, 6438–6443.
16 S. Weber, A. J. Spakowicz and J. A. Theriot, *Phys. Rev. Lett.*, 2010, **104**, 238102.
17 J. Szymanski and M. Weiss, *Phys. Rev. Lett.*, 2009, **103**, 038102.
18 W. Pan, L. Filobelo, N. D. Q. Pham, O. Galkin, V. V. Uzunova and P. G. Vekilov, *Phys. Rev. Lett.*, 2009, **102**, 058101.
19 G. Guigas and M. Weiss, *Biophys. J.*, 2008, **94**, 90–94.
20 I. Bronstein, Y. Israel, E. Kepten, S. Mai, Y. Shav-Tal, E. Barkai and Y. Garini, *Phys. Rev. Lett.*, 2009, **103**, 018102.
21 M. A. Lomholt, I. M. Zaid and R. Metzler, *Phys. Rev. Lett.*, 2007, **98**, 200603.
22 I. M. Zaid, M. A. Lomholt and R. Metzler, *Biophys. J.*, 2009, **97**, 710–721.
23 E. Falck, T. Rog, M. Karttunen and I. Vattulainen, *J. Am. Chem. Soc.*, 2008, **130**, 44.
24 P. F. F. Almeida, W. L. C. Vaz and T. E. Thompson, *Biochemistry*, 1992, **31**, 6739–6747.
25 D. Turnbull and M. H. Cohen, *J. Chem. Phys.*, 1961, **34**, 120–125.
26 D. Turnbull and M. H. Cohen, *J. Chem. Phys.*, 1970, **52**, 3038–3041.
27 T. Apajalahti, P. Niemela, P. N. Govindan, M. S. Miettinen, E. Salonen, S. J. Marrink and I. Vattulainen, *Faraday Discuss.*, 2010, **144**, 411–430.
28 S. Busch, C. Smuda, L. C. Pardo and T. Unruh, *J. Am. Chem. Soc.*, 2010, **132**, 3232.
29 P. S. Niemela, M. Miettinen, L. Monticelli, H. Hammaren, P. Bjelkmar, T. Murtola, E. Lindahl and I. Vattulainen, *J. Am. Chem. Soc.*, 2010, **132**, 7574.
30 P. G. Saffman and M. Delbrück, *Proc. Natl. Acad. Sci. U. S. A.*, 1975, **72**, 3111–3113.
31 M. Weiss, H. Hashimoto and T. Nilsson, *Biophys. J.*, 2003, **84**, 4043.
32 M. Frick, K. Schmidt and B. J. Nichols, *Curr. Biol.*, 2007, **17**, 462–467.

33 S. Wieser, J. Weghuber, M. Sams, H. Stockinger and G. J. Schutz, *Soft Matter*, 2009, **5**, 3287–3294.
34 C. Eggeling, C. Ringemann, R. Medda, G. Schwarzmann, K. Sandhoff, S. Polyakova, V. N. Belov, B. Hein, C. von Middendorff, A. Schonle and S. W. Hell, *Nature*, 2009, **457**, 1159–1162.
35 K. Ritchie, X.-Y. Shan, J. Kondo, K. Iwasawa, T. Fujiwara and A. Kusumi, *Biophys. J.*, 2005, **88**, 2266–2277.
36 V. Mueller, C. Ringemann, A. Honigmann, G. Schwartzmann, R. Medda, M. Leutenegger, S. Polyakova, V. N. Belov, S. W. Hell and C. Eggeling, *Biophys. J.*, 2011, **101**, 1651–1660.
37 S. Ramadurai, A. Holt, V. Krasnikov, G. van den Bogaart, J. A. Killian and B. Poolman, *J. Am. Chem. Soc.*, 2009, **131**, 12650–12656.
38 J. Domanski, S. J. Marrink and L. V. Schafer, *Biochim. Biophys. Acta, Biomembr.*, 2012, **1818**, 984–994.
39 E. Flenner, J. Das, M. C. Rheinstadter and I. Kosztinh, *Phys. Rev. E*, 2009, **79**, 011907.
40 T. Akimoto, E. Yamamoto, K. Yasuoka, Y. Hirano and M. Yasui, *Phys. Rev. Lett.*, 2011, **107**, 178103.
41 G. R. Kneller, K. Baczynski and M. Pasenkiewicz-Gierula, *J. Chem. Phys.*, 2011, **135**, 141105.
42 R. Veldhuizen, K. Nag, S. Orgeig and F. Possmayer, *Biochim. Biophys. Acta, Mol. Basis Dis.*, 1998, **1408**, 90–108.
43 M. Javanainen, L. Monticelli, J. de la Serna and I. Vattulainen, *Langmuir*, 2010, **26**, 15436–15444.
44 O. Berger, O. Edholm and F. Jahnig, *Biophys. J.*, 1997, **72**, 2002–2013.
45 M. Holtje, T. Forster, B. Brandt, T. Engels, W. von Rybinski and H.-D. Holtje, *Biochim. Biophys. Acta, Biomembr.*, 2001, **1511**, 156–167.
46 W. L. Jorgensen, J. Chandrasekhar, J. D. Madura, R. W. Impey and M. L. Klein, *J. Chem. Phys.*, 1983, **79**, 926.
47 B. Hess, C. Kutzner, D. van der Spoel and E. Lindahl, *J. Chem. Theory Comput.*, 2008, **4**, 435–447.
48 D. J. Evans and B. L. Holian, *J. Chem. Phys.*, 1985, **83**, 4069.
49 T. Darden, D. York and L. Pedersen, *J. Chem. Phys.*, 1993, **98**, 10089.
50 B. Hess, H. Bekker, H. J. C. Berendsen and J. Fraaije, *J. Comput. Chem.*, 1997, **18**, 1463–1472.
51 S. J. Marrink, A. H. de Vries and A. E. Mark, *J. Phys. Chem. B*, 2004, **108**, 750–760.
52 S. J. Marrink, H. J. Risselada, S. Yefimov, D. P. Tieleman and A. H. de Vries, *J. Phys. Chem. B*, 2007, **111**, 7812–7824.
53 L. Monticelli, S. K. Kandasamy, X. Periole, R. G. Larson, D. P. Tieleman and S.-J. Marrink, *J. Chem. Theory Comput.*, 2008, **4**, 819–834.
54 M. Sansom, K. Scott and P. Bond, *Biochem. Soc. Trans.*, 2008, **36**, 27–32.
55 M. Parrinello and A. Rahman, *J. Appl. Phys.*, 1981, **52**, 7182–7190.
56 W. Deng and E. Barkai, *Phys. Rev. E*, 2009, **79**, 011112.
57 S. Burov, J.-H. Jeon, R. Metzler and E. Barkai, *Phys. Chem. Chem. Phys.*, 2011, **13**, 1800–1812.
58 J.-H. Jeon and R. Metzler, *Phys. Rev. E*, 2012, **85**, 021147.
59 Y. He, S. Burov, R. Metzler and E. Barkai, *Phys. Rev. Lett.*, 2008, **101**, 058101.
60 M. Patra, M. Karttunen, M. T. Hyvönen, E. Falck, P. Lindqvist and I. Vattulainen, *Biophys. J.*, 2003, **84**, 3636–3645.
61 M. Patra, M. Karttunen, M. T. Hyvönen, E. Falck and I. Vattulainen, *J. Phys. Chem. B*, 2004, **108**, 4485–4494.
62 V. Tejedor, O. Benichou, R. Voituriez, R. Jungmann, F. Simmel, C. Selhuber-Unkel, L. B. Oddershede and R. Metzler, *Biophys. J.*, 2010, **98**, 1364–1372.
63 M. Magdziarz, A. Weron, K. Burnecki and J. Klafter, *Phys. Rev. Lett.*, 2009, **103**, 180602.
64 B. A. Scalettar, J. R. Abney and J. C. Owicki, *Proc. Natl. Acad. Sci. U. S. A.*, 1988, **85**, 6726–6730.
65 D. F. Kusic, E. L. Elson and M. P. Sheetz, *Biophys. J.*, 1999, **76**, 314–322.
66 M. R. Horton, F. Hofling, J. O. Radler and T. Franosch, *Soft Matter*, 2010, **6**, 2648–2656.
67 K. A. Dill, K. Ghosh and J. D. Schmit, *Proc. Natl. Acad. Sci. U. S. A.*, 2011, **108**, 17876–17882.

VI

PROTEIN CROWDING IN LIPID BILAYERS GIVES RISE TO NON-GAUSSIAN ANOMALOUS LATERAL DIFFUSION OF PHOSPHOLIPIDS AND PROTEINS

by
Jae-Hyung Jeon, Matti Javanainen, Hector Martinez-Seara Monne, Ralf Metzler, and Ilpo Vattulainen, 2016
Physical Review X vol 6, 021006,
DOI: 10.1103/PhysRevX.6.021006

Protein Crowding in Lipid Bilayers Gives Rise to Non-Gaussian Anomalous Lateral Diffusion of Phospholipids and Proteins

Jae-Hyung Jeon,[1,2] Matti Javanainen,[2,3] Hector Martinez-Seara,[2,4] Ralf Metzler,[2,5] and Ilpo Vattulainen[2,3,6]

[1]*School of Physics, Korea Institute for Advanced Study, Seoul 130-722, Republic of Korea*
[2]*Department of Physics, Tampere University of Technology, FI-33101 Tampere, Finland*
[3]*Department of Physics, P. O. Box 64, FI-00014 University of Helsinki, Finland*
[4]*Institute of Organic Chemistry and Biochemistry, Academy of Sciences of the Czech Republic, CZ-16610 Prague, Prague, Czech Republic*
[5]*Institute for Physics and Astronomy, University of Potsdam, D-14476 Potsdam-Golm, Germany*
[6]*Memphys–Center for Biomembrane Physics, University of Southern Denmark, DK-5230 Odense, Denmark*

(Received 31 August 2015; revised manuscript received 23 December 2015; published 12 April 2016)

Biomembranes are exceptionally crowded with proteins with typical protein-to-lipid ratios being around $1:50-1:100$. Protein crowding has a decisive role in lateral membrane dynamics as shown by recent experimental and computational studies that have reported anomalous lateral diffusion of phospholipids and membrane proteins in crowded lipid membranes. Based on extensive simulations and stochastic modeling of the simulated trajectories, we here investigate in detail how increasing crowding by membrane proteins reshapes the stochastic characteristics of the anomalous lateral diffusion in lipid membranes. We observe that correlated Gaussian processes of the fractional Langevin equation type, identified as the stochastic mechanism behind lipid motion in noncrowded bilayer, no longer adequately describe the lipid and protein motion in crowded but otherwise identical membranes. It turns out that protein crowding gives rise to a multifractal, non-Gaussian, and spatiotemporally heterogeneous anomalous lateral diffusion on time scales from nanoseconds to, at least, tens of microseconds. Our investigation strongly suggests that the macromolecular complexity and spatiotemporal membrane heterogeneity in cellular membranes play critical roles in determining the stochastic nature of the lateral diffusion and, consequently, the associated dynamic phenomena within membranes. Clarifying the exact stochastic mechanism for various kinds of biological membranes is an important step towards a quantitative understanding of numerous intramembrane dynamic phenomena.

DOI: 10.1103/PhysRevX.6.021006 Subject Areas: Biological Physics, Soft Matter

I. INTRODUCTION

The dynamics of biomembranes plays a crucial role in the regulation of numerous cellular processes. This is largely due to the fact that membrane proteins carry out a substantial fraction of cellular functions. For instance, they are involved in cellular signaling, in which the functional complex can be a single protein as well as an oligomer [1–3] together with an appropriate pool of lipids modulating the protein function by protein-lipid interactions [4–7]. Since the formation of protein-lipid complexes is reversible, proteins and lipids are repeatedly probing the membrane for functionally favorable surroundings, thereby allowing the diffusive motion to largely control their reaction kinetics.

Cell membranes are known to be extremely complex fluids characterized by heterogeneity [6,8] and compartmentalization [9,10]. Similar to the crowded cytoplasm of biological cells [11], membranes are crowded with proteins and other macromolecules [12]. These effects substantially complicate the relationship between the dynamics and function of cell membranes. Notably, crowding has been a neglected feature of the intracellular environment [11] until recently, when numerous studies have identified the role of crowding in multiple phenomena including, *inter alia*, protein stability [13], signaling [14,15], and gene transcription [16]. Most notably, crowding shapes the reaction kinetics [11,17–19] by modifying the mobility [20] as well as association rates [21–25]. This multitude of examples together with the shift in dimensionality from three to two hints that, besides the cytoplasm, crowding plays a substantial role also in cellular membranes. Indeed, similarly to the cytoplasm [26–28], one can argue that reaction kinetics in two dimensions are optimized by the

degree of crowding as the slower mobility is compensated by the higher reactant concentration [29,30].

Cytoplasmic crowding in living biological cells is known to cause anomalous diffusion with a mean-squared displacement (MSD) of the form [31,32]

$$\langle \mathbf{r}^2(t) \rangle \simeq K_\alpha t^\alpha, \tag{1}$$

with the generalized diffusivity K_α of physical dimension m^2/s^α and the anomalous diffusion exponent α [33–35]. Normal Brownian motion corresponds to the limit $\alpha = 1$. For passively moving tracer particles in living cells such as green fluorescent proteins [36], fluorescently labeled messenger RNA [37,38], and chromosomal loci [38,39], as well as visible, submicron tracer particles [40,41], subdiffusion with $0 < \alpha < 1$ is observed. Control experiments in artificially crowded environments consistently reveal subdiffusion [42–44]. In the presence of active driving, superdiffusive motion with $1 < \alpha < 2$ is also observed [45–47] in living cells.

In cellular membranes crowding is known to induce heterogeneous and confined motion. While some studies argue that crowding leads to the slowing-down of diffusion in terms of an effective diffusivity in an otherwise Brownian diffusion scenario [48], others suggest that diffusion becomes anomalous instead [48–58]. Anomalous diffusion of the form Eq. (1) was observed in various cellular membranes [32,55,57,58], emphasizing its general nature in membranes. Intriguingly, while anomalous diffusion would be expected to hinder the efficiency of diffusion-limited processes, in suitably crowded conditions it can surprisingly also result in favorable effects, such as to enhance the search of nearby reaction partners, which further leads to increased protein complex formation and a subsequent boost in reaction rates [59,60]. Confinement and corralling effects can also lead to enhanced protein oligomerization [61] and bursts in reaction rates [62]. Another important effect is the observation of aging [63], the explicit dependence of the dynamics of different membrane proteins on the length of the observation time [55,58].

While a lot of work has been conducted on the development of reaction-diffusion theories in the subdiffusive regime [64,65], such theories have not been widely applied to biological systems [15,32,66,67]. Therefore, resolving the diffusion mechanisms of molecules in crowded and compartmentalized conditions of cellular membranes could greatly improve our understanding of diffusion-controlled reactions in the cells. Moreover, membrane protein complexes [2,68] are targeted by a major fraction of current drugs. Therefore, understanding and thereafter altering the dynamics that govern the formation of functional protein–protein [69,70], lipid–protein [71,72], or domain–protein [73] units is an intriguing approach to the treatment of numerous diseases.

Single-particle superresolution techniques, such as stimulated emission depletion fluorescence (lifetime) correlation spectroscopy (STED-FCS) and single-particle tracking, have recently improved the understanding of biomolecular motion quite dramatically, identifying lateral nanoscale membrane heterogeneities as well as anomalous motion [51,55,58,74,75], yet the limit of probing nanoscale single-particle motion is still a formidable experimental challenge. Here, the added value given by molecular simulation approaches can be impressive [49,52,53,76–79].

In this work, we show through extensive molecular simulations and theoretical analysis that protein crowding changes the membrane dynamics drastically. We find that the dynamics of lipids in crowded conditions is no longer described by the mechanism consistent with the fractional Langevin equation (FLE) typically associated with the lipid motion in noncrowded membranes [52,53], or by any single known mechanism. Instead, the motion becomes non-Gaussian and heterogeneous, yet maintains its ergodic properties. In particular, while the time-averaged MSD scales sublinearly, no aging is observed. Concurrently, a strong dynamic heterogeneity is observed among different lipids as well as membrane-embedded proteins. Our findings are central to resolving the mechanisms governing how molecules move along crowded membranes and, therefore, to understanding how the multitude of processes occurring in cellular membranes are controlled by anomalous diffusion-reaction dynamics.

This paper is structured as follows. After a brief introduction to the model and simulations in Sec. II, we present our results in Sec. III. In particular, we demonstrate that the motion of the membrane constituent molecules is multifractal and anomalous. In contrast to noncrowded membranes, significant non-Gaussian shapes for the particle diffusion are observed and the inhomogeneity of the motion of individual particles is shown to be slowly varying with time. In Sec. IV, we discuss our results and conclude the paper. Additional results to support those presented in the main text are given in Supplemental Material [80].

II. MODELS AND SIMULATION

For our investigation of the stochastic characteristics of the lateral molecular diffusion in protein-crowded lipid membranes, we simulate three lipid bilayer systems similar to those employed in our study of the emergence of anomalous diffusion in the presence of membrane-embedded proteins [49]. Two protein-crowded membrane systems are modeled by embedding a total of 16 NaK channels (Protein data bank (PDB) entry 2AHY), respectively, in bilayers of 1600 1,2-dipalmitoyl-sn-glycero-3-phosphocholine (DPPC) and 1,2-dilauroyl-sn-glycero-3-phosphocholine (DLPC) lipids. The lipid-to-protein ratio is 1:50 per leaflet, corresponding to a protein surface

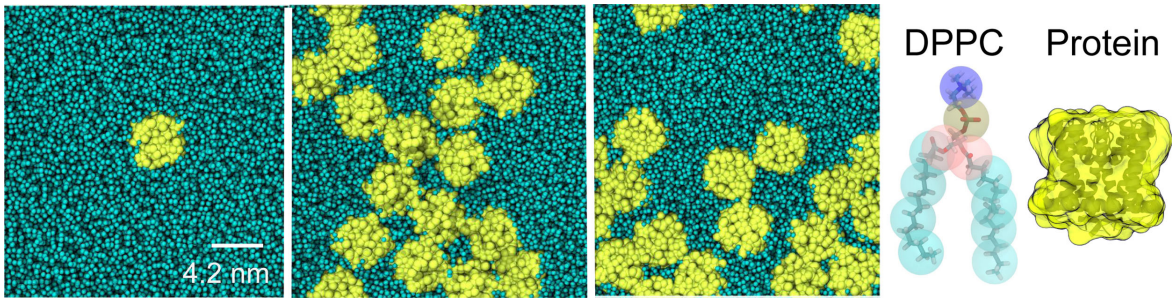

FIG. 1. Snapshots of the membrane systems at the end of the respective simulations runs. From left to right: (i) protein-poor membrane composed of 2045 DPPC phospholipids and a single NaK channel protein; (ii) protein-rich membrane system composed of 1600 DPPC lipids and 16 NaK proteins: aggregating system; (iii) protein-rich membrane system composed of 1600 DLPC lipids and 16 NaK proteins: nonaggregating system; (iv) schematic structures of a DPPC phospholipid and a NaK channel protein employed in our coarse-grained simulations. For both DPPC and the NaK channel, the transparent coarse-grained structure is shown on top of the atomistic representation.

coverage of approximately 34%, which is known as a typical value in cellular membranes [81]. Both systems span a lateral membrane area of approximately $25\times25\,\mathrm{nm}^2$ with periodic boundary conditions. The main difference between the two systems, as shown in Fig. 1, is that the NaK proteins tend to strongly aggregate with the others to form a larger complex in the DPPC system while they do so to a much lesser extent in the DLPC membrane. This is most likely due to a different hydrophobic mismatch of the proteins with the two lipid environments. In this spirit, the two systems chosen for this study are used to gauge the dynamics in two physically different settings often found in cell membranes—protein aggregating and protein nonaggregating. As a reference, we also simulate a protein-poor membrane composed of 2045 DPPC lipids and a single NaK channel.

In order to study large systems consisting of multiple proteins over a time scale of 100 μs, the computationally efficient coarse-grained Martini-based [82,83] force field [84] is employed. The protein-poor case is simulated for 25 μs, which corresponds to 100 μs of efficient time when the commonly used coarse-grained-to-atomistic comparison factor of 4 is taken into account. Compared to the protein-poor case, the protein-crowded systems turn out to have slower lateral dynamics [49]. Because of this, in this work, we simulate them for 100 μs (corresponding to 400 μs of effective time), which is fourfold longer than our previous simulation (25 μs) for similar systems. All simulation parameters are identical to our previous simulation study [49]. The analyses on the simulation results below are carried out in terms of the real simulation time.

III. RESULTS

In this section, we showcase the various aspects of the protein and lipid motion in the simulated lipid membranes. As we see, major changes are effected at higher protein crowding fractions.

A. Protein crowding induces multifractal anomalous lateral diffusion in membranes

We start our analysis by examining the diffusion properties of single phospholipid and protein molecules in our model membranes. From an individual two-dimensional trajectory $\mathbf{r}_i(t)$ encoding the motion of such a single molecule, the time-averaged MSD,

$$\overline{\delta_i^2(\Delta)} = \frac{1}{T-\Delta}\int_0^{T-\Delta}[\mathbf{r}_i(t+\Delta)-\mathbf{r}_i(t)]^2 dt, \qquad (2)$$

is evaluated as a function of the lag time Δ and the overall observation time T. Here and throughout the study, $\mathbf{r}_i(t)$ refers to the in-plane coordinate of the center of mass of a given ith lipid or protein molecule with respect to the center of mass of the entire membrane, thus removing the effect of membrane drift during the simulations [53]. In protein-rich membranes the membrane drift does not need to be removed separately with respect to each leaflet because the drift of the monolayers with respect to each other is negligible due to the anchoring effect of the proteins; see Figs. S1 and S2 in Supplemental Material [80]. The advantage of the time-averaged MSD Eq. (2) over the ensemble average Eq. (1) is that for sufficiently long trajectories $\mathbf{r}_i(t)$ resolves differences between the motion of individual particles, as we show below. We note that in so-called weakly nonergodic systems the long-time scaling of the time-averaged MSD $\overline{\delta_i^2(\Delta)}$ may differ fundamentally from the corresponding ensemble average $\langle\mathbf{r}^2(t)\rangle$, reflecting the nonstationarity of the underlying motion [31,32,35,85,86]. Experimentally and from simulations, such weak nonergodicity was indeed observed in the cytoplasm [40,41] and the plasma membrane [55,58] of living cells, as well as quite different systems such as blinking quantum dots [87] or granular gases [88].

Figure 2 depicts time-averaged MSD of all lipid molecules (thin gray lines) and proteins (thick red lines) in

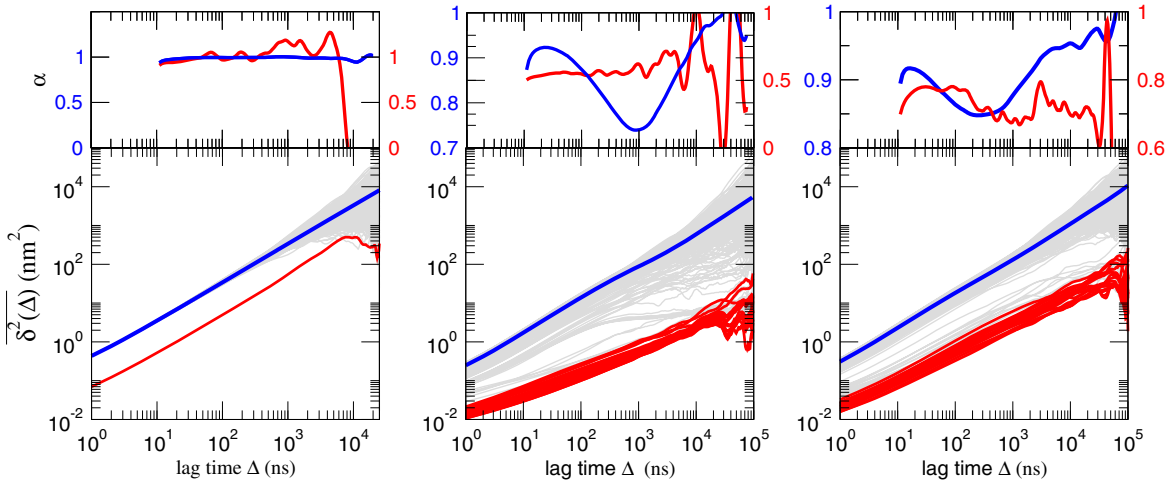

FIG. 2. Time-averaged MSD traces $\overline{\delta^2(\Delta)}$ for both individual lipids (gray thin lines) and NaK proteins (red thick lines) in protein-poor DPPC (left), protein-rich DPPC (middle), and protein-rich DLPC (right) membranes. In each panel, the blue thick line represents the mean time-averaged MSD $\langle\overline{\delta^2(\Delta)}\rangle$ for all lipids in the membrane. The upper panels represent the variation of the scaling exponent α versus the lag time Δ for lipids (blue line) and proteins (red line) in each membrane system from fits to the corresponding mean time-averaged MSDs. In this plot, the offset $\Delta = 10$ ns is due to the finite interval in fitting the instantaneous slope of the time-averaged MSD. Note the different scales of the ordinates in the different panels. We check that the change of the fit range does not seriously alter the $\alpha(\Delta)$ curves. Note that, in general, the scaling exponents α of the proteins exhibit larger fluctuation than those of the lipids. In particular, its sudden decrease for $\Delta > 5$ μs shown in the noncrowded membrane reflects the statistically insignificant fluctuation of a single time-averaged MSD curve.

noncrowded and crowded membranes. Along with the individual time-averaged MSDs, the mean

$$\langle\overline{\delta^2(\Delta)}\rangle = \frac{1}{N}\sum_{i=1}^{N}\overline{\delta_i^2(\Delta)} \tag{3}$$

as the blue solid line is plotted for all lipids. From this averaged curve, the anomalous scaling exponents α are estimated as a function of the lag time Δ, shown in the upper panels in Fig. 2. The results show that protein crowding significantly affects the character of the lateral diffusion in the membranes. While the lipids and the single protein in the noncrowded membrane exhibit trivial Brownian diffusion at lag times Δ longer than some 10 ns, consistent with previous studies [52–54,89,90], those in the crowded membrane exhibit significant anomalous diffusion. The plot of α as a function of Δ tells us that the lipid carries out multifractal subdiffusion until *tens of microseconds*, where the scaling exponent α is temporally varied with Δ in a broad spectrum of values. Additionally, the subdiffusive dynamics extends for around 3 orders of magnitude longer than for noncrowded lipid membranes. The variation in α indicates that the lipid motion is strongly affected by the proteins until around 10 μs. The behavior at time scales of > 10 μs is not conclusive for our analysis due to the limited simulation time. It appears that the strong fluctuation in the scaling exponent $\alpha(\Delta)$ for the proteins stems from the comparatively small numbers of proteins and will be different for independent runs. Interestingly, the diffusion dynamics of the proteins is affected by their own crowded state. In contrast to the normal diffusion of a single protein in a noncrowded membrane, 16 proteins in the crowded membranes exhibit strong subdiffusion. This effect is also clearly seen in the corresponding trajectories (see Fig. S3 in Supplemental Material [80]). Without any signature of transient behavior, it persists until the end of the simulations at 100 μs with an anomalous diffusion exponent that is smaller than the value for the lipids. The magnitude of α becomes smaller when the proteins are aggregated in the DPPC membrane compared to the case where they do not aggregate in the DLPC membrane. These results are consistent with our earlier study [49], even though the exact lag time dependence of α is affected by the confinement effects which strongly depend on the incidental aggregation geometry of the proteins. Note that the lateral dynamics of the proteins is about 10 times slower than the lipid dynamics.

It is also noteworthy that, owing to the protein crowding, individual lipids have various diffusion patterns which are distinct from the averaged behavior $\langle\overline{\delta^2(\Delta)}\rangle$; in both protein-rich DPPC and DLPC membranes there are some lipids whose time-averaged MSD curves almost completely follow those of the proteins, which suggests that these lipids move together with the proteins during the entire simulation time, possibly in nonannular binding sites.

In line with this view, it is found that approximately 30 lipids in the vicinity of a protein are considerably slowed down compared to lipids far from the protein (see Fig. S13 in Supplemental Material [80]). For the case of the

protein-aggregating DPPC membrane, some other lipids, while unbound from the proteins, undergo restricted subdiffusion in confined space in between aggregated proteins; see the sample trajectory in Fig. S3 in Supplemental Material [80]. Such a confined diffusive pattern is not observed if the lipids easily move through the nonaggregating proteins in the DLPC membrane. The majority of lipids appear to carry out unrestricted anomalous diffusion in the bulk. We quantify the effect of protein crowding on the mobility of individual lipids by comparison of the amplitude scatter in the time-averaged MSD for the protein-poor and protein-rich membranes in Fig. S4 in Supplemental Material [80]. The amplitude scatter has a markedly broader distribution in the protein-crowded membrane. Notably, in this case, the shape of the distribution becomes asymmetric with respect to the average because of the existence of a fraction of less mobile lipids caused by the presence of the proteins.

B. Protein crowding induces non-Gaussian anomalous diffusion

We now proceed to investigate whether the fractional Langevin equation, identified previously as a governing process for the lateral diffusion in pure lipid bilayers [52–54], is still able to reproduce the behavior of the lateral motion in protein-crowded membranes. The FLE, a special case of the generalized Langevin equation [91] with power-law friction kernel compensating the power-law correlations of the driving fractional Gaussian noise, typically describes the motion of tracer particles in viscoelastic media [92].

We first examine the (non-)Gaussianity of the diffusion process by looking at the cumulative distribution of the squared displacements $\Pi(r^2,\Delta)=\int_0^r P(\mathbf{r}',t=\Delta)2\pi r' dr'$ for the two-dimensional motion [55,93,94]. Here, P is the propagator, i.e., the probability density that the spatial increment of the particle is found to be at $[\mathbf{r},\mathbf{r}+\mathrm{d}\mathbf{r}]$ over the lag time interval Δ. Gaussian anomalous diffusive processes such as the FLE are described by the propagator in free space $P(\mathbf{r},\Delta)=\exp[-r^2/(2\sigma_\Delta)]/(2\pi\sigma_\Delta)$, with $\sigma_\Delta=2K_\alpha\Delta^\alpha$, which yields the cumulative distribution $\Pi(r^2,\Delta)=1-\exp[-r^2/(4K_\alpha\Delta^\alpha)]$. Thus, the plot of $-\log[1-\Pi(r^2,\Delta)]$ versus r^2 displays a power-law scaling with the exponent 2 [94]. As we show in Fig. 3, the lipids in the noncrowded membrane are in very good accord with the Gaussian scaling law.

However, both protein-crowded systems in Fig. 3 clearly show that the lateral diffusion is not Gaussian. It appears that the cumulative distributions for the crowded membranes follow a power-law relation $-\log[1-\Pi(r^2,\Delta)]\sim r^\delta$, with a single or multiple scaling exponent $\delta<2$ over the entire range of r^2 plotted. It turns out that these non-Gaussian scaling curves are found to be consistently preserved at different overall observation times T (see Fig. S5 in Supplemental Material [80]). Such a

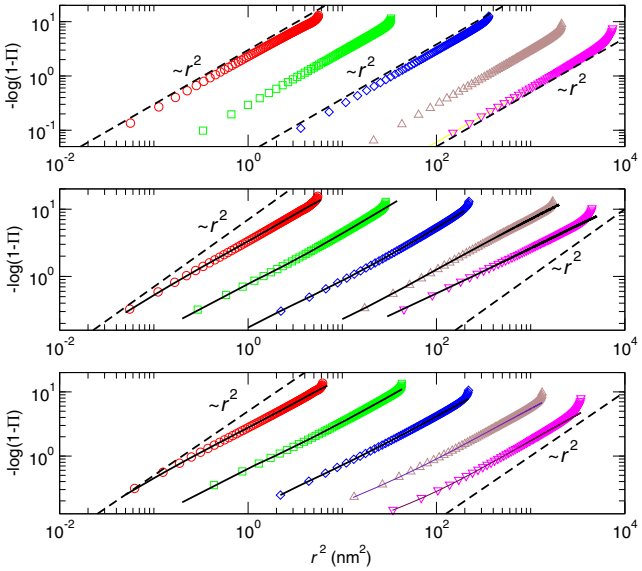

FIG. 3. Cumulative distribution $\Pi(r^2,\Delta)$ for squared displacements $r^2=[\mathbf{r}(t+\Delta)-\mathbf{r}(t)]^2$ of individual lipids. The value $-\log[1-\Pi(r^2,\Delta)]$ is plotted against r^2 at lag times $\Delta=1$ ns (red), 10 ns (green), 100 ns (blue), 1000 ns (brown), and 5000 ns (magenta), from left to right. For a Gaussian process the scaling of $-\log(1-\Pi)\sim r^2$ is obtained [94] as indicated with dashed lines in the plot. Data are for the noncrowded DPPC (top), aggregating protein-crowded DPPC (middle), and nonaggregating protein-crowded DLPC (bottom) systems. For the latter two cases the exponent deviates substantially from a value of 2, as seen from the Gaussian guide lines. The solid lines depict the theoretical curves [Eq. (5)] of $-\log(1-\Pi)$ expected from the non-Gaussian propagator P fitting to the simulation data shown in Fig. 4.

power-law scaling with an exponent $\delta\neq 2$ may be explained with a non-Gaussian propagator P of the form

$$P_r(r,\Delta)\propto\exp\left[-\left(\frac{r}{c\Delta^{\alpha/2}}\right)^\delta\right], \tag{4}$$

which leads to a cumulative distribution $-\log[1-\Pi(r^2,\Delta)]\sim(r/c\Delta^{\alpha/2})^\delta$ in the large-displacement limit. Here, $P_r(r,\Delta)$ is the radial part of the propagator given by $P_r(r,\Delta)=\int_0^{2\pi}d\theta P(r,\theta,\Delta)$, with $r\geq 0$, and c is a scaling constant of dimension $[\mathrm{m/s}^{\alpha/2}]$. We confirm the non-Gaussianity of the propagators in Fig. 4 by examining the profiles of $\log P_r(r,\Delta)$ at several lag times with the fit curves based on the above non-Gaussian (solid lines) and the Gaussian (dashed lines) propagators. The lipids in the protein-poor membrane (Fig. 4, top left) have the anticipated Gaussian propagator at all given times. In the protein-crowded DPPC membrane (Fig. 4, top right and bottom), the two fit curves unambiguously suggest that the propagators are non-Gaussian with exponents $\delta<2$. Moreover, we find that the propagators require a composite fit function involving two non-Gaussian components (see

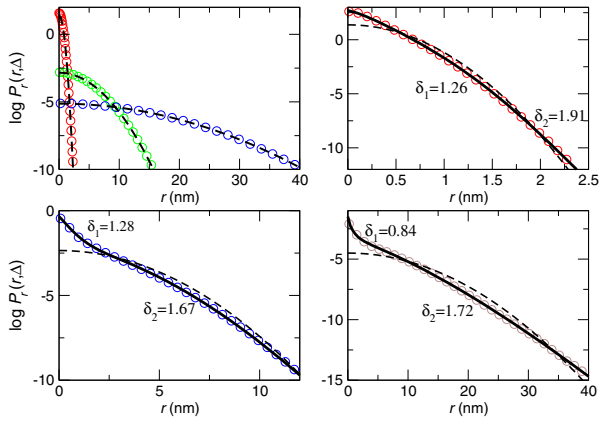

FIG. 4. Radial propagator $P_r(r,\Delta)$ for DPPC lipids in protein-poor and protein-rich membranes. In all cases the dashed and solid lines, respectively, represent the fitting curve to the simulation result: (dashed) Gaussian propagator $F_G(r) = c_1 \exp[-(r/2\sigma_1)^2]$, (solid) non-Gaussian propagator $F_{NG}(r) = c_1 \exp[-(r/2\sigma_1)^{\delta_1}] + c_2 \exp[-(r/2\sigma_2)^{\delta_2}]$, where the annotated δ values are the fit values. (Top left) The protein-poor case with $\Delta = 1$ ns (red), 10 ns (green), and 100 ns (blue). The other panels are for the protein-rich case with $\Delta = 1$ ns (top right), 100 ns (bottom left), and 1000 ns (bottom right). The two-component Gaussian fit to the P is supplemented in Fig. S7 in Supplemental Material [80].

the caption of Fig. 4 and also Fig. S7 in Supplemental Material [80]) to fully explain the behavior at both small and large displacements. For the two-component non-Gaussian propagator (shown in the caption of Fig. 4), its cumulative distribution can be exactly obtained as

$$\log[1-\Pi(r^2)] = \log\{1 - 4c_1\delta_1^{-1}\sigma_1^2\gamma[2\delta_1^{-1}, (r/2\sigma_1)^{\delta_1}] - 4c_2\delta_2^{-1}\sigma_2^2\gamma[2\delta_2^{-1}, (r/2\sigma_2)^{\delta_2}]\}, \quad (5)$$

where $\gamma(s,x) = \int_0^x t^{s-1}\exp(-t)dt$ is an incomplete gamma function. The solid lines in Fig. 3 depict the theoretical cumulative distribution Eq. (5) expected from the non-Gaussian propagator, which fits the simulation data in Fig. 4. For all cases, the theoretical curves display excellent agreement with the cumulative distribution, which in turn supports the validity of the proposed non-Gaussian propagator. We notice that the theoretical curves do not show a tip at the end. This suggests that the sharp bending at the tip in the simulation likely results from insufficient statistics. As we discuss further below, the character of the above non-Gaussian propagator is different from the non-Gaussian propagators in other complex soft matter systems found in recent experimental studies [95–99]. There is no single master curve describing all propagators obtained at different times, since the estimated δ values vary with time. The variation trend of δ in time appears to be system specific depending on the extent of the transient confinement effect due to protein crowding; see Fig. S6 in Supplemental Material [80]. For the protein-crowded DPPC system (where many lipids experience strong transient confinement), the values of effective δ tend to decrease with increasing lag time Δ. This indicates that the non-Gaussianity is enhanced until, at least, $\Delta = 5$ μs as time elapses. In contrast, the tendency is opposite in the nonaggregating DLPC system, in which δ increases and thus P becomes more Gaussian over time.

As our analysis shows, the non-Gaussian lateral anomalous diffusion revealed by Π and P cannot be explained by the model of multiple-component Gaussian processes that has often been introduced for modeling complicated anomalous diffusion processes found in experiment [93,100]. For our protein-crowded membranes, one can invoke a two-component (anomalous) diffusion model composed of slowly diffusing lipids in the proximity of the proteins and fast lipids in bulk [101], with the propagator $P(\mathbf{r},\Delta) = m\exp[-r^2/(2\sigma_{\text{slow}})]/(2\pi\sigma_{\text{slow}}) + (1-m)\exp[-r^2/(2\sigma_{\text{fast}})]/(2\pi\sigma_{\text{fast}})$, with $0 < m < 1$. As demonstrated in Fig. S7 in Supplemental Material [80], this model does not properly fit the distribution of displacements at various lag times. Additionally, we examine in Fig. S8 [80] whether the propagators are explained by the two-component model composed of a Gaussian center and a non-Gaussian tail as employed in some recent studies [95–97]. While this model explains the propagators better than the two-component Gaussian model, it also shows a deviation from the propagators, especially when the center is sharply peaked.

The protein diffusion exhibits similar characteristics. The corresponding cumulative distributions and propagators are plotted in Fig. 5. This analysis demonstrates that an isolated single protein in the noncrowded membrane (top panels) shares the property of Gaussian diffusion. The plot of $-\log[1-\Pi(r^2,\Delta)]$ scales as r^2, and $P_r(r,\Delta)$ follows the Gaussian propagator (dashed lines). The inconsistent cumulative distribution curve for $\Delta = 5$ μs is statistically inconclusive because it was obtained from a single trajectory of length $T = 25$ μs. The proteins in the crowded DPPC (middle panels) and DLPC (bottom panels) membranes display non-Gaussian scaling with δ being significantly below 2 at any analyzed displacements. The depicted solid lines are the expected cumulative distributions [Eq. (5)] from the fitted non-Gaussian propagators. The non-Gaussian protein diffusion appears to be more complex than the non-Gaussian behavior of the lipids, presumably due to the slow lateral dynamics of the proteins and nontrivial, effective lipid-mediated interactions among proteins. The cumulative distributions are typically characterized by multiple scaling curves.

We perform additional analyses to cross-check the failure of the FLE model for the protein-crowded membranes. Figure 6 presents the results of the moment ratios $\langle\mathbf{r}^4\rangle/\langle\mathbf{r}^2\rangle^2$ (regular) and $\langle\mathbf{r}^4_{\text{MME}}\rangle/\langle\mathbf{r}^2_{\text{MME}}\rangle^2$ (mean maximal excursion [102]) for lipids in the protein-poor and protein-rich membranes [53,102]. Note that in the literature the

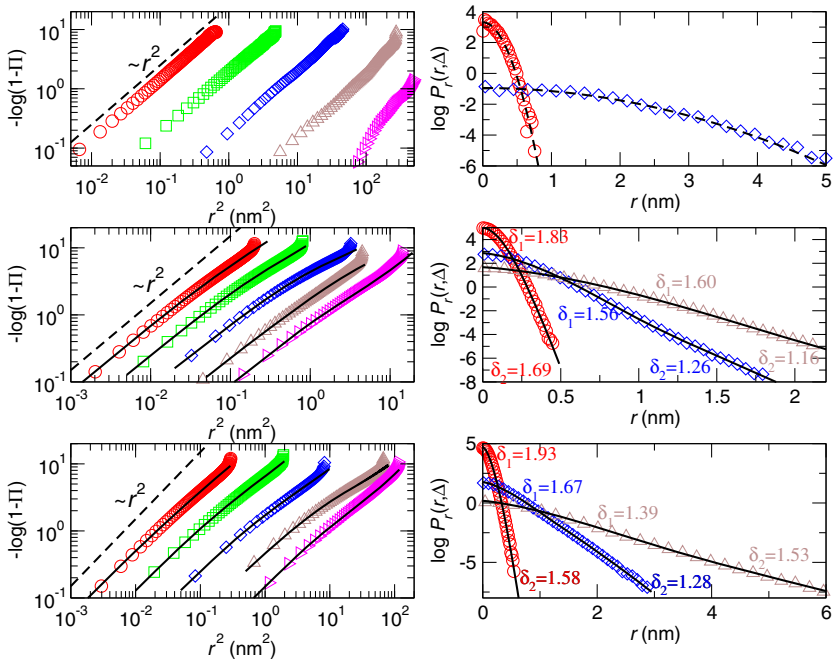

FIG. 5. Cumulative distribution $\Pi(r^2, \Delta)$ and propagator $P_r(r, \Delta)$ for proteins: (top) Protein-poor DPPC, (middle) protein-rich DPPC, and (bottom) protein-rich DLPC membranes. For all panels the color code denotes the results at $\Delta = 1$ ns (red), 10 ns (green), 100 ns (blue), 1000 ns (brown), and 5000 ns (magenta). As in Fig. 4, the dashed and solid lines in $\log P_r(r, \Delta)$ represent the fit curve using the Gaussian and the non-Gaussian propagators, respectively. The annotated δ values are the estimated non-Gaussian exponents δ from fitting.

regular moment ratio is alternatively redefined to a non-Gaussian parameter $\alpha_2(t) = (1/2)\langle \mathbf{r}^4(t)\rangle / \langle \mathbf{r}^2(t)\rangle^2 - 1$ [32,103]. It was theoretically shown that for a two-dimensional Gaussian process including FLE motion the moment ratio should be 2 for the regular moment and < 1.49 for the MME [53,102]. The lipids in the non-crowded membrane are in good agreement with these criteria. In contrast, in Fig. 6, the lipids in the crowded membranes are shown to have regular moments > 2 and the MME > 1.49 (dashed line), thus disobeying the Gaussianity criteria. Again, the obtained moment ratios are inconsistent with the FLE Gaussian model. We also note that the obtained moment ratios do not satisfy the criteria for anomalous diffusion in fractal media, which is characterized by moment ratios < 2 for the regular and < 1.49 for the mean maximal excursion [102]. This rules out the possibility that the protein-induced non-Gaussian diffusion in our model membranes is caused by a fractal-like obstacle structure formed by proteins.

The velocity autocorrelation function

$$C(\Delta) = \langle \mathbf{v}_{\delta t}(t + \Delta) \cdot \mathbf{v}_{\delta t}(t) \rangle \tag{6}$$

is also found to be inconsistent with the FLE model. From the trajectory, we obtain $C(\Delta)$ for average velocities $\mathbf{v}_{\delta t}(t) = [\mathbf{r}(t + \delta t) - \mathbf{r}(t)]/\delta t$, with a varying time interval δt [53,104], comparing them to the corresponding theoretical curve of the FLE model. Previously it was shown

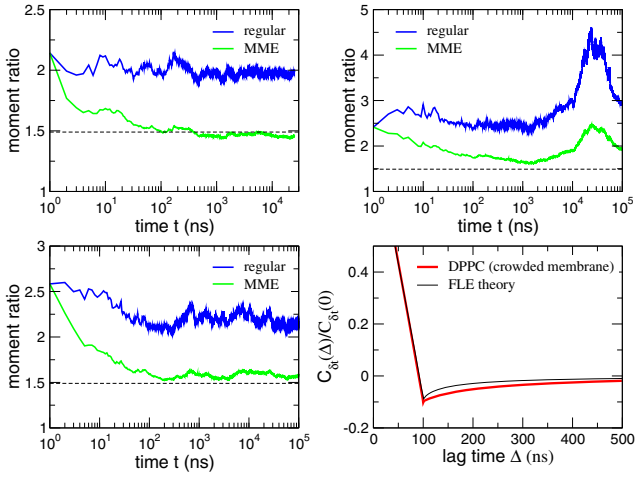

FIG. 6. Moment ratio of lipid molecules, $\langle \mathbf{r}^4\rangle / \langle \mathbf{r}^2\rangle^2$ (regular) and $\langle \mathbf{r}^4_{\mathrm{MME}}\rangle / \langle \mathbf{r}^2_{\mathrm{MME}}\rangle^2$ (mean maximal excursion). (Top left) DPPCs in the protein-poor membrane, (top right) DPPCs in the protein-rich membrane, (bottom left) DLPCs in the protein-rich membrane. Here, the MME distance $\mathbf{r}_{\mathrm{MME}}(t)$ refers to the maximum distance reached from the origin until time t [102]. For two-dimensional FLE motion with $0 < \alpha < 1$, the moment ratio is 2 for regular and < 1.49 (dashed line) for MME. (Bottom right) Velocity autocorrelation function $C(\Delta) = \langle \mathbf{v}_{\delta t}(t + \Delta) \cdot \mathbf{v}_{\delta t}(t)\rangle$ for the average velocity $\mathbf{v}_{\delta t}(t) = [\mathbf{r}(t + \delta t) - \mathbf{r}(t)]/\delta t$ with the chosen time interval $\delta t = 100$ (ns). The result for DPPCs in the protein-rich membrane is compared to the corresponding theoretical curve of FLE [53].

that the $C(\Delta)$ is excellently explained by the FLE model in the noncrowded case [53,54]. Figure 6 (bottom right) shows the result for DPPC lipids in the protein-rich membrane. While the antipersistent tendency in the lipid motion is observed, the relaxation profile does not follow the FLE model.

C. Protein crowding induces spatiotemporal heterogeneity in lateral diffusion

In order to obtain more insight into the physical nature of the protein-induced non-Gaussian diffusion, we visualize the spatiotemporal character of the lateral diffusion through diffusion maps at different times in Fig. 7. Since in our membrane systems the diffusion is anomalous with a time-dependent scaling exponent, neither the map of the generalized diffusion coefficient $K_\alpha(x, y, t)$ nor the scaling exponent $\alpha(x, y, t)$ properly quantify the degree of the local diffusion preference. We thus generate a 2D contour map of the local mean-squared displacements $[\mathbf{r}(t + t_0) - \mathbf{r}(t)]^2$ at time t over a short time interval t_0 set to be 1 ns in our analysis. Usually there are only 1–2 particles (or even none) at each site of the square grid in space, so the averaged local mean-squared displacements can be highly fluctuating in space regardless of the true local diffusional preference. To obtain a statistically meaningful contour map averaged over these fluctuations, we evaluate the diffusion map at time t by averaging 10 consecutive contour maps evaluated at times t, $t + 1, \ldots, t + 9$ ns, based on the observation that during 10 ns the protein position remains almost unchanged compared to that of the lipids. By this procedure, the diffusion maps of lipids are evaluated at $t = 1$, 10, 100, and 1000 ns.

Figure 7 compares the diffusion maps of DPPC molecules in protein-poor and protein-rich cases. Therein, the blue regions represent the unoccupied space by the lipids, which almost overlaps with the dashed circles denoting the positions of the NaK proteins at that moment, as estimated from the trajectory. In the case of the protein-poor membrane, the profile of the diffusion map changes with time. Except for the tendency that the lipid diffusion becomes slowed down in the proximity of a protein, the hot regions in which large lipid diffusion occurs emerge randomly in space. The rapidly varying spatiotemporal heterogeneity effectively produces homogeneous lipid diffusion over time, as seen above in the time-averaged MSD curves and their distribution. In sharp contrast to this, the diffusion map for the protein-crowded membrane exhibits a heterogeneous profile that strongly depends on the protein configuration in space. The diffusion tends to be slower in the protein-crowded regions and faster in between two distant protein complexes. It is surprising that the protein-induced diffusion heterogeneity has a very long life span. The given pattern of the diffusion map is maintained for more than 1 μs. Thus, a lipid molecule will experience a space-dependent diffusivity while diffusing across the membrane, as quantified below. The persistent pattern of the diffusion map originates from the slow diffusion dynamics of the protein complexes compared to the lipid motion in the investigated time range.

The spatiotemporal heterogeneity in the lateral diffusion of the lipids is further corroborated in Fig. 8. Here, we present the time-averaged MSD traces as a function of measurement time T for DPPC molecules in protein-poor and crowded membranes. To quantify the degree of amplitude fluctuations of the time-averaged MSDs upon

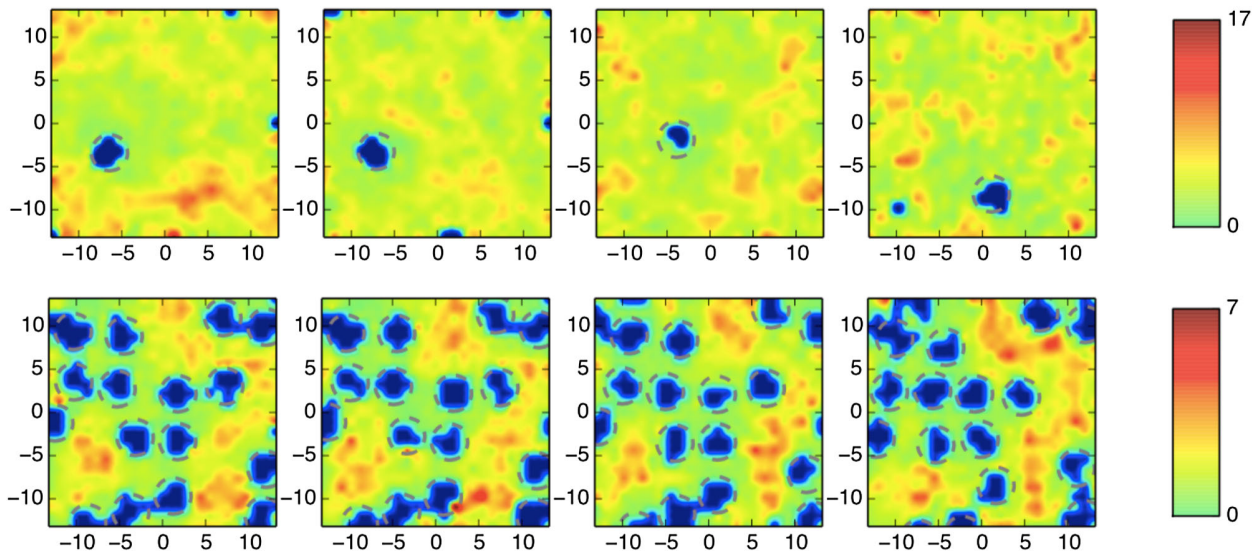

FIG. 7. Diffusion maps of DPPC lipid molecules in protein-poor (top) and protein-rich (bottom) membranes. In each case the four plots depict the diffusion maps at $t = 1$, 10, 100, and 1000 ns from left to right. Blue regions are the unoccupied space by the lipid at the given time, while the gray dashed circles illustrate the position of the proteins. Axis coordinates are in nanometers.

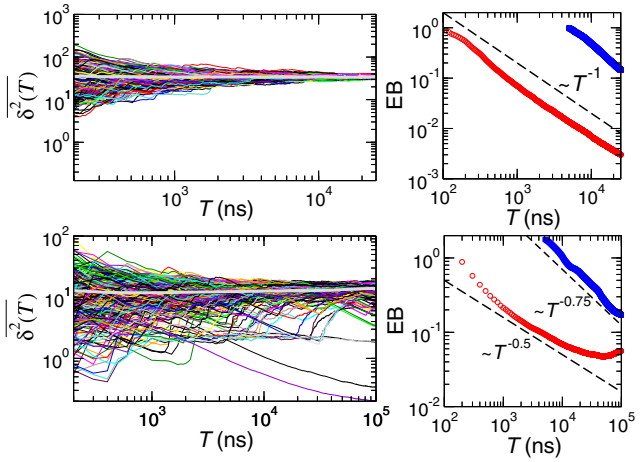

FIG. 8. Spatiotemporal fluctuations of the lipid diffusion in noncrowded (top) and crowded (bottom) DPPC membranes. (Left) Individual time-averaged MSD curves are plotted as a function of measurement time T at fixed $\Delta = 100$ ns. The thick gray lines represent the mean time-averaged MSD $\langle\overline{\delta^2(T)}\rangle$. (Right) Ergodicity breaking parameter EB(T), Eq. (7), depicted for $\Delta = 100$ ns (red circle) and 5000 ns (blue squares).

the increase of T, we evaluate the ergodicity breaking parameter [35,104,105]

$$\mathrm{EB}(T) = \frac{\left\langle (\overline{\delta^2(T)})^2 \right\rangle - \left\langle \overline{\delta^2(T)} \right\rangle^2}{\left\langle \overline{\delta^2(T)} \right\rangle^2}. \tag{7}$$

In the noncrowded membrane the heterogeneity of the time-averaged MSD in Fig. 8 is consistent with that for typical homogeneous ergodic diffusion, such as FLE motion. While individual time-averaged MSD traces show an erratic profile, their mean depicted by the thick gray line is independent of the observation time T, $\langle\overline{\delta^2(T)}\rangle \simeq T^0$, and the time-averaged MSD heterogeneity decreases with increasing T in accordance with the expected convergence law $\mathrm{EB}(T) \sim T^{-1}$ as for FLE [106–109]. Meanwhile, the lipids in the protein-rich membranes suffer strong heterogeneous diffusion. There exist lipids showing continuously decreasing, aginglike time-averaged MSDs upon increasing T. Additionally, it is observed that a fraction of lipids experience a sudden increase in the time-averaged MSD at a certain T' while having been independent of T for shorter observation times $T < T'$. From the diffusion map it can be inferred that those lipids diffusing successively through slow and fast diffusivity regions in space can have such temporal mobility heterogeneities. This new picture on the lipid diffusion in protein-crowded membranes is corroborated in Fig. 9, where we plot the temporal fluctuation of the diffusivity K_α for some individual lipid molecules and the probability density $\mathcal{P}(K_\alpha)$ for the obtained diffusivity from all trajectories. The traces of $K_\alpha(t)$ indeed show that the individual lipids display fluctuating diffusivity. The

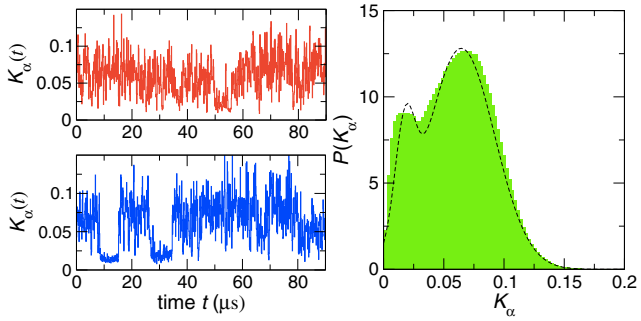

FIG. 9. (Left) Temporal fluctuation of the diffusivity $K_\alpha(t)$ for two chosen individual lipid molecules in the protein-crowded DPPC membrane. The diffusivity K_α is given in units of $\mu\mathrm{m}^2/\mathrm{ns}^\alpha$ and the temporal resolution is 100 ns. (Right) Probability density $\mathcal{P}(K_\alpha)$ for the obtained K_α value from all DPPC lipid molecules in the protein-crowded membrane. The dashed line represents a double-Gaussian fit to the data. Plots corresponding to the protein-poor system and nonaggregating systems can be found in Figs. S11 and S10 in Supplemental Material [80].

bimodal profile of $\mathcal{P}$ tells us that the diffusivity fluctuates within a finite range of values with two favorable diffusivity states. For some lipids (e.g., Fig. 9, bottom left), the transitions between the high and low diffusivity states are clearly seen. In this case, the lipids explore the low diffusivity region with a surprisingly long sojourn time of ~10 μs. Such patterns of diffusivity fluctuation lead to the decrease or the increase of time-averaged MSD $\overline{\delta^2(T)}$ with increasing T, as observed in Fig. 8. A supporting simulation described in Sec. S7 in Supplemental Material [80] suggests that the temporal fluctuation in $\overline{\delta^2(T)}$ may be attributed to a temporal change of the diffusivity whether or not the particle is under transient confinement. Geometrical effects like confinement are unable to change the amplitude of $\overline{\delta^2(T)}$, which can be decreased or increased if the diffusivity is changed with time. In spite of the strong heterogeneity on the single molecule level, on average the lipid diffusion does not age in the sense of $\langle\overline{\delta^2(T)}\rangle \simeq T^0$. This ergodic nature of the lipid diffusion is consistent with the diffusivity fluctuation in Fig. 9 in that a typical sojourn time for a given diffusivity state is always bounded. In other words, no diverging sojourn time exists for a low diffusivity state, which may be necessary for inducing nonergodicity, as shown in recent studies on the fluctuating diffusivity model [58,110,111]. The EB parameter indicates that the space-dependent diffusivity only leads to a slower ergodic convergence than the conventional Brownian case $\mathrm{EB}(T) \sim T^{-1}$. This observation indicates the importance of the proper averaging procedure in the analysis of the crowded membrane dynamics.

IV. DISCUSSION AND CONCLUSIONS

Based on extensive computer simulations and single trajectory analyses, we here provide a systematic

investigation of the anomalous lateral molecular diffusion of lipid molecules and embedded proteins in protein-crowded membranes. Recently, several experimental and computational studies reported that anomalous lipid diffusion is present in protein-crowded membranes up to time scales of microseconds to milliseconds and even up to 100 s in living cells [49,55,58,100]. Going beyond these studies, our focus here is to pin down the stochastic character and physical origins of the anomalous lateral diffusion induced by protein crowding. The three major results of this work are as follow. (1) The protein crowding significantly enhances the anomalous lateral diffusion in membranes. The subdiffusive lipid dynamics becomes much slower and spans up to several orders of magnitude longer than the typical crossover time of a few nanoseconds in a protein-poor membrane. This observation is in line with the above-discussed previous studies for crowded artificial or cellular membranes [49,55,58,100]. The protein channel motion observed in the plasma membranes of living cells also exhibits pronounced aging effects [55,58,63], a phenomenon not observed in our much simpler model membranes. (2) The protein crowding effects a non-Gaussian character in the anomalous diffusion, which is incompatible with the known models describing lateral diffusion. Previously, several groups, including us, found that in protein-free lipid bilayers, at any lipid phases, the lateral diffusion is consistently governed by the Gaussian FLE process (or, equivalently, fractional Brownian motion [112–114]), which thus appears to be a universal platform for the description of lateral diffusion in membranes [52–54]. However, our current study demonstrates that the inclusion of proteins in the membranes drastically changes the diffusion character: the picture suggested earlier no longer holds under protein crowding, thereby implying that the current paradigm of anomalous diffusion in membranes has to be revised. We show in this work that in protein-rich membranes, regardless of the lipid species, the lateral diffusion of phospholipids and proteins becomes highly non-Gaussian, and can no longer be explained by the Gaussian FLE model. This is clearly seen in the propagator $P_r(r,\Delta)$ obtained from the simulated lipid trajectories, which obeys a compressed (or stretched) exponential form [Eq. (4)]. The analyses also show that the observed non-Gaussian character is not explained by some other lateral diffusion models, such as the anomalous diffusion in fractal space [32,115], the free-volume jump diffusion [116,117], or the nonergodic continuous time random walk model [55,89]. (3) Protein crowding creates significant spatiotemporal heterogeneity in lateral diffusion dynamics with a very long life span of > 1 μs (Fig. 7). An individual lipid, while diffusing across such an environment, undergoes a spatially varying diffusivity, stemming largely from slowed-down diffusion in the vicinity of membrane proteins [101] compared to fast diffusion in protein-free regions. This results in strong heterogeneity in the motion of individual lipids, as seen in the amplitude scatter of the time-averaged MSD curves shown in Fig. 8 and also in Fig. S4 in Supplemental Material [80], but does not give rise to nonergodic properties.

Collecting these findings, it can be concluded that the protein crowding completely reshapes the lateral anomalous dynamics in membranes in its duration and stochastic character.

There are a few remarks on the non-Gaussian lateral diffusion observed in this work. Often, complicated diffusion patterns found in living cells have been modeled heuristically by a multicomponent Gaussian model [93,100]. Our computational study shows that this approach is not valid even in our crowded model membranes although they are much simpler than crowded cellular membranes. That is, the lateral diffusion in highly protein-crowded environments is not decomposed into the superposition of slow Gaussian diffusion in the proximity of proteins and fast Gaussian diffusion away from the proteins. This is mainly because a lipid molecule, whose dynamics is much faster than the protein dynamics, explores both slow and fast regions in space multiple times during its lateral diffusion and, thus, there is no distinction between slow and fast particles. While our study does not invalidate the use of multicomponent Gaussian approximation in general, it cautions the excessive interpretation of the results in terms of multiple-component Gaussian models when no further information is available.

Recently, a series of experimental and computational studies reported non-Gaussian diffusion dynamics in various soft complex systems [95–99]. Examples include colloidal beads on lipid bilayer tubes, particle diffusion in entangled actin networks, liposomes in nematic actin filaments, and colloidal suspensions. In these studies it was shown that the complex environments give rise to transient non-Gaussian diffusion on a certain time scale over which the propagator P typically has an exponential tail notwithstanding the diffusion dynamics maintaining the normal Einstein scaling law. On the one hand, the non-Gaussian lateral diffusion reported in this work is in line with these cases in that it is a phenomenon arising from the spatial complexity of the system. On the other hand, it is distinguished from them in that the non-Gaussian displacements are described by the compressed-exponential propagator [Eq. (4)] and lead to the anomalous diffusion dynamics $\overline{\delta^2} \sim \Delta^{\alpha}$.

What physical origins govern the observed non-Gaussian anomalous diffusion present in the protein-crowded membranes? Is it a system-specific phenomenon only shown in the protein-crowded membrane or a universal character commonly valid for similar crowded systems? Through additional computational work, we find that a very similar non-Gaussian anomalous diffusion can take place in a much simpler crowded, quasi-two-dimensional Lennard-Jones (argon) system. Simulation results are summarized in

Fig. 10. The inert atoms, otherwise displaying normal Brownian self-diffusion, undergo multifractal non-Gaussian anomalous diffusion when placed in an obstacle-crowded space where the immobile obstacles are aligned to give a transient confining effect to the diffusing particles. It is remarkable that an analogous profile of $\alpha(\Delta)$ over a long time window, similar to that observed in the protein-rich DPPC membrane (Fig. 2), is obtained when the obstacles are aligned in a similar fashion to the aggregating proteins [Fig. 10(e)]. The propagators are also shown to have a similar non-Gaussian character as in the case of the crowded membranes studied [Fig. 10(h)]. These results strongly suggest that the obstacle-induced hindrance and the transient confinement have a major responsibility for the non-Gaussian anomalous diffusion found in this work. We also find that the specific aggregation dynamics of proteins and the associated transient effect, as well as finite-size effects, are not significantly attributing to the non-Gaussian anomalous lipid dynamics. This is corroborated by the fact that the spatial correlation lengths and correlation times of proteins and lipids are considerably smaller than the membrane size and the simulation time (see Sec. S9 in Supplemental Material [80]). Our speculation on the origin of the observed non-Gaussian diffusion also gives an explanation of why the FLE Gaussian model, seemingly a universal dynamic model for the anomalous diffusion in protein-free membranes in all physical phases, fails to reproduce the diffusion characteristics in the protein-crowded membranes. This is because the observed non-Gaussianity is an effect of geometrical origin due to protein alignment, not from the viscoelasticity of a lipid membrane stemming from the lipid polymeric tail.

What dynamic model then replaces the Gaussian FLE model for the description of the non-Gaussian heterogeneous diffusion occurring in protein-crowded membranes? While it will be a challenging task to establish the quantitatively accurate model, we speculate that it will be based upon a hybrid model combining the obstructed diffusion with a diffusion process with space-dependent or fluctuating diffusivity. Several versions of the latter model were introduced recently where the local diffusivity is deterministically given by a specific functional form $K_1(x,y)$ or randomly given with a probability density $\mathcal{P}(K_1)$ [58,96,99,110,118–120]. These models were shown to generate heterogeneous diffusion processes having pronounced fluctuations in the time-averaged MSDs and in some cases induce weak ergodicity breaking. It was demonstrated that the fluctuating diffusivity model describes the nonergodic subdiffusion of a DC-SIGN receptor in the living-cell membranes [58] and the reptation dynamics in entangled polymer systems [111]. As we learn from the diffusion map and the trace of the diffusivity fluctuation in Figs. 7 and 9, the heterogeneous lateral diffusion in our protein-crowded membranes may be understood within the framework of the fluctuating diffusivity model. While in the literature heavy-tailed distributions of the diffusivity and the sojourn time are usually introduced to explain a nonergodic subdiffusion [58,110,111], in our membrane systems the diffusivity fluctuation is shown to have a finite variance and bounded sojourn times. Such moderate diffusivity fluctuation induces heterogenous lateral diffusion without weak ergodicity breaking.

Expanding the idea introduced in Ref. [99], we consider a Gaussian subdiffusive process with a fluctuating diffusivity $K_\alpha(t)$, where the evolution dynamics of K_α is modeled by stochastic motion of a particle confined in the double-well potential landscape of $-\log\mathcal{P}(K_\alpha)$ shown in Fig. 9. The physical scenario for this description is that the individual lipids experience an annealed fluctuating diffusivity induced by the protein crowding, while they carry out a FLE-like Gaussian subdiffusion if the presence of the obstacles (i.e., the proteins) is ignored. Then, in the long-time limit where $K_\alpha(t)$ reaches the stationary state with $\mathcal{P}(K_\alpha)$, the average propagator for this heterogeneous process is given by

$$P(x,\Delta)=\int_0^\infty dK_\alpha\frac{\mathcal{P}(K_\alpha)}{\sqrt{4\pi K_\alpha\Delta^\alpha}}\exp\left(-\frac{x^2}{4K_\alpha\Delta^\alpha}\right). \quad (8)$$

It can be shown that a non-Gaussian propagator P is attained for the given form of $\mathcal{P}$ found in Fig. 9 (see Fig. S15 in Supplemental Material [80]). This means that the non-Gaussian, heterogeneous anomalous diffusion we find in our crowded membranes can be reasonably explained within the framework of the fluctuating diffusivity model. However, it turns out that the propagator Eq. (8) based on the Gaussian kernel does not successfully explain the obtained propagator for the lipids in the simulations (see Fig. S15 in Supplemental Material [80]). Previous studies [58,96,110,118,120] inform us that a multifractal anomalous diffusion is not seen in these space-dependent diffusion processes. It is speculated that the heterogeneous lateral diffusion attains the additional non-Gaussian, multifractal nature by the effect of obstruction in space. Thus, the proper diffusion model for the protein-crowded membranes should integrate the non-Gaussian feature associated with the obstruction in space into the above-discussed fluctuating diffusivity model. In line with this idea, we find that the propagator Eq. (8) with a non-Gaussian kernel stemming from the presence of obstacles shows reasonable agreement with the propagator for the lipids; see Fig. S16 in Supplemental Material [80]. A thorough theoretical investigation of this model remains for future work. Complementary stochastic analysis tools will be of crucial assistance in this task [35,121–123]. Finally, we note in passing that our proposed diffusion mechanism for the protein-crowded membranes does not negate other possible diffusion mechanisms in other

crowded artificial or living-cell membranes [124–126]. Various diffusion patterns markedly different from the current non-Gaussian heterogeneous diffusion can emerge due to the presence of additional complexity.

Is the non-Gaussian anomalous diffusion expected to be biologically relevant? There are many reasons to assume so. First, as cell membranes are crowded with proteins [81], their influence on membrane dynamics has to be accounted for. Second, a great fraction of cellular functions are due to proteins working in unison as protein dimers or higher oligomeric complexes, and in order to function, the proteins have to form a complex where the relative orientation and the distance of individual proteins renders the function possible. This implies that the proteins should sample their relative conformational space for sufficiently long times in order to find the functional structure for the protein complex, and this sampling process is obviously fostered by correlated motion of the proteins. In the same spirit, in agreement with the lipid raft paradigm [3], it is known that for a number of membrane proteins there are lipid binding sites [127] where a specific lipid binds to a protein in a manner where it is able to modulate protein conformation and dynamics, and thus also activation and function. Here, too, the formation of the protein-lipid complex may be a slow process where correlated motion of the lipids next to the protein would increase the formation rate of the functional protein-lipid unit.

As we learn from this study, a new component in complexity may significantly affect the diffusion dynamics in protein-crowded membranes, thereby reshaping the stochastic character of the motion. A systematic understanding of the role of various complex components in living cellular membranes for the lateral membrane dynamics will be a challenging task in the future.

ACKNOWLEDGMENTS

We thank Touko Apajalahti for the tool used to estimate the correlation of lipid motion. We acknowledge financial support from the Academy of Finland [Finland Distinguished Professorship (R. M.), Centre of Excellence Programme (IV)] and the European Research Council (Advanced Grant project CROWDED-PRO-LIPIDS). For computing resources, we thank CSC–IT Center for Science (Espoo, Finland).

J.-H. J. and M. J. contributed equally to this work.

APPENDIX: MOLECULAR DYNAMICS SIMULATION ON THE CROWDED SIMPLE FLUID SYSTEMS

Here, we support our observations on the anomalous non-Gaussian lipid dynamics reported in the main text with additional simulations on a much simpler two-dimensional crowded system, i.e., a Lennard-Jones (LJ) fluid. The dynamics of this fluid are studied by simulating both obstacle-free [Fig. 10(a)] and obstacle-containing [Figs. 10(b) and 10(c)] systems. In the obstacle-containing case, two different arrangements of the obstacles are considered in order to produce the effects of transient weak and strong confinement.

The obstacle-free system consists of 9000 particles, whereas in the two obstacle-containing systems 20 obstacles are placed among 1900 particles. Each of these obstacles is built of an aggregate of 55 particles that are permanently fixed in space.

The simulations are run in the NVT ensemble at the boiling point of argon (87.3 K), whose LJ parameters ($\epsilon = 0.996$ kJ/mol, $\sigma = 0.3405$ nm [128]) are used for the particles. The area of the obstacle-free system is adjusted so that its 2D diffusion coefficients correspond to the value calculated for the same model in 3D at the same temperature and at a pressure of 1 bar. The areas of the two obstacle-containing systems are fixed to provide a very similar surface density and liquidlike behavior.

The obstacle-free system is simulated for 100 ns, whereas the obstacle-containing systems showing weak and strong confinement are simulated for 500 ns and 1 μs, respectively. All simulations are performed using an integration time step of 2 fs. The LJ interactions are cut off at 1 nm and a dispersion correction is applied to both energy and pressure. The temperature is kept constant at 87.3 K using the Berendsen thermostat [129]. Periodic boundary conditions are employed in the xy plane where diffusion takes place. The simulations are performed with the GROMACS simulation package version 4.5.x [130].

Figure 10 presents the highlights of the simulation results. The time-averaged MSD and the anomalous diffusion exponent α in Figs. 10(d) and 10(e) show that the obstacles in space induce anomalous diffusion. In the case of strong transient confinement [Fig. 10(c)], mimicking the protein-crowded DPPC (aggregating) case in Fig. 2(b), the variation of α in time reproduces the behavior of α for the lipids in the crowded membrane. Further, the duration of anomalous diffusion in the argon system, as also in the DPPC membrane, is significantly elongated.

It is important to note that here the anomalous diffusion (consistent with the results we discuss in the main text) is observed for simple LJ particles with static obstacles. This suggests that the effect of protein-aggregating dynamics in Fig. 2(b) is not essential for the observed strong anomalous lipid diffusion. Once the obstacles give rise to transient but strong confinement, the diffusing particles carry out anomalous dynamics. Moreover, the analyses of the propagators for the three systems in Figs. 10(f)–10(h) show that the anomalous diffusion in the strongly confined case [Fig. 10(c)] is indeed non-Gaussian. Analogously to the membrane system, P is described by a combination of two stretched-exponential propagators. Further, to rule out possible finite-size effects, we repeat this analysis for a LJ argon system whose size is 9 times (3×3) larger than

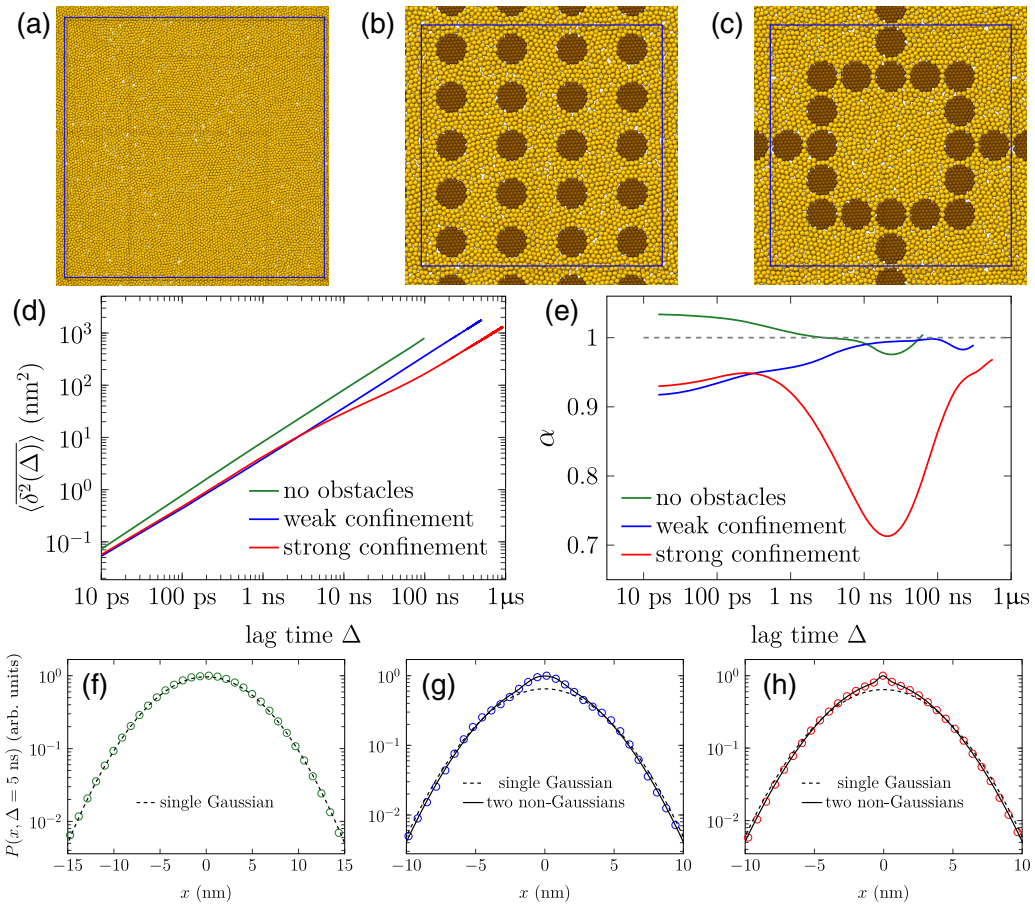

FIG. 10. (a)–(c) The Lennard-Jones (LJ) argon fluid systems simulated in our study. (a) The 2D argon fluid without obstacles. (b) The argon fluid particles with an obstacle arrangement that leads to weak confinement. (c) The argon fluid with an obstacle arrangement that gives rise to strong confinement. Note that the effect of confinement in (b) and (c) is transient. (d) The averaged time-averaged MSD curves for the argon particles in (a)–(c) systems. (e) The anomalous diffusion exponent α versus lag time Δ estimated from the mean time-averaged MSDs in (d). (f) The x component propagator $P(x, \Delta = 1\ \text{ns})$ with a single-Gaussian fit (dashed line) for the obstacle-free case. (g) The propagator P for the weakly confined argon particles with a single-Gaussian (dashed line) and double-non-Gaussian (solid line) fits. (h) The propagator P for the strongly confined argons with a single-Gaussian (dashed line) and double-non-Gaussian (solid line) fits.

the one discussed here. Consistent non-Gaussian diffusive behavior is observed (data not shown).

Summarizing, our simulation study on the simple LJ fluid systems corroborates the validity of the non-Gaussian anomalous lateral diffusion observed in protein-crowded membranes. The non-Gaussian lateral diffusion is not a system-specific, out-of-equilibrium transient dynamic property dependent upon the system preparation. Instead, it is a general dynamic equilibrium property induced by obstacle crowding.

[1] S. Angers, A. Salahpour, and M. Bouvier, *Dimerization: An Emerging Concept for G Protein-Coupled Receptor Ontogeny and Function*, Annu. Rev. Pharmacol. Toxicol. **42**, 409 (2002).

[2] S. R. George, B. F. O'Dowd, and S. P. Lee, *G-Protein-Coupled Receptor Oligomerization and Its Potential for Drug Discovery*, Nat. Rev. Drug Discov. **1**, 808 (2002).

[3] D. Lingwood and K. Simons, *Lipid Rafts as a Membrane-Organizing Principle*, Science **327**, 46 (2010).

[4] A. Laganowsky, E. Reading, T. M. Allison, M. B. Ulmschneider, M. T. Degiacomi, A. J. Baldwin, and C. V. Robinson, *Membrane Proteins Bind Lipids Selectively to Modulate Their Structure and Function*, Nature (London) **510**, 172 (2014).

[5] R. Phillips, T. Ursell, P. Wiggins, and P. Sens, *Emerging Roles for Lipids in Shaping Membrane-Protein Function*, Nature (London) **459**, 379 (2009).

[6] K. Simons and E. Ikonen, *Functional Rafts in Cell Membranes*, Nature (London) **387**, 569 (1997).

[7] M. Manna, T. Rog, and I. Vattulainen, *The Challenges of Understanding Glycolipid Functions: An Open Outlook Based on Molecular Simulations*, Biochim. Biophys. Acta-Mol. Cell Biol. Lipids **1841**, 1130 (2014).

[8] A. Kusumi, T. K. Fujiwara, R. Chadda, M. Xie, T. A. Tsunoyama, Z. Kalay, R. S. Kasai, and K. G. N. Suzuki, *Dynamic Organizing Principles of the Plasma Membrane that Regulate Signal Transduction: Commemorating the Fortieth Anniversary of Singer and Nicolson's Fluid-Mosaic Model*, Annu. Rev. Cell Dev. Biol. **28**, 215 (2012).

[9] D. M. Andrade, M. P. Clausen, J. Keller, V. Mueller, C. Wu, J. E. Bear, S. W. Hell, B. C. Lagerholm, and C. Eggeling, *Cortical Actin Networks Induce Spatio-Temporal Confinement of Phospholipids in the Plasma Membrane—A Minimally Invasive Investigation by STED-FCS*, Sci. Rep. **5**, 11454 (2015).

[10] A. Kusumi, C. Nakada, K. Ritchie, K. Murase, K. Suzuki, H. Murakoshi, R. S. Kasai, J. Kondo, and T. Fujiwara, *Paradigm Shift of the Plasma Membrane Concept From the Two-Dimensional Continuum Fluid to the Partitioned Fluid: High-Speed Single-Molecule Tracking of Membrane Molecules*, Annu. Rev. Biophys. Biomol. Struct. **34**, 351 (2005).

[11] R. J. Ellis, *Macromolecular Crowding: An Important but Neglected Aspect of the Intracellular Environment*, Curr. Opin. Struct. Biol. **11**, 114 (2001).

[12] D. M. Engelman, *Membranes Are More Mosaic Than Fluid*, Nature (London) **438**, 578 (2005).

[13] Y. Wang, M. Sarkar, A. E. Smith, A. S. Krois, and G. J. Pielak, *Macromolecular Crowding and Protein Stability*, J. Am. Chem. Soc. **134**, 16614 (2012).

[14] M. Hellmann, D. W. Heermann, and M. Weiss, *Enhancing Phosphorylation Cascades by Anomalous Diffusion*, Europhys. Lett. **97**, 58004 (2012).

[15] L. E. Sereshki, M. A. Lomholt, and R. Metzler, *A Solution to the Subdiffusion-Efficiency Paradox: Inactive States Enhance Reaction Efficiency at Subdiffusion Conditions in Living Cells*, Europhys. Lett. **97**, 20008 (2012).

[16] H. Matsuda, G. G. Putzel, V. Backman, and I. Szleifer, *Macromolecular Crowding as a Regulator of Gene Transcription*, Biophys. J. **106**, 1801 (2014).

[17] A. P. Minton, *The Influence of Macromolecular Crowding and Macromolecular Confinement on Biochemical Reactions in Physiological Media*, J. Biol. Chem. **276**, 10577 (2001).

[18] J. S. Kim and A. Yethiraj, *Effect of Macromolecular Crowding on Reaction Rates: A Computational and Theoretical Study*, Biophys. J. **96**, 1333 (2009).

[19] D. Ridgway, G. Broderick, A. Lopez-Campistrous, M. Ruaini, P. Winter, M. Hamilton, P. Boulanger, A. Kovalenko, and M. J. Ellison, *Coarse-Grained Molecular Simulation of Diffusion and Reaction Kinetics in a Crowded Virtual Cytoplasm*, Biophys. J. **94**, 3748 (2008).

[20] D. S. Banks and C. Fradin, *Anomalous Diffusion of Proteins due to Molecular Crowding*, Biophys. J. **89**, 2960 (2005).

[21] A. P. Minton, *Implications of Macromolecular Crowding for Protein Assembly*, Curr. Opin. Struct. Biol. **10**, 34 (2000).

[22] M. Tabaka, T. Kalwarczyk, J. Szymanski, S. Hou, and R. Holyst, *The Effect of Macromolecular Crowding on Mobility of Biomolecules, Association Kinetics, and Gene Expression in Living Cells*, Front. Phys. **2**, 54 (2014).

[23] G. Wieczorek and P. Zielenkiewicz, *Influence of Macromolecular Crowding on Protein-Protein Association Rates—A Brownian Dynamics Study*, Biophys. J. **95**, 5030 (2008).

[24] Y. Phillip and G. Schreiber, *Formation of Protein Complexes in Crowded Environments—From in Vitro to in Vivo*, FEBS Lett. **587**, 1046 (2013).

[25] A. Bhattacharya, Y. C. Kim, and J. Mittal, *Protein-Protein Interactions in a Crowded Environment*, Biophys. Rev. Lett. **5**, 99 (2013).

[26] K. A. Dill, K. Ghosh, and J. D. Schmit, *Physical Limits of Cells and Proteomes*, Proc. Natl. Acad. Sci. U.S.A. **108**, 17876 (20111).

[27] O. Stiehl, K. Weidner-Hertrampf, and M. Weiss, *Kinetics of Conformational Fluctuations in DNA Hairpin-Loops in Crowded Fluids*, New J. Phys. **15**, 113010 (2013).

[28] K. Aoki, M. Yamada, K. Kunida, S. Yasuda, and M. Matsuda, *Processive Phosphorylation of ERK MAP Kinase in Mammalian Cells*, Proc. Natl. Acad. Sci. U.S.A. **108**, 12675 (2011).

[29] J. D. Schmit, E. Kamber, and J. Kondev, *Lattice Model of Diffusion-Limited Bimolecular Chemical Reactions in Confined Environments*, Phys. Rev. Lett. **102**, 218302 (2009).

[30] P. D. Calvert, V. I. Govardovskii, N. Krasnoperova, R. E. Anderson, J. Lem, and C. L. Makino, *Membrane Protein Diffusion Sets the Speed of Rod Phototransduction*, Nature (London) **411**, 90 (2001).

[31] E. Barkai, Y. Garini, and R. Metzler, *Strange Kinetics of Single Molecules in Living Cells*, Phys. Today **65**, No. 8, 29 (2012).

[32] F. Höfling and T. Franosch, *Anomalous Transport in the Crowded World of Biological Cells*, Rep. Prog. Phys. **76**, 046602 (2013).

[33] J.-P. Bouchaud and A. Georges, *Anomalous Diffusion in Disordered Media: Statistical Mechanisms, Models and Physical Applications*, Phys. Rep. **195**, 127 (1990).

[34] R. Metzler and J. Klafter, *The Random Walk's Guide to Anomalous Diffusion: A Fractional Dynamics Approach*, Phys. Rep. **339**, 1 (2000).

[35] R. Metzler, J.-H. Jeon, A. G. Cherstvy, and E. Barkai, *Anomalous Diffusion Models and Their Properties: Non-Stationarity, Non-Ergodicity, and Ageing at the Centenary of Single Particle Tracking*, Phys. Chem. Chem. Phys. **16**, 24128 (2014).

[36] C. Di Rienzo, V. Piazza, E. Gratton, F. Beltram, and F. Cardarelli, *Probing Short-Range Protein Brownian Motion in the Cytoplasm of Living Cells*, Nat. Commun. **5**, 5891 (2014).

[37] I. Golding and E. C. Cox, *Physical Nature of Bacterial Cytoplasm*, Phys. Rev. Lett. **96**, 098102 (2006).

[38] S. C. Weber, A. J. Spakowitz, and J. A. Theriot, *Bacterial Chromosomal Loci Move Subdiffusively through a Viscoelastic Cytoplasm*, Phys. Rev. Lett. **104**, 238102 (2010).

[39] I. Bronstein, Y. Israel, E. Kepten, S. Mai, Y. Shav-Tal, E. Barkai, and Y. Garini, *Transient Anomalous Diffusion of Telomeres in the Nucleus of Mammalian Cells*, Phys. Rev. Lett. **103**, 018102 (2009).

[40] J.-H. Jeon, V. Tejedor, S. Burov, E. Barkai, C. Selhuber-Unkel, K. Berg-Sørensen, L. Oddershede, and R. Metzler,

In Vivo Anomalous Diffusion and Weak Ergodicity Breaking of Lipid Granules, Phys. Rev. Lett. **106**, 048103 (2011).

[41] S. M. Ali Tabei, S. Burova, H. Y. Kim, A. Kuznetsov, T. Huynh, J. Jureller, L. H. Philipson, A. R. Dinner, and N. F. Scherer, *Intracellular Transport of Insulin Granules Is a Subordinated Random Walk*, Proc. Natl. Acad. Sci. U.S.A. **110**, 4911 (2013).

[42] J.-H. Jeon, N. Leijnse, L. B. Oddershede, and R. Metzler, *Anomalous Diffusion and Power-Law Relaxation of the Time Averaged Mean Squared Displacement in Worm-Like Micellar Solutions*, New J. Phys. **15**, 045011 (2013).

[43] W. Pan, L. Filobelo, N. D. Q. Pham, O. Galkin, V. V. Uzunova, and P. G. Vekilov, *Viscoelasticity in Homogeneous Protein Solutions*, Phys. Rev. Lett. **102**, 058101 (2009).

[44] J. Szymanski and M. Weiss, *Elucidating the Origin of Anomalous Diffusion in Crowded Fluids*, Phys. Rev. Lett. **103**, 038102 (2009).

[45] A. Caspi, R. Granek, and M. Elbaum, *Enhanced Diffusion in Active Intracellular Transport*, Phys. Rev. Lett. **85**, 5655 (2000).

[46] N. Gal and D. Weihs, *Experimental Evidence of Strong Anomalous Diffusion in Living Cells*, Phys. Rev. E **81**, 020903(R) (2010).

[47] J. F. Reverey, J.-H. Jeon, H. Bao, M. Leippe, R. Metzler, and C. Selhuber-Unkel, *Superdiffusion Dominates Intracellular Particle Motion in the Supercrowded Cytoplasm of PathogenicAcanthamoeba castellanii*, Sci. Rep. **5**, 11690 (2015).

[48] J. A. Dix and A. S. Verkman, *Crowding Effects on Diffusion in Solutions and Cells*, Annu. Rev. Biophys. **37**, 247 (2008).

[49] M. Javanainen, H. Hammaren, L. Monticelli, J.-H. Jeon, M. S. Miettinen, H. Martinez-Seara, R. Metzler, and I. Vattulainen, *Anomalous and Normal Diffusion of Proteins and Lipids in Crowded Lipid Membranes*, Faraday Discuss. **161**, 397 (2013).

[50] M. R. Horton, F. Höfling, J. Rädler, and T. Franosch, *Development of Anomalous Diffusion among Crowding Proteins*, Soft Matter **6**, 2648 (2010).

[51] C. Eggeling, C. Ringemann, R. Medda, G. Schwarzmann, K. Sandhoff, S. Polyakova, V. N. Belov, B. Hein, C. von Middendorff, and A. Schönle, *Direct Observation of the Nanoscale Dynamics of Membrane Lipids in a Living Cell*, Nature (London) **457**, 1159 (2009).

[52] G. R. Kneller, K. Baczynski, and M. Pasenkiewicz-Gierula, *Consistent Picture of Lateral Subdiffusion in Lipid Bilayers: Molecular Dynamics Simulation and Exact Results*, J. Chem. Phys. **135**, 141105 (2011).

[53] J.-H. Jeon, H. M.-S. Monne, M. Javanainen, and R. Metzler, *Anomalous Diffusion of Phospholipids and Cholesterols in a Lipid Bilayer and Its Origins*, Phys. Rev. Lett. **109**, 188103 (2012).

[54] E. Bakalis, S. Höfinger, A. Venturini, and F. Zerbetto, *Crossover of Two Power Laws in the Anomalous Diffusion of a Two Lipid Membrane*, J. Chem. Phys. **142**, 215102 (2015).

[55] A. V. Weigel, B. Simon, M. M. Tamkun, and D. Krapf, *Ergodic and Nonergodic Processes Coexist in the Plasma Membrane as Observed by Single-Molecule Tracking*, Proc. Natl. Acad. Sci. U.S.A. **108**, 6438 (2011).

[56] S. Stachura and G. R. Kneller, *Probing Anomalous Diffusion in Frequency Space*, J. Chem. Phys. **143**, 191103 (2015).

[57] M. Weiss, H. Hashimoto, and T. Nilsson, *Anomalous Protein Diffusion in Living Cells as Seen by Fluorescence Correlation Spectroscopy*, Biophys. J. **84**, 4043 (2003).

[58] C. Manzo, J. A. Torreno-Pina, P. Massignan, G. J. Lapeyre, Jr., M. Lewenstein, and M. F. Garcia Parajo, *Weak Ergodicity Breaking of Receptor Motion in Living Cells Stemming From Random Diffusivity*, Phys. Rev. X **5**, 011021 (2015).

[59] G. Guigas and M. Weiss, *Sampling the Cell with Anomalous Diffusion—The Discovery of Slowness*, Biophys. J. **94**, 90 (2008).

[60] M. J. Saxton, *Chemically Limited Reactions on a Percolation Cluster*, J. Chem. Phys. **116**, 203 (2002).

[61] P. J. Woolf and J. J. Linderman, *Self Organization of Membrane Proteins via Dimerization*, Biophys. Chem. **104**, 217 (2003).

[62] Z. Kalay, T. K. Fujiwara, and A. Kusumi, *Confining Domains Lead to Reaction Bursts: Reaction Kinetics in the Plasma Membrane*, PLoS One **7**, e32948 (2012).

[63] J. H. P. Schulz, E. Barkai, and R. Metzler, *Aging Renewal Theory and Application to Random Walks*, Phys. Rev. X **4**, 011028 (2014).

[64] V. A. Volpert, Y. Nec, and A. A. Nepomnyashchy, *Fronts in Anomalous Diffusion-Reaction Systems*, Phil. Trans. R. Soc. A **371**, 20120179 (2013).

[65] I. M. Sokolov, M. G. W. Schmidt, and F. Sagués, *Reaction-Subdiffusion Equations*, Phys. Rev. E **73**, 031102 (2006).

[66] E. Melo and J. Martins, *Kinetics of Bimolecular Reactions in Model Bilayers and Biological Membranes. A Critical Review*, Biophys. Chem. **123**, 77 (2006).

[67] M. A. Lomholt, I. M. Zaid, and R. Metzler, *Subdiffusion and Weak Ergodicity Breaking in the Presence of a Reactive Boundary*, Phys. Rev. Lett. **98**, 200603 (2007).

[68] M. A. Yıldırım, K.-I. Goh, M. E. Cusick, A.-L. Barabási, and M. Vidal, *Drug-Target Network*, Nat. Biotechnol. **25**, 1119 (2007).

[69] A. I. Archakov, V. M. Govorun, A. V. Dubanov, Y. D. Ivanov, A. V. Veselovsky, P. Lewi, and P. Janssen, *Protein-Protein Interactions as a Target for Drugs in Proteomics*, Proteomics **3**, 380 (2003).

[70] M. R. Arkin and J. A. Wells, *Small-Molecule Inhibitors of Protein-Protein Interactions: Progressing towards the Dream*, Nat. Rev. Drug Discov. **3**, 301 (2004).

[71] M. R. Wenk, *The Emerging Field of Lipidomics*, Nat. Rev. Drug Discov. **4**, 594 (2005).

[72] H. J. Kaiser, A. Orlowski, T. Rog, W. Chai, T. Feizi, D. Lingwood, I. Vattulainen, and K. Simons, *Lateral Sorting in Model Membranes by Cholesterol-Mediated Hydrophobic Matching*, Proc. Natl. Acad. Sci. U.S.A. **108**, 16628 (2011).

[73] P. V. Escribá, *Membrane-Lipid Therapy: A New Approach in Molecular Medicine*, Trends Mol. Med. **12**, 34 (2006).

[74] A. Honigmann, V. Mueller, H. Ta, A. Schoenle, E. Sezgin, S. W. Hell, and C. Eggeling, *Scanning STED-FCS Reveals*

Spatiotemporal Heterogeneity of Lipid Interaction in the Plasma Membrane of Living Cells, Nat. Commun. **5**, 5412 (2014).

[75] G. Vicidomini, H. Ta, A. Honigmann, V. Mueller, M. P. Clausen, D. Waithe, S. Galiani, E. Sezgin, A. Diaspro, S. W. Hell, and C. Eggeling, *STED-FLCS: An Advanced Tool to Reveal Spatiotemporal Heterogeneity of Molecular Membrane Dynamics*, Nano Lett. **15**, 5912 (2015).

[76] J. E. Goose and M. S. P. Sansom, *Reduced Lateral Mobility of Lipids and Proteins in Crowded Membranes*, PLoS Comput. Biol. **9**, e1003033 (2013).

[77] G. Guigas and M. Weiss, *Membrane Protein Mobility Depends on the Length of Extra-Membrane Domains and on the Protein Concentration*, Soft Matter **11**, 33 (2015).

[78] E. Falck, T. Róg, M. Karttunen, and I. Vattulainen, *Lateral Diffusion in Lipid Membranes through Collective Flows*, J. Am. Chem. Soc. **130**, 44 (2008).

[79] M. Javanainen, L. Monticelli, J. B. de la Serna, and I. Vattulainen, *Free Volume Theory Applied to Lateral Diffusion in Langmuir Monolayers: Atomistic Simulations for a Protein-Free Model of Lung Surfactant*, Langmuir **26**, 15436 (2010).

[80] See Supplemental Material at http://link.aps.org/supplemental/10.1103/PhysRevX.6.021006 for additional results and figures that complement those given in the main Letter.

[81] A. D. Dupuy and D. M. Engelman, *Protein Area Occupancy at the Center of the Red Blood Cell Membrane*, Proc. Natl. Acad. Sci. U.S.A. **105**, 2848 (2008).

[82] S. J. Marrink, H. J. Risselada, S. Yefimov, D. P. Tieleman, and A. H. De Vries, *The MARTINI Force Field: Coarse Grained Model for Biomolecular Simulations*, J. Phys. Chem. B **111**, 7812 (2007).

[83] L. Monticelli, S. K. Kandasamy, X. Periole, R. G. Larson, D. P. Tieleman, and S.-J. Marrink, *The MARTINI Coarse-Grained Force Field: Extension to Proteins*, J. Chem. Theory Comput. **4**, 819 (2008).

[84] P. J. Bond and M. P. Sansom, *Insertion and Assembly of Membrane Proteins via Simulation*, J. Am. Chem. Soc. **128**, 2697 (2006).

[85] I. M. Sokolov, *Models of Anomalous Diffusion in Crowded Environments*, Soft Matter **8**, 9043 (2012).

[86] M. J. Skaug, A. M. Lacast, L. Ramirez-Piscin, J. M. Sancho, K. Lindenberg, and D. K. Schwartz, *Single-Molecule Diffusion in a Periodic Potential at a Solid-Liquid Interface*, Soft Matter **10**, 753 (2014).

[87] F. D. Stefani, J. P. Hoogenboom, and E. Barkai, *Beyond Quantum Jumps: Blinking Nanoscale Light Emitters*, Phys. Today **62**, No. 2, 34 (2009).

[88] A. Bodrova, A. V. Chechkin, A. G. Cherstvy, and R. Metzler, *Quantifying Non-Ergodic Dynamics of Force-Free Granular Gases*, Phys. Chem. Chem. Phys. **17**, 21791 (2015).

[89] T. Akimoto, E. Yamamoto, K. Yasuoka, Y. Hirano, and M. Yasui, *Non-Gaussian Fluctuations Resulting from Power-Law Trapping in a Lipid Bilayer*, Phys. Rev. Lett. **107**, 178103 (2011).

[90] E. Flenner, J. Das, M. C. Rheinstädter, and I. Kosztin, *Subdiffusion and Lateral Diffusion Coefficient of Lipid Atoms and Molecules in Phospholipid Bilayers*, Phys. Rev. E **79**, 011907 (2009).

[91] P. Hänggi, *Correlation Functions and Master Equations of Generalized (Non-Markovian) Langevin Equations*, Z. Phys. B **31**, 407 (1978).

[92] I. Goychuk, *Viscoelastic Subdiffusion: Generalized Langevin Equation Approach*, Adv. Chem. Phys. **150**, 187 (2012).

[93] G. J. Schütz, H. Schindler, and T. Schmidt, *Single-Molecule Microscopy on Model Membranes Reveals Anomalous Diffusion*, Biophys. J. **73**, 1073 (1997).

[94] M. Weiss, *Single-Particle Tracking Data Reveal Anticorrelated Fractional Brownian Motion in Crowded Fluids*, Phys. Rev. E **88**, 010101(R) (2013).

[95] B. Wang, S. M. Anthony, S. C. Bae, and S. Granick, *Anomalous yet Brownian*, Proc. Natl. Acad. Sci. U.S.A. **106**, 15160 (2009).

[96] B. Wang, J. Kuo, S. C. Bae, and S. Granick, *When Brownian Diffusion Is Not Gaussian*, Nat. Mater. **11**, 481 (2012).

[97] G. Kwon, B. J. Sung, and A. Yethiraj, *Dynamics in Crowded Environments: Is Non-Gaussian Brownian Diffusion Normal?*, J. Phys. Chem. B **118**, 8128 (2014).

[98] G. David and J. Phillies, *In Complex Fluids the Gaussian Diffusion Approximation Is Generally Invalid*, Soft Matter **11**, 580 (2015).

[99] M. V. Chubynsky and G. W. Slater, *Diffusing Diffusivity: A Model for Anomalous, yet Brownian, Diffusion*, Phys. Rev. Lett. **113**, 098302 (2014).

[100] S. J. Sahl, M. Leutenegger, M. Hilbert, S. W. Hell, and C. Eggeling, *Fast Molecular Tracking Maps Nanoscale Dynamics of Plasma Membrane Lipids*, Proc. Natl. Acad. Sci. U.S.A. **107**, 6829 (2010).

[101] P. S. Niemelä, M. Miettinen, L. Monticelli, H. Hammaren, P. Bjelkmar, T. Murtola, E. Lindahl, and I. Vattulainen, *Membrane Proteins Diffuse as Dynamic Complexes with Lipids*, J. Am. Chem. Soc. **132**, 7574 (2010).

[102] V. Tejedor, O. Benichou, R. Voituriez, R. Jungmann, F. Simmel, C. Selhuber-Unkel, L. Oddershede, and R. Metzler, *Quantitative Analysis of Single Particle Trajectories: Mean Maximal Excursion Method*, Biophys. J. **98**, 1364 (2010).

[103] J.-P. Hansen and I. McDonald, *Theory of Simple Liquids*, 3rd ed. (Academic Press, Amsterdam, 2006).

[104] S. Burov, J.-H. Jeon, R. Metzler, and E. Barkai, *Single Particle Tracking in Systems Showing Anomalous Diffusion: The Role of Weak Ergodicity Breaking*, Phys. Chem. Chem. Phys. **13**, 1800 (2011).

[105] Y. He, S. Burov, R. Metzler, and E. Barkai, *Random Time-Scale Invariant Diffusion and Transport Coefficients*, Phys. Rev. Lett. **101**, 058101 (2008).

[106] W. Deng and E. Barkai, *Ergodic Properties of Fractional Brownian-Langevin Motion*, Phys. Rev. E **79**, 011112 (2009).

[107] J.-H. Jeon and R. Metzler, *Fractional Brownian Motion and Motion Governed by the Fractional Langevin Equation in Confined Geometries*, Phys. Rev. E **81**, 021103 (2010).

[108] J.-H. Jeon and R. Metzler, *Inequivalence of Time and Ensemble Averages in Ergodic Systems: Exponential Versus Power-Law Relaxation in Confinement*, Phys. Rev. E **85**, 021147 (2012).

[109] J. Kursawe, J. Schulz, and R. Metzler, *Transient Aging in Fractional Brownian and Langevin-Equation Motion*, Phys. Rev. E **88**, 062124 (2013).

[110] P. Massignan, C. Manzo, J. A. Torreno-Pina, M. F. Garca-Parajo, M. Lewenstein, and G. J. Lapeyre, Jr., *Nonergodic Subdiffusion from Brownian Motion in an Inhomogeneous Medium*, Phys. Rev. Lett. **112**, 150603 (2014).

[111] T. Uneyama, T. Miyaguchi, and T. Akimoto, *Fluctuation Analysis of Time-Averaged Mean-Square Displacement for the Langevin Equation with Time-Dependent and Fluctuating Diffusivity*, Phys. Rev. E **92**, 032140 (2015).

[112] A. N. Kolmogorov, *Curves in Hilbert Space, which Are Invariant With Respect to a One-Parameter Group of Motions*, Dokl. Akad. Nauk SSSR **26**, 6 (1940).

[113] A. M. Yaglom, *Correlation Theory of Stationary and Related Random Functions*, 1st ed. (Springer, New York, 1987).

[114] B. B. Mandelbrot and J. W. van Ness, *Fractional Brownian Motions, Fractional Noises and Applications*, SIAM Rev. **10**, 422 (1968).

[115] M. J. Saxton, *Anomalous Diffusion due to Obstacles: A Monte Carlo Study*, Biophys. J. **66**, 394 (1994).

[116] W. L. C. Vaz and P. F. Almeida, *Microscopic versus Macroscopic Diffusion in One-Component Fluid Phase Lipid Bilayer Membranes*, Biophys. J. **60**, 1553 (1991).

[117] P. F. F. Almeida, W. L. C. Vaz, and T. E. Thompson, *Lateral Diffusion in the Liquid Phases of Dimyristoylphosphatidylcholine/Cholesterol Lipid Bilayers: A Free Volume Analysis*, Biochem. J. **31**, 6739 (1992).

[118] A. G. Cherstvy and R. Metzler, *Population Splitting, Trapping, and Non-Ergodicity in Heterogeneous Diffusion Processes*, Phys. Chem. Chem. Phys. **15**, 20220 (2013).

[119] A. G. Cherstvy, A. V. Chechkin, and R. Metzler, *Anomalous Diffusion and Ergodicity Breaking in Heterogeneous Diffusion Processes*, New J. Phys. **15**, 083039 (2013).

[120] A. G. Cherstvy, A. V. Chechkin, and R. Metzler, *Particle Invasion, Survival, and Non-Ergodicity in 2D Diffusion Processes with Space-Dependent Diffusivity*, Soft Matter **10**, 1591 (2014).

[121] K. Burnecki, E. Kepten, Y. Garini, G. Sikora, and A. Weron, *Estimating the Anomalous Diffusion Exponent for Single Particle Tracking Data with Measurement Errors—An Alternative Approach*, Sci. Rep. **5**, 11306 (2015).

[122] A. Godec, M. Bauer, and R. Metzler, *Collective Dynamics Effect Transient Subdiffusion of Inert Tracers in Flexible Gel Networks*, New J. Phys. **16**, 092002 (2014).

[123] Y. Meroz and I. M. Sokolov, *A Toolbox for Determining Subdiffusive Mechanisms*, Phys. Rep. **573**, 1 (2015).

[124] T. Fujiwara, K. Ritchie, H. Murakoshi, K. Jacobson, and A. Kusumi, *Phospholipids Undergo Hop Diffusion in Compartmentalized Cell Membrane*, J. Cell Biol. **157**, 1071 (2002).

[125] A. Kusumi, C. Nakada, K. Ritchie, K. Murase, K. Suzuki, H. Murakoshi, R. S. Kasai, J. Kondo, and T. Fujiwara, *Paradigm Shift of the Plasma Membrane Concept from the Two-Dimensional Continuum Fluid to the Partitioned Fluid: High-Speed Single-Molecule Tracking of Membrane Molecules*, Annu. Rev. Biophys. Biomol. Struct. **34**, 351 (2005).

[126] M. J. Saxton and K. Jocobson, *Single-Particle Tracking: Applications to Membrane Dynamics*, Annu. Rev. Biophys. Biomol. Struct. **26**, 373 (1997).

[127] F. X. Contreras, A. M. Ernst, F. Wieland, and B. Brugger, *Specificity of Intramembrane Protein-Lipid Interactions*, Cold Spring Harbor Persp. Biol. **3**, a004705 (2011).

[128] L. A. Rowley, D. Nicholson, and N. G. Parsonage, *Monte Carlo Grand Canonical Ensemble Calculation in a Gas-Liquid Transition Region for 12-6 Argon*, J. Comput. Phys. **17**, 401 (1975).

[129] H. J. C. Berendsen, J. P. M. Postma, W. F. van Gunsteren, A. DiNola, and J. R. Haak, *Molecular Dynamics with Coupling to an External Bath*, J. Chem. Phys. **81**, 3684 (1984).

[130] S. Pronk *et al.*, *GROMACS 4.5: A High-Throughput and Highly Parallel Open Source Molecular Simulation Toolkit*, Bioinformatics **29**, 845 (2013).

Tampereen teknillinen yliopisto
PL 527
33101 Tampere

Tampere University of Technology
P.O.B. 527
FI-33101 Tampere, Finland

ISBN 978-952-15-4230-5
ISSN 1459-2045